A.S. Balasubramanian
7/3/69

SOME FACTORS INFLUENCING

THE STRESS-STRAIN BEHAVIOUR OF CLAYS

by

A.S.BALASUBRAMANIAM

VOLUME I

TEXT

A Dissertation submitted for the
Degree of Doctor of Philosophy
at
Cambridge University

Churchill College

March 1969

Summary

This dissertation is mainly concerned with the experimental investigation of the stress-strain behaviour of remoulded saturated clays for all possible types of imposed stress paths, under stress controlled conditions in the axi-symmetric triaxial apparatus. The conventional triaxial apparatus was modified to improve the uniformity of strains of the deforming specimens during all stages of the tests, as the state of the samples changed from the initial condition of a slurry to that of failure. This complete set of data, in the stress plane in which the principal axes of stress and strain coincide and with two principal stresses and strains always equal, was used to study the regions in these stress planes for which any, or all, of the stress-strain theories developed so far at Cambridge are valid. From the data constitutive equations were developed to describe the stress-strain behaviour in these bounded stress regions; no appeal was made to concepts such as those developed in the theory of plasticity.

The use of a radiographic technique for locating lead shot within soil specimens was found to be most satisfactory for the study of the local deformations in triaxial samples which are generally assumed to be straining uniformly. Using this technique it was shown that (i) the deformation is uniform during one dimensional and isotropic consolidation, (ii) during shear the conventional lubricated ends significantly reduce the effects of end restraint on the deformation behaviour of the samples; the strains are substantially uniform up to about 75 per cent of the peak stresses. The local deformations during shear when plotted in the form of histograms approximated to normal distribution curves.

The effects of history such as (i) the initial moisture content (ii) the initial 1-D stress used in sample preparation (iii) the subsequent isotropic consolidation prior to shear (iv) the load increment duration, and (v) the load increment size, on the stress-strain behaviour are studied in detail. It is shown that these factors do influence the deformation characteristics to a considerable extent. Methods, which take account of these effects, are proposed to correlate all the test results.

Specimens were sheared to failure under a wide variety of imposed stress paths from an initial isotropic stress state; it is shown that a unique peak stress envelope exists for all such specimens. This peak stress envelope coincides with the

critical state line for pressures higher than the maximum pre-consolidation pressure but lies on a Hvorslev type surface for pressures lower than the preconsolidation pressure.

The assumption used in the three main Cambridge stress-strain theories for clays are critically examined and expressed in mathematically similar form for ease of comparison. The precise regions in the stress plane in which each theory is valid are defined.

The stress plane is divided into regions within which the deformation characteristics are, to a first approximation, path independent. Characteristic surfaces are plotted relating the stresses and associated strains in each of these regions and are expressed by simple constitutive equations.

Preface

I am very grateful to Professor K.H.Roscoe for the opportunity to work under his direction and to use the excellent equipment and techniques which have been developed at Cambridge for fundamental research in Soil Mechanics. I am also deeply indebted to him for his unstinted help and advice at all stages of my work. I am deeply indebted to my supervisor, Dr.R.G.James, for his guidance, help and encouragement and the amount of time he has devoted in discussing every aspect of the work presented in this dissertation.

I wish to thank the staff of the Soil Mechanics group, particularly Professor A.N.Schofield for many stimulating and helpful discussions.

Special acknowledgements are due to Drs.A.Thurairajah, D.G.Coumoulos and Ting, W.H., for encouragement and assistance during the initial phase of my work.

I wish to express my appreciation to all my research colleagues, in particular to Messrs.E.C.Hambly, N.K.Tovey, P.J.Avgherinos and B.L.Tennekoon for many valuable discussions.

My special thanks are also due to Mr.R.E.Ward of the Soil Mechanics Laboratory and his assistants W.Gwizdala and A.Cooke for the invaluable service they gave me while carrying out my experimental work.

I would also like to record my thanks to Mr.A.A.Barker and his staff in the Engineering Laboratory Workshop for making the necessary apparatus.

Mrs.N.Chapman for the patience and care she took in preparing the bulk of the data for computation.

Mr.P.E.Clarkson for his assistance in Computing.

Mr.E.Nisbet and his staff of the Photographic Department.

Professor O.R.Frisch of the Nuclear Physics Group of the Cavendish Laboratory for granting permission to use the film measuring machine (CLARA).

Mrs.R.E.Ward for the great care with which she has typed this dissertation.

I am grateful to the Government of Ceylon for the financial support given by them and in particular for extending the period of my Scholarship for three months beyond the normal period of three years.

I am also appreciative of the facilities provided by the Cambridge University and Churchill College.

Last but not least, I am greatly indebted to the generous hospitality and kindness shown by Professor and Mrs.K.H.Roscoe to me throughout my stay in Cambridge.

I certify that except where specific reference is made in the text to the work of others, the contents of this dissertation are original and have not been submitted to any other university.

A.S.Balasubramanian

7-3-1969.

CONTENTS

Page No.

CHAPTER 7. CONSTITUTIVE EQUATIONS FOR THE STRESS-STRAIN BEHAVIOUR OF CLAYS IN BOUNDED STRESS REGIONS

CHAPTER 1

GENERAL INTRODUCTION

1.1 Foreword

A wide variety of soil mechanics problems need for their satisfactory solution, a stress-strain relationship dependent on fundamental soil constants. Such a relationship between the stresses and strains should cover all possible forms of stress and strain paths. The fundamental soil constants should depend only on the properties of the soil and be independent of such factors as the geometry of the apparatus in which the soil is tested or the type of tests carried out. The research work in Cambridge is mainly aimed at achieving relationships between stresses and strains for both cohesive and cohesionless soils.

In order to derive a stress-strain theory, several basic assumptions have to be made of which one or more may not alone be capable of being verified experimentally. However it is possible to compare the theoretical predictions with the observed overall behaviour. Hence it is essential that new and more sophisticated apparatus should be designed to control both stresses and strains independently at any stage of testing. Such types of apparatus will necessarily be of complicated geometry and hence during any process of deformation, the uniformity of stresses and strains throughout the sample should be ascertained. Non-destructive techniques using X and Gamma rays have been developed in Cambridge for the measurements of internal strains and voids ratio in deforming soil specimens. Also methods have been developed to investigate the orientation of clay particles in soil specimens using transmission and scanning electron microscopes. Further, load cells of varying forms have been developed to measure the normal and shear stresses on the boundaries of the samples. Attempts have been made to develop semiconductor pressure probes for the measurement of internal pore pressures.

In this thesis the investigation of the stress-strain behaviour is restricted to the axi-symmetric conditions of the conventional triaxial system of stresses on cylindrical specimens, where in the principal axes of stress and strain are at all times

compelled to coincide and (ii) the intermediate principal stress is always equal to the major or the minor principal stress. The observations from this simple system of stresses are compared with those from the other types of apparatus such as the simple shear apparatus and the biaxial apparatus (Hambly (1969)) where the specimens are subjected to plane strain conditions. Hereafter the simple shear apparatus will be referred to as the S.S.A. Non-destructive radiation techniques are developed for the measurement of internal strains and voids ratio in cylindrical specimens under different applied stress conditions. The effects of several factors that influence the stress-strain behaviour during sample preparation and testing are investigated. Finally sections of the specimens are observed in the scanning electron microscope to study the changes of the orientation of clay particles during one dimensional consolidation, isotropic consolidation and shear.

1.2 Basic Concepts and Definitions

1.2.1 Stress

The stress parameters used in the analysis of triaxial test results are

$$p = \tfrac{1}{3} (\sigma_1' + 2 \sigma_3')$$

$$\text{and} \quad q = (\sigma_1' - \sigma_3') \text{ since } \sigma_2' = \sigma_3'$$

where σ_1', σ_2' and σ_3' are the principal effective compressive stresses. The parameters p and q are functions of the first and second invariants of the stress tensor

$$\begin{vmatrix} \sigma_1' & 0 & 0 \\ 0 & \sigma_2' & 0 \\ 0 & 0 & \sigma_3' \end{vmatrix}$$

1.2.2 Strain

In terms of the principal compressive strains ϵ_1, ϵ_2 and ϵ_3 the relevant strain parameters for use under the axi-symmetric conditions of the triaxial test are

$$\upsilon = (\epsilon_1 + 2 \epsilon_3)$$

$$\text{and} \quad \epsilon = \tfrac{2}{3} (\epsilon_1 - \epsilon_3) \text{ since } \epsilon_2 = \epsilon_3$$

The parameters υ and ϵ are functions of the first and second

invariant of the strain tensor $\begin{vmatrix} \epsilon_1 & 0 & 0 \\ 0 & \epsilon_2 & 0 \\ 0 & 0 & \epsilon_3 \end{vmatrix}$

1.2.3 The axial and volumetric strains of a triaxial sample

Using the definition of natural strains (Nadai 1950), the axial strain in a triaxial sample of initial length L_o and initial volume V_o is

$$\epsilon_1 = \int_L^{L_o} \frac{dL}{L} = \log\left(\frac{L_o}{L}\right) \quad \text{(compression being positive)}$$

and the volumetric strain is

$$\upsilon = \int_V^{V_o} \frac{dV}{V} = \log\left(\frac{V_o}{V}\right) \quad \text{(compression being positive)}$$

or expressed in terms of the voids ratio (e) is

$$\upsilon = \log\left(\frac{1+e_o}{1+e}\right)$$

where e is the initial voids ratio.

The stresses p, q and the voids ratio e are quantities which can be measured absolutely. The strains υ and ϵ are always measured with respect to a datum. In the present thesis, unless otherwise stated, υ and ϵ will be measured from the state of the sample at the end of its preparation under isotropic stress conditions and just prior to shear. (All samples are prepared from a slurry which is first subjected to one dimensional, and subsequently to isotropic, consolidation. Some samples are then permitted to swell under isotropic stress conditions. Deviatoric stresses are then applied to the samples at the end of their history under isotropic stress conditions.) Consequently the datum of υ varies and depends on the initial isotropic consolidation pressure. The four quantities p, q, υ and ϵ are extensively used throughout the analysis. It should be noted that no attempt will be made to classify them as dependent or independent variables. However it must be emphasised that it is not possible to vary less than (i) two of the four quantities p, q, υ and ϵ during isotropic consolidation and swelling and (ii) three of the four parameters for all other stress paths.

1.2.4 Loading, unloading and reloading

In this dissertation, the term loading refers to an increase in deviator stress higher than its previous maximum value. Unloading and reloading refer to a decrease or an increase, respectively in the deviator stress which is never greater than its previous maximum value. The terms loading, unloading and reloading do not refer to the mean normal stress p or to the parameters q/p, q/p_e etc. In general the author defines the imposed stress path in terms of q and p but occasionally when discussing unloading and reloading tests it will be necessary to also use the previous maximum values of these parameters.

1.3 Previous Work on Yielding of Clays

1.3.1 The constant voids ratio contours of Rendulic

A proper study of the yielding of cohesive soils started with Rendulic (1936). Rendulic performed a series of stress controlled compression and extension triaxial tests on remoulded saturated clay. The results were plotted in a σ_1' , $\sqrt{2}\,\sigma_3'$ space and Rendulic found that the stress paths followed by specimens sheared at constant voids ratio (undrained tests) are in close agreement with the constant voids ratio contours derived from drained tests and isotropic consolidation tests. Further, by assuming that these contours are reproducible in the $\sigma_1' = \sigma_3'$ and $\sigma_1' = \sigma_2'$ planes, Rendulic suggested that the constant voids ratio contours form surfaces of revolution about the space diagonal $\sigma_1' = \sigma_2' = \sigma_3'$ when plotted in three dimensional stress space. His results were obtained from only three types of triaxial test:

(i) 4 tests in isotropic consolidation
(ii) 3 fully drained tests with cell pressures of 28.4, 35.6 and 42.7 psi respectively
(iii) 7 undrained tests at 14.2, 28.4, 35.6, 42.7, 56.8 and 71 psi respectively.

These contours are reproduced in Fig. 1:1.

1.3.2 The effective stress, water content relationships of Henkel.

Henkel (1960) provided experimental results on Weald clay and London clay to illustrate the existence of a unique relationship between the effective stresses and the water content for

each clay. The compression test results provided by Henkel are of three types with stress paths of slope (dq/dp) equal to $-\frac{3}{2}$, 3 and ∞ respectively. Similar stress paths are also imposed on the extension side. The stress paths imposed, and typical constant moisture content contours interpolated from them, are shown in Figs. 1.2(a), (b) and (c). Fig.1.2(c) shows that the constant water content contours obtained from drained tests are similar in form to the stress paths corresponding to the conventional undrained tests.

1.3.3 The (p,q, e) space of Roscoe, Schofield and Wroth.

Roscoe, Schofield and Wroth (1958) put forward a basic concept of the existence of a unique surface in the three dimensional space relating the voids ratio and the stress parameters q and p. Such a surface for normally and lightly overconsolidated clays is represented by ABCD in Fig.1.3 which is based on triaxial test data from Imperial College on Weald clay. The surface CDEF corresponding to overconsolidated specimens is based on less reliable evidence than that supporting ABCD. Also the authors suggested that it is not possible for the specimen to exist at a state (defined by p, q and e) outside the domain bounded by the two surfaces ABCD and CDEF unless tensile stresses are imposed. These two surfaces were subsequently called the state boundary surface. In developing the surface ABCD in Fig.1.3, Roscoe, et.al.(1958) only used the results of undrained tests.

1.3.4 The similarity of undrained stress paths and the state boundary surface in two dimensional plot

Assuming that all e = constant sections of the state boundary surface are geometrically similar Roscoe and Roorooshasb (1963) transformed this three dimensional surface relating (p, q and e) into a two dimensional curve. The relevant parameters selected were q/p and $\frac{1}{p}\exp\left(\frac{e_a - e}{\lambda}\right)$, denoted by η and ξ respectively. The function $\exp\left(\frac{e_a - e}{\lambda}\right)$ is equivalent to the parameter p_e defined by Hvorslev (1937), as

$$p_e = \exp\left(\frac{e_a - e}{\lambda}\right) \qquad 1.1$$

where e_a corresponds to the voids ratio at unit pressure on the virgin consolidation line and p_e is the equilibrium pressure corresponding to the instantaneous voids ratio e on this line. Subsequent workers (e.g. Burland 1965) have used the alternative parameters q/p_e and p/p_e for the two dimensional representation of

the state boundary surface. A unique curve can only be expected in this two dimensional plot for that part of the state path followed in any type of triaxial text that lies on the state boundary surface representing the state paths obtained from undrained tests.

1.3.5 The uniqueness of state boundary surface, Roscoe and Thurairajah (1964)

A detailed investigation of the stress paths followed by specimens in the $(\eta, \xi_T)^*$ space for tests carried out on Weald clay, Cambridge Gault clay and Kaolin was reported by Roscoe and Thurairajah (1964). The results for Weald clay and Cambridge Gault clay were from conventional drained and undrained compression tests in the triaxial apparatus. The results for Kaolin include tests carried out both in the triaxial apparatus and in the S.S.A. The following observations are noted.

(i) For Weald clay the state paths for drained and undrained tests form a unique curve in the (η, ξ_T) space.

(ii) For Gault clay the state paths for drained and undrained tests give different curves in the (η, ξ_T) space. The drained test path has higher values of η for a given value of ξ_T than the undrained test path.

(iii) For Kaolin in the triaxial apparatus the drained and undrained test paths in the (η, ξ_T) space were different as shown in Figs.1.4(a) and (b). Again the value of η corresponding to a given value of ξ_T was greater for the drained test path than for the undrained. The state paths followed during anisotropic consolidation seem to deviate from the drained and undrained surfaces as shown in Fig.1.4(c). This deviation can be seen to be smaller for anisotropic consolidation paths initiated from the drained test path at high stress ratios.

(iv) For Kaolin tested in the simple shear apparatus the drained and undrained tests lie on the same unique curve in the $(\eta', \xi_T')^{**}$ space as shown in Fig.1.5(a) and (b). The parameters η' and ξ_T' refer to the S.S.A. where

$$\eta' = \frac{\tau}{\sigma'} \quad \text{and} \quad \xi' = \frac{1}{\sigma'} \exp\left(\frac{e_a' - e}{\lambda}\right)$$

e_a' is the voids ratio corresponding to unit pressure of σ'

* $\xi_T = \frac{1}{\xi} \exp\left(-\frac{e_a}{\lambda}\right)$

** $\xi_T' = \frac{1}{\xi'} \exp\left(-e_a'/\lambda\right)$

These authors did not present any data concerning the shear strains experienced by specimens in the triaxial apparatus and the S.S.A. during tests. Fig.1.6 illustrates the strain paths relating the volumetric strain υ and the shear strain ϵ, followed in the two types of apparatus for the so called conventional drained tests. In a conventional drained compression test in the triaxial apparatus the cell pressure $\sigma_2' = \sigma_3'$ is maintained constant while in a fully drained test in the S.S.A. the vertical stress σ' is kept constant. It would therefore be somewhat more logical to compare the results of fully drained tests in the S.S.A. with the results of p = constant tests in the triaxial apparatus. The strain path for the latter type of test is also shown in Fig.1.6. It should be noted that the volumetric strains observed in both types of triaxial test, for a given shear strain, are considerably greater than in the S.S.A. test. Hence the state path for fully drained tests are bound to be nearer to the state paths in undrained tests in the S.S.A. than in the triaxial apparatus. (Note: It has been assumed, when plotting Fig.1.6, that the angle of shear imposed on the sample by the S.S.A. is equal to the shear strain ϵ. For justification of this see equation (2) of Arthur, James and Roscoe (1964).)

Roscoe and Thurairajah (1964) concluded that

(i) the reason Weald clay appeared to have one unique surface in (p, q, e) space was due to the presence of air in the samples and they also stated that if the air is removed then there would be probably two independent apparent surfaces for drained and undrained tests on Weald clay as shown by the triaxial data for the Cambridge Gault clay and the Kaolin.

(ii) if the voids ratio had been correctly measured in the most deforming part of the samples in the triaxial drained and partially drained tests, then one unique surface would exist in the (p,q, e) space for all compression tests regardless of the extent of the dilation.

These conclusions will be discussed further in Chapter 4 in the light of the author's results.

1.3.6 The stress-strain theory of Roscoe and Poorooshasb based on unique (p,q,e) surface for normally and lightly overconsolidated clays

Assuming a unique (p,q,e) surface, an incremental stress-strain theory was proposed by Roscoe and Poorooshasb (1963) in the form

$$d\epsilon_1 = \left(\frac{d\epsilon_1}{d\eta}\right)_v d\eta + \left(\frac{d\epsilon_1}{dv}\right)_\eta . dv \qquad 1.2$$

where $\left(d\epsilon_1/d\eta\right)_v$ corresponds to the variation of ϵ_1 with η in an undrained test and $\left(d\epsilon_1/dv\right)_\eta$ represents the variation of ϵ_1 with v in a constant η stress path. The total strain experienced at any instant for any state path on the state boundary surface ABCD in Fig.1.3 is calculated by integrating equation 1.2.

$$\epsilon_1 = \int_0^{\epsilon_1} d\epsilon_1 = \int_0^{\eta} \left(\frac{d\epsilon_1}{d\eta}\right)_v d\eta + \int_0^{\eta} \left(\frac{d\epsilon_1}{dv}\right)_\eta . dv \qquad 1.3$$

The limitations of this theory will be discussed further in Chapters 6 and 7 in the light of the author's test results.

1.3.7 The critical state concept and associated stress-strain theories

Roscoe, Schofield and Wroth (1958) put forward the basic concept that the end points of all tests performed on remoulded saturated clay lie on a unique line in the (p,q,e) space. This line was subsequently defined as the critical state line. At the critical state, the material is capable of having unlimited shear distortion without any further change in stresses or volume. The critical state line is assumed (i) to have a constant slope M in the (q,p) space and (ii) to be parallel to the virgin compression line in the (e-log p) plot. These statements about the critical state line will be studied in relation to the author's results in Chapter 5. The parameter M is assumed to be a fundamental property of the material; it was used by Roscoe, Schofield and Thurairajah (1963a) in deriving an expression for the energy dissipated internally in plastic distortion. A stress-strain theory was proposed by these authors based on an energy equation and some of the concepts of the theories of plasticity as developed for metals. This stress-strain theory was subsequently presented in a concise form and

the ideal material which satisfies all the assumptions made, was called the Cam clay (Roscoe and Schofield 1963). The expression for energy dissipation was later modified by Roscoe and Burland (1968) and a Modified theory was presented in the light of the new energy equation. The Cam clay theory and the Modified theory will be discussed in detail in Chapter 6. Wroth (1965), using the energy equation of Roscoe, Schofield and Thurairajah (1963a) proposed an independent theory based on an empirical strain equation which does not depend on theories of plasticity for metals. This theory predicts identical strains to those obtained from the Cam clay theory for normally consolidated clays.

1.4 Outline of the contents of the present thesis

The first chapter of this dissertation (already presented above) begins with a general introduction of the broad aspects of the work carried out at Cambridge into the fundamental study of the stress-strain behaviour of soils. This is followed by a section which includes definitions of the stress and strain parameters and some of the basic concepts. The literature published on the yielding of cohesive soils is reviewed, but only briefly in Chapter 1, since further details are given when discussing the author's results in later chapters.

Since a major portion of this dissertation is devoted to a careful investigation of the experimental behaviour of clays, Chapter 2 summarises the apparatus used, the measurements carried out and the errors involved. Possible improvements in test techniques are suggested. Chapter 2 begins with a brief description of modifications of conventional triaxial test apparatus including those required for the application of non-destructive techniques to study the distributions of strains within the samples. The overall test programme carried out by the author is then presented in tabular form. Chapter 2 concludes with an illustration of the methods used in the computations of the localised strains and of the stresses.

In Chapter 3, the use of non-destructive techniques for the measurement of local strains and local voids ratio is fully described. They include a lead shot technique which is used to study the distribution of strains during the one dimensional consolidation, isotropic consolidation and subsequent shear of triaxial samples. The effect of end restraint on the strains

of triaxial specimens with conventional ends (i.e. porous stones or unpolished metal, both of which induce friction) is investigated. The internal displacements and strains in specimens with lubricated ends are also studied during the deformation of normally and overconsolidated clays both in compression and in extension. This investigation is carried out both on 1.5 inch diameter by 3 inch high samples and on 4 inch diameter by 4.5 inch high samples. In developing the X-ray absorption method for the determination of local voids ratio from the optical density of radiographs it was necessary to study the effects of scattered radiation on the X-ray films. These effects were most satisfactorily reduced by making use of a Bucky grid. An alternative Gamma ray method developed by Coumoulos (1967) to study the distribution of voids ratio in saturated clay samples was found to be unsatisfactory for the conditions of the triaxial test equipment. It could perhaps be used for this purpose by some means which would increase the difference in absorption coefficient of the fluid and solid phase in the sample.

Chapter 4 is devoted to a study of the several factors that influence the stress-strain behaviour as represented in the $(q/p, \epsilon)$, $(q/p, v)$ and $(q/p_e, p/p_e)$ spaces. These factors include the effects of (a) the initial moisture content of the slurry from which the specimens are prepared; (b) the one dimensional stress used in the sample preparation; (c) the similarity of strains for tests with similar applied stress paths performed at different levels of isotropic stress; (d) the end restraint, the sample size and the load increment; (e) time on the undrained and fully drained tests.

In Chapter 5 the behaviour of the specimens at peak stresses is investigated. (The peak stresses correspond to the values of q and p at the instant that the maximum value of q is observed. For special tests in which q is held constant or is reduced the peak stresses will refer to conditions at which the ratio is observed to be a maximum.) This investigation includes the effects of end restraint, initial one dimensional consolidation, load increment duration and the applied stress paths on the peak stresses. The peak stress envelopes in $(\Delta e_f, \log q_f)$ and $(\Delta e_f, \log p_f)$ spaces are studied in relation to the critical state line assumed by Roscoe, Schofield and Thurairajah (1963a).

Chapter 6 is concerned with the comparisons of the observed deformation behaviour with those predicted from a number of theories. The observed deformation characteristics correspond

to all possible forms of stress paths. The basic concepts of the yield surface, the strain hardening law and the flow rule as derived from the simple Cam clay model and its Modification are examined in relation to the experimental observations. The stress-strain theory of Roscoe and Poorooshasb is also investigated. The stress paths reported in Chapter 6 cover all the possible forms of deformation in the stable and unstable regions and clearly illustrate the effects of anisotropy, Bauchinger effect and the hysteresis loops in the stress-strain behaviour for large unloading and reloading paths.

In Chapter 7 the stress paths are classified by their slopes into different groups for which different characteristic surfaces are developed. Constitutive equations are then proposed to describe these surfaces.

The thesis is concluded in Chapter 8 with a brief summary of the experimental findings, the limitations of the existing stress-strain theories and recommendations for future work.

CHAPTER 2

THE APPARATUS, TEST PROCEDURE, METHODS OF MEASURING AND ASSOCIATED ERRORS

2.1 The consolidometer for use with X-rays.

2.1.1 The selection of the material of the consolidometer

The consolidometer was mainly used for X-ray work. Hence it was essential to select a material which has an absorption coefficient which is as small as possible. Perspex and aluminium were selected because of their relatively low X-ray absorption coefficients.

2.1.2 Description of the base load cell and the consolidometer

A detailed description of the way in which the pedestal of the base of a commercially available triaxial cell was modified to incorporate a load cell has been given by Burland (1967) (see his pages 73-4). Three diagrams of it are shown in Fig.2.1. The load cell is machined from an aluminium alloy. The four active webs A (0.25 inch wide and 0.025 inch thick) have Saunders Roe Foil strain gauges ($\frac{1}{4}$ inch) stuck to either side. The dummy gauges are mounted on a hollow hexagonal shaped pillar D made from a separate piece of duralumin which can be screwed into position after all the gauges are connected to the terminal board T. The top of the pedestal is $1\frac{1}{2}$ inch diameter and is polished and smeared with silicone grease. The active face of the load cell is 1 inch diameter and there is a clearance of 2×10^{-3} inches between it and the surrounding pedestal. The rubber cap C covers the whole pedestal; it is held to it by Gaco rings. The output from the load cell was recorded on a 6 channel Foster recorder described by James (1965). The load cell was calibrated by subjecting it to water pressure in a conventional triaxial cell.

The special consolidometer to study the uniformity of strains during the one dimensional (1-D) initial consolidation of the clay while preparing samples for triaxial tests is shown in Fig.2.2 mounted on the modified triaxial base K which has been described above. It consists of a perspex tube made in two parts and connected by a collar. The internal face of the tube is highly polished and is $1\frac{1}{2}$ inch diameter. The two parts are held together by two metal end plates connected by four screwed rods L. The bottom metal plate forms a seal against the rubber

cap C (Fig.2.1) on the pedestal containing the load cell. The piston M is made of PTFE to reduce friction between it and the side walls. Its lower face contains a porous stone ($\frac{3}{16}$ inch thick and type UNI 150 KV) and this is the only drainage face for the sample. The casette N for the X-ray films rests in a special holder with reference markers such as P in Fig.2.2, fixed in two rows on both sides of this holder. The whole apparatus is mounted on the square base plate Q which can be fixed at one end of a test bed while the X-ray head is mounted at the other end. Loads are applied to the piston M by a hanger.

One test, to investigate the effects of side friction during 1-D consolidation was carried out with the perspex tubes (J in Fig.2.2) replaced by tubes of duralumin.

2.2 The triaxial formers for conventional and enlarged ends

When not wishing to study deformation during 1-D consolidation clay samples were prepared in an adaption of the sand sample formers made by Thurairajah (1961). It is shown in Fig.2.3 in an assembled position. It consists essentially of a split mould 'A' (similar to that shown in Fig.2.4) positioned in an outer casing C. The whole unit is clamped to the base of a triaxial cell. A low vacuum is applied through the outlet F to keep the rubber membrane G in position in the mould. The extension piece E is clamped to the casing C with an outer ring D. The load is applied through a piston P by a hanger resting on a steel ball placed on the top of rod M. During consolidation drainage takes place at both ends of the sample. Walker (1965) made a former of similar design for preparing $1\frac{1}{2}$ inch diameter triaxial samples on enlarged polished pedestals (2.25 inch diameter). After the samples had been prepared initially by 1-D consolidation they were mounted in standard Clockhouse triaxial cells which had been slightly modified. The triaxial apparatus was placed on a turntable thus enabling the specimen to be rotated through 90 degrees. Three types of end conditions were used. (i) The conventional rough end was of a 1.5 inch diameter porous stone ($\frac{3}{16}$ inch thick type UNI 150 KV) at the base (ii) Lubricated ends were provided by replacing this porous stone by a $\frac{3}{16}$ inch thick highly polished brass disc covered with a thin layer of silicone grease. Drainage was permitted through a $\frac{1}{4}$ inch diameter porosint (Grade B) stud recessed at the centre of this brass disc.

(iii) The enlarged end used is of the same type as that of Walker (1965) (see his pages 75-79). In all tests in the triaxial cells the top cap was of duralumin with a highly polished lower face covered with a thin layer of silicone grease. The volume change of the specimen was measured by a 10 c.c burette calibrated to 0.02 cc, connected directly to the triaxial cell base. The axial load was applied through a G shaped hanger.

2.3 The triaxial former and apparatus for 4 inch diameter sample

A new triaxial former was made for the 4 inch diameter specimen. This former was similar to that used by Thurairajah (as described in section 2.2) with modifications to suit the 4 inch diameter standard Clockhouse triaxial cell and for radiographic work. Fig.2.4 shows the various components of this 4 inch diameter former. The 4 inch triaxial cell in an assembled position is shown in Fig.2.5. It had been necessary to respace the reinforcement rods Q, which hold the outer perspex casing of the triaxial cell together, so that they were at the corners of a square. This enabled the specimen to be radiographed in two perpendicular directions.

2.4 The experimental set up for taking radiographs

2.4.1 The compression triaxial tests

Each test lasted for about 30 to 45 days and therefore it was necessary to carry out about three to four tests at the same time. All tests with radiographic work were carried out in an X-ray compound shielded with double-lined lead screens L as shown in Fig.2.5. With 1.5 inch diameter samples a focal film distance of four feet was found to be necessary for good definition of the images of the lead markers on the radiographs. Test beds six feet long were made (the top of one can be seen at the bottom of Fig.2.5, a better view is given in Fig.2.8). The 4 inch triaxial cell A in Fig.2.5 was mounted on a turntable B at one end of the test bed.

The $1\frac{1}{2}$ inch triaxial cells were each mounted on a special base plate with a highly polished upper surface covered with a thin layer of lubricant. The $1\frac{1}{2}$ inch triaxial cell could then be rotated about a vertical axis and could be clamped in two mutually perpendicular positions. The casette holder H was mounted on the same base plate at the back of the triaxial cell.

Two vertical columns of lead markers, each 0.080 inch diameter were fixed to both sides of the casette holder., The images of these markers were used as references to allocate the true axes of the triaxial system in the radiographs. During compression tests with 1.5 inch diameter samples the load was applied through a G shaped hanger. With the 4 inch diameter sample it was necessary to design a special hanger so as to be clear of the triaxial cell and its ancilliary equipment.during rotation. The triaxial cell pressure was supplied through a flexible pressure tubing connected to the base of the triaxial cell. The X-ray head X was mounted on a similar base plate at the other end of the same test bed. The positions of the two base plates could be varied along the length of the test bed. A new carriage system on which the X-ray head is mounted enables it to be shifted with ease from one test bed to another.

2.4.2 The extension triaxial tests

During extension triaxial tests (in which the triaxial cell pressure exceeded the axial stress) a metal frame F (in Fig.2.5) carrying two pulleys P1 and P2 was fixed to the top of the test bed. A proving ring was fixed to the upper end of the ram and this system of ram plus proving ring was counter balanced by a weight supported by the wire attached to the pulley system. The axial load was applied to the top of the ram through the proving ring by placing dead weights on the counter balance hanger. A modified ram (Loudon 1967) was used for the extension tests with 1.5 inch diameter samples. Fig.2.6 gives the details of this ram. The ram was hollow and contained three equally spaced vertical slots at its lower end. The ram R was lowered into the guide H of the top cap. A conical wedge W inside the lower end of the ram could be drawn upwards by tightening the screw S thereby causing the lower end of the ram to expand and grip the top cap. The screw S is supported by the plate T which is fixed to the proving ring. Leakage of the cell fluid through the ram was prevented by small Gaco "O" rings clamped round the shaft by tightening the nut N.

For the 4 inch triaxial cell a similar ram was made but it was fixed to the top cap by a different arrangement. A hard metal pin was driven horizontally through the ram at its lower end and could be made to lock itself in grooves machined in the sides of the guide H in the top cap.

2.4.3. The perspex jig and probe for placing lead markers

Fig.2.4 shows the perspex jig and the probe used for placing lead markers in the clay samples. The perspex jig can be slid into the top of the extension piece of the triaxial former so that it is located by the two pins projecting above this former. The lower surface of the jig is then nearly in contact with the upper surface of Kaolin. The holes in the jig are equally spaced on any of the three pairs of mutually perpendicular diameters with the spacing different for each pair. The probe has a small cavity at one end in which the lead markers sit while being forced down to their respective positions. This method of placing lead markers was found to be satisfactory even with the four inch diameter sample, in which some of the lead markers were located correctly at a depth of 17 inches below the jig. Fig.2.7 is a typical radiograph of a 4 inch diameter sample at the end of the isotropic consolidation. The images of the lead shot within the sample can be clearly seen, as can those of the reference markers down each side of the radiograph.

2.5 The triaxial sample preparation

Air-dried Kaolin* was mixed with 160 p.c. of distilled water in a commercial pugmill for about three hours under a vacuum of 20 inches of mercury. The highly polished brass disc with a thin layer of silicone grease, and containing the central porous stone was then placed on top of the pedestal and was just covered with distilled water. The conventional cylindrical rubber membrane was then attached to the base pedestal with Gaco "O" rings. The split mould (see Fig.2.3 or 2.4) was assembled around the membrane and the membrane was sucked to the inner surface of the mould with a vacuum of about 20 inches of mercury. A thin layer of silicone grease was applied to the inner surface of the membrane. Kaolin slurry was then carefully placed inside the membrane with a long handled spoon. Care was taken to prevent trapping any air bubbles. When the extension piece was nearly filled, the perspex jig was placed in position. The lead markers were then forced into position in a regular pattern. After placing all the markers, the perspex jig was removed, the upper surface of the Kaolin was levelled and a little distilled water was added. The piston was then inserted into the extension

* Liquid limit = 74, Plastic limit = 42, Plasticity Index = 32, Specific gravity = 2.61

piece. With the 1.5 inch diameter specimens the first load was the weight of the hanger itself (about 5 lbs.). Subsequent loads were applied in increments of 5 lbs at 12 hour intervals. Except where otherwise stated, all specimens were prepared under a maximum 1-D consolidation pressure of 22.6 psi. The last increment of load was normally applied for a day. The loads were proportionally increased for the four inch diameter specimens to give the same pressures.

At the end of one dimensional consolidation the outer ring that clamps the extension piece to the base (D in Fig.2.3) was removed. The sample was trimmed with a wire saw through the gap between the extension piece and the base. After removing the extension piece (E in Fig.2.3) the level of the upper surface of the sample was checked and distilled water was added to prevent the absorption of air. The top cap with a thin layer of silicone grease applied to its lower polished surface was placed in position and a cylindrical rubber membrane was sealed to it with three or four "hard" Gaco "O" rings (initially $1\frac{1}{16}$ inch internal diameter).

The sample former was then removed and the top portion of the triaxial cell was placed in position and clamped to the base. The cell was filled with the appropriate cell fluid from the upper end. The ram was inserted into the top cap guide and locked in position.

2.6 The sample preparation of specimens for the scanning electron microscope

The following is an abstract of the methods adopted and described in detail by Tovey (1969) for the preparation of specimens of the samples to be viewed in the scanning electron microscope. The following specimens were investigated in the scanning electron microscope: (i) at the end of 1-D consolidation. (ii) at the end of isotropic consolidation. (iii) after the failure of a sheared sample. The samples at the end of 1-D consolidation and of isotropic consolidation were dismantled quickly from the state corresponding to their maximum stresses and specimens about one cm. cube were cut from them while still wet. The 1-D consolidated specimens were then freeze-dried, while the isotropically consolidated specimens were air-dried. Ideally all specimens should have been dried by the same method but this system was adopted at Tovey's request. All samples after shear in the triaxial were oven-dried. All the dried specimens were then

fractured to obtain a clear fractured surface and the remaining sides were trimmed to give a fractured surface área of about $\frac{3}{16}$ inch x $\frac{3}{16}$ inch. Each small specimen was then mounted on the end of a small $\frac{1}{8}$ inch diameter brass tube. The sides of the specimen were coated with silver dag and the fractured surface was vacuum coated with a layer of carbon 50 to 100°A units thick and this was followed by a layer of gold about 200°A units thick.

2.7 The triaxial cell pressure

The cell pressures were obtained from constant head equipment described by Bishop and Henkel (1962). The cell pressures were measured on Bourdon gauges to an accuracy of 0.1 psi or 0.01 Kgm per sq.cm. Except in one test where water was used all the other tests were carried out with silicone oil (350 centi stoke) as cell fluid.

2.8 The equipment for non-destructive tests.

2.8.1 The X-ray set

The X-ray equipment used was a Meuller M.G.150 Industrial set. Detailed descriptions of the set are given in O'Loughlin (1964) and James (1965). Briefly, the X-ray set can be operated either with a fine focal spot of 1.5 mm or with a coarse focal spot of 4 mm. Since the completion of the author's experimental program provisions have been made to use a finer focal spot of 0.4 mm. The maximum range of tube voltage was from 50 kV to 150 kV. The maximum tube current was 20 milliamp with the coarse focal spot and 8 milliamp with the fine focal spot. O'Loughlin found that the intensity of radiation was uniform within a cone of semivertical angle of 22.5°. The input voltage was stabilised within 0.1 p.c. using a regulator in the range 190 to 260 volts.

2.8.2 The X-ray films

Kodak Industrex type D (fast and High contrast) films were used for almost all the work carried out with lead shot technique. Occasionally Crystallex films were used for better contrast but exposure times were much longer than for the Industrex D film. The film was placed between two lead screens (0.004 inch thick at the back and 0.006 inch thick in the front) inside a standard Kodak steel casette. The casette was placed in position by sliding it inside the casette holder as shown in

Fig.2.5. It is then firmly pressed against the front face of the casette holder by tightening the wing nuts on the back face.

2.8.3 The exposure of X-ray film

The exposure time was selected by trial and error to obtain an optimum film density of 1.0 as suggested by James (1964). The exposure time used for the 1-D consolidation tests on 1.5 inch diameter samples varied from 1.5 to 2 minutes at 70 kV with a tube current of 15 mA and the fine focal spot. A focal film distance of 50 inches was employed. Approximately identical exposure conditions were used for all triaxial work on 1.5 inch diameter samples. Two types of exposure conditions were employed with the four inch diameter samples depending on the focal film distance (f.f.d.). With f.f.d.'s of 50 and 120 inches, exposures of 4 mA for one minute and 6 mA for 8 minutes at 130 kV were used.

2.8.4 The processing of exposed films

The exposed films were developed in DX-80 developer for four minutes, according to the manufacturer's instructions. The films were agitated while being developed for about ten times at the end of each minute. The films were then fixed in acid fixative for 12 minutes. Afterwards they were washed in running water and dried. The developed films were kept in boxes and stored in a cool dark place.

2.8.5 The measurement of the positions of the images of the lead shot markers on the X-ray films

The radiographs taken in the earliest tests carried out by the author were measured in the Orthogonal displacement meter described by Roscoe, Arthur and James (1963). Since fifteen to twenty radiographs were taken in each test, a faster method of measuring the displacement of the coordinates of the images of the lead markers had to be obtained. Subsequent measurements were therefore carried out in the Cavendish Laboratory using a new machine (called CLARA) which is described in detail by Lord (1969). CLARA had the disadvantage of not being able to take films broader than 2 inches in width. This was a handicap because it was necessary to cut the radiographs to this dimension before measurements could be made with CLARA. Late in the author's test programme a new measuring machine designed and developed by James (1968) became available and was used for a

third series of measurements on the 4 inch diameter samples and a few on the 1.5 inch diameter samples. A detailed description of the apparatus is given in James (1968).

2.8.6 The Baldwin densitometer for the measurement of film density

Film densities were measured on a Baldwin densitometer. The apparatus will not be described in detail here since it was operated according to the manufacturer's manual. The instrument was capable of measuring film density to an accuracy of 0.01 in the range 0 - 3 and to an accuracy of 0.005 in the ranges 0 - 0.5, 1.0 - 1.5 and 2.0 - 2.5. A $\frac{3}{16}$ inch aperture was used and the density recorded was an average value over this area.

2.8.7 The Parallel plate Collimator

The parallel plate collimator described in Appendix 1 was first designed by Sirwan (1965) and consists essentially of a series of 4 x 2 x 0.036 inch steel plates. The spacing between the plates was adjusted so that they were in the same plane as the X-ray beams, thus producing images of the least possible thickness on the radiograph.

2.8.8 The Bucky grid and the Mechanism for its movement

The most efficient method of counteracting the effects of scattered radiation is by the use of a Potter-Bucky diaphragm or grid (Bucky, 1938). This diaphragm consists essentially of alternate thin strips of lead and of paper. The central strip is normal to the plane of the diaphragm and other strips are arranged so that when viewed from the focus of the grid they appear to be as thin as possible. All radiations other than the primary (and those which do not make too small an angle with the primary rays) are absorbed by the lead lamellae. The grid was moved during exposure to prevent the formation of the images of the lead strips on the radiograph. To achieve uniform film density it is essential for the grid to remain focussed during the motion. The mechanism for the movement of the grid is shown in Fig.2.8. The grid was mounted on a frame carrying a roller at its bottom end which moves on the surface of a constant velocity rotating cam. Further details showing the linear displacement of the grid with time while the cam is rotating is given in Appendix 1.

2.8.9 The Gamma ray apparatus and ancilliary equipment

Only a limited amount of experiments have been carried out with the Gamma ray apparatus for reasons stated in Chapter 3. A few additional experiments were carried out for the author by Donnelly (1966). The apparatus was designed and used by Coumoulos (1967) and will therefore only be described briefly here. Fig.2.9 shows the apparatus mounted on a test bed with a triaxial specimen of Kaolin. The apparatus consists of a main frame F which supports the radioactive source S and the detector D. The source and the detector are carefully aligned using a light source and both remain aligned during any subsequent movement. It is possible to move them either horizontally or vertically by means of the hand wheels S_1 and S_2. A low energy Americium source Am^{241} with a half life of 458 years and a peak energy of 60 keV was used. A scintillation counter with a thulium activated sodium iodide crystal was used as the detector. The advantages of using a low energy source and a scintillation counter are discussed in detail by Coumoulos (1967). A scalar directly connected to the counter amplifies the signal from the photomultiplier and records those photons that lie between selected energies.

2.9 The types of tests and their designations

2.9.1 The designation of the tests

All tests are classified into 5 groups according to the following designation:

Group 1: The bulk of the tests on $1\frac{1}{2}$ inch diameter samples are designated by alphabetical letter systems in the following sequence (i) A,B,C,.....Z; (ii) AB,AC,.....AZ; (iii) BA, BB,BC.....BZ; (iv) CA,CB,CC.....CZ; (v) DA,DB,.....DZ

Group 2: A few tests on $1\frac{1}{2}$ inch diameter samples were carried out in a special constant temperature room. These are designated by the letter T with a numeral suffix, namely T_1, T_2,.....T_{26}.

Group 3: Large 4 inch diameter triaxial tests are designated with alphabetical letters beginning with the letter O. E.g. OA, OB, OC.....etc.

Group 4: A series of tests with the Bucky grid are designated by the letters BG followed by a numeral. E.g. BG1, BG2,..... etc.

Group 5: A series of tests with Gamma ray measurements are designated by the letter G followed by a number.
E.g. G1, G2.....etc.

2.9.2. Types of tests

All tests were further classified by subdividing them according to the stress or strain paths imposed upon them as shown in Tables 2.1 to 2.22 inclusive. For ease of reference the headings of these tables are quoted (unless otherwise stated all tests are on $1\frac{1}{2}$ inch diameter samples).

Table Number	Type of test
2.1 (a-c)	The one dimensional consolidation and swelling tests.
2.2 (a-c)	The isotropic consolidation tests.
2.3	Drained and undrained compression tests on $1\frac{1}{2}$ inch diameter sample with different end conditions.
2.4 (a-b)	Shear tests on specimens prepared with different initial one dimensional consolidation stress.
2.5	Shear tests with different load increment sizes.
2.6	Tests on 4 inch diameter specimens.
2.7	Constant volume compression tests.
2.8	Constant p compression tests.
2.9	Drained tests with applied stress path $\frac{dq}{dp} = 3$.
2.10	Other drained tests with $dq > o$ $dp > o$ and $\infty \geq \frac{dq}{dp} > 0$.
2.11	Extension tests.
2.12	Anisotropic consolidation tests.
2.13	Tests with linear strain paths i.e. v/ϵ = constant.
2.14	Tests on overconsolidated specimens.
2.15	Tests with stress paths, where $dp < o$ $dq > o$ and below the undrained test path in a (p.q) space.
2.16	Tests with stress paths, where $dp < o$, $dq < o$ and $d(\frac{q}{p}) > o$.
2.17	Tests with stress paths where $dp < o$, $dq < o$ and $d(\frac{q}{p}) \leq o$.
2.18	Constant q tests.
2.19	Tests with stress paths where $dp > o$, $dq < o$, $\frac{dq}{dp} < (\bar{s})$; $\bar{s}$ denoting the slope of undrained stress path in the (p,q) space in a direction in which q is decreasing.

Table Number	Type of tests
2.20	Tests with stress paths where $dp > o$, $dq < o$ and $\frac{dq}{dp} > (\bar{s})$; $\bar{s}$ denoting the slope of undrained stress path in the (p,q) space in a direction in which q is decreasing.
2.21	Tests on specimens which have been initially sheared and subsequently subjected to stress paths where q and p increase.
2.22	Tests with stress paths (where $\frac{dq}{dp}$ = constant) originating from stress ratios higher than zero.

2.10 The computation of overall stresses and strains

2.10.1 The axial stress and the ram friction in triaxial tests

The axial load transmitted to the specimen was measured outside the triaxial cell and it was assumed that the frictional loss was negligible. A $\frac{1}{2}$ inch diameter ram was used with the 1.5 inch diameter specimens and a $\frac{3}{4}$ inch diameter ram with the 4 inch diameter specimens. As stated by Bishop and Henkel (1962), provided the ram and bushing are smooth and have adequate clearance between them, friction can only arise as a result of lateral forces which push the ram against the bushing. The following note has been taken from Bishop and Henkel "Theoretical studies on tests by Haussler indicate that in a well designed cell the friction should not exceed about 1.2 p.c. of the axial load provided oily lubricants are used. Warlam in a study of methods of loading used in triaxial tests concluded that the friction using a $\frac{3}{4}$ inch diameter ram would lie between 1 p.c. and 3 p.c. of the axial load for most of the load range." It was observed by the author that a load of $\frac{1}{4}$ lb was sufficient to move the ram in the bushing and often this was achieved by the self weight of the ram alone. Further, all the tests were carried out with silicone fluid as cell fluid, which acted as a lubricant and minimised the effect of friction.

However friction due to non-uniform deformation of the sample cannot be avoided. It will be seen later that the deformation of all specimens tested with frictionless ends was approximately uniform up to the peak stress ratio. Nevertheless it is desirable to develop techniques for the measurement of axial stress inside the cell, such as those proposed by Holubec (1966).

The alternative method of reducing the friction with the use of a rotating ram, or a rotating bushing suggested by Anderson and Simon (1960) and used by Mitchell (1967) needs further investigation to show that this rotation does not induce torsional stresses in the specimen. Bishop and Henkel (1962) stated that "a limited number of tests at Imperial College in which the load had been measured both with and without the rotation of the bushing or ram indicate that the errors normally lie between 1 p.c. and 3 p.c. when no rotation is used..... In some cases however additional accuracy is required and under these conditions, a rotating bushing appears to be the simplest satisfactory way of reducing friction. Rotation of the piston itself can transmit torsional stresses to the specimen which may alter the stress system sufficiently to nullify to a large extent, the increased accuracy in the measurement of axial load." With the high accuracy of the lead shot measurement in James' new measuring machine it is possible to detect the magnitude of torsional strains by a stereoscopic method using X-rays. For the interpretation of the results in this thesis, the author assumes that the effect of ram friction is negligible.

2.10.2 The cell pressure

As stated previously (section 2.7) the cell pressure was measured to an accuracy of 0.1 psi, or 0.01 Kgm per sq.cm.

2.10.3 The pore pressure measurement

Except for two tests where a Bishop type null indicator was used, for all other tests the pore pressure was measured with Bell and Howell "range flush mounted type" transducers. The outputs from these transducers were measured on a digital voltmeter. The transducers were capable of measuring pore pressures in the range 0-150 psi to an accuracy of 0.01 psi. All tests with pore pressure measurements were carried out in a constant temperature room ($25^{\circ}C \pm \frac{1}{2}^{\circ}C$). It is desirable for the flexibility of the pore water pressure measuring system to be as low as possible. By simple calculation of the flexibility of a transducer and the dead volume of the measuring system, Ting (1968) showed that the volumetric change of this system was $2 \times 10^{-7} in^3/psi$. This figure may be compared with $5 \times 10^{-6} in^3/psi$ for the Bishop null indicators. Ting also showed that the flexibility of the transducer system corresponds to an error of 19×10^{-6} in the volumetric strain of a $1\frac{1}{2}$ inch

diameter triaxial specimen. At present, the volumetric strains cannot be measured to a better accuracy than 0.001. Therefore it is apparent that the Bell and Howell transducers were quite satisfactory for the measurement of pore pressure.

2.10.4 The local measurement of pore pressures

The four inch diameter triaxial cell was originally designed to carry five miniature semi conductor transducers $\frac{1}{8}$ inch long and $\frac{1}{8}$ inch diameter for the local measurement of pore pressures. These transducers were buried in the specimen together with the lead markers. These transducers were originally used by Burland (1967) for the measurement of local pore pressures in a Model clay footing. Burland stated that these transducers were most desirable since they eliminated the long length of flexible pore-water lead and therefore had the minimum possible flexibility. It should be noted that the pore pressure probes used by Blight (1963) and McDermott (1965) had a length of flexible tubing, leading from the porous element to the pressure measuring device. The author carried out only one undrained test with the semi-conductor transducer probes used by Burland. It was observed that the range of pressure (0-20 psi) of these transducers was not sufficient for triaxial testing. Alternate transducers of the same shape are now under construction by Ward and Hambly at Cambridge. Further work on local pore pressure measurements will have to be deferred until these transducers become available.

2.10.5 The area correction for constant deviator stress

At high stress ratios the deformations are large for small increases in deviator stress. Therefore it was necessary to add small weights of the magnitude of 0.25 lb at intervals of time to maintain the deviator stress approximately constant, for a known increment of deformation.

For constant deviator stress

$$\frac{W + \Delta W}{Ao + \Delta A} = \frac{W}{Ao} \qquad 2.1$$

where $Ao = (\frac{Vo}{Ho})$ and

W is the deviator load at volume Vo and height Ho, while $W + \Delta W$ is the deviator load at volume $(Vo - \Delta V)$ and height $(Ho - \Delta H)$. The additional weight W was calculated from equation 2.1 for known values of W, Vo, Ho, ΔV and ΔH.

2.10.6 The membrane correction

A membrane correction was applied to the measured value of the deviator stress. The corresponding Δq for the measured deviator stress (as given by Bishop and Henkel 1962) is

$$\Delta q = \frac{\pi D M \epsilon_1}{a} \qquad 2.2$$

where D is the average diameter of the specimen, M is the compression modulus of the membrane, ϵ_1 is the axial strain and a is the corrected area of the sample.

2.10.7 The overall axial strain

The axial strain was computed from the initial height and the change in height of the specimen. The change in height was measured by a dial gauge to 10^{-4}inch or 10^{-3}mm accuracy.

2.10.8 The overall volumetric strain

The overall volumetric strain was computed from the initial volume and the change in volume of the specimen as recorded from the burette readings.

2.10.9 The effects of leakage

The leakage of cell fluid into the specimen and the leakage of water from the specimen and from the drainage connections caused errors in the measurements of pore water pressure in undrained tests and in the volumetric strains recorded in drained tests. The investigations carried out by Poulos (1964) and Walker (1965) indicated that leakage past the "O" rings could be reduced to negligible proportions provided tight "O" rings were used to seal the rubber sheath to the end caps and provided the end caps were highly polished with a thin layer of silicone grease at the sides. Further, the use of teflon sleeves for the Klinger cocks and soft copper washers for the joints proved to be satisfactory for the elimination of leakage at these joints. A detailed theoretical and experimental investigation was carried out by Ting (1968) into membrane leakage using different cell fluids. He concluded that "(a) the use of water as cell fluid causes diffusion of water from the cell into the specimen, (b) the use of castor oil as cell fluid causes reverse leakage of water from the specimen into the cell fluid, (c) with silicone oil as the cell fluid no leakage was detected. For the present purposes the performance of silicone oil as a cell fluid to

prevent membrane leakage is extremely satisfactory."

The author computed the volumetric strain from the displacements of the lead markers buried in the soil. The results are presented in Chapter 3 and they confirm the conclusions reached by Ting, that the use of silicone oil as cell fluid prevents membrane leakage.

2.11 The computation of local strains from the lead shot measurements

2.11.1 The method of computation of strains as given by Roscoe, Arthur and James (1963)

Roscoe, Arthur and James (1963) described a method of determining strains in the plane strain condition from the displacements of four neighbouring lead shot markers buried in the soil. Fig.2.10 gives the original positions and the displacements of the four markers 1,2,3 and 4 lying in one plane within a soil mass. The distances between these markers ~~being~~ are ℓ_x and ℓ_y. The displacement of the markers with respect to axes x and y as shown are (u_1, v_1), (u_2, v_2), (u_3, v_3) and (u_4, v_4). Assuming the displacements to be small compared to the diagonal lengths, the strains $\delta\epsilon_x$, $\delta\epsilon_y$ and $\delta\gamma_{xy}$ are given by

$$\delta\epsilon_x = (u_1 - u_3)/\ell_x \qquad 2.3$$

$$\delta\epsilon_y = (v_2 - v_4)/\ell_y \qquad 2.4$$

and $$\delta\gamma_{xy} = (v_1 - v_3)/\ell_x + (u_2 - u_4)/\ell_y \qquad 2.5$$

From Mohr's circle of strain, the magnitude and directions of the major and minor principal strains are given by

$$\begin{bmatrix}\delta\epsilon_1\\ \delta\epsilon_3\end{bmatrix} = \tfrac{1}{2}(\delta\epsilon_x + \delta\epsilon_y) \pm \tfrac{1}{2}\sqrt{\left[(\delta\epsilon_x - \delta\epsilon_y)^2 + (\delta\gamma_{xy})^2\right]} \qquad 2.6$$

and $$\alpha = \tfrac{1}{2}\tan^{-1}\left[\delta\gamma_{xy}/(\delta\epsilon_x - \delta\epsilon_y)\right] \qquad 2.7$$

where α defines the direction of ϵ_1 and is positive when measured clockwise from the x-axis.

2.11.2 Sirwan's method for the computation of strains from the displacements of lead markers buried in triaxial specimens of sand

Sirwan (1965) determined the strains in triaxial specimens of sand by arranging the lead markers at the vertices of regular tetrahedra as indicated in Fig.2.11. Sirwan computed the radial

strains in two perpendicular directions at any section B from the radial displacement of the markers in this plane. The axial strain along the centre line was computed from the axial displacement of the markers in planes such as A.

2.11.3 The author's methods of arrangement of lead shot markers in the triaxial specimens.

(i) The arrangement of lead markers for 1.5 inch diameter samples

The lead markers were arranged in two mutually perpendicular vertical planes containing the axis of the sample as shown in Fig.2.12 (a) and (b). During the computation of strains in plane 1, the markers were again separated into two sets called 1A and 1B as shown in Fig.2.13. Plane 1A contains all the rows that have 3 shot in a row while plane 1B contains all the rows containing only a pair of shot. This method was adopted to be able to compare the strains from one plane with those in the orthogonal plane. For example in studying the distribution of axial strain along the centre line and at the circumference, it is convenient to use plane 1A since all markers at the circumference and at the centre are in the same horizontal plane. Again when radial strains are compared at the same horizontal section, it is convenient to use plane 1B and plane 2. The average volumetric strain for the whole sample when computed from the lead shot measurements will be a truer value when the number of slices is increased to the maximum possible i.e. use is made of the displacements of all the shot.

(ii) The arrangement of markers in 4 inch diameter specimen

With the 4 inch diameter sample, lead markers were arranged in two perpendicular planes. At any one horizontal section the arrangement of markers was symmetrical across the two perpendicular diameters. In individual tests the number of columns in any one plane varied from 6 to 9 while the number of rows varied from 8 to 16.

2.11.4 The computation of coordinates of markers

Two vertical rows of reference markers were fixed to the casette holder. These markers lie outside the dimensions of the specimen. For computation purposes a pair of Cartesian axes was selected with its origin coinciding with one of the reference markers and one axis coinciding with one vertical row. These axes are fixed in space and were used as reference axes to

give the coordinates of any point within triaxial specimens. However during measurements in CLARA or in James' machine, each of these machines has a pair of separate coordinate axes fixed within themselves. Consequently the measurements were always carried out with respect to Cartesian axes of the respective machine. To obtain from these measurements the coordinates of any desired point with respect to the triaxial reference axes it was necessary to carry out the computations indicated below. The computations allow for the shift and rotation of the machine axes that are required to make them coincide with the triaxial reference axes, as indicated in Fig.2.14.

The respective transformation relations are (see Fig.2.15)

$$x = (x^1 - h)\cos\Theta - (y^1 - k)\sin\Theta$$
$$y = (y^1 - k)\cos\Theta + (x^1 - h)\sin\Theta \qquad 2.8$$
$$\tan\Theta = \left(\frac{\bar{x} - h}{\bar{y} - k}\right)$$

where x^1 and y^1 are the coordinates with respect to the machine axes; x and y are coordinates with respect to the triaxial reference axes. The point A is the origin of the triaxial reference axes and has coordinates (h,k) with reference to the machine axes prior to any shift or rotation. The second marker point B is another point defining the triaxial reference axes. This point B has coordinates $(\bar{x},\bar{y})$ with respect to the initial machine axes which were used for all the measurements.

2.11.5 The calculation of strains from the coordinates of markers and their displacements

(i) Method 1

In this method the axial and radial strains were computed directly from the axial displacements and the radial displacements of four markers lying in the same vertical plane. The axial strain ϵ_y and the radial strain ϵ_x are given by

$$\epsilon_x = \log\left[(x_1 - x_2)/\{(x_1 - x_2) + (c_1 - c_2)\}\right]$$
$$\epsilon_y = \log\left[(y_3 - y_4)/\{(y_3 - y_4) + (d_3 - d_4)\}\right] \qquad 2.9$$

where x_1, x_2 are the x coordinates of the markers in the same horizontal plane and c_1 and c_2 are the corresponding displacements in the x direction. y_1 and y_2 are the y coordinates of the markers in the same vertical line and d_1, d_2 are their corresponding displacements.

(ii) Method 2

In this method the strains were computed from the displacements of 3 markers, by assuming a linear homogenous function for the displacements in terms of the coordinates. Consider the three markers A, B and C with coordinates (x_1, y_1), (x_2, y_2) and (x_3, y_3). The corresponding displacements of these markers being (u_1, v_1), (u_2, v_2) and (u_3, v_3)

$$\text{then } u = ax + by + c \qquad 2.10$$

$$\text{and } v = dx + ey + f \qquad 2.11$$

where a, b, c.....f are constants

$$\delta \epsilon_x = \frac{\partial u}{\partial x} = a \qquad 2.12$$

$$\delta \epsilon_y = \frac{\partial v}{\partial y} = e \qquad 2.13$$

$$\text{and } \delta \epsilon_{xy} = \tfrac{1}{2}\left(\frac{\partial u}{\partial y} + \frac{\partial v}{\partial x}\right) = \tfrac{1}{2}(b+d) \qquad 2.14$$

Also the principal strain rates $\delta\epsilon_1$ and $\delta\epsilon_3$ are

$$\begin{bmatrix} \delta\epsilon_1 \\ \delta\epsilon_3 \end{bmatrix} = \tfrac{1}{2}(\delta\epsilon_x + \delta\epsilon_y) \pm \tfrac{1}{2}\sqrt{\left[(\delta\epsilon_x - \delta\epsilon_y)^2 + (2\delta\epsilon_{xy})^2\right]}$$

a, e, b and d are obtained from the equations

$$\begin{bmatrix} x_1 & y_1 & 1 \\ x_2 & y_2 & 1 \\ x_3 & y_3 & 1 \end{bmatrix} \begin{bmatrix} a \\ b \\ c \end{bmatrix} = \begin{bmatrix} u_1 \\ u_2 \\ u_3 \end{bmatrix} \qquad 2.16$$

$$\text{and } \begin{bmatrix} x_1 & y_1 & 1 \\ x_2 & y_2 & 1 \\ x_3 & y_3 & 1 \end{bmatrix} \begin{bmatrix} d \\ e \\ f \end{bmatrix} = \begin{bmatrix} v_1 \\ v_2 \\ v_3 \end{bmatrix} \qquad 2.17$$

The computation of the coordinates, displacements and the strains was carried out using the Titan Computer.

2.11.6 Selection of triangular elements for strain measurements

Fig.2.13 illustrates the method of selection of triangles. For plane 1A each rectangular element bounded by the six markers A, B, C, D, E and F were split into 4 triangles. The strains were computed for each triangle and this procedure was repeated for the rest of the rectangular elements. For planes 1B and 2, each rectangular element was broken into 2 triangles.

2.12 Errors and improvements

The accuracy of the measurement of strains from the lead shot technique in triaxial specimen is dependent on several factors.

(i) The precise repositioning of the casette and the X-ray tube between successive radiographs.

(ii) The change in size and the distortion of the film due to such causes as humidity and temperature changes.

(iii) The accuracy of the measurement of the positions of the markers in the film.

(iv) The deviation of the arrangement of the markers from the assumed planes.

With the use of fixed base plates for the X-ray head and for the casette holders errors due to the repositioning of the casette and the X-ray tube were reduced to a very small order.

The number of markers used in the triaxial specimens were about 30 for the 1.5 inch diameter sample and about (100-150) for the 4 inch diameter sample. Hence the time taken for the measurement of each radiograph was about 10 minutes for the 1.5 inch diameter sample and was about 30 minutes for the 4 inch diameter sample. During measurement the radiographs were covered by a thick sheet of perspex to reduce the expansion of the films (due to the heat from the projector of the measuring machine) to a very small order. The time taken for the measurement of each shot was of the order of 15 to 20 seconds.

Although every effort was made to arrange the markers in one plane it was not possible to guarantee that all the shot were exactly in the plane in which they were assumed to be during the initial arrangement and deformation. The markers were probed into the samples when the clay was in the form of a slurry at 160 p.c. moisture content. To check the possibility of the deviations of the markers from the assumed plane, radiographs were taken in mutually perpendicular directions.

With the four inch diameter specimen, the contrast on the radiographs of the images of the markers close to the ends of the specimen was considerably reduced by the effect of scattered radiation from the end plattens. The use of a Bucky grid was found to eliminate the effects of scattered radiation and improve the quality of the contrast and definition of lead markers in thick specimens (7 inch) of sand. A similar method could be adopted for the clay specimens. However with the automatic

measuring device designed by James the contrast and definition of the marker are not critical. Due to the lack of time the author has not done any measurements with the automatic device.

CHAPTER 3

THE USE OF DESTRUCTIVE AND OF NON-DESTRUCTIVE TECHNIQUES FOR THE STUDY OF THE DEFORMATION CHARACTERISTICS OF KAOLIN.

3.1 General Introduction

Non-destructive techniques using X and Gamma rays have been developed in Cambridge for the determination of internal strains and voids ratio in deforming soil masses. These methods are mainly used to (i) check the uniformity of deformation of soil specimens in various types of soil test equipment such as the conventional triaxial apparatus (described by Bishop and Henkel (1962), Rowe and Barden (1964)), the simple shear apparatus (described by Roscoe (1953)), etc.; and (ii) determine the patterns of internal strains and changes of voids ratio in deforming soil masses in boundary value problems, e.g. wall and footing problems in sand (James (1965)) and clay (Burland (1967)). X-ray techniques were first developed by Roscoe, Arthur and James (1963) for determining such patterns under plane strain conditions from the measurements of the displacements of lead shot markers embedded in sand. X-ray absorption techniques for the measurement of local voids ratios in laboratory specimens were initiated by O'Loughlin (1964) and further developed by Sirwan (1965). The limitations of the latter method for saturated triaxial clay specimens will be discussed in section 3.7. Attempts have been made during the past decade to use Gamma rays to determine the density of soil both in the field and in the laboratory. Two techniques have been used: (i) the back-scattering method and (ii) the direct absorption method. Schematic diagrams of both methods are shown in Fig.3.1. In the back-scattering technique the Gamma rays emitted from the radioactive source are scattered by the soil and during this process the energy of the photons is usually decreased. Some of the scattered photons return to the detector and are counted. The back-scattering method was used by Skopek (1957) for surface measurements and by Cameron and Bourne (1958) for subsurface measurements. In the direct absorption method, the transmitted radiation consisting of unscattered (primary) and some scattered photons is measured. Bernhard and Chasek (1955) obtained empirical expressions for the intensity of primary and scattered radiation in terms of the wet density and the source-detector distance. In both the back-scatter and direct absorption methods, the determination of voids ratio invariably depends on some form of calibration

curve relating the transmitted counting rates to the densities of a number of specially prepared soil samples each of which is assumed to be uniform. While these techniques may provide valuable (but approximate) information in field problems the accurate determination of voids ratio in laboratory specimens used for research purposes required intensive experimental and theoretical investigation. A detailed study of the use of Gamma rays for this latter purpose was carried out by Coumoulos (1967). This method will be further discussed in section 3.7. In this chapter, however, the author's main study of the deformation of cylindrical specimens of Kaolin was achieved by employment of the lead shot technique.

3.2 The assumptions made in the measurement of strains with the lead shot technique

The general assumptions made in the derivation of strains from the measurements of displacements of lead shot markers are: (i) the mass of soil within the smallest grid, deforms uniformly (ii) there is no relative movement between the lead markers and the surrounding soil. The experimental assumptions in support of these assumptions have already been presented for sand by Roscoe, Arthur and James (1963). The validity of these assumptions for clay will be considered in sections 3.3.5 and 3.5.3(e).

3.3 The one dimensional consolidation tests with the lead shot technique for the measurement of local strains.

3.3.1 Introduction

The structure of clay particles is assumed to have no preferred orientation after remoulding. However such orientation may develop during subsequent consolidation. Hvorslev (1960) suggested that during the uniaxial consolidation of a remoulded clay ~~that~~ the particles developed a preferred orientation in a direction perpendicular to that of the major principal stress. Thompson (1962) suggested that this preferred orientation did not develop to the same extent simultaneously throughout any such sample, but he did not measure local strains within his samples. Sirwan (1965) using the lead shot technique to measure local strains in consolidometer samples observed that the consolidation during the first application of load was larger in layers close to the free draining surfaces than for the other layers in the samples. For subsequent load increments he observed that the consolidation was larger in layers which were

remote from the free draining surfaces than for those that were close. It must be emphasised that the mechanism of one dimensional consolidation is further complicated by the effects of side friction. Side friction measurements in consolidometers have been carried out by Leonards and Girault (1961), Thompson (1962) and Burland (1967) among others. These measurements indicate that the magnitude of side wall friction can be reduced to a very small order by lubricating the walls with silicone grease. The author's one dimensional consolidation experimental results using the lead shot technique will be presented in this section. In addition to the strains the magnitude of side friction was measured by making use of the load cell (described in section 2.1.2) at the base of the sample. The apparatus used and the method of sample preparation have already been described in sections 2.1 to 2.5.

3.3.2 The results of the side friction tests

Figs.3.2 (a-c) indicate the percentage load lost in friction of the specimen, during one dimensional consolidation in the perspex and the duralumin consolidometers and in the triaxial former with the rubber lining. A layer of silicone grease (about 0.01 inch thick) was smeared over the inside surfaces of these consolidometers prior to introducing clay. The dashed lines in Fig.3.2 refer to the percentage load lost in friction immediately after applying a load increment. The full lines refer to conditions two days after applying an increment. It is evident that the side friction was a minimum in the triaxial former which was lined with a rubber membrane.

3.3.3 The equilibrium voids ratio (e) vs log (stress (σ_1')) plot for one dimensional consolidation

In Figs.3.3(a-c), the full lines give the observed relationship between the equilibrium overall voids ratio (as measured from the final moisture content and the measured heights of the sample and the logarithm of the axial stress as calculated from the piston load. The dashed curves show the same relationship but now the stress is as recorded by the load cell at the base of the sample. The full lines have a slope $\lambda = 0.31$, while for the dashed lines $\lambda = 0.29$. For both types of swelling curve, their slopes k were approximately identical and equal to 0.045. The value of $\lambda = 0.29$ may be compared to that of 0.25 - 0.26 obtained during isotropic consolidation in conventional triaxial specimens (see section 3.4.5).

3.3.4 The variation of consolidation with depth during 1-D consolidation

(i) Consolidation during the first increment of stress

Fig.3.4 illustrates the vertical displacement Δy of lead shot markers with respect to their vertical coordinate y as measured from the impermeable boundary of the sample. The three different symbols in this diagram refer to three different vertical columns or markers within the sample. It is evident that the sample was deforming uniformly, since the displacements of all markers were linearly proportional to their initial vertical coordinates, for this first stress increment of 3 psi. During this increment of stress the clay, in the form of a slurry at 157 per cent moisture content, was consolidated from a height of 8.5 inches to about 5.7 inches; (The corresponding dimensions in the radiograph become scaled up by a factor of 1.09.); The corresponding cumulative vertical strain being approximately 33 per cent. In Fig.3.4 the topmost layer of lead shot markers is about 0.7 inches below the free draining surface. Since no markers were arranged along this surface, the consolidation in the element of clay closest to it (which is about 0.7 inch thick) can not be included in Fig.3.4. Similar lead shot measurements carried out by Sirwan (1965) during one dimensional consolidation of a slurry with an initial stress increment of only 0.26 psi, indicated that the consolidation in layers closest to the free draining surface is higher than the rest of the sample for this first increment of stress. The author has not sufficient experimental results to confirm Sirwan's observations.

(ii) The consolidation during subsequent increment of stress

The subsequent stress increments were applied with a stress increment ratio of one, up to a maximum stress of 102 psi. Figs. 3.5 to 3.8 show the variation of consolidation in mm/cm with the major principal effective stress (at the end of each stress increment) for four horizontal elements A, D, E and H at depths close to the free draining surface (element A), the mid-height of specimen (elements D & E), and the impermeable boundary (element H). It is observed in Figs.3.5 to 3.7 that the consolidation of any horizontal element was uniform over its three vertical columns up to the maximum consolidation stress of 100 psi. Also in Fig.3.8, the element A which was closest to the free draining surface had the least consolidation. The greatest

consolidation was observed on the element H which was closest to the impermeable boundary. Elements D and E which were approximately at mid section had roughly the average value of the consolidation of elements A and H. A similar phenomenon was observed by Sirwan (1965) during increments subsequent to the first.

3.3.5 The comparison of the average overall voids ratio from boundary measurements with the overall average of the local values computed from the lead shot measurement

The overall average voids ratio at the end of each increment of stress was computed from the final moisture content, diameter and change in height of the sample. Using the overall average voids ratio thus computed at the end of the first increment of stress subsequent local voids ratio were calculated from the displacements of the lead markers. When doing this the specimen was divided into eight horizontal sections A to H and the voids ratio of each element was calculated from its axial strain using the expression

$$e = e_o - \frac{\epsilon_1}{100}(1 + e_o) \qquad 3.1$$

where e was the voids ratio at a cumulative strain of ϵ_1 percent and e_o was the initial voids ratio prior to the application of any load. The average voids ratio over the whole specimen was then also computed from these local voids ratios. Fig.3.9 illustrates the variation of voids ratio from boundary measurements with respect to those computed from the average of the local voids ratio, for the range of stress 0-100 psi. The excellent agreement between the two values indicates the power of the lead shot technique for the measurement of strains and voids ratio in clay specimens.

3.3.6 The variation of voids ratio with respect to time during a stress increment

The axial strain within each element A-H at specific intervals of time after the application of a stress increment was computed from the displacement of the lead markers. The corresponding local voids ratio was determined from equation 3.1. Using the Modified theory of consolidation of Davis and Raymond (1965), the local voids ratio change with time at different depths in the specimen was calculated by the numerical method reported by Richart (1957) from his equation (43). The

experimental observations and the theoretical predictions are compared in Figs.3.10 and 3.11. The local voids ratio computed from the displacements of the lead markers are in good agreement with the theoretical predictions for the top half of the sample. However for elements far from the free draining surface ($\frac{Z}{H} > 0.6$, see Fig.3.10) the experimental observations deviate from the theoretical predictions. These deviations may in part be due to the effects of secondary consolidation occuring simultaneously with the primary consolidation. Such a model incorporating primary and secondary consolidation is described by Brinch Hansen (1961).

3.3.7 Pore pressure isochrones as determined from the local voids ratio

The local effective stresses were calculated from the local voids ratio, using the logarithmic relationship between the voids ratio and the major principal effective stress shown in Fig.3.3(a). The local pore pressures in the elements were then determined from the applied total stress and the calculated local effective stress. Figs.3.12 (a-b) illustrate the pore pressure isochrones determined in this way with the curves drawn through the mean of the experimental points. These isochrones are similar in form to those observed by actual local pore pressure measurements by Burland (1967) during one dimensional consolidation in a large consolidometer.

3.4 Isotropic consolidation and swelling using the lead shot technique for strain measurement

3.4.1 General

In the investigation discussed in this section, specimens of Kaolin initially prepared by one dimensional consolidation were subsequently further consolidated in the triaxial apparatus under isotropic stress conditions. The patterns of the axial and radial strain distributions during this isotropic consolidation are studied in detail for both the 1.5 inch diameter and the 4 inch diameter triaxial samples.

3.4.2 The effect of end restraint on the local strains during isotropic consolidation of $1\frac{1}{2}$ inch diameter x 3 inch high samples

Figs.3.13 (a-d) show the distribution, along the axis of a 1.5 diameter sample, of the local (a) axial, (b) radial, (c)

volumetric and (d) shear, strains respectively that occur during the application of three successive increments of isotropic stress; the sample was contained between conventional friction type ends (see section 2.2). In Figs.3.13 (a) and (b) it was observed for each increment of stress that (i) the axial strain was lowest at the top of the specimen and increased towards the bottom and (ii) the radial strain was a maximum at the top and a minimum at the base. These distributions of strains are as to be expected if significant friction is present on the ends of the sample. A large porous stone (type UNI 150 kv) of 1.5 inch diameter was used at the base of the specimen. The effect of friction due to the porous rough surface was to reduce the lateral movement of the sample at the base and thereby decrease the radial strain. Fig.3.13(c) shows that the volumetric strain was virtually uniform throughout the sample. This indicates that consolidation due to the isotropic stress increment is also uniform throughout the sample despite the observed non uniformities of axial and radial strain. From Fig.3.13(d) it can be seen that the shear strain varies from -2 to +3 per cent within the specimen. This may be due to the development of local anisotropy within the sample and will be discussed further in section 3.4.5. As can be seen in Figs.3.13 (a-d) most of the non uniformity in the distribution of strain occurs during consolidation under the first increment of isotropic stress. Figs.3.14 (a-d) and 3.15 (a-d) each refer to a similar series of tests to those discussed for Figs.3.13 (a-d) but instead of frictional conventional ends the samples had lubricated conventional ends and lubricated enlarged ends respectively. The strains throughout the samples with these lubricated ends was far more uniform than for those with frictional ends.

3.4.3 The distributions of vertical and horizontal displacements of lead markers during isotropic consolidation in a 4 inch diameter x 4 inch high sample

From section 3.3.2 it was concluded that the lubricated end condition produces more uniform strains during isotropic consolidation than the rough end condition. A detailed investigation of the radial and axial displacements of the lead markers in two perpendicular vertical planes passing through the axis of the specimen was then carried out in a 4 inch diameter triaxial sample. The objective was twofold in that (i) the radial strain

distribution cannot be studied in detail with the 1.5 inch diameter sample and (ii) any effect of the increase in length of drainage paths due to the small porous stones which were used with the lubricated ends should show up markedly in a larger sample. The markers were arranged in the two perpendicular planes as illustrated in Figs.3.16(a) and (b). The vertical displacement patterns with respect to height within the sample and the horizontal displacement patterns at different radii within the sample, for the lead markers in both planes are shown in Figs.3.17(a-d). The remarkably linear variations of the displacement patterns indicate that both the axial and radial strains are uniform in both perpendicular planes and therefore the assumption that $\epsilon_2 = \epsilon_3$, in the calculation of strains in triaxial specimens is justified.

3.4.4 The effect of anisotropy on the axial and radial strains during consolidation under isotropic stress

It has already been stated that all the specimens were initially prepared under a one dimensional consolidation conditions. Hence all specimens were subjected to an initial shearing process. The subsequent application of increasing isotropic stress gradually erases the effect of the initial one dimensional consolidation. This is best illustrated in Figs.3.14(d) and 3.15(d) where it is observed that during the application of the first increment of isotropic stress, a shear strain with a maximum value of approximately -1 per cent is observed. Subsequent increments of isotropic stresses do not produce any further increase in the shear strain, indicating that the strains due to these increments of stress are isotropic. The data suggests that specimens isotropically consolidated to approximately three times the initial one dimensional stress can be assumed to have lost their previous shear stress history effects. A similar observation was also noted by Loudon (1967) using a different technique for the strain measurements.

3.4.5 The slopes of the isotropic consolidation lines in the e-logp plot for overall voids ratio as determined from the average local voids ratio

The average volumetric strain in the sample during an increment of isotropic stress was determined from the local measurements of strains. The average overall voids ratio at the end of each increment was obtained from the final overall

average voids ratio of the sample(obtained from the final moisture content determination) and the average volumetric strains computed from the lead shot measurements. Figs.3.18(a-c) illustrate the variation of these voids ratio with log p for tests carried out with the three types of end conditions. These relationships are linear in the (e-logp) plot with λ varying in the range 0.25 to 0.26.

3.4.6 The distributions of vertical and horizontal displacements of the lead markers during isotropic swelling

Figs.3.19(a-b) and 3.20(a-b) illustrate the vertical and horizontal displacements of the lead markers in two orthogonal planes in the sample during isotropic swelling. (These planes were as shown in Figs.3.16(a) and (b).) The displacements are seen to be linear in the two directions in both planes. However the slopes of the lines corresponding to the horizontal displacements at the bottom end of the sample are considerably less than for the other lines. This indicates that the radial strains at the bottom end of the sample were lower than in the rest of the sample. This reduction in strain was in part due to errors in measurement as the markers were placed extremely close to the cell pedestal and the scattered radiation from this pedestal tended to blurr the images of the markers in the radiograph, thereby reducing the contrast and definition of these images.

3.4.7 The effect of anisotropy during swelling under isotropic stress.

The average axial and radial strains as determined from the mean slopes of the lines in Figs.3.19(a) and (b) and 3.20(a) and (b) during swelling under isotropic stress are -2.66 and -1.34 per cent respectively. These results indicate that the strains were anisotropic during swelling under isotropic stress conditions. A similar phenomenon was also observed by Burland (1967) (see his Fig.2.3.1) during isotropic swelling using a different technique for the measurement of strains.

3.5 The displacement patterns and strain distributions in cylindrical specimens during shear

3.5.1 General

The nonuniform deformation of soil specimens during shear has been considered by most research workers to be the largest

source of error in the experimental study of the stress-strain relationships of soils. Theoretical investigations of the distributions of stresses and strains in cylindrical specimens under compression and in extensions have been carried out by Filon (1902), Pickett (1944), D'Appolonia and Newmark (1951), Balla (1960) and other research workers. The theoretical methods developed by all these workers are only applicable for elastic media. The deformation of clay specimens are mainly plastic and hence these methods have only limited application in soil mechanics problems. Besides the theoretical studies carried out by the above authors, experimental evidence confirming the nonuniformity of deformation in triaxial specimens were cited by a number of authors; notably, Geuze and Tan (1950), Rowe and Barden (1964) who worked with saturated clay samples and Shockley and Ahlvin (1960) who worked with sand samples. The method adopted by these workers and others was to determine the moisture content of portions of clay and frozen sand cut from the test specimens. This procedure takes time and the moisture content can only be determined at the end of the test. In contrast to this procedure, Roscoe, Schofield and Thurairajah (1963b) described a method of measuring the local variation of strains throughout a triaxial sample both in compression and in extension. The same method was used by Sirwan (1965) to study the local variation of voids ratio as well as of the strains. In this method a number of horizontal lines had been painted on the membrane of the triaxial sample. The height and diameter of each element was measured by means of a theodolite and the corresponding axial and radial strains were determined. While this method was far from precise, it gave an overall idea of the local strains and voids ratio in the triaxial specimens. Accurate measurements of the strains were limited by the assumptions, namely (i) each element deformed uniformly within itself (ii) the reference lines defining the boundaries of the element was circular in horizontal planes throughout the testing, (iii) no soil passed from one element to another, during the deformation of the soil and (iv) the volume of an element was determined by assuming that it was a truncated cone. In addition to the above method, Sirwan (1965) also studied the local variations of strains and voids ratio of triaxial specimens using (i) the lead shot technique and (ii) the X-ray absorption method with film density measurements.

Most of the experimental work mentioned above was carried

out on sand samples. Very little progress has been made in the study of local strains in clay specimens. In the present section the author carried out a detailed investigation, predominantly using the X-ray lead shot technique, of the distributions of strains in normally and over consolidated clay specimens both in compression and in extension. This type of study can not only give a better understanding of the behaviour of clay under all combinations of applied stresses but also helps to establish practical limits for the reliability of conventional triaxial test results.

3.5.2 The effect of end restraint on the strains of 1.5 inch diameter triaxial samples during shear in compression tests

(i) General

The three types of end conditions used in the triaxial specimens during shear were described in section 2.2. The local strain distributions were determined both during a fully drained shear test and during an undrained shear test. The procedure of testing adopted in any particular type of test was the same for tests on specimens with all the three types of end conditions. The details of the tests are summarised in Table 2.3. The observations were only used to evaluate the effects of end restraint on the distribution of the strains and to select the best type of end condition for conventional tests. The results are also useful in evaluating the large bulk of test data already available with the conventional friction end tests on triaxial specimens of Kaolin.

(ii) The fully drained test results

Figs.3.21(a) and (b) illustrate the axial and radial strain distributions in a fully drained test on a specimen contained between conventional frictional type ends. In these figures each line corresponds to the equilibrium strain distribution in the specimen at the end of each stress increment. The results indicate that both the axial and radial strains are smallest at the two ends of the specimen. Also, for each increment of stress, the maximum strain was observed approximately at one third of the height from the base. The axial strain distribution up to an average value of 4 per cent was reasonably uniform; these strains correspond to a stress ratio of 0.4.

The radial strains were everywhere small in this range of stress ratio. Beyond a stress ratio of 0.4 the axial and radial strains became nonuniform. This development of nonuniformity caused a localised region near the base to bulge. Figs.3.22(a) and (b) refer to a similar test to that discussed for Figs.3.21(a) and (b), but instead of conventional frictional ends the sample had the conventional lubricated ends. There is a marked improvement in the uniformity of the distributions of the axial and the radial strains in the sample with the lubricated end condition. The strains were reasonably uniform up to 9 per cent overall axial strain. This strain corresponded to a stress ratio of 0.59 which was approximately $\frac{4}{5}$ th the peak stress ratio. Moreover even at the peak stress ratio, the distribution of strains in the sample with the lubricated ends was far more uniform than the sample contained between the frictional ends. Figs.3.23(a) and (b) illustrate the corresponding distribution of strains during a fully drained test in a specimen contained between the enlarged lubricated ends. With this end condition the strains were again reasonably uniform up to 12 per cent overall axial strain which corresponded to a stress ratio of 0.55. Beyond this level of stress, the strains in the specimen contained between the enlarged lubricated ends were less uniform than those in the specimen between the conventional lubricated ends. In this particular test with the enlarged ends, the author used a lubricated rubber membrane in between the specimen and the enlarged end plattens. These rubber discs had a tendency to expand more than the ends of the soil specimen, thereby imposing a lateral thrust on the sample. For the subsequent experiments discussed in this dissertation, the author did not use any rubber discs in between the specimen and the lubricated end plattens.

(iii) The results of undrained tests

Figs.3.24(a) and (b) show the distributions of axial and radial strains in a specimen of Kaolin contained between conventional frictional ends and subjected to an undrained test. The behaviour of the specimen was similar to that observed during the drained test with the same end condition (see Figs.3.21(a) and (b)). The local axial and radial strains were larger in a region approximately at one third the height from the base, than within the rest of the sample. Figs.3.25(a) and (b) illustrate the distribution of strains in a sample contained between the

enlarged lubricated ends, during an undrained test. The strains were far more uniform in this specimen than the corresponding specimen contained within the frictional ends.

The internal strain patterns discussed above illustrate that with the use of the lubricated ends the strains within triaxial specimens are substantially uniform up to about $\frac{4}{5}$ th of the peak stresses. Beyond this value of the stresses, the deformation is large for small increments of stress and the strains begin to develop nonuniformity. In the above analysis all the radiographs were measured on the Orthogonal displacement meter where the accuracy of the measurements was limited (section 2.12). The accuracy of the measurement is improved about three-fold on CLARA and on James' measuring machine. A detailed investigation of the internal strains and displacements in normally and overconsolidated clay specimens will be discussed in the next section. In these tests the radiographs were measured either on CLARA or on James' machine.

3.5.3 Compression tests on 1.5 inch diameter x 3 inch high specimens of normally consolidated Kaolin with different applied stress paths.

(a) General

In the present section a detailed study of the displacement patterns and strain distributions inside a 1.5 inch diameter normally consolidated specimen of Kaolin is carried out when the sample was sheared under two different applied stress paths of slope $\frac{dq}{dp}$ of 3 and 1.5 respectively.

The strains were computed employing (i) Sirwan's method and (ii) the author's method (see section 2.11). The arrangement of lead markers are given in Figs.2.12 and 2.13.

(b) The displacement patterns and strain patterns in specimens AB ($\frac{dq}{dp}$= 3) and AX ($\frac{dq}{dp}$ = 1.5).

Figs.3.26(a), (b) and (c) illustrate the incremental vertical displacements of 3 columns of markers in one axial plane within the sample AB (normally consolidated to 60 psi and then sheared with applied stress path of slope 3) with respect to the height of the sample, for stress increments applied at stress ratios of 0.28, 0.43 and 0.62 respectively. In these figures the vertical displacements of the markers were found to vary linearly with the height of the markers above the base, indicating that the axial

strain was uniform throughout the sample for all three increments.

The data presented in Figs.3.27(a),(b) and (c) includes that given in Fig.3.26 for one plane of the sample and also shows the corresponding strains as recorded from radiographs taken on the mutually perpendicular vertical plane. Both displacement patterns are almost identical indicating that the axial strains in both planes were the same. Figs.3.28(a-c) and 3.29(a-c) illustrate a similar phenomenon for the sample AX which was normally consolidated to 60 psi and then sheared with an applied stress path of slope 1.5

(c) <u>The comparison of the strains computed from (i) Sirwan's method and (ii) the Author's method for three increments of stresses in the sample AB.</u>

In Sirwan's method of computation of strains it was assumed that the principal axes of strain coincide with the vertical and the horizontal axes of the specimen. Hence he calculated $\Delta\epsilon_y$ and $\Delta\epsilon_x$ which he assumed were the local axial and radial strains respectively. This assumption would only be true if the torsional strain $d\gamma_{xy}$ in any element of the soil was zero. In the Author's method of computation of strains, using triangular elements (described in section 2.11.5 as method 2), it was possible to calculate the magnitudes and directions of the incremental principal strains ($\Delta\epsilon_1$ and $\Delta\epsilon_2$) corresponding to each increment of stress. Fig.3.30 shows the lead shot markers that were used in calculating the local strains by both methods. (They correspond to the markers in Plane 2 as shown in Fig.2.12(b).) In Sirwan's method the local vertical axial strain was calculated directly from the relative displacements of two neighbouring markers, one being directly above the other. Similarly radial strains were obtained from two neighbouring shot which were assumed to be in the same horizontal plane. With the Author's method the triangles used are numbered (i)-(x) as shown in Fig.3.30. In Fig.3.31(a) the local axial incremental strains obtained from Sirwan's method ($\Delta\epsilon_y$) and from the Author's method ($\Delta\epsilon_1$) are compared in the left hand diagram for all the odd numbered triangles and in the right hand diagram for all the even numbered triangles in Fig.3.30. These local incremental strains were all for an increment of stress ratio $\Delta\eta = 0.08$ from a stress ratio at the start of the increment of $\eta = 0.28$. The corresponding comparison for local radial strains ($\Delta\epsilon_x$ for Sirwan and $\Delta\epsilon_2$ for the Author) is given in Fig.3.31(b) for the

same increment of stress ratio. Similar comparisons, to those shown in Fig.3.31, are given for a later stage in test AB in Fig.3.32 for η = 0.44 and $\Delta\eta$ = 0.07, while Fig.3.33 refers to η = 0.62 and $\Delta\eta$ = 0.06 in the same test.

In Figs.3.31, 3.32 and 3.33, the lines are equally inclined to the abscissa and ordinate axes of each diagram. If the experimental points all lie on these lines then it follows that the local principal axes of strain are vertical and horizontal throughout the sample. This can be seen to be the case in Figs.3.31 and 3.32 but there are very slight deviations at the high stress ratio as shown in Fig.3.33. If the sample had strained uniformly throughout, then all the points on each diagram would have been superposed. It can be seen that this does not appear to be the case for any of the increments. The detailed distribution of the local axial strain, at the three stages of test AB discussed above, are shown in Fig.3.34 while Fig.3.35 gives the corresponding data for the radial strains. From these two figures it is evident that the strains are moderately uniform throughout the first two increments of stress ratio but not for the third. This would appear to contradict the conclusion in section 3.5.3(b) from Fig.3.27(c) that the vertical displacement of any shot was approximately linearly related to its height above the base. This matter will be discussed later in the light of the data from tests on 4 inch diameter samples.

(d) Comparison of the overall strains from the average of local measurements and from the boundary measurements.

In this section the results of three tests, AX, AB and AQ are presented. They correspond to tests started from an initial isotropic stress of 60 psi and sheared along stress paths of slope 1.5, 3 and ∞ respectively. The overall axial and radial strains were obtained from the average of local measurements in both plane 1 and plane 2 (see Fig.2.12) for each increment of stress ratio in these tests. From these strains the overall volumetric strain was computed at each stage of the test. The overall axial and volumetric strains were also computed from the measured changes in height and volume of the sample. The measurements will be referred to as the boundary measurements.

In Figs.3.36(a-b) to 3.38(a-b) the lines are equally inclined to the coordinate axes of the diagrams. Since the experimental points all lie on these lines it is evident that the strains

computed from the boundary measurements are in agreement with the overall strains obtained by averaging the local measurements. The points in each figure correspond to the strains at the end of each increment in a continuous test. The excellent agreement between the overall volumetric strains as obtained from burette readings and as calculated from the lead shot displacements indicates that there was no leakage through the membrane: the cell fluid was silicone oil.

3.5.4 The displacement and strain patterns in a 4 inch diameter sample of normally consolidated Kaolin during a fully drained test (OB) at a constant cell pressure of 30 psi.

The lead shot markers were arranged within the sample in two mutually perpendicular vertical planes 1 and 2 as illustrated in Fig.3.16(a) and (b). In this case however plane 1 contained 6 columns (1-6) and 10 rows (A-J) of lead shot and in plane 2 there were 6 columns (1-6) and 8 rows (A-H).

Figs.3.39(a) illustrates the vertical displacements of the markers in plane 1 plotted against the height of the markers above the base, caused by an increment of stress ratio $\Delta\eta = 0.05$ from an initial stress ratio $\eta = 0.5$. It can be seen that for any one column of markers the vertical displacements are approximately linear with heights of the markers indicating that the vertical strains are uniform throughout that column. Since the lines are approximately parallel the vertical strains in all columns are identical hence the vertical strain is approximately uniform throughout the sample.

Fig.3.39(b) gives the corresponding information for the horizontal displacements (when $\eta = 0.5$ and $\Delta\eta = 0.05$) plotted against the positions of the markers along the sample diameter. The observed data now only lies very approximately on straight lines and these are approximately parallel except for the rows A and J which were only 0.1 inch from the end platens. (When inspecting Fig.3.39(b) it must be noted that the observed displacements correspond to local horizontal strains of magnitude 0.3 per cent approximately. It will be shown later that 27 per cent of these very small local strains have errors exceeding $\pm$ 0.2 per cent and 4 per cent exceeding $\pm$ 0.4 per cent.) Figs. 3.40(a) and (b) give the corresponding data for plane 2, and from inspection of Figs.3.39 and 3.40 it may be deduced that the strains are below average in the regions close to the ends of the specimen, especially near the bottom.

The above incremental displacement patterns were typical of those obtained for each increment of stress ratio prior to the attainment of its peak value at which $0.65 > \eta > 0.55$. An attempt was made to determine the distribution of incremental displacements and strains during failure as defined by the maximum stress ratio η. When η was 0.55 the sample was stable and radiographs of planes 1 and 2 were taken. An increment $\triangle\eta = 0.10$ was then applied and the ram of the triaxial cell began to move slowly downwards with a small acceleration. At intervals during this process the ram was temporarily locked in position for about 15 minutes while radiographs were taken of planes 1 and 2. Fig.3.41(a) and (b) show typical distribution of local incremental displacements that occurred in an interval between successive radiographs in plane 1. The patterns for plane 2 were similar to those for plane 1 and for all tests discussed from hereon in this thesis data will only be presented for plane 1. These patterns clearly indicate that the strains were not uniform.

The strain distributions corresponding to the displacement patterns given in Fig.3.39 for $\eta = 0.5$ and Fig.3.41 for failure are shown for plane 1 in Figs.3.42(a) and (b) and in Figs.3.43 (a) and (b) respectively. In the (a) diagrams the values of the local vertical strains are plotted between the relevant pair of markers, while the (b) diagrams give in the same way the local horizontal strains. There is considerable variation of both strains throughout the sample, with significantly greater variation for the failure case. These variations appear to be random and this is confirmed by the histograms plotted in Figs.3.44(i)-(ix). In these histograms the number of meshes of the lead shot network having a particular value of the local axial strain are plotted against this strain in all the (a) diagrams. The (b) diagrams refer to horizontal strains. Figs.3.44(i)-(ix) refer to each successive increment during test OB and the particular increment corresponding to $\eta = 0.5$ and $\triangle\eta = 0.05$ is shown in Fig.3.44(vi) while the failure increment discussed above is given in Fig.3.44(vii). All these histograms approximate to normal distribution curves as used in statistics. It is only when the histogram is a true normal distribution curve that the conventional procedure of using overall average strains, when developing stress-strain relationships, is warranted. Some of the scatter in these

histograms will be due to errors in the technique of measuring the displacements of the lead markers. To assess the magnitude of these errors a given radiograph was measured twice by the Author under, as near as possible, identical conditions. The results are shown in Figs.3.45(a) and (b) for the axial and radial strains respectively. The scatter in these readings is of the order of one third of that shown in the histograms in Fig.3.44. Consequently these histograms do really represent the type of variation of strain throughout the triaxial samples.

3.5.5 The deformation of a lightly overconsolidated specimen (1.5 inch diameter) of Kaolin in a drained test

In this section the local deformation characteristics of a lightly overconsolidated specimen (1.5 inch diameter and 3 inch high) is described. The specimen was subjected to a maximum consolidation pressure of 145 psi, subsequently swollen to an isotropic stress of 90 psi and then sheared by imposing a stress path of slope 3.

The incremental vertical displacement patterns of the markers inside the sample in plane 1 for three stress increments are shown in Figs.3.46(a-c). The incremental displacement patterns were found to be linear for the three stress increments applied at stress ratios of 0, 0.23 and 0.52 respectively. During the first increment the strains were extremely small and the scatter from a straight line will be due to errors in measuring these small strains.

The incremental axial and radial strain distributions along the sample height for the three increments of stress are illustrated in Figs.3.47 and 3.48 respectively. The results indicate that the strains were approximately uniform over the centre two thirds of the sample, and the strains close to the ends of the sample were found to be of lower magnitude than in the middle two thirds. These differences in strains increased with the stress ratio.

3.5.6 The deformation of a 1.5 inch diameter heavily overconsolidated specimen during a drained compression test BZ.

In this section the internal displacements and the strain patterns in a heavily overconsolidated specimen are presented. The sample was subjected to a maximum isotropic preconsolidation pressure of 90 psi, subsequently isotropically swollen to 8.2 psi,

and then sheared by imposing a stress path of slope 3.

Figs.3.49(i-v) illustrate the incremental vertical displacements of the markers in plane 1 for five increments of stress applied at stress ratios of 0, 0.6, 0.8, 1.0 and 1.1. The incremental displacement was found to vary linearly with the height of the sample.

Figs.3.50(i)-(v) show the incremental axial strain distribution inside the specimen, for the displacement patterns provided in Fig.3.49(i-v). The strains were found to be approximately uniform up to a stress ratio of 1, and the sample failed when the stress ratio was just greater than 1.1. The corresponding incremental radial strain distributions are illustrated in Fig.3.51 (i-v).

At high stress ratios the radial strains at the ends of the sample were considerably smaller than those corresponding to the central two thirds of the specimen which themselves were moderately uniform.

3.5.7 The deformation of a 4 inch diameter heavily overconsolidated specimen in drained test OC.

The deformation characteristic of a 4 inch diameter heavily overconsolidated specimen will now be discussed. The sample was subjected to a maximum isotropic consolidation pressure of 60 psi, and swollen back to an isotropic stress of 5 psi. Subsequently the specimen was sheared along an applied stress path of slope 3. The incremental axial and radial displacements of the markers are plotted against the height and diameter of the sample in Figs.3.52(a) and (b) respectively. Both the axial and radial displacements were found to vary linearly with the height and diameter of the sample. The slopes of the lines corresponding to the radial displacement patterns were found to be lower towards the bottom of the sample.

The actual local incremental axial and radial strains as computed from the displacements of the markers are presented in Figs.3.53(a) and (b) respectively and 3.54(a) and (b) respectively for two stress increments. In view of the apparent random variation of the strains the results are also presented in the form of histograms in Figs.3.55 and 3.56. The histograms in Fig.3.55 which refer to $\eta = 0$ and $\Delta\eta = 0.63$ can be approximated to normal distribution curves, but this is hardly possible for the histograms of Fig.3.56 for which $\eta = 0.63$ and $\Delta\eta = 0.21$. This latter picture may imply that local failure surfaces are

developing across the sample.

3.5.8 The distribution of strains in a 1.5 inch diameter normally consolidated specimen sheared along a constant p path in extension.

The internal displacements and strain patterns in a 1.5 inch diameter specimen sheared in extension will now be considered. The specimen was subjected to a maximum isotropic consolidation pressure of 60 psi and subsequently sheared along a constant p stress path. The incremental vertical displacements of the markers at 4 stages of test BE are shown in Figs.3.57(i)-(iv). The displacement patterns were linear for the first two increments of stress applied at stress ratios of 0 and 0.42 respectively. Beyond this stress level, the displacement pattern is nonlinear, indicating that the strain was nonuniform. The maximum displacement rate with respect to the height occurs in the centre of the sample. This is well illustrated in Fig. 3.57(iii) where $\eta = 0.5$ and is most marked in Fig.3.57(iv) where $\eta = 0.58$. The sample failed in the next increment but it can be seen in Fig.3.57(iv) that all the strain in that increment occurred in the middle third of the sample and none at its ends.

The corresponding incremental axial strain distributions are provided in Figs.3.58(i)-(iv). The strains were approximately uniform for the first two increments of stress.

Marked nonuniformity was observed in the strains for the third increment of stress and in the fourth there was gross nonuniformity. The radial strain distributions in Figs. 3.59(i)-(iv) reveal similar phenomena to those observed for the axial strains.

In contrast to their behaviour in compression tests, specimens in extension tests are more liable to develop local regions of high deformation. Fig.3.60(i)-(v) shows photographs of radiographs taken during the compression test BZ at five stages of strain of the heavily overconsolidated sample discussed in section 3.5.6. Fig.3.60(v) corresponds to conditions after a failure plane has developed well after the attainment of the peak stress ratio. Fig.3.61(i)-(v) represent corresponding radiographs during the extension test BE. Figs.3.61(i)-(iv) correspond to similar stages of strain to those plotted in Figs.3.58(i)-(iv) and 3.59(i)-(iv). The onset of the development of the neck is clearly seen in Fig.3.61(iv) and its full

development in Fig.3.61(v). Between these two radiographs all deformation was occurring in this neck region. Close inspection of Figs.3.61(iii)-(v) shows the development of thin cracks just before and after the peak stress ratio condition was attained.

3.5.9 The deformation of a 4 inch diameter specimen sheared along a constant p path in extension test OE.

The displacement and strain patterns in a 4 inch diameter sample are presented in this section. The specimen was subjected to a maximum isotropic consolidation pressure of 30 psi and subsequently sheared in extension along a constant p path. In this sample there were 8 columns (1-8) and eleven rows (A-K) of lead shot markers. The incremental vertical displacement patterns of the markers are plotted in Fig.3.62(a) for an increment of stress ratio $\Delta\eta = 0.15$ applied at a stress ratio of $\eta = 0.31$. It can be seen that the vertical displacements vary linearly with the height of the sample. The slopes of these lines are nearly the same suggesting that the axial strain was uniform throughout the sample. The horizontal displacement of the markers are plotted against the diameter of the sample in Fig.3.62(b). At any horizontal section in the sample the horizontal displacement of the markers are linearly related to the positions of the markers along the diameter of the sample. These lines are also parallel suggesting that the radial strain was uniform throughout the sample. The incremental axial and radial strain distributions as computed from the displacement of the markers are given in Figs. 3.63 and 3.64 for two increments of stress applied at stress ratios of 0.31 and 0.45 respectively. There was considerable variation in the magnitudes of the local strains as shown in the histograms in Figs.3.65(i)-(v). These histograms of strain distributions can be approximately represented by normal distribution curves.

3.6 The deformation characteristics during failure in compression and in extension.

3.6.1 The formation of rigid end zones in the normally consolidated specimen OB failing in compression.

The formation of rigid end zones during destructive tests in materials with low cohesion has been reported by several

authors. These zones develop due to the end conditions and the lack of continuity and isotropy of the material tested. Zelenin and Lomize (1961) introduced coloured layers of soils in clay specimens and demonstrated the formation of such rigid end zones in their sample during deformation. By extending the theorem of Bishop, Gree and Hill (1956) which states that "any region shown to be necessarily rigid for a particular stress field must be rigid in all complete solutions", Haythornthwaite (1960) isolated conical regions at the ends of the specimens as being rigid. He reported that this conical region subtends a semivertical angle of $(45-\frac{\phi}{2}^{\circ})$ with the axis of the specimen. For a value of ϕ of 20°, this angle will be 35°. The tests carried out by the Author on Kaolin had maximum stress ratios corresponding to 20° approximately.

In Fig.3.66 the mesh of continuous lines was made by connecting images of the lead shot markers on a radiograph taken at a given instant during the early stages of progressive failure of the sample. The dotted lines were obtained from the positions of the same markers in a subsequent radiograph which was taken after appreciable progressive failure had occurred. In Fig.3.66 the shape of a mesh in the second radiograph is superposed on its shape in the first in such a way that the mesh has not rotated and the geometric centres of both shapes coincide. Consequently while the full lines in Fig.3.66 represent the initial shapes of the meshes, the dotted lines represent the shapes of the meshes after deformation. If the gaps between neighbouring dotted lines is of uniform width round every mesh then the sample will have strained uniformly throughout. Where the gap is widest the greatest deformation will have occurred and where the dotted lines coincide with the full lines then no deformation will have taken place at this point. In Fig.3.66 when dotted lines do not appear they have coincided with the full lines. It can be seen that no deformations have occurred in the conical zones at the ends of the sample. The zones are therefore rigid, the mesh size of the lead shot network should have been reduced to specify them accurately. The conical zones are much smaller than those predicted by Haythornthwaite since their semi vertical angle is 69° compared to his predicted value of 35°. It is interesting to note that the angle α in Fig.3.66 is 21° which is very close to the value $\phi = 20^{\circ}$ for the Kaolin.

In Fig.3.67(a) the axial displacements and the heights of the markers above the sample base are plotted for the 6 vertical columns of markers for a strain increment just before rupture planes were seen visually to develop during test OB. The bottom of the sample is to the left of this diagram so that in effect the sample is on its side. The axial strains, which are proportional to the slopes of the dotted lines (with respect to the base of the diagram), can be seen to be ~~the~~ largest in the outer ring of a horizontal layer in the sample represented by the shaded region in this diagram. In Fig.3.67(b) the corresponding information is given for the radial displacements of the markers in the horizontal rows AA, ... HH, with respect to the position of the markers along the diameter. The slope of the dotted curve is a measure of the radial strain at that point. It can be seen that ~~the vast majority~~ most of the radial strain is occurring in the central cylindrical core shown shaded in Fig.3.67(b).

3.6.2 The "mesh" displacement pattern in a specimen during failure in extension

Fig.3.68 illustrates the displacement pattern inside specimen OE while failing in extension and may be compared with the corresponding pattern in Fig.3.66 for a specimen failing in compression. It is evident that for specimens failing in extension, there are no rigid zones forming at the ends of the specimen as developed in the compression sample. The theoretical analysis of Haythornthwaite indicates rigid zones at the ends of the specimen even in extension. These rigid zones were reported by him to subtend an angle of $(45 - \phi/2)^{\circ}$ with the base of the sample.

3.7 The X and Gamma absorption techniques for the study of the local voids ratio changes in triaxial specimens of Kaolin

3.7.1 The Gamma ray technique

A specimen of Kaolin was isotropically consolidated to 30 psi in the triaxial apparatus. At the end of isotropic consolidation, a number of readings were taken at different levels along the axes of the sample by transmitting radiation from a low energy Gamma ray source. The average of these counts over a time interval of 400 seconds was found to be 26000. The specimen of Kaolin was isotropically consolidated to 60 psi. This change in stress caused a compressive volumetric strain of 7 p.c. A second series of readings were then taken and the average count was found to be 25700, for the same interval of time. This difference is approximately the same magnitude as the standard deviation (322)

corresponding to 26000. Hence it is apparent, that in order to improve the sensitivity of measurements the counting period should be increased considerably and this would not be practicable. Alternate techniques should therefore be developed to increase the sensitivity of the method for the measurement of local voids ratio in triaxial specimens of Kaolin.

3.7.2 The X-ray absorption technique applied to triaxial samples of clay

In addition to the limitation stated in section 3.7.1, the X-ray absorption technique is further restricted by the effect of scattered radiation. Attempts were made to eliminate the effect of scattered radiation by the use of a parallel plate collimator (Sirwan (1965)) and by the use of a Bucky grid Hondius Boldingh (1964). A detailed investigation was carried out and indicated that

(i) the film density variation along the film height was about 12 p.c. and across the film was 5.6p.c. without the use of a parallel plate collimator on the grid.

(ii) the use of the parallel plate collimator reduced the variation in film density to about 7.7 p.c. in both directions on the film.

(iii) The use of the Bucky grid reduced the variation in film density to 1.33 p.c. across the film. However the variation in film density along the film height was found to be 16 p.c.

The high variation in the film density along the height, when the Bucky grid was used, was entirely due to the variation in thicknesses of the lead lamellae in the grid.

Because of the high variation in film density observed, further investigation of the use of grids is required. A brief note on the study of the effects and elimination of scattered radiation is given in Appendix 1.

3.8 A preliminary study on the orientation of clay particles in specimens of Kaolin under 1-D consolidation, isotropic consolidation and shear

The experimental observations provided in this dissertation indicate that the deformation behaviour of specimens of Kaolin is anisotropic. This anisotropic deformation is considered to be a result of the preferred orientation of the flake shaped Kaolin particles. Quantitative methods to describe the degree of anisotropy from the orientation of the clay particles are now

being developed in Cambridge by Tovey (1969). The experimental observations provided in this section were carried out with a view to using these methods in the study of the stress-strain behaviour of Kaolin. At the moment the interpretation of the results is only qualitative. The methods of sample preparation for scanning electron microscope are outlined in section 2.

3.8.1 The random orientation of clay particles in the slurry

The micrographs in Fig.6.39 are of specimens as prepared from the slurry taken from the pugmill. The micrographs (a) and (b) are a stereo pair and indicate that the orientations of the clay particles are completely random.

3.8.2 The effect of 1-D consolidation on the orientation of clay particles

Fig.3.70 contains the micrographs taken of specimens of Kaolin at the end of 1-D consolidation. These micrographs indicate that the Kaolin particles are orientated into groups in the form of packets. The orientation of the packets of particles are random. The micrographs are again mounted in stereo pairs.

3.8.3 The effect of isotropic consolidation on the orientation of clay particles

Illustrated in Fig.3.71 are the micrographs taken at the end of isotropic consolidation. These micrographs also indicate that the particles are orientated parallel to one another in groups. These groups are arranged at random. Visual observation of the micrographs suggests a preferred orientation although this is not as intense as in 1-D consolidation. The results, though preliminary, indicate that additional isotropic consolidation does not have appreciable effect in altering the orientation of clay particles. Once the structure corresponding to the packets of clay particles is formed, at the end of 1-D consolidation, it will remain so during the subsequent isotropic consolidation.

3.8.4 The failure plane and the failure zone as observed in the scanning microscope

The micrographs in Fig.3.72(a) and (b) illustrate a typical failure plane. The sheared sample was oven dried and split open on the failure plane. Visual observations on these micrographs indicate a high degree of orientation to give face on particles with their planes lying in the direction of the sheared zone.

The sheared zone was further investigated and it was found that along a thin layer of the sheared zone thé particles are highly orientated in a parallel direction. The regions closer to this thin zone and on either side of it include regions with random groups of particles. The thin sheared zone where the maximum degree of parallel orientation is observed is about 20 μ wide. The micrographs indicating the sheared zone are illustrated in Fig.3.73.

CHAPTER 4

THE EFFECTS OF SAMPLE PREPARATION AND TESTING METHODS ON THE STRESS-STRAIN BEHAVIOUR AND THE $(\frac{q}{p_e}, \frac{p}{p_e})$ RELATIONSHIP FOR NORMALLY CONSOLIDATED KAOLIN.

4.1 General Introduction

The successful development of a theory for the adequate description of the stress-strain relationships of clays requires a detailed experimental investigation of the material behaviour. Almost all the experimental observations presented in this dissertation are based on stress controlled triaxial (axi-symmetric) tests performed on specimens of Kaolin prepared from a slurry of 160 per cent moisture content. Often the sample preparation, and the method of testing, influence the stress-strain behaviour. A knowledge of the magnitude of these effects is needed to establish approximate limits for the variability of the test results. The major factors that influence the stress-strain behaviour during shear are (i) the initial moisture content of the slurry from which the specimen is prepared and (ii) the initial one dimensional consolidation stress applied during the sample preparation.

Experiments performed by Olson (1962) indicate that the voids ratio of a specimen at the end of isotropic consolidation varies according to the initial moisture content of the slurry. Two methods were adopted by Olson for the sample preparation.

Method I. Clay at a moisture content of 60 to 65 per cent was hand packed into a 1.5 inch diameter plastic tube fitted with a piston. As more and more soil was added, the piston was drawn down into the tube, until a specimen of 3 inches length was obtained. This sample was then extruded and set up in the triaxial cell. These specimens were referred to by him as the remoulded samples.

Method II. A dilute suspension of the clay at a water content of 1000 per cent (Liquid Limit 85 per cent) was transferred to a 20 inch long plastic tube of 1.5 inch internal diameter. The base of the tube was fitted with a porous stone and drainage fittings. After a period of several weeks the clay was consolidated under a uniaxial stress of 7 psi. At the end of the primary consolidation, the samples were extruded and set up in the triaxial cell. These specimens were referred to

by him as sedimented samples.

Olson found that the remoulded samples had a lower equilibrium voids ratio than the sedimented samples for a given consolidation pressure. Also the stress-strain behaviour of the two samples were different. He attributed these variations to the differences in soil structure of the two types of specimens.

Henkel and Sowa (1963) compared the results of triaxial tests performed on specimens $_{N}$ prepared under one dimensional and subsequent isotropic consolidation with samples prepared under K_o consolidation conditions. The stress paths followed by these specimens during an undrained test were observed to be different. It should be emphasised that these authors carried out experiments on materials other than Kaolin and the testing methods employed were quite different to those adopted by the present writer. Though their observations are helpful in giving an overall idea of the deviations in the stress-strain characteristics, these deviations were not necessarily due to the effects of the methods employed for the sample preparation. Several additional variables were introduced during the method of testing. For example if adequate time is not allowed for the isotropic consolidation prior to shear, the volumetric strain observed during shear will not represent the true magnitude. Further, the stress-strain characteristics can also depend on the magnitude of the isotropic consolidation to which the specimen is subjected prior to shear. In stress-controlled tests, the behaviour may also depend on the size of stress increment and its duration of application. Additional restrictions are imposed on the deformation characteristics by the geometry of the apparatus. A complete study of these factors and their effects are beyond the scope of the present work. However, in this chapter the author has comprehensively studied the effects of some of the factors, and a preliminary study of others, by careful control of the other variables.

4.2 The duration of isotropic consolidation prior to shear

The complete duration of the shearing phase of a test varied from 2 to 4 weeks. It was essential to ascertain that the effect of secondary consolidation due to the isotropic stress during shear was not of the same order as that of the volume change due to shear. Hence all specimens, prior to shear were left under a constant isotropic stress for a period of seven to ten days. Fig.4.1 illustrates the variation of volume change

with respect to time (plotted on a log-scale) for the final increments of isotropic stress on three samples AF, Z and AD. It is evident that at the end of these periods (approximately 7 days for each increment), the volume change due to secondary consolidation was small (approximately 0.014 cc/day). Thus over the duration of a shear test (2 to 4 weeks) one may expect a sample to consolidate a further 0.2 - 0.4 cc. This volume is small in relation to the volume change observed during the shear phase in a typical drained test which is of the order of 7 cc.

4.3 The behaviour of specimens prepared from different initial Moisture content

4.3.1 The effect of initial moisture content of the slurry on the equilibrium voids ratio

In the present investigation three specimens of Kaolin were prepared from slurries of initial moisture content of 120, 160 and 180 per cent. They were one dimensionally consolidated under an axial stress of 22.6 psi and subsequently isotropically consolidated to 60 psi. It can be seen in the data tabulated in Fig.4.2 that the specimen prepared from an initial moisture content of 120 per cent had, after isotropic consolidation to 60 psi, a lower voids ratio (e_o = 1.306) than the specimen prepared from the higher moisture content of 180 per cent (e_o = 1.361). The voids ratio (e_o = 1.368) at 60 psi of the specimen prepared from 160 per cent moisture content was approximately the same as that prepared from the 180 per cent moisture content. The latter two specimens were prepared from different batches of Kaolin and hence a direct comparison of voids ratio is not strictly valid. The results do however indicate that a reduction in the moisture content of the slurry can cause considerable change in the voids ratio. These results are in agreement with the observations of Olson.

4.3.2 The stress-strain behaviour and the (q/p_e, p/p_e) characteristics

Fig.4.2 illustrates the (q/p, v) characteristic of the three specimens during fully drained tests at a constant cell pressure of 60 psi. It can be seen that at high stress ratio, the specimen prepared from a slurry with the lowest moisture content has a volumetric strain appreciably smaller than the other two specimens. Fig.4.3 illustrates that the (q/p_e, p/p_e) relationships of the three specimens are different. It is unwise to generalise from the

results of only three tests and Fig.4.3 should not be taken necessarily to imply that the state boundary surface is different for each and every moisture content of the slurry. Further work is needed to decide this point. It must be borne in mind that the initial voids ratios of the samples just prior to shear will be different for specimens prepared with different initial one dimensional stresses. However it is interesting to observe in Fig.4.4 that these specimens have a unique (v, ϵ) characteristic, indicating that the behaviour is unique when plotted in strain space. Apart from the (v, ϵ) characteristics being unique, the results indicate that the stress-strain behaviour of remoulded specimens does depend on the initial moisture content of the slurry. In order to be consistent with the previous research workers in Cambridge the author chose a figure of 160 per cent for the initial moisture content of the slurry in the preparation of all his other samples.

4.4 The effect of initial one dimensional consolidation stress on the shearing phase of fully drained tests

4.4.1 General

Fig.4.5 illustrates the stress paths followed by three specimens which were subjected to different one dimensional consolidation pressures and subsequently brought to the same isotropic stress. In this figure points A, B and C correspond to the stress states at the end of one dimensional consolidation. Points A^1, B^1 and C^1 correspond to the stress state at the end of the first increment of isotropic stress. Point O^1 represents the stress state for all samples at the end of isotropic consolidation and prior to shear. The details of these shear tests are summarised in Table 2.4(a). The experimental observations are discussed in section 4.4.2 and attempts will be made in sections 4.4.3 and 4.4.4 to study the effect of the initial shear stress imposed during the one dimensional consolidation on the subsequent stress-strain behaviour.

4.4.2 The experimental observations on fully drained tests

Since all the specimens were subjected to the same applied stress path of slope 3, commencing from the same isotropic stress of 60 psi any stress point (q,p) can be uniquely represented by the parameter $(\frac{q}{p})$. Figs.4.6 and 4.7 illustrate the variation of the volumetric and shear strain with respect to this parameter. It is clear that, (a) at any particular stress ratio, the specimens

with high initial one dimensional consolidation pressure have low volumetric and shear strain and (b) except for the specimen with a 1-D stress of 55 psi, the $(\frac{q}{p} - \upsilon)$ characteristics for the two specimens with 1-D stress of 22 psi and 11 psi are approximately the same. Hence any further reduction below 11 psi of the 1-D stress will not have an appreciable effect on the volumetric strain, stress ratio characteristic. Fig.4.8 illustrates that the (υ, ϵ) characteristic for the three specimens is approximately unique. The $(\frac{q}{p_e}, \frac{p}{p_e})$ characteristics of the three specimens are illustrated in Fig.4.9. It is observed that the specimen with the initial 1-D stress closest to the isotropic stress of 60 psi has the highest value of $\frac{p}{p_e}$, for any specific value of $\frac{q}{p_e}$. It will now be shown that specimens which have lower volumetric strains (at any particular stress-ratio) will have higher values of $\frac{p}{p_e}$ for any specific $\frac{q}{p_e}$. By definition

$$p_e = p_o \exp\left(\frac{e_o - e}{\lambda}\right) \qquad 4.1$$

where e_o corresponds to the voids ratio at pressure p_o on the isotropic consolidation line.

$$v = \log\left(\frac{1 + e_o}{1+e}\right) \qquad 4.2$$

Hence from 4.1 and 4.2

$$p_e = p_o \exp\left(\frac{1 + e_o}{\lambda}\right)(1 - \exp(-\upsilon)) \qquad 4.3$$

Contours of constant $(\frac{q}{p})$ are straight lines on the $(\frac{q}{p_e}, \frac{p}{p_e})$ plot even if p_e varies during the tests; this is illustrated in Fig.4.10. Hence at any particular stress ratio the position of a point on the state path in $\frac{q}{p_e}$, $\frac{p}{p_e}$ space corresponding to a drained test can shift towards or away from the origin along the constant stress ratio line and its position will depend on the magnitude of p_e. As indicated by equation 4.3, high volumetric strain results in high values of p_e and therefore tends to move the point towards the origin along BA. The data presented in Fig.4.6 indicated that the specimen with 1-D stress of 55 psi had a lower volumetric strain compared to the other two specimens. Correspondingly this specimen will have a higher value of $\frac{p}{p_e}$, than the other two specimens for any particular value of $\frac{q}{p_e}$ on the $\frac{q}{p_e}$, $\frac{p}{p_e}$ plot.

4.4.3 The correlation of the drained test results of specimens prepared with different initial 1-D stress

The following assumptions will be made in the calculation of

the initial shear stress experienced by a specimen during 1-D consolidation. The ratio of the minor principal stress to the major principal stress is a constant during the initial 1-D consolidation. This ratio is taken to be 0.7 (K_o) and is in agreement with the lateral pressure measurements carried out by Thompson (1962) and Burland (1967) during 1-D consolidation of cylindrical specimens. The corresponding value of ($\frac{q}{p}$) is 0.375.

Two methods will be studied for the correlation of the observations on the specimens prepared with different initial 1-D stress. These methods are based on two different additional assumptions.

Method 1 In this method it will be assumed that there would be a unique relationship between $\frac{q}{p}$ and v, and $\frac{q}{p}$ and ϵ, during shear under a given applied stress path of all specimens if they had been initially prepared under truly isotropic stress condition (i.e. these specimens are assumed to be initially isotropically consolidated from the slurry, instead of being subjected to a 1-D consolidation). Since all specimens prepared by the author were initially sheared to a stress ratio of 0.375 during 1-D consolidation, one would expect them to exhibit strains of small magnitude during the initial phases of subsequent shear in the triaxial apparatus, until the stress ratio of 0.375 (experienced by the specimen during 1-D consolidation) was exceeded. Therefore the behaviour of all these specimens beyond a stress ratio of 0.375 should be identical in the ($\frac{q}{p}$ - v) and ($\frac{q}{p}$ -ϵ) spaces irrespective of their initial 1-D stress. Figs.4.11(a) and (b) indicate that the ($\frac{q}{p}$ -ϵ) and the ($\frac{q}{p}$ - v) characteristics of the specimen for stress ratios higher than 0.375. It is observed that even after allowing for the initial shear stress effects based on the K_o condition the stress strain behaviour in the ($\frac{q}{p}$,v) and ($\frac{q}{p}$,ϵ) spaces is not unique.

Method 2 In Method 2 only one different assumption will be made to those used in Method 1. In Method 1 it was assumed that the stress-strain behaviour during shear of all the specimens might be unique once the stress ratio $\frac{q}{p}$ had exceeded the K_o value attained during the initial 1-D consolidation. In Method 2 it will be assumed instead that the behaviour of all specimens might be unique once the deviator stress q had exceeded the value attained during the initial 1-D consolidation. The initial shear stress experienced by the three specimens prepared under

the initial 1-D stresses of 11, 22 and 55 psi were, 3.3, 6.6 and 16.5 psi respectively. The (q, ϵ) and the (q, v) relationships for the three specimens during the whole of the shearing phase from the initial isotropic stress of 60 psi are shown in Figs. 4.12 and 4.13. The points A, B and C on the curves correspond to the three deviator stresses quoted above, namely A = 3.3, B = 6.6 and C = 16.5 psi. In this method of correlation of the tests results it is suggested that the behaviour of the three specimens before they reach the initial shear stresses of 3.3, 6.6 and 16.5 psi respectively may be different.

However thereafter the behaviour of the specimens should be identical. In Fig.4.12 the points G and H on the curve OAK correspond to the same level of deviator stresses as the points B and C respectively. Let ϵ_A, ϵ_B, ϵ_C, ϵ_G and ϵ_H be the shear strains as recorded in Fig.4.12 at the points A, B, C, G and H respectively. Then the modified $(q-\epsilon)$ relation for the specimen having the stress-strain curve CM is obtained by adding the shear strain difference $\epsilon_H - \epsilon_C$ for all values of ϵ on the curve CM. Similarly the modified $(q-\epsilon)$ relation for the specimen having the stress-strain curve BL is obtained by adding $\epsilon_G - \epsilon_B$ for all values of ϵ on the curve BL. These modified relations for the specimens with the stress-strain curve OAK are replotted in Fig.4.14. A similar procedure is adopted for the (q-v) characteristics of the specimens in Fig.4.13 and the results are replotted in Fig.4.15. It is observed that the behaviour of the three specimens in Figs.4.14 and 4.15 are still not unique; however the correlation is somewhat better than that produced by Method 1.

An alternate method by which the author was able to correlate the stress-strain behaviour of the three specimens satisfactorily will now be described.

<u>The shifts of the origin of the stress-strain curves depending on the magnitudes of the initial 1-D stress</u>.

In this method it is suggested that the behaviour of the specimens in the plots (q^*, ϵ^*) and (q^*, v^*) are unique where

$$q^* = q - q_{Ko} \qquad 4.4$$

$$v^* = v - v_{Ko} \qquad 4.5$$

$$\text{and} \quad \epsilon^* = \epsilon - \epsilon_{Ko} \qquad 4.6$$

where q_{Ko} is the magnitude of the initial shear stress due to

one dimensional consolidation and v_{Ko} and ϵ_{Ko} correspond to the volumetric and shear strain experienced by the specimens during the subsequent shear in the triaxial apparatus up to a deviator stress of q_{Ko}. The results are presented in the modified plot (q^*, ϵ^*) and (q^*, v^*) in Figs.4.16 and 4.17. The unique relationships revealed by these plots indicate that the origins of the stress-strain curve denoted by D, E and F in the (q, ϵ) and (q, v) plots shift by the amount ($-q_{Ko}, -\epsilon_{Ko}$) and ($-q_{Ko}, -v_{Ko}$) respectively. It is of interest to note that the stress-strain behaviour for deviator stresses less than q_{Ko}, i.e. for negative values of q^*, ϵ^* and v^* also appears to be unique and occurs as a continuous extension of the curve describing the behaviour in the positive range of q^*.

The method suggested in this section for the correlation of the stresses and strains of specimens subjected to varying 1-D stresses and subsequently sheared from an isotropic stress condition, has an important field application. Specimens which are in the normally consolidated state and under a Ko condition in the field, when tested in the triaxial apparatus at an isotropic stress (greater than the initial 1-D stress) will only give unique behaviour in the (q^*, ϵ^*) plot and not in the conventional q, ϵ or ($\frac{q}{p}, \epsilon$) plots. The initial one dimensional consolidation stress experienced in the field by the specimen could be determined by performing a single 1-D consolidation test in the laboratory on the specimen. Then by doing a single drained triaxial test after isotropic consolidation at a cell pressure higher than the initial 1-D stress, it is now possible to establish the (q^*, ϵ^*) and (q^*, v^*) behaviour of the field specimen.

It would be interesting to study the effect of different initial 1-D stresses prior to isotropic consolidation at 60 psi for other test paths under drained conditions than those discussed above which had a slope $dq/dp = 3$. If the modified relation in the (q^*, v^*) plot is unique for a given imposed stress path, then the ($\frac{q^*}{p_e}$, $\frac{p^*}{p_e}$) plot should also be unique for that type of test, provided the voids ratio of these samples are approximately the same at the end of isotropic consolidation (see equation 4.3 which indicates that p_e is constant when e_o and v are constant). Note that $p^* = p_o + \frac{1}{3} q^*$. In addition to the voids ratios being identical at any one isotropic stress if the constant ($\frac{q^*}{p^*}$) lines are linear in the (Δe, log p^*) plot with

slope ($-\lambda$) for all types of tests, then there would be a unique ($\frac{q^*}{p_e}$, $\frac{p^*}{p_e}$) curve for all these tests.

4.5 The effect of initial 1-D consolidation stress on the undrained test results

4.5.1 General

The observations during undrained tests on two specimens T_7 and T_4 will now be presented and an attempt will then be made to correlate ~~this~~ these data. Specimen T_7 was prepared from a slurry by initial 1-D consolidation under a vertical stress of 3 psi, which corresponds to an applied deviatoric stress of 1 psi. This specimen was then isotropically consolidated under a pressure of 60 psi and was then subsequently sheared in a conventional undrained triaxial compression test. Sample T_4 was subjected to a similar treatment but was given more initial 1-D consolidation since it was subjected to a vertical stress of 22 psi, corresponding to an initial shear stress of 6.6 psi.

4.5.2 The experimental data from undrained tests T_7 and T_4

In Fig.4.18 the ($\frac{q}{p}$, ϵ) relationships observed during triaxial shear tests T_7 and T_4 are plotted and can be seen to be virtually identical. The magnitudes of the parameters ϵ and q were both taken to be zero at the commencement of the triaxial shear phase of the tests (i.e. after the isotropic consolidation to 60 psi). This unique ($\frac{q}{p}$, ϵ) relationship is therefore independent of the previous shear stress (or strain) history which had been imposed on the samples during the initial 1-D consolidation. The fact that no such uniqueness was observed in drained tests (see Fig.4.7) will be discussed in section 4.5.3

When the same data was plotted on a ($\frac{q}{p_e}$, $\frac{p}{p_e}$) plot as shown in Fig.4.19, the undrained state boundary surface corresponding to specimen T_7, which had only experienced a previous shear stress of 1 psi during 1-D consolidation, was much higher than that for T_4 (previously subjected to a shear stress of 6.6 psi). It would therefore seem that if no allowance is made for stress or strain history, the undrained state boundary surface is not unique but does depend on the stress history. This statement is confirmed by the different (q,u) relationships for specimens T_7 and T_4, shown in Fig.4.20.

4.5.3 The correlation of the undrained test results on specimens T_7 and T_4 which have experienced different initial shear stresses during 1-D consolidation

Two methods attempting to correlate the results of undrained tests T_7 and T_4 will now be considered. The first is the same as the (q^*, v^*, ϵ^*) method used in correlating drained tests results in section 4.4.3.

Method 1

If during the initial 1-D consolidation, a sample is subjected to a shear stress q_{K_o} and undergoes a shear strain of ϵ_{Ko} then during subsequent shear in the triaxial shear phase of a test $q^* = q - q_{Ko}$ and $\epsilon^* = \epsilon - \epsilon_{Ko}$. The ($q^*$, ϵ^*) relations for specimens T_7 and T_4 can be seen to be completely different in Fig.4.21. The ($\frac{q^*}{p^*}$, ϵ^*) are also different as shown in Fig.4.22. In deriving p^*, it was assumed that

$$p^* = p_o + \tfrac{1}{3}q^* - u \qquad 4.8$$

A possible explanation for the fact that both the (q^*, ϵ^*) and the ($\frac{q^*}{p^*}$, ϵ^*) relationships are not unique for undrained tests on samples with different shear stress (or strain) histories, whereas they were for drained tests, will be deferred until Method 2 has been described.

Method 2

In this method it will be assumed that (i) a unique (q,u) relationship should exist during triaxial shear of any specimen that had been prepared from a slurry under isotropic conditions only (i.e. without any initial 1-D consolidation) and (ii) the changes of q and u actually observed during triaxial shear of a sample, which had in its history previously experienced a shear stress of q, would only be the same as those for an isotropic sample for values of $q > q_1$. In Fig.4.20 the values of q_1 for samples T_7 and T_4 correspond to points A and B respectively. If the two assumptions stated above are correct then curve BY when B is displaced to C (where C is at the same value of q as B) should coincide with curve CX. This can be seen to be the case in Fig.4.23. Hence the (q,u) relations for the two specimens are identical for all values of q larger than the highest value of q_1 imposed on either specimen during the preliminary 1-D consolidation. If however the values of u shown in Fig.4.23 are used to calculate revised values of p during the shear tests on specimens T_7 and T_4 it is found that the

$(\frac{q}{p}, \epsilon)$ relationship is not unique at higher values of $(\frac{q}{p})$ as shown in Fig.4.24. It will be recalled in Fig.4.18, that where the experimentally observed values of u were used to calculate p, ~~that~~ the $(\frac{q}{p}, \epsilon)$ curve was unique for all values of $\frac{q}{p}$. In the light of the evidence provided so far it is concluded that the $(\frac{q}{p}, \epsilon)$ relation actually observed in undrained tests is unique and is not affected by the previous shear stress q_1 imposed during 1-D consolidation. Furthermore the pore pressures observed during triaxial shear are dependent on q_1, but deviations from the values observed with isotropically prepared samples occur in the range $o < q \leqslant q_1$. It will be recalled that in section 4.4.3 the $(\frac{q}{p}, \epsilon)$ relationship observed in drained tests was affected by the initial shear stress. The apparent contradiction between this and the conclusion made above for undrained tests may be explained by appealing to the hypothesis of Roscoe and Poorooshasb (1963) or its modification by Roscoe and Burland (1968).

The basic equation used by Roscoe and Poorooshasb has been discussed in section 1.3.6 and is given in equation 1.2. This equation can be expressed in terms of shear strain (ϵ) namely

$$d\epsilon = (\frac{d\epsilon}{d\eta})_v \cdot d\eta + (\frac{d\epsilon}{dv})_\eta \cdot dv \qquad 4.7$$

Consequently an increment of shear strain during any test in which there is a reduction of volume can be considered to be made up of two components namely (i) an undrained component as represented by the first term on the right hand side of equation 4.7 and (ii) an anisotropic consolidation component as represented by the second term in this equation. Hence it is possible for the undrained components of the shear strain to be independent of the initial shear stress history while the anisotropic consolidation component does depend on the initial shear stress history for the range $o < q \leqslant q_1$.

It can be seen that the anisotropic consolidation component in equation 4.7 is itself the product of two components, namely (i) a component $(\frac{d\epsilon}{dv})_\eta$ which is obtained from the results of anisotropic consolidation tests and (ii) the volume change dv which is predicted by projecting the imposed stress increment on to the state boundary surface. This latter surface is assumed to be unique and to be best represented by data from undrained tests. The author believes that his own data and that of Poorooshasb (1961) and Thurairajah (1961) shows that

$(\frac{d\epsilon}{dv})_\eta$ is not dependent on the magnitude of the shear stress q_1. This implies that the volumetric strains experienced during triaxial shear tests with geometrically similar stress paths are not uniquely related to $\frac{q}{p}$ until $q > q_1$.

4.6 The stress-strain curves and the $(\frac{q}{p_e} - \frac{p}{p_e})$ characteristics of specimens initially consolidated 1-dimensionally to 22 psi and then under different isotropic stresses prior to shear with geometrically similar applied stress or strain paths

4.6.1 General

In this section the author has studied the stress-strain behaviour of specimens sheared from isotropic stress levels of 30, 60 and 90 psi when subjected to three different types of imposed stress path. The stress paths were those of (i) an undrained test (ii) a constant p test and (iii) a fully drained test. All specimens were initially prepared under a 1-D stress of 22 psi and subsequently isotropically consolidated to the relevant levels of isotropic stress. The experimental observations on each type of test are first presented and subsequently discussed.

4.6.2 The experimental observations on undrained tests

Fig.4.25 illustrates the variation of shear strain ϵ with stress ratio $\frac{q}{p}$ for three undrained compression tests. It is noted that the variation of $\frac{q}{p}$ with ϵ is unique for all three tests. The $(\frac{q}{p_e}, \frac{p}{p_e})$ characteristics for the three tests are shown in Fig.4.26. The stress paths followed by the three specimens in this plot are significantly different. Also the specimens which has been sheared at the highest isotropic stress is found to have a higher value of $\frac{p}{p_e}$, than the other two specimens for any particular value of $\frac{q}{p_e}$. The $(\frac{q}{p_e}, \frac{u}{p_e})$ relationships of the three tests are also different as seen in Fig.4.27.

4.6.3 The correlation of undrained stress paths based on the initial shear stress q_1 imposed during the preliminary 1-D consolidation

In section 4.5.3, two methods were employed for the correlation of undrained test results and it was noted that the method 2 gave better correlation of these results. This method will now be used to correlate the stress paths of the undrained tests discussed in section 4.6.2. In addition to the two assumptions stated at the beginning of Method 2 in section 4.5.3 it will

also be assumed that geometrically similar (q,u) relationships, to that stated in assumption (i), apply whatever the stress level of the initial isotropic consolidation prior to shear. The validity of these assumptions will now be investigated in relation to the experimental observations. The three specimens T_3, T_4 and T_5 were all initially subjected to deviator stresses of 6.6 psi. The points A, B and C in Fig.4.27 correspond to this level of deviator stress. In this figure two points D and E are selected on the curve OAF such that the deviator stresses of D and E are the same as those of B and C respectively. Let the values of $\frac{u}{p_e}$, corresponding to the points A, B E be denoted by $(\frac{u}{p_e})_A$, $(\frac{u}{p_e})_B$.....$(\frac{u}{p_e})_E$. Then the modified relation for specimen T_5 is obtained by subtracting $(\frac{u}{p_e})_C - (\frac{u}{p_e})_E$ from every value of $(\frac{u}{p_e})$ lying on the curve CH. Similarly the modified relation for specimen T_4 is obtained by subtracting $(\frac{u}{p_e})_B - (\frac{u}{p_e})_D$ from every value of $(\frac{u}{p_e})$ lying in the curve BG. These modified relations and the curve OAF are replotted in Fig.4.28 for the three specimens. The unique relationship observed in this plot illustrates that assumptions made above for the correlation of test results, are valid. Since the modified $(\frac{q}{p_e}, \frac{u}{p_e})$ is unique it follows that the $(\frac{q}{p_e}, \frac{p}{p_e})$ plot (where $p = p_o + \frac{1}{3}q - (u)mod$ and (u)mod corresponds to values of u in Fig.4.28) for all the undrained tests will also be unique. Because of the method of obtaining (u)mod this latter curve will coincide with that shown for the 90 psi specimen in Fig.4.26.

4.6.4 The experimental observations for constant p tests AJ, AQ and AO at isotropic stresses of 30, 60 and 90 psi respectively.

Fig.4.29 illustrates the variation of shear strain ϵ with stress ratio $(\frac{q}{p})$ for three specimens sheared from isotropic stresses of 30, 60 and 90 psi respectively. It is noted that the $(\frac{q}{p}, \epsilon)$ characteristic corresponding to the 30 psi specimen (Test AJ) is quite different from the other two. A similar deviation is observed in the $(\frac{q}{p}, v)$ relationships of the three specimens shown in Fig.4.30. The $(\frac{q}{p_e}, \frac{p}{p_e})$ characteristics of the three specimens presented in Fig.4.31 are also different. At any particular level of $(\frac{q}{p_e})$, the corresponding value of $(\frac{p}{p_e})$ is significantly larger for the specimen which had been subjected to the lowest isotropic stress p_o of 30 psi. It is interesting to note that the $(\frac{q}{p_e}, \frac{p}{p_e})$ characteristic of this specimen (i.e.

p_o= 30 psi 1-D consolidation pressure = 22 psi) is approximately the same as that shown in Fig.4.9, where the specimen AR was subjected to a similar high ratio of 1-D to isotropic stress levels. (For the specimen AR the initial 1-D stress was 55 psi and the subsequent isotropic stress was 60 psi. The ratio of initial 1-D stress to the isotropic stress of this specimen was therefore = $\frac{55}{60} \simeq 0.9$; the corresponding ratio for the specimen AJ in Fig.4.31 was $\frac{22}{30} = 0.73$.) The (v, ϵ) characteristics for the three specimens AJ, AQ and AO presented in Fig.4.32 are approximately unique. During a constant p test, the volumetric strain experienced by a specimen is entirely due to shear. If elastic volumetric strain is assumed to be only a function of the mean normal stress p and if elastic shear strain is neglected, then the ($v-\epsilon$) relationship illustrated in Fig.4.32 will refer to plastic strains. Consequently the slope of this curve will represent that of the plastic strain rate vector $\frac{dv^p}{d\epsilon^p}$ which has been used extensively in some of the Cambridge stress-strain theories for 'wet' ~~days~~ clays.

4.6.5 The correlation of constant p tests based on the initial shear stress q_1 imposed during consolidation

For the correlation of the experimental observations of constant p tests, two assumptions will be made:

(i) unique relations exist between (a) q* and ϵ* and (b) q* and v*, where q*, ϵ* and v* are as defined in section 4.4.3, and

(ii) the unique relationships (a) and (b) stated in assumption 1 are similar for all specimens sheared from isotropic stress states. This entails the use of the parameter $(\frac{q^*}{p^*})$ for the comparison of specimens sheared after consolidation to different isotropic stress levels.

In Figs.4.33 and 4.34 the points A, B and C correspond to the strains ϵ_{Ko} and v_{Ko} experienced by the three specimens in reaching the stress state q_{Ko}. The results are replotted in the (q*, ϵ*) and (q*,v*) spaces in Figs.4.35 and 4.36 respectively and are presented again in the $(\frac{q^*}{p^*}, \epsilon^*)$ plot and $(\frac{q^*}{p^*}, v^*)$ plot in Figs.4.37 and 4.38 respectively. The unique relationships in both these plots indicate that the assumptions (i) and (ii) above are valid for the correlation of the test results. Furthermore, since q*, ϵ* and q* v* are unique the relationship between ϵ* and v* is also unique.

Note: Since the voids ratio e_o of the three specimens will be different at the end of consolidation under the three isotropic stresses, it follows from equation 4.3 that the value of p_e for each of the three specimens will be different at any particular $(\frac{q^*}{p^*})$. Hence the $(\frac{q^*}{p_e}, \frac{p^*}{p_e})$ curves of the three specimens will not be unique.

4.6.6 The experimental observations on fully drained tests AF, Z and AD at cell pressures of 30, 60 and 90 psi respectively after 1-D consolidation to 22 psi

Fig.4.39 illustrates the variation of ϵ with $\frac{q}{p}$ for the fully drained tests carried out from the three isotropic stresses of 30, 60 and 90 psi. These characteristics are all different. A similar phenomenon was also noted in the $(\frac{q}{p}, v)$ characteristics in Fig.4.40. In both figures the specimen sheared from the 30 psi isotropic stress had smaller strains than the other two specimens. Fig.4.41 shows that the $(\frac{q}{p_e}, \frac{p}{p_e})$ characteristics of the three specimens are also different. Similar to the results of constant p tests, these drained tests also indicate that for the test at 30 psi, the value of $\frac{p}{p_e}$ corresponding to any value of $\frac{q}{p_e}$ is larger than those for the other two specimens. The (v, ϵ) characteristics of the three specimens are illustrated in Fig.4.42. In this the (v, ϵ) characteristic for the specimen AF (initially consolidated at 30 psi) is different from those of specimen Z (60 psi) and specimen AD (90 psi). It will be shown in the next section (4.6.7) how these results may be correlated.

4.6.7 The correlation of fully drained tests on specimens sheared from isotropic stresses of 30, 60 and 90 psi after initial 1-D consolidation under a stress of 22 psi

The assumptions now made for the correlation of the stress-strain behaviour of the fully drained tests are the same as those mentioned in section 4.6.5 for the correlation of constant p test results.

In Figs.4.43 and 4.44 the points A, B and C correspond to the strains ϵ_{Ko} and v_{Ko} experienced by the three specimens in reaching the stress state q_{Ko}. The results are replotted in the (q^*, ϵ^*) and (q^*, v^*) spaces in Figs.4.45(a) and (b) respectively. These results are then presented in the $(\frac{q^*}{p^*}, \epsilon^*)$ plot and $(\frac{q^*}{p^*}, v^*)$ plot in Figs.4.46(a) and (b). The unique relationships in these plots indicate that the relationship between v^* and ϵ^* must be

unique and furthermore that the assumptions (i) and (ii) made in section 4.6.5 are valid for the correlation of the fully drained test results. Since the voids ratio of the three specimens were different at the three isotropic stresses, the quantity p_e, for the three specimens will be different at any particular $(\frac{q^*}{p^*})$, therefore the $(\frac{q^*}{p_e}, \frac{p^*}{p_e})$ curves for the three specimens will not be unique.

4.6.8 The $(\frac{q}{p_e}, \frac{p}{p_e})$ characteristics of specimens sheared with different applied stress paths from three isotropic stress states

Figs.4.47(i)-(iii) show the experimentally observed $(\frac{q}{p_e}, \frac{p}{p_e})$ characteristics for three types of tests (undrained, constant p and fully drained) at each of the three isotropic stresses of 30, 60 and 90 psi. All the samples had been previously 1-D consolidated under a vertical stress of 22 psi. The maximum deviation between the three types of stress paths is observed in the case of the tests on the samples consolidated at 30 psi isotropic stress. The extent of this type of deviation diminishes as the isotropic stress increases from 3o to 90 psi. The behaviour at 90 psi is approximately unique for all three stress paths. These observations may be compared with those of Roscoe and Thurairajah (1964) presented in section 1.3.5. They also noted a difference in the state boundary surface followed by the drained and undrained specimens of Kaolin in the alternating plot $(\frac{q}{p}, \frac{1}{p} \exp(\frac{e_a - e}{\lambda}))$ which is similar to the $(\frac{q}{p_e}, \frac{p}{p_e})$ plot. The one dimensional stress used in the preliminary preparation of his samples (Thurairajah (1961)) was of the order of 33 psi which is larger than the 22 psi used by the present Author. Hence the differences observed by Roscoe and Thurairajah (1964) in the $(\frac{q}{p_e}, \frac{p}{p_e})$ plot of the drained and undrained state boundary surfaces in triaxial specimens of Kaolin can be attributed to the predominant effect of the initial 1-D stress.

4.7 The effects of time on the stress-strain behaviour of Kaolin

4.7.1 General Introduction

In this section the effects of time on the stress-strain behaviour of Kaolin are investigated both during undrained tests and fully drained tests. The undrained test results are studied in relation to the recent investigation made by Ting (1968). The investigation of the stress-strain behaviour during drained

tests is complementary to that of Walker (1967) whose experiments were carried out in the SSA as well as in the triaxial apparatus. No attempt has been made to repeat the survey of literature on time effects as this has already been done by Thompson (1962), Walker (1967) and Ting (1968). For a reliable study of the time effects in fully drained and undrained tests it will be necessary to make considerable improvements in the present experimental techniques. These techniques should incorporate facilities to measure (i) the distribution of stresses at the end plattens (ii) local pore pressures and (iii) the local strains using the lead shot technique; all measurements being required to a high degree of accuracy. If local strains and local pore pressures are measured, then it is possible to study the effects of time during the pore pressure dissipation in drained tests, and the pore pressure equalisation in undrained tests. Experimental observations provided in later sections of this chapter, indicate that the deformation of Kaolin can be considered to be in two phases, (i) time dependent (where the effects of time on the strains are predominant) and (ii) time stable (where the effects of time are small and can be allowed for by linear logarithmic relations). The time dependent range of Kaolin for the $1\frac{1}{2}$ inch diameter samples was found to be small, and if this region is to form a subject for detailed investigation it would be desirable to select a clay which had a larger time dependent range than that of Kaolin.

4.7.2 The experimental observations in the time study of undrained tests.

Figs. 4.48 and 4.49 illustrate the (ϵ, t) and the (u,t) characteristics for several increments of stress ratio applied at different stress levels in a continuous undrained test (T_4), at 60 psi cell pressure. The stress ratio ($\eta = \frac{q}{p}$) at the end of each increment of stress is indicated along each curve. The time required for the shear strain to reach a stable value increases with increase of stress ratio and is about 500 mins. for $\eta = 0.57$ and after about 1500 mins. for $\eta = 0.78$. The time taken for the pore pressure to reach a stable value also increases with increase of stress ratio being 400 and 800 mins. for $\eta = 0.57$ and 0.78 respectively.

The shear strains and the pore pressures can be expressed as functions of time and of the shear stress i.e.

$$\epsilon = \phi(q,t) \qquad 4.8$$

and $u = \chi(q,t)$ 4.9

A detailed investigation carried out by Ting (1968) indicated that equation 4.7 can be expressed as

$$\epsilon = \phi_1(q) + \phi_2(q) \cdot \phi_3(t) \quad 4.10$$

For specimens sheared under undrained conditions from the same isotropic stress $p_o = p_e$ (a constant) and therefore

$$\epsilon = \psi_1\left(\frac{q}{p_e}\right) + \psi_2\left(\frac{q}{p_e}\right) \phi_3(t) \quad 4.11$$

To the author's knowledge no attempts have been made so far to study the form of equation (4.9) for the variation of pore pressure with time. However if equation 4.9 assumes a form

$$u = \chi_1\left(\frac{q}{p}\right) + \chi_2\left(\frac{q}{p}\right) \cdot \chi_3(t) \quad 4.12$$

then it is evident that the elimination of time from equations 4.11 and 4.12 would give

$$\epsilon = F(q,u) \quad 4.13$$

Two of the three equations 4.11, 4.12 and 4.13 are sufficient to describe the variation of pore pressure and the shear strain during the time dependent range. These equations may then be used, as shown below, to describe the deviations in strain and pore pressure during the time dependent phase for the undrained component of shear strain used in the stress-strain theory of Roscoe and Poorooshasb (1963) or that of Roscoe and Burland (1968). At present pore pressures are only measured at the ends of the specimens, and there has been no guarantee that these measured values of pore pressures represent the true magnitude throughout the sample during the time dependent phase. In an attempt to determine the form of the functions in equation 4.12 (which describes the variation of pore pressure with time) the author tried to use semiconductor pressure probes for the local measurements of pore pressures. Unfortunately all six of these very expensive transducers were not satisfactory and attempts are still in progress at Cambridge to develop suitable replacements.

4.7.3 The effects of time on fully drained tests

The effects of time on the observed stress-strain behaviour in fully drained tests will now be considered in the next four sub-section.

(i) The uniqueness of stress-strain behaviour in the time stable regions

Figs.4.50 and 4.51 show the (ϵ, t) characteristics and the (v,t) characteristics corresponding to stress increments at various levels of deviator stress, in a fully drained test at 60 psi. The observations indicate that beyond a period of about 700 minutes for each increment of deviator stress the volumetric strains and the shear strain reach an approximately constant value, but nevertheless are still increasing at a very small rate with respect to time.

The uniqueness of the stress-strain behaviour in a continuous stress controlled drained test was investigated by carrying out fully drained tests at 60 psi cell pressure with load increment durations of $\frac{1}{2}$ day, 1 day and 2 days respectively. The sizes of the load increments used and the methods of testing adopted were identical in all three tests. Figs.4.52 to 4.54 illustrate the ($\frac{q}{p}$,v), ($\frac{q}{p}$, ϵ) and the ($\frac{q}{p_e}$, $\frac{p}{p_e}$) characteristics of all three tests. From these observations it is apparent that for load increment durations of half a day or greater, the stress-strain behaviour corresponding to continuous tests performed with constant load increment durations, is approximately unique. These observations are in agreement with those of Walker (1967). He performed stress-controlled drained tests in the S.S.A and came to the conclusion that the stress-strain curves obtained from a continuous test (in which sufficient time had been allowed for the dissipation of pore pressure after each increment has been applied) is unique and is independent of the load increment duration.

For stress paths lying between the undrained and drained paths, this unique stress-strain behaviour can be predicted using the incremental stress-strain theory of Roscoe and Poorooshasb (1963) or the modified theory of Roscoe and Burland (1968). However if the variations of volumetric and shear strains with time have to be predicted during any increment which is applied for a long time these secondary strains should be added to those predicted by the above theories. These additional secondary strains will now be investigated for a fully drained test.

(ii) <u>Secondary shear strains and volumetric strains as linear functions of log t in the time stable region</u>

The variations of shear strains and volumetric strains with respect to log t at various levels of stress ratios ($\eta = \frac{q}{p}$) are shown in Figs.4.55(a-h) and 4.56(a-h) respectively during a

fully drained test (R). Similar observations on Kaolin have been noted during 1-D consolidation by Thompson (1962) and during fully drained tests in the S.S.A and in the triaxial apparatus by Walker (1967). These linear relationships can be expressed as

$$\frac{dv}{d(\log t)} = \mathcal{F}(\eta) \qquad 4.14$$

and

$$\frac{d\epsilon}{d(\log t)} = \Lambda(\eta) \qquad 4.15$$

The functions $\mathcal{F}$ and $\Lambda(\eta)$ are plotted against η in Figs.4.57 and 4.58. The function $\mathcal{F}(\eta)$ is approximately a constant and is independent of the stress levels. The function $\Lambda(\eta)$ varies linearly with η and can therefore be expressed as

$$\Lambda(\eta) = m.\eta \qquad 4.16$$

where m is a constant.

Equations 4.14, 4.15 and 4.16 would give

$$\frac{dv}{d\epsilon} = \bar{m}.\frac{1}{\eta} \qquad 4.17$$

where $\bar{m} = \left(\frac{\mathcal{F}}{m}\right)$.

The equations 4.14, 4.15 and 4.16 are the same as those observed by Walker in the triaxial apparatus. Walker used $\left(\frac{\tau}{\sigma}\right)$ as a parameter in the S.S.A and his corresponding relations were of the form

$$\left.\begin{aligned} \frac{dv}{d(\log t)} &= \mathcal{F}^*\left(\frac{\tau}{\sigma}\right) \\ \frac{d\epsilon}{d(\log t)} &= \Lambda^*\left(\frac{\tau}{\sigma}\right) \\ \mathcal{F}^*\left(\frac{\tau}{\sigma}\right) &= \mathcal{F}^* \quad \text{a constant} \\ \Lambda^*\left(\frac{\tau}{\sigma}\right) &= m^*\left(\frac{\tau}{\sigma}\right) \end{aligned}\right\} \qquad 4.18$$

where m* is a constant

(iii) <u>A note on equation 4.17</u>

It is interesting to note that equation 4.17 which describes the dilatancy rate $\left(\frac{dv}{d\epsilon}\right)$ during the deformation in the time stable region is of the form

$$\left(\frac{dv}{d\epsilon}\right)_{\text{time stable}} = \bar{m}.\frac{1}{\eta} \qquad 4.17$$

where the dilatancy rate is only a function of the stress ratio. It is appropriate at this point to compare equation 4.17 with the corresponding variation of $(\frac{dv}{d\epsilon})_\eta$ with η during anisotropic consolidation. It is shown in Chapter 6 that $(\frac{dv}{d\epsilon})_\eta$ during anisotropic consolidation can be expressed as

$$(\frac{dv}{d\epsilon})_\eta = (\frac{\lambda}{\lambda - k}) \quad (\frac{M^2 - \eta^2}{2\eta}) \qquad 4.19$$

where $\lambda = 0.26$, $k = 0.06$ and $M = 0.9$ (for Kaolin)
Thus the dilatancy rate $(\frac{dv}{d\epsilon})$ during anisotropic consolidation and during the secondary consolidation are both only dependent on the stress ratio.

(iv) <u>The incremental stress-strain theory of Roscoe and Poorooshasb (1963) in the time dependent and the time stable regions.</u>

For stress paths satisfying the conditions $dv \geq o$ and $d\eta \geq o$, the stress-strain behaviour in a continuous test can be described as

$$d\epsilon = (d\epsilon)_{undrained} + (\frac{d\epsilon}{dv})_\eta \cdot dv \qquad 4.7 \text{ bis}$$

If equations 4.13 and 4.12 are valid for the deformation behaviour in undrained tests in the time dependent region then

$$(d\epsilon)_{undrained} = \frac{\partial F}{\partial q} \cdot dq + \frac{\partial F}{\partial u} \cdot du \qquad 4.20$$

where $u = \chi_1(\frac{q}{p}) + \chi_2(\frac{q}{p})\ \chi_3(t)$ 4.12 bis

The equations 4.20 and 4.12 can be considered as a particular case of equation 4.7 when $dv = o$. Thus for the undrained case a prediction of the time dependent stress can be made. However for $dv > o$, the validity of equation 4.7 in the time dependent (i.e. pore pressure dissipation) range has not been verified. The validity of equation 4.7 during pore pressure dissipation may be ascertained by obtaining local measurements of the pore pressures and the strains. From these measurements it would be possible to determine the variation of $(\frac{dv}{d\epsilon})$, dv, u, and $d\epsilon$ with time and hence if equation 4.20 is valid for the undrained component of shear strain equation 4.7 may then be shown to be valid, or otherwise, for the drained case.

Now considering the time stable region in which deformations occur under constant stress it has been shown that

$$dv = \mathcal{J}\, d(\log t) \qquad 4.14 \text{ bis}$$

for $dv > o$ where $\mathcal{J}$ is a constant.

and $d\epsilon = \Lambda(\eta)\, d(\log t)$ 4.15 bis

where $\Lambda(\eta) = m \cdot \eta$. Hence the strains may be predicted during this phase of deformation.

4.8 The effect of load increment size on the stress-strain behaviour in fully drained tests on specimens 1-D consolidated to 22 psi and subsequently isotropically consolidated to 60 psi.

4.8.1 General

The experimental observations presented in this dissertation are based on stress controlled triaxial tests. In studying the effect of stress paths on the stress-strain behaviour, it is essential to keep the magnitude of pore pressure associated with a stress increment, as low as possible. Fully drained compression tests at constant cell pressures with large increments can cause high pore pressures to develop and hence the specimen will be virtually subjected initially to an undrained stress path and subsequently to a constant q stress path. Though these types of stress paths are more likely to occur in engineering practice they would give a totally misleading picture in the laboratory if it was there assumed that they referred to the stress-strain behaviour under fully drained conditions. The stress path followed by a test specimen subjected to a large increment is indicated in Fig.4.59, it is evident that the specimen has been subjected to stress paths which are totally different from that which had been intended. Also the stress ratio at the end of the undrained phase is higher than the stress ratio at the end of the constant q phase. Hence the specimens would have been subjected to a higher stress ratio, than the recorded value, at the end of its pore pressure dissipation. In this section the effects of the load increment size on the stress strain behaviour of specimens (sheared under fully drained conditions from a cell pressure of 60 psi) will be investigated. The stress history of the specimens were identical prior to shear, namely 1-D stress of 22 psi and isotropic stress of 60 psi.

4.8.2 Experimental observations illustrating the effects of load increments size on fully drained tests

Experimental observations on four fully drained tests Z, R, X and Y are presented in this section. In test Z stress increments of 0.7 psi were applied at 3 hour intervals. Five stress increments were applied during a day and the equilibrium readings

were taken before applying the next increment and the following morning. In test R stress increments of 7 psi were applied at two day intervals. Stress increments of 14 psi were applied in text X at two day intervals and in test Y, a single stress increment of 26 psi was used. The (q, ϵ) characteristics of the specimens are as shown in Fig.4.60. It is noted that the shear strain corresponding to any particular deviator stress is different for each of the tests indicating that the magnitude of the applied stress increment has an important effect on the results obtained in drained tests. The results indicate that ϵ is path dependent. The (q, ϵ) characteristic of the specimen Z before and immediately after the application of load increments is illustrated in Fig.4.61. It is evident that the difference in strains caused by each stress increment is so small that the deviations of shear strains before and immediately after the application of the stress increment are within the limits of the experimental accuracy.

Fig.4.62 illustrates the (q,v) characteristics of all the specimens. The (q,v) characteristics are found to be different. There is no orderly behaviour in the (q,v) characteristics of the specimen. One would expect this discrepancy as it has already been established, in section 4.6.8 and Fig.4.47, that the pore pressures developed in undrained tests and the volumetric strains experienced in drained tests are affected by the initial shear stress effects caused by the preliminary 1-D consolidation. This is illustrated in Fig.4.63 where the state paths followed by specimens with the larger increments (namely R, X and Y) always lie between the undrained state path and the path followed by the specimen (namely Z) which had a large number of smaller increments. It is suggested that if the effect of the initial shear stress history had not been there, then there would have been a unique (q,v) characteristic independent of the load increment size.

Figs.4.64 and 4.65 illustrate the (q,v) characteristics and the $(\frac{q}{p_e}, \frac{p}{p_e})$ characteristics corresponding to test Z in which the increments were small. It is again observed that the increment size is so reduced that the stress-strain behaviour before and immediately after the application of the stress increments lie within a narrow band. A similar increment size was selected for all subsequent tests in which the stress path effects were investigated.

4.9 The effects of sample size on the stress-strain behaviour

Most of the experimental observations presented in this thesis were made during triaxial tests carried out on 1.5 inch diameter by 3 inch high specimens. A few tests were carried out with 4 inch diameter by 4.5 inch high samples. The ratio of the volumes of the two sizes of samples is 1:9.5. In some respects it would be advantageous if the size of the specimen were to be reduced below the conventional size of 1.5 inch diameter and 3 inch high, since smaller specimens would reduce the maximum drainage path and hence the total period required for a test, especially a drained test. In fact the maximum drainage path in samples in the S.S.A is very much smaller than in conventional triaxial specimens. The stress-strain behaviour as observed in a 1.5 inch diameter specimen (T.1) will now be compared with that obtained for a 4 inch diameter specimen (OB). The increment sizes used in both tests were such that the increment of deviator stress was approximately the same for each. Both specimens were initially prepared under the same one dimensional stress of 22 psi. The 1.5 inch diameter specimen was sheared after isotropic consolidation at 25 psi and the 4 inch diameter specimen was sheared after isotropic consolidation at 30 psi. Ideally the two specimens should have been sheared from the same isotropic stress. The author did not have a test result at 30 psi on the 1.5 inch diameter sample with the same stress increment size as that of the 4 inch diameter sample. Figs.4.66 - 4.68 illustrate the behaviour of the two specimens in the $(\frac{q}{p}, v)$, $(\frac{q}{p}, \epsilon)$ and $(\frac{q}{p_e}, \frac{p}{p_e})$ plots respectively. The behaviour of the two specimens was approximately the same, indicating that the stress-strain behaviour from small laboratory specimens can be used to predict the strains for larger size specimens. The small differences which do exist can be attributed to the effect of the 1-D consolidation i.e. the ratio of the 1-D to isotropic stress is slightly different for the two specimens. This statement is, of course, only based on tests with a volume factor of 1 to 9.5. For the measurements of local pore pressures and local strains, it may be necessary to increase the size of specimen even further.

4.10 The effect of end restraint on the stress-strain behaviour on fully drained tests

Figs. 4.69 - 4.71 illustrate the behaviour of two specimens (contained between the frictional ends and the lubricated ends) in

the $(\frac{q}{p}, v)$, $(\frac{q}{p}, \epsilon)$ and $(\frac{q}{p_e}, \frac{p}{p_e})$ plots.

The average stress-strain behaviour of the two specimens are similar in spite of the discrepancies observed in the $(\frac{q}{p_e}, \frac{p}{p_e})$ plot. This difference may be attributed to the marked nonuniformity in strains noted during shear in Chapter 3 for specimens contained beteen frictional ends.

CHAPTER 5

THE PEAK STRESS ENVELOPES AND THEIR RELATIONS TO THE CRITICAL STATE LINE.

5.1 Introduction

In this chapter the data corresponding to the peak deviator stress condition of tests with a large variety of imposed stress paths is presented and is discussed in detail in relation to the critical state concept of Roscoe, Schofield and Wroth (1958) and The Hvorslev criterion of failure. The critical state concept and the associated previous experimental work on clays is summarised in section 5.2. A detailed study of the effects of miscellaneous test conditions such as (i) end restraint (ii) initial 1-D consolidation stress (iii) subsequent isotropic consolidation stress and (iv) the load increment duration is made in section 5.3. In the following section 5.4, all tests starting from an isotropic consolidation state (p_o) are classified into four types depending on the increments of mean normal stress and deviator stress and it is shown that a unique peak stress envelope exists in the (Δe_f, p_f, q_f) space for three of the four types of tests. p_f and q_f correspond to the values of p and q at the peak deviator stress condition and Δe_f is the change in voids during the shear phase of a test as measured from the condition after isotropic consolidation under a stress p_o. This peak stress envelope is shown to coincide with the conventional critical state line for $p_f \geq p_o$ and to be a Hvorslev type envelope for $p_f < p_o$. In section 5.5, experimental results are presented which confirm the uniqueness of the peak stress envelope for a wide range of isotropic stresses. The results of the three types of tests at all isotropic stress levels are then correlated in section 5.6 in the non-dimensional 3-D space (Δe_f, $\frac{p_f}{p_o}$, $\frac{q_f}{p_o}$), in which they lie on a unique curve. As before this unique curve coincides with the conventional critical state line for $\frac{p_f}{p_o} \geq 1$, and is found to lie on a Hvorslev type surface for $\frac{p_f}{p_o} < 1$. The results of a series of miscellaneous tests in each of which there are several changes of direction of the imposed stress path prior to failure are presented in section 5.7. They show that for specimens subjected to stress paths with $\Delta p < o$ from $p > p_o$ (i) the peak stress point lies on the unique (Δe_f, $\frac{p_f}{p_o}$, $\frac{q_f}{p_o}$) curve, provided the specimen has undergone volumetric yielding during the phase in which $\Delta p < o$ and (ii) the

peak stress point lies on a series of (Δe_f, p_f/p_o) and (Δe_f, q_f/p_o) curves originating from the same unique curve (mentioned in (i) above), provided the specimen has experienced only elastic volumetric strains during the phase in which $\Delta p < o$. The projections of these curves on the ($\frac{q_f}{p_o}$, p_f/p_o) plane being still unique.

5.2 The critical state concept and the associated previous experimental work on clays

The critical state concept was outlined at the beginning of section 1.3.7 and a typical critical state line in (p,q,e) space was represented by curve AB in Fig.1.3. In the previous section (1.3.5) detailed evidence was presented by Roscoe and Thurairajah (1964) concerning the uniqueness of the state boundary surface for wet clays. In this evidence they also discussed at some length, the uniqueness of the critical state line for a number of saturated remoulded clays. The majority of the evidence was restricted to results of undrained and fully drained (constant cell pressure) compression triaxial tests, though some data from S.S.A tests was presented for Kaolin. In all cases the critical state line from the drained tests appears to differ slightly from that of the undrained tests, though both lines appear to have the same slope on an (e, log p) plot. Roscoe and Thurairajah presumed that the undrained data was more reliable than the drained, since the critical state was achieved at smaller strains in the undrained than in the drained tests. From these two types of test results, they suggested that there was in fact a unique critical state line for both these tests and this line was best represented by the undrained data. They implied at the large stress in the drained tests the samples were probably not deforming uniformly, nor were the stresses so reliable as in the undrained tests. The author therefore decided to investigate this phenomenon fully by studying in detail the strain patterns during triaxial tests in which the effect of each variable was considered in turn. Some of these data have been presented in Chapter 4, but most of these were concerned with the behaviour of the samples at all stress levels prior to the attainment of peak deviator stress. If the Cambridge concepts of the critical state line are correct then for wet clays the peak stress should coincide with the attainment of the critical state. In this chapter a detailed study will be made of the results at peak deviator stress (q_f) for a wide variety of imposed stress paths

with the corresponding state paths on an (e, log p) plot ranging between AL and AD in Fig.5.12. In all the author's tests, the samples were sheared from a state of virgin consolidation, such as represented by point A in Fig.5.12. Henkel (1959) had carried a series of drained and undrained tests on samples with varying degree of overconsolidation from the same initial maximum virgin preconsolidation pressure $(p_o)_{max}$. He confirmed the unique critical state concept for normally consolidated samples, but suggested for a given $(p_o)_{max}$ the peak stress was observed for overconsolidated samples on another unique curve which deviated progressively from the critical state line as the degree of overconsolidation was increased. Roscoe, Schofield and Wroth (1959) argued that Henkel's overconsolidated samples became unstable when they attained the peak value of q_f and that only the portion of the sample within the thin failure zone would then proceed to the critical state during subsequent deformation under inherently unstable condition. Since in the author's stress controlled tests it is not possible to study conditions beyond the attainment of peak deviator stress the work in this chapter will be restricted to peak stress conditions and in cases where samples contract in volume during shear it can be reasonably expected that these will coincide with the attainment of critical state. Before presenting the peak stress data for a very wide variety of stress paths, the results of some tests specially devised to study the effect of (i) end restraint (ii) the initial 1-D consolidation stress (iii) the subsequent isotropic consolidation stress and (iv) load increment duration, on the observed peak stresses will be outlined.

5.3 The effect of miscellaneous test conditions on the observed peak stresses

(i) End restraint

To study the effect of end restraint three specimens were prepared under (as nearly as possible) identical conditions, namely 1-D consolidation to 22 psi followed by consolidation under isotropic stress to 60 psi. Each sample was then subjected to shear under fully drained (constant cell pressure) conditions, but the first sample (T) had "rough" ends, the second (R) conventional lubricated ends and the third (Q) enlarged ends with rubber membranes. Details of these end conditions are given in section 2.2. The peak stresses observed in these three tests,

which were nearly as possible identical except for end restraints, are given in Table 5.1. In this table p_f is the value of p, when q attains its peak value q_f. It can be seen that the value of (q_f/p_f) for all three tests is virtually identical (within ± 2 p.c.), though the value of q_f ranges from ± 5 p.c. of the mean value. If it is assumed that the cohesion of the clay is zero, the value of $\phi = \tan^{-1}(q_f/p_f)$ ranges from 19.2° to 20.0°. When combined with the evidence provided by Bishop and Green (1965) for sand, it would appear that end restraint does not have a significant effect on the value of (q_f/p_f), for Kaolin specimens with 2:1 height to diameter ratio.

(ii) The initial one-dimensional consolidation stress

To study the effect of the magnitude of the preliminary one-dimensional consolidation stress used in the preparation of samples from a slurry three samples were prepared under 1-D stresses of 11, 22 and 55 psi respectively. These samples were then isotropically consolidated under 60 psi, and subsequently sheared under fully drained condition (constant cell pressure) with conventional lubricated ends. The observed peak stresses and stress ratios are presented in Table 5.2. The result for even test AB in Table 5.2 should not be compared directly with those presented in Table 5.1, since the former only had half a day load increment duration, while for the latter each increment was applied for two days. However it is interesting to note that the value of (q_f/p_f) for tests AU and AB are very similar to those in Table 5.1. In test AR the low value of q_f and especially q_f/p_f correspond to an unexpected premature failure of the sample which cannot be explained by the author. According to the discussion in section 4.4.3 the value of q_f should have increased with increase in the 1-D stress as observed in tests AU and AB, but the effect on (q_f/p_f) does not appear to be very significant

(iii) Isotropic consolidation stress

Four samples were subjected to preliminary 1-D consolidation under a vertical stress of 22 psi and then isotropically consolidated to 30, 60, 90 and 120 psi respectively. They were subsequently sheared under fully drained conditions (constant cell pressure) and the peak stresses and stress ratios are quoted in Table 5.3. The results indicate that the peak stress ratio tends to decrease from 0.8 at 30 psi to 0.735 at 120 psi. The end points when plotted in Fig.5.1 illustrate linear relationship

between q_f and p_f with a mean value of (q_f/p_f) of 0.765 corresponding to a ϕ of 19.5. The slightly higher values of (q_f/p_f) observed in Table 5.3 compared to those in Table 5.1 may be in part described not only to the difference in isotropic stress but also to the effect of the magnitude of the stress increments. This can be best seen by comparing test Z with test R, since the only difference in these tests was in test Z each increment was about 0.5 psi (five increments per day) while in test R the increments were about 5 psi at 2 day intervals.

(iv) Load increment duration

Three identical specimens were prepared with preliminary 1-D consolidation under 22 psi followed by isotropic consolidation under 60 psi. These samples were then subjected to shear with identical load increments. But on the first sample the duration of each increment was 12 hours where-as for the other two specimens it was 24 and 48 hours respectively. It can be seen (table 5.4) that both the peak stresses tend to increase slightly with increase in load increment duration. However the variation of (q_f/p_f) is less than $\pm$ 1.5 p.c of the mean of the three values.

Any variation that can be detected in Table 5.1 to 5.4 inclusive, will be reduced to the minimum possible in the data presented and discussed in the remainder of this chapter, by insuring the following test conditions. All samples will have conventional lubricated ends, and will be subjected to an identical 1-D stress of 22 psi. The isotropic consolidation stresses were, for the majority of the samples 30, 60 or 90 psi respectively. The duration of each of the stress increments during the shear phase of all tests was approximately the same (5 increments per day) and their magnitudes proportional to the maximum isotropic stress used during sample preparation.

5.4 The relationship between peak stresses and change in voids ratio of specimens sheared from the isotropic stress state

In this section the peak stresses observed in 43 tests with widely differing stress paths will be presented and discussed. Each of these tests took 25 to 30 days to complete. In all the author carried out about 100 tests of this duration but in the other 57 was interested in the stress-strain behaviour prior to

failure as discussed in Chapters 4, 6 and 7. All the specimens of the 43 tests discussed in the present section were one-dimensionally consolidated to 22 psi, 25 were then isotropically consolidated to 90 psi, 4 to 30 psi, 9 to 60 psi, and the five remaining tests at miscellaneous cell pressures. Four of the tests on samples isotropically consolidated to 60 psi were extension tests which include and undrained test and tests with constant values of $(\frac{dq}{dp}) = \infty$, 3 and 1.5 respectively. All the other tests were compression tests, details of which will be given as each test is discussed in the subsections below.

The tests in the remaining subsections of this section 5.4, are divided for convenience into the following four types:-

Type 1 Tests on samples normally consolidated to an isotrppic preconsolidation pressure of p_o and subsequently sheared under stress paths in which $p \leqslant p_o$, and for compression tests $\Delta q \geqslant o$ for $q > o$. The full range of the paths of this type are illustrated in Fig.5.2 in which point A represents the samples after normal consolidation under the isotropic pressure p_o. The path AP corresponds to constant effective pressure test with $p = p_o$ throughout. The path AU represents an undrained test. The path AK corresponds to isotropic swelling and is shown as a curve based on the experimental evidence of the author and Loudon (1967). The region between paths AU and AK is generally only investigated in the laboratory by carrying out tests on heavily overconsolidated samples following paths of the type AKJ or ABC. However, as it is important in all practical problems involving reduction of p (say by excavation) paths of the type AE are investigated. Fortunately for most practical problems on normally consolidated clay the voids ratio of the soil will be decreasing as represented by the path AG.

Type 2 This type of test is identical to Type 1 except that $p \geqslant p_o$ and $\Delta p \geqslant o$. As shown in Fig.5.3, the point A corresponds (as in Fig.5.2) to samples after normal consolidation under the isotropic pressure p_o. The path AP again corresponds to a constant p test. The path AD represents a conventional fully drained test (with constant cell pressure so that $dq/dp = 3$) usually carried out in the laboratory. The path AQ corresponds to a test in which both the deviator stress and the cell pressure are increased. It is apparent that for stress paths lying between the line AH (parallel to the critical state line) and the p axis in Fig.5.3(a), it is not possible for a specimen to reach

the critical state. The points D^1 and Q^1 correspond to the states on the normal consolidation line NN', with the same value of p as those of D and Q respectively. Since the critical state line XX' is assumed to be parallel to the line NN', the change in voids ratio corresponding to state D from that of A, along the path AD can be considered to be due to the isotropic consolidation phase AD^1 and the constant p shear phase D^1D.

Type 3 In this type of test, as shown in Fig.5.4(a), after initial consolidation under isotropic stress p_o to point A, the samples were subjected to the condition $\Delta p \leqslant o$ during the initial phase of shear and then to the condition $\Delta p \geqslant o$, such that the specimens finally failed with $p > p_o$. At the point of reversal of Δp the samples were in a lightly overconsolidated state as shown in Fig.5.4(b). In a sense these samples were initially of Type 1 and then when p becomes greater than p_o, they reverted to Type 2 tests.

Type 4 In this type of test the samples were initially sheared with $p > p_o$ corresponding to Type 2 tests as represented by AW in Fig.5.5. Subsequently and prior to failure the value of p was reduced, while the deviator stresses were continuously increased (path WY) until the peak stresses were reached at Y. During the second phase it will be shown that the samples only behave as in Type 1 tests provided the relevant value of p_o for stage WY is taken to be p_o' as shown in Fig.5.5.

Note: For the extension tests the deviator stresses are negative and hence $\Delta q \leqslant o$ for all values of q.

5.4.1 The results of all compression triaxial tests from samples isotropically consolidated to 90 psi

The conditions at peak deviator stress observed in all the types 1, 2 and 3 tests that were carried out on samples initially isotropically consolidated to 90 psi are shown in Figs.5.6 to 5.8 inclusive. The imposed stress paths are shown in Fig.5.6 and are also given in greater detail in the tables A2.1, A2.2 and A2.3 in Appendix 2 for tests of Type 1, Type 2 and Type 3 respectively. The overall change in voids ratio Δe_f throughout each test, as measured from point A, are plotted against the value of p_f at failure in Fig.5.7. Failure is defined as the attainment of the maximum observed deviator stress q_f. It can

be seen that the peak stress points for all three types of tests lie on a unique curve. A similar unique curve for peak stress conditions of all the tests is obtained when $\Delta e'_f$ is plotted against q_f, as shown in Fig.5.8. The upper dotted line LPX in Fig.5.6 is obtained directly from the smooth curves drawn through the experimental data in Figs.5.7 and 5.8. It is evident in Fig.5.6 that for all stress paths of Types 2 and 3 that the peak stresses lie on a line PX which is remarkably close to the line OX of slope 0.7, which passes through the origin. It will be shown later that the line OX can be taken to be the critical state line. In contrast to this, the peak points for all tests of Type 1 lie above this line OX. In fact they approximate closely to a state line of slope 0.6 as represented by PL in Fig.5.6. This line PL, appears to be similar to a constant voids ratio section of the Hvorslev surface corresponding to a maximum preconsolidation pressure of p_o. It is in fact different since the voids ratios of the specimens are different for all values of the peak stresses along the line PL.

In his original work, Hvorslev expressed the equation of his surface by

$$\tau_f = \mu_o \sigma'_f + \mathfrak{Z} \exp(-B\, e_f) \qquad 5.1$$

where μ_o, $\mathfrak{Z}$ and B are fundamental soil constants τ_f, σ'_f and e_f are the peak shear stress, mean normal stress and voids ratio respectively in the plane of failure at the moment of failure. Roscoe, Schofield and Wroth's representation of Hvorslev's surface in (p,q,e) space is CDEF in Fig.1.3. The section of this surface by a constant e_f plane is given by UL in Fig.5.9; it can be expressed as

$$q_f = \bar{\mu} p_f + \bar{c} \qquad 5.2$$

where $\bar{c} = \bar{\mathfrak{Z}} \exp(\frac{-e_f}{\lambda})$

and $\bar{\mathfrak{Z}}$ is a constant.

i.e. $$q_f = \bar{\mu}\, p_f + \bar{\mathfrak{Z}} \exp(-\frac{e_f}{\lambda}) \qquad 5.3$$

The projection of the author's failure surface PL in the (q,p) plane shown in Fig.5.10 can be expressed as

$$q_f = M p_f + c(1 - \frac{1}{\bar{n}}) \qquad 5.4$$

where M is the slope of the critical state line OX, c is the magnitude of the apparent cohesion OL and $\bar{n}$ is the ratio of the maximum consolidation pressure p_o to the peak stress p_f.

i.e. $$\bar{n} = \frac{p_o}{p_f} \qquad 5.5$$

Equation 5.4 can also be expressedaas

$$q_f = Mp_f + \Sigma_1 \left\{\exp\left(-\frac{e_f}{\lambda}\right)\right\} \quad \left(1 - \frac{1}{\bar{n}}\right) \quad , 5.6$$

The peak stress envelope for Type 1 tests corresponding to the line PL in Fig.5.6, 5.7 and 5.8 is replotted in a $(\Delta e_f, \ln(n-1))$ space in Fig.5.11. It is evident that the relationship between Δe_f and $\ln(n-1)$ is linear in the range $1.2 \leqslant \bar{n} \leqslant 9$.

In this range the relationship may be expressed as

$$\Delta e_f - B_1 = B_2 \ln(n-1) \qquad 5.7$$

where, as will be shown later, B_1 and B_2 are fundamental soil constants.

Therefore $\bar{n} - 1 = \exp\left(\frac{\Delta e_f - B_1}{B_2}\right)$

i.e. $\bar{n} = 1 + \exp\left(\frac{\Delta e_f - B_1}{B_2}\right)$

and therefore $\left(1 - \frac{1}{\bar{n}}\right) = \dfrac{\exp\left(\frac{\Delta e_f - B_1}{B_2}\right)}{1 + \exp\left(\frac{\Delta e_f - B_1}{B_2}\right)}$

Therefore equation 5.6 can be expressed as

$$q_f = Mp_f + \Sigma_1 \left(\exp\left(\frac{-e_f}{\lambda}\right)\right) \left[\frac{\exp\left(\frac{\Delta e_f - B_1}{B_2}\right)}{1 + \exp\left(\frac{\Delta e_f - B_1}{B_2}\right)}\right] \qquad 5.8$$

for $1.2 \leqslant 1 + \exp\left(\frac{\Delta e_f - B_1}{B_2}\right) \leqslant 9$.

For the Type 1 tests, the failure strength q_f as given by equation 5.8, is found to be dependent on the critical state parameter M giving the frictional component, together with a cohesion component dependent on e_f and Δe_f.

It will be interesting at this stage to replot the unique relationships shown in Figs.5.7 and 5.8 on semi-logarithmic scale. Figs.5.12 and 5.13 represent the relationships in the $(\Delta e_f, \log p_f)$ and $(\Delta e_f, \log q_f)$ spaces respectively. In Fig.5.12 NN' represents the isotropic consolidation line passing through A(=90 psi). XX' represents a line parallel to the isotropic consolidation line and displaced along the p_o axis through A by a distance AP equivalent to the peak change in voids ratio Δe_f in a constant p test. The line LPX represents the unique curve from Fig.5.7.

AE is drawn asymptotic to the curve PL. It is observed that for pressures higher than 90 psi, the curve LPX coincides approximately with the line XX'. Also for pressures lower than 20 psi the curve LPX is coincident with the asymptotic AE. Hence from Figs.5.6 and 5.12 it can be concluded that for pressures higher than the maximum preconsolidation pressure, the unique curve LPX coincides with the critical state line as defined by Roscoe, Schofield and Thurairajah (1963). For pressures lower than the maximum preconsolidation pressure the slope of the curve LPX changes smoothly from a value of $\lambda = 0.26$ to the slope of the line AE which is approximately 0.07 and is distinctly higher than any value of k recorded by any worker at Cambridge (for whom the range is 0.02 to 0.06).

In Fig.5.13 the curve LPX corresponds to the unique curve in Fig.5.8. The line XX^1 is of the same slope λ (= 0.26) as that of the isotropic consolidation line in an (e, log p) plot. The line EE^1 has a slope of 0.09. Therefore the results in the $(\Delta e_f, \log q_f)$ plot also indicate that for pressures higher than the initial maximum consolidation pressure p_o the curve LPX is of slope λ.

It is therefore concluded that for pressures higher than the maximum consolidation pressure the behaviour of the specimens is in close agreement with the assumptions made by Roscoe, Schofield and Thurairajah that the "critical state line is parallel to the virgin compression line". However for pressures lower than this maximum the peak stress envelope deviates from the critical state line and will be discussed in the next section.

5.4.2 The peak stress envelope LPX and its relationship to the isotropic consolidation line

The following assumptions are made in the derivation of the function that describes the peak stress envelope in the $(\Delta e_f, \log p_f)$ plot, presented in Fig.5.12; (i) the peak stress envelope is smooth and continuous and (ii) the tangent $T'T''$ to the envelope at any arbitrary point T can be expressed in the form

$$\Delta e_f - \Delta e^* = - \lambda^* \left(\log \frac{p_f}{p_o}\right) \qquad 5.9$$

where Δe^* is the magnitude of the intercept AT'' made by the tangent with the ordinate AP in Fig.5.12 as measured from A and λ^* is the slope of the tangent $T'T''$. Figs.5.14(a) and (b) illustrate the variations of λ^* and Δe^* with $\left(\frac{p_f}{p_o}\right)$.

For $0 < \frac{p_f}{p_o} \leq 0.25$ $\Delta e^* = o$ and $\lambda^* = \theta$

and therefore equation 5.9 becomes

$$\Delta e_f = - \theta . \log \left(\frac{p_f}{p_o}\right) \qquad 5.10$$

for $0.25 \leq \frac{p_f}{p_o} \leq 0.7$

$$\Delta e^* = B_3 - B_4 \log \left(\frac{p_f}{p_o}\right) \text{ where}$$

B_3 and B_4 are soil constants

and $\lambda^* = \lambda \left(\frac{p_f}{p_o}\right)$

and therefore equation 5.9 becomes

$$\Delta e_f - B_3 = - \left(\lambda \frac{p_f}{p_o} + B_4\right) \log \left(\frac{p_f}{p_o}\right) \qquad 5.11$$

For $0.7 \leq \frac{p_f}{p_o} \leq 1$

$\Delta e^* = G_1$ (a constant which depends on λ-K)

and $\lambda^* = \lambda \left(\frac{p_f}{p_{max}}\right)$

and therefore equation 5.9 becomes

$$\Delta e_f - G_1 = - \lambda \left(\frac{p_f}{p_o}\right) \left(\log \left(\frac{p_f}{p_o}\right)\right) \qquad 5.12$$

Since $p_{max} = p_o$

For $\frac{p_f}{p_o} \geq 1$ $\Delta e^* = G_2$ (constant)

and $\lambda^* = \lambda$

and therefore equation 5.9 becomes

$$e_f - G_1 = - \lambda \log \left(\frac{p_f}{p_o}\right) \qquad 5.13$$

5.5 The peak points of specimens sheared after initial consolidation under isotropic stresses of (i) 60 psi (ii) 30 psi and (iii) miscellaneous pressures respectively

(i) 60 psi

The results of five compression and four extension triaxial tests after isotropic consolidation under 60 psi are presented in Figs.5.15, 5.16 and 5.17 in a manner similar to those already presented in Figs.5.6, 5.7 and 5.8 respectively for samples sheared from 90 psi. The data for these tests with point A corresponding to 60 psi a_{ve} is given in Table A2.4 in Appendix 2. In these diagrams the crosses represent the peak conditions in the extension tests while the circles refer to the compression tests. Furthermore the curves and lines plotted are not the mean through the experimental points but have been scaled directly from Figs.5.6, 5.7 and 5.8 in the ratio of 60 to 90 (i.e. the ratio of the initial isotropic stresses for each for a given change of voids ratio Δe_f). It is evident that the results of tests for samples prepared at 60 psi, are geometrically identical to those obtained from samples prepared at 90 psi.

(ii) 30 psi

The corresponding data for four compression tests on samples initially consolidated to 30 psi are presented in Figs.5.18, 5.19 and 5.20 and the data are presented in Table A2.5 in Appendix 2. As before, the lines and curves have been scaled directly from Figs.5.6, 5.7 and 5.8 respectively, except for the line OX in Fig.5.18. This line OX has slope of 0.8 compared to slopes of OX in all previous diagrams. These higher values may have been caused by the effects of any anisotropy developed during the 1-D consolidation to 22 psi not having been eliminated during the subsequent isotropic consolidation to 30 psi. In all other respects the agreement with the previous data presented in this subsection is entirely satisfactory.

(iii) Miscellaneous pressures

Time was only available to complete five tests, on samples, which had been initially consolidated under isotropic stresses other than 30, 60 or 90 psi. The imposed stress paths are shown in Fig.5.21 and the change in voids ratio Δe_f are plotted against p_f/p_o and q_f/p_o in Figs.5.22 and 5.23 respectively. The

data for these tests are given in Table A2.6 in Appendix 2. As before the curves and lines in these diagrams are not the mean through the experimental data, but are scaled from Figs. 5.6, 5.7 and 5.8 respectively. Again there is satisfactory agreement.

5.6 The unique peak stress curves in (Δe_f, p_f/p_o, q_f/p_o) space

The peak conditions for all the tests discussed in sections 5.4 and 5.5 are collected together and presented in Figs.5.24, 5.25 and 5.26 in the (q_f/p_o, p_f/p_o), (Δe_f, $\ln(p_f/p_o)$) and (Δe_f, $\ln(q_f/p_o)$) plots respectively. It will be noticed that the point lettered Z in each of these plots refers to a Type 4 test which is considered in section 5.7. It is evident that for all cases where (p_f/p_o) ≥ 1, the peak conditions coincide with the critical state, as represented by the ~~state~~ straight line portions PX of the curves LPX. Hence if (p_f/p_o) ≥ 1 the relevant equations are

$$q_f = M\, p_f \qquad 5.14$$

and $$\Delta e_f - G_1 = \lambda \log\left(\frac{p_f}{p_o}\right) \qquad 5.13 \text{ bis}$$

where G_1 is a fundamental soil constant representing the magnitude of Δe_f in a constant p test, i.e. the distance measured parallel to the e-axis between the normally consolidated line NN' and the critical state line XX' in an (e_f, p_f/p_o) or (e_f, $\ln(p_f/p_o)$) plot. On the other hand when $p_f/p_o < 1$, the peak conditions coincide with the unique curve LP, for which the relevant equations have already been derived namely equations 5.5, 5.7 and 5.8

$$\bar{n} = p_o/p_f \qquad 5.5 \text{ bis}$$

$$\Delta e_f - B_1 = B_2 \ln(\bar{n} - 1) \qquad 5.7 \text{ bis}$$

$$q_f = Mp_f + \Lambda_1 \left(\exp\left(-\frac{e_f}{\lambda}\right)\right)\left[\frac{\exp\left(\frac{\Delta e_f - B_1}{B_2}\right)}{1+\exp\left(\frac{\Delta e_f - B_1}{B_2}\right)}\right] \qquad 5.8 \text{ bis}$$

The unique curve LPX shown in Fig.5.24 to 5.26, is represented in 3-D (p,q,e) space in Fig.5.27, where the actual curve XPL corresponds to a p_o of 90 psi. As p_o varies, so do the positions of A,P and L; e.g. they may become A', P' and L' respectively. In Fig.5.27 the curves AP and A'P' correspond to the state paths followed in constant p tests.

When it is recalled that the Hvorslev equation (see equation 5.3) represents a constant e section of the state boundary surface C C' X' X in Fig.5.27 and since the Author's equation 5.8

reduces to Hvorslev's equation when $\Delta e_f = o$, then it is apparent that the curves PL (and P'L') lie on the Hvorslev state boundary surface.

5.7 The peak points of specimens in Type 4 tests

5.7.1 The peak stress point for specimens subjected to volumetric yielding during the shear phase in which $\Delta p < o$

A typical stress path imposed in a Type 4 test is shown in Fig.5.5 and is described in detail in section 5.4. In this type of test, the mean normal stress p is increased for the initial phase of shear (path AW) and is decreased for the subsequent shear phase (path WY). The Author has carried out only one such test (Test T_{12}). The path ABCD followed by this specimen T_{12} is shown in the (q,p), (Δe, log p) and (Δe, log q) spaces in Figs.5.27(a) to (c). The critical state line PX and the Hvorslev envelopes LP and L'P' corresponding to isotropic stresses of A(p_o = 90) and A' (p_o = 117.8 psi) are also shown in these figures. It is observed that the peak point D of the specimen T_{12} lies closer to the envelope L'P' than to the envelope LP. It is therefore concluded that the peak point of specimen subjected to stress path of Type 4 (where $\Delta p > o$ for the initial phase and $\Delta p < o$ for the final phase) ~~the peak point~~ lies on the Hvorslev envelope corresponding to an isotropic stress p_o equivalent to the maximum p ever experienced by the specimen, provided that the specimen had undergone volumetric yielding during the phase in which Δp was less than zero.

The peak point of the specimen T_{12} has already been plotted in Figs.5.25 and 5.26 in the (q_f/p_o, p_f/p_o), (Δe_f, p_f/p_o) and (Δe_f, q_f/p_o) spaces respectively. For this specimen p_o and Δe_f are taken to be the isotropic stress corresponding to A', and the ordinate A'C', respectively in Fig.5.27(b).

5.7.2 The peak points of specimens subjected to stress paths (i) that cause elastic volumetric changes and (ii) cycles of deviator stress

Figs.5.28(a) to (d) illustrate the stress paths followed by four specimens T_{17}, BR, BO and BS. These specimens were subjected to stress cycles, in which both the deviator stress and the mean normal stress have been considerably reduced. The peak points of these four specimens are shown in Figs.5.29, 5.30 and 5.31 in relation to the peak stress envelope LPX originally

shown in Figs.5.24, 5.25 and 5.26. It can be seen that the peak points for all specimens lie approximately on the projection of the Hvorslev envelope LP in the stress plane of Fig.5.29. However, the peak points are found to deviate from the envelope LP in Figs.5.30 and 5.31 which entail the parameter Δe_f. At present the Author has not sufficient information to explain these apparent deviations observed in the peak stress points of the samples subjected to stress cycles. Perhaps the envelope LP in Figs.5.30 and 5.31 is not unique. It is suggested for specimens which have been subjected to a previous stress ratio of η (as represented by B in Fig.5.30) with increasing deviator stress, and subsequently failed along stress paths which only cause elastic volumetric changes, that the corresponding Hvorslev envelope may be of the form L'P' in Fig.5.30. The line L'P' is of the same slope as the asymptotic AL and passes through B. The limiting positions of the envelope L'P' being LP'' and L'' P corresponding to $(\Delta e_\eta)_p$ being zero and $(\Delta e_f)_p$ respectively. Using the unique envelope for q_f/p_o and p_f/p_o given by LP in Fig.5.29 and the corresponding projection L'P' in Fig.5.30 relating Δe_f and p_f/p_o it is possible to obtain the projection in the $(\Delta e_f, q_f/p_o)$ space as represented by L'P' in Fig.5.31. The apparent shift $(\Delta e_\eta)_p$ in Fig.5.31 of the envelope P'L' is only a function of the plastic volumetric strain experienced by a specimen in a constant p test and therefore

$$(\Delta e_\eta)_p = f(\eta) \qquad 5.15$$

5.8 Conclusion on the data of peak stress conditions

Experimental observations have been provided in this Chapter to illustrate that the peak stress conditions coincide with the conventional critical state condition for values of $p_f/p_o > 1$. However for values of $p_f/p_o < 1$, the peak stress points are found to lie on a Hvorslev type curve in the $(q_f/p_o, p_f/p_o)$ space. This curve has a unique projection in the $(\Delta e_f, p_f/p_o)$ and $(\Delta e_f, q_f/p_o)$ for all specimens which undergo volumetric yielding during the shear phase in which $\Delta p < o$. For specimens which experience only elastic volumetric change, from states with stress ratio $\eta > o$, it appears that a series of parallel curves (starting from the original unique curve) exist in the $(\Delta e_f, p_f/p_o)$ and $(\Delta e_f, q_f/p_o)$ spaces. Further experimental work is needed before a proper interpretation can be made of these parallel curves.

The Author's main conclusions concerning the unique critical

state line and the unique Hvorslev peak stress curve have only been shown to be valid for the conditions of the conventional triaxial (axi-symmetric) type of test. In this system the intermediate principal stress is always equal to the major or minor principal stress and the principal axes of stress and strain are always coincident. These restrictions limit the general investigation of failure criteria for soils. Hambly and Roscoe (1969) have shown that under plane strain conditions the value of the intermediate stress σ_2' is always $K(\sigma_1' + \sigma_3')$ where K is a constant. Hence the main conclusions of the Author are likely to be applicable for plane strain conditions. Before these concepts can be extended to generalised 3-D stress systems an extensive series of tests must be carried out in a truly triaxial test apparatus in which each of the three principal stresses, or strains, can be varied independently. Such an apparatus is now being developed at Cambridge.

CHAPTER 6

THE THEORY OF PLASTICITY APPLIED TO THE DEFORMATION OF CLAYS

6.1 General Introduction

A considerable amount of theoretical knowledge on the stress-strain properties of plastically deforming materials has been developed in the last 30 years. The lack of experimental data on the mechanical properties of soils has limited the possibility of assessing the application of these theories for the mathematical description of their stress-strain behaviour. However with the experimental evidence available attempts have been made by various research workers to develop stress-strain theories for cohesive and cohesionless soils. The aim of this chapter is to study experimentally the mechanical behaviour of s-aturated remoulded Kaolin and to investigate how far its stress-strain behaviour may be explained by the concepts of plasticity. Four of the basic concepts in the theory of plasticity, as developed for materials such as metals, will now be discussed.

(i) The concept of a yield surface

For elasto-plastic materials the strains due to any increment of stress are often divided into two components; (i) elastic and (ii) plastic. A yield surface is defined in stress space as one which separates the regions of stress for which the strains are elastic from those for which the strains include a plastic component. For conditions of stress inside the yield surface an infinitesimal increment of stress can cause only elastic deformation. If the stress conditions correspond to a point on the yield surface and if the material is stable (as defined by Drucker (1959)) an infinitesimal increment of stress directed outside the yield surface produces only plastic strains for a perfectly plastic material and additional elastic strains if the material work hardens. An infinitesimal increment imposed inside the yield surface can only cause elastic deformation. Any work hardening effect due to plastic deformation can be accounted for by considering that the yield surface shifts or changes in shape. The possible shape of yield surface for Kaolin will be studied in section 6.2.1.

(ii) The strain hardening law

The strain hardening law is a relationship between the position of the yield surface in the stress space and the plastic strains experienced by the material in arriving at the specific stress point under consideration. Such a relationship for Kaolin will be investigated in section 6.2.2.

(iii) The flow rule

The flow rule provides a relationship between the strain rate vector during plastic deformation and the imposed stress vector. For increments of plastic deformation to occur the stress point should lie on the yield surface and the stress increment be directed outside this surface. If normality (Drucker (1959)) holds then the plastic strain rate vector at that point is normal to the yield surface. At any point on a smooth part of the yield surface the direction of the plastic strain rate vector is independent of the direction of the stress increment. However if the stress point is at a corner of the yield surface, the plastic strain rate vector can lie anywhere between the outward normals at points immediately adjacent to the corner. A flow rule can also be derived independently without any appeal to concepts such as normality, by equating the energy supplied to the energy stored and also dissipated in the material during plastic deformation (Roscoe, Schofield and Thurairajah (1963a p.219)). An experimental investigation of the direction of the strain rate vector at various levels of stress ratio is given in section 6.3.

(iv) The principal axes of stress, stress increment and strain increment

In the theory of plasticity it is often assumed that the principal axes of stress and strain increment coincide. An experimental investigation of this assumption can only be carried out in an apparatus in which the principal axes of stress and strain increment can be rotated and their directions recorded independently. At present the simple shear apparatus is the only apparatus in which the principal axes of stress and strain increment can be rotated while maintaining a uniform distribution of strain within the soil specimen. A detailed investigation carried out by Cole (1967) on Leighton Buzzard sand in this apparatus showed that the principal axes of stress and strain increment did coincide, for all except the initial stages of a

test. See also Roscoe, Bassett and Cole (1967).

6.2 The predictions of the Cam-clay theory and the Modified theory (Roscoe and Burland (1968))

In the Cam-clay theory of Roscoe and Schofield (1963) a simple mathematical expression for the yield surface of "wet clay" is derived using two basic concepts.

(i) the plastic strain rate vector at any point on the yield locus is normal to the yield locus.

i.e. $$\frac{d\epsilon^p}{dv^p} = -\left(\frac{dp}{dq}\right)_y \qquad 6.1$$

where the suffix y implies that the sample is yielding.

(ii) an energy balance where the external energy supplied $\delta E'$, is equated to the sum of the energy stored in the system δU and the energy dissipated during plastic deformation δW

i.e. $$(\delta E')_{ext} = (\delta U)_{stored} + (\delta W)_{dissip.} \qquad 6.2$$

Three features of equations 6.1 and 6.2 will now be considered.

(a) Stored energy per unit volume

Assuming that the energy stored in the system is only due to elastic volumetric strain Roscoe, Schofield and Thurairajah (1963), derived the following expression for the stored energy per unit volume of the soil

$$(\delta U)_{stored} = p\,\delta v^e \qquad 6.3$$

where δv^e corresponds to the elastic volumetric strain increment caused by a stress increment (δq, δp) from an initial stress condition (q,p).

(b) The expression for energy dissipation

The Cam-clay theory assumes that energy is only dissipated due to plastic shear distortion. Its magnitude due to an increment of stress (δq, δp) applied at the stress condition (q,p) is given by

$$(\delta W)_{dissipation} = M p\,\delta\epsilon^p \qquad 6.4(a)$$

where M is defined as the slope of the critical state line in a (q,p) plot and $\delta\epsilon^p$ is the plastic component of the incremental shear strain. On the contrary the modified theory of Roscoe and Burland (1968) assumes that energy can be dissipated both

due to plastic volumetric strains and plastic shear strains. The corresponding expression is

$$(\delta W)_{\text{dissipation}} = p\sqrt{(\delta v^p)^2 + M^2(\delta \epsilon^p)^2} \qquad 6.4(b)$$

where δv^p is the plastic component of the volumetric strain. The Cam-clay theory and the modified theory only differ in their expressions for energy dissipation.

(c) <u>The expression for $(d\epsilon^p/dv^p)$</u>

By assuming that the principal axes of stress and plastic strain increment coincide the expression for energy dissipation is

$$(\delta W)_{\text{dissipation}} = p\,\delta v^p + q\,\delta \epsilon^p \qquad 6.5$$

From equations 6.4(a) and 6.5

$$\frac{d\epsilon^p}{dv^p} = \left(\frac{1}{M-\eta}\right) \qquad 6.6(a)\ \text{Cam-clay theory}$$

and from equations 6.4(b) and 6.5

$$\frac{d\epsilon^p}{dv^p} = \left(\frac{2\eta}{M^2-\eta^2}\right) \qquad 6.6(b)\ \text{Modified theory}$$

(d) <u>The equation for the yield locus based on the normality and the energy concepts</u>

From equations 6.6(a) and 6.1

$$\left(\frac{dp}{dq}\right)_y = -\frac{1}{(M-\eta)} \qquad 6.7(a)\ \text{Cam-clay theory}$$

From equations 6.6(b) and 6.1

$$\left(\frac{dp}{dq}\right)_y = -\frac{2\eta}{M^2-\eta^2} \qquad 6.7(b)\ \text{Modified theory}$$

Equations 6.7(a) and 6.7(b) are the differential equations of the yield locus based on the Cam-clay theory and the modified theory respectively. Integrating equations 6.7(a) and (b) and substituting the condition $p = p_o$ when $\eta = o$, the equations for the yield locus become

$$q = M p \log\left(\frac{p_o}{p}\right) \qquad 6.8(a)\ \text{Cam-clay theory}$$

and

$$q = M p \left(\frac{p_o}{p} - 1\right)^{\frac{1}{2}} \qquad 6.8(b)\ \text{Modified theory}$$

Fig.6.1 illustrates the yield loci based on equations 6.8(a) and (b) for three different values of p_o. It has to be noted that the expression for the yield locus contains only one material constant i.e.M which is taken to be 0.9 for Kaolin for reasons which are discussed later.

6.2.1 The experimental investigation of the form of the yield locus

In this investigation specimens of Kaolin were taken to five different positions in the (q,p) stress plane and were then sheared in a triaxial (axi-symmetric) apparatus along the stress paths indicated in Figs.6.2(a) to (e).

(i) The application of stress cycles on specimen CD

In Fig.6.2(a), the specimen CD was isotropically consolidated to the stress point A and was then subjected to the stress cycles AB_1A, AB_2A.....AB_8A. The undrained stress path through A is represented by the dashed line. The stress cycles AB_1A, AB_2A, AB_3A, AB_4A and AB_5A lie inside the undrained stress path. Indicated along each path is the net plastic volumetric strain experienced by the specimen when reaching the stress state A at the end of each cycle. It is noted that at the end of each complete stress cycle the specimen has experienced plastic volumetric strains of 0.4, 0.34, 0.34, 2 and 0.45 p.c. respectively; i.e. for the five stress cycles imposed, the specimen has suffered a total plastic volumetric compressive strain of 3.53 p.c. The same specimen was then taken along the stress paths AB_6A and AB_7A. These two stress paths lie outside the undrained stress path through A. During the stress cycle AB_6A, the specimen experienced a plastic volumetric strain of 0.65 p.c. Hence the total plastic volumetric strain at the end of the stress cycle AB_6A is 4.19 p.c. During the constant p stress cycle AB_7A, the plastic volumetric strain experienced by the specimen is seen to be 0.7 p.c. bringing the total strain to 4.89 p.c. However, a specimen at the end of isotropic consolidation when sheared from A to B_7 along a constant p stress path would have undergone a plastic volumetric strain of 4.6 p.c. (as measured in the constant p test AO). From the experimental observations of tests CD and AO it is evident that (i) the plastic volumetric strain experienced by the specimen CD in reaching the stress state BZ, along the stress path AB_1AB_2.....B_6AB_7 is approximately the same as that experienced by the specimen AO along the direct stress path AB_7 and (ii) in test CD the majority of the plastic

volumetric strain i.e. 3.53 p.c. out of 4.89 p.c. occured for the stress cycles which lie inside the undrained stress path (shown dotted).

(ii) The application of stress cycles on the heavily over-consolidated specimen T_{19}

In this investigation specimen T_{19} was isotropically consolidated to 90 psi as represented by the point A in Fig.6.2(b). Subsequently it was allowed to swell back isotropically to 8 psi as represented by the point B so that it was heavily over-consolidated (degree of overconsolidation R = 11.2). The stress cycles BC_1B, BC_2B and BC_3B were then imposed on the specimen. The incremental plastic volumetric strain experienced by the specimen during the completion of each stress cycle is indicated along each stress path. It can be seen that the specimen has experienced large plastic volumetric strains for each of the stress cycles BC_1B, BC_2B and BC_3B. These results indicate that heavily overconsolidated specimens, having a maximum preconsolidation pressure (A), undergo large plastic volumetric strains when sheared along stress paths lying below the state boundary surface. At the end of the stress cycle BC_3B, the specimen was reconsolidated isotropically to the stress point A. At this stage it can be seen that the specimen had suffered a total plastic volumetric strain of 5 p.c. At the end of the stress cycle $ABC_1BC_2BC_3BA$ the specimen T_{19} was sheared along the stress path AD. The volumetric strain experienced by the specimen when sheared along this path was 2.3 p.c. giving a total of 7.3 p.c. for all paths. In test T_9 the corresponding volumetric strain when the specimen was sheared directly from the isotropic state i.e. from A to D, was 4.4 p.c. It is evident that the volumetric strain experienced by the specimen T_9 when sheared from A to D is considerably higher than the volumetric strain experienced along the same path by the specimen T_{19}, which had been previously subjected to the stress cycles. The total volumetric strain of specimen T_{19} at the stress state D was 7.3 p.c. This specimen had been subjected to a stress ratio of 0.66 (corresponding to C_2) during the cycle BC_2B which is higher than that corresponding to point D. Hence it is suggested that the volumetric strain experienced by the specimen T_{19} would only be identical to that of T_9, when the stress ratio of both specimens corresponding to 0.66 along the stress path AD.

(iii) The application of stress cycles on specimens CR and CF which have previously been subjected to shear

It was shown in the previous section that it is possible for specimens sheared from the normally, or overconsolidated, states along stress paths lying inside the state boundary surface to experience plastic volumetric strains. It would therefore be interesting to see if there are any particular stress regions in the (q,p) plane in which the application of stress cycles do not cause any plastic volumetric strains as assumed in the theories discussed above.

In Fig.6.2(c) the sample CR was isotropically consolidated to A (90 psi) and was then sheared to B (η = 0.7) along the stress path AB. From B, the sample was subjected to stress cycles BC_1B, BC_2B and BAB. The incremental plastic volumetric strain experienced by the specimen during each stress cycle is indicated along the stress path for that cycle. It is evident that the specimen has experienced a considerable amount of plastic volumetric strain for each of these three stress cycles. In Fig.6.2(d) the sample CF was sheared from the isotropic stress state A (p = 90 psi) to B (η = 0.25, p = 90 psi) along a constant p stress path. The specimen was then sheared to C (η = 0.25, p = 160 psi) along the stress path BC (with constant dq/dp). The sample CF was then subjected to stress cycles CD_1C, CD_2C, CD_3C.....CD_6C. The incremental plastic volumetric strain suffered by the specimen during each cycle of stress is indicated along the stress path for that cycle. It is again apparent that plastic volumetric strains of appreciable magnitude have been experienced by the specimen for all the six stress cycles. The tests described in this, and the previous, section have stress paths below the state boundary surface covering all regions except that represented by D_1CD_4 in Fig.6.2(e). This narrow region will now be investigated by applying stress cycles on specimen T_{16}.

(iv) The application of stress cycles on specimen T_{16}

In Fig.6.2(e) a sample T_{16} was isotropically consolidated to the stress state A (p = 90 psi) and was sheared to B (η = 0.33, p = 90 psi) along a constant p stress path. From B the specimen was sheared to C (η = 0.66, p = 60 psi) along a constant volume stress path. The sample was then subjected to stress cycles CD_1C, CD_2C, CD_3C and CD_4C. The incremental plastic volumetric strain experienced by the specimen during each stress cycle is

indicated along each stress path. These strains, in relation to those that occurred along other stress cycle paths are small, indicating that for the stress cycles CD_1C, CD_2C, CD_3C and CD_4C, the magnitude of the plastic volumetric strain increments during each cycle can be assumed to be zero.

The conclusion from the experiments performed on specimens CD, T_{19}, CR, CF and T_{16}

The above experimental results illustrate that the volumetric strains during state paths beneath the state boundary surface are only recoverable for stress cycles applied to a specimen in a limited zone (D_1CD_4 in Fig.6.2(e)) in the (q,p) plane. Outside this narrow zone, the application of stress cycles on samples of Kaolin cause irrecoverable volumetric strains. The precise nature of the boundaries of this zone requires further investigation. According to the Cam-clay theory and its modification the regions in which plastic volumetric strains cannot take place are much wider than the limited zone indicated in Fig.6.2(e), indicating that the yield surfaces predicted by the above theories are possibly oversimplifications. As stated by Palmer (1965) yield surfaces in practice are necessarily a matter of the definition of yield. If yielding is defined by a strain of a given magnitude then the nature and form of the yield surface will differ depending on this magnitude. However the magnitudes of the plastic volumetric strains observed in the experiments cited above are too large to be neglected. These deviations require further theoretical and experimental investigation.

6.2.2 The prediction of strains from the Cam-clay theory and the Modified theory

As discussed at the beginning of this chapter the strain hardening law is a relationship between the position of the yield surface in stress space and the plastic strains experienced by the material in arriving at a specific stress point. In this section expressions are derived for the total strains experienced by the specimen when sheared from the isotropic consolidation state to any specific stress state. The following assumptions are made in the Cam-clay theory and its modification:-

(i) During isotropic consolidation the voids ratio is linearly related to the logarithm of the mean normal stress. The slope of this line is denoted by $(-\lambda)$

i.e. $$e_o - e_a = -\lambda \log p_o \qquad 6.9$$

where e_a corresponds to the voids ratio at unit pressure.

(ii) During isotropic swelling the voids ratio is linearly related to the logarithm of mean normal stress. The slope of this line is (-K)

i.e. $e - e_o = - k \log \left(\frac{p}{p_o}\right)$ 6.10

(iii) There exists a unique relation between e, q and p for all states of the specimen for which q and p lie on the yield locus.

(iv) The shear strains are always irrecoverable.

(v) The soil is assumed to be stable in the sense that the normality condition of Drucker (1959) is applicable.

i.e. $(dq/dp) = - \delta v^p / d\epsilon^p$ 6.11

(vi) The soil is assumed to be isotropic.

(vii) The energy balance stated in section 6.2 is valid

i.e. $(\delta E')_{ext} = (\delta U)_{stored} + (\delta W)_{dissipated}$ 6.2 bis

Consider a sample in its initial state (e_o, p_o) subjected to an increment of isotropic stress δp_o, then from equation 6.9

$$(\delta v)_{\eta=o} = \left(\frac{\lambda}{1+e_o}\right)\left(\frac{\delta p_o}{p_o}\right)_{\eta=o} \qquad 6.12$$

and of this total volumetric strain a part is recoverable and is given by equation 6.10

$$(\delta v^r)_{\eta=o} = \left(\frac{k}{1+e_o}\right)\left(\frac{\delta p_o}{p_o}\right)_{\eta=o} \qquad 6.13$$

Combining the relation

$$(\delta v)_{\eta=o} = (\delta v^p)_{\eta=o} + (\delta v^r)_{\eta=o} \qquad 6.13(a)$$

with equations 6.12 and 6.13

$$(\delta v^p)_{\eta=o} = \left(\frac{\lambda-k}{1+e_o}\right)\left(\frac{\delta p_o}{p_o}\right)_{\eta=o} \qquad 6.14$$

From equation 6.8(a) the expression for the yield locus in the Cam-clay theory is

$$\frac{q}{Mp} = \log\left(\frac{p_o}{p}\right) \qquad 6.8(a) \text{ bis}$$

Differentiating 6.8(a) and rearranging the terms,

$$\frac{dp_o}{p_o} = \frac{dp}{p}\left[1 + \frac{1}{M}\left(\frac{dq}{dp} - \frac{q}{p}\right)\right] \qquad 6.15$$

The quantity (dp_o/p_o) is a measure of the shift of the yield locus and hence for any infinitesimal increment of stress (dq, dp) from the state (q,p,e) the increment in plastic volumetric strain is given by

$$d\upsilon^p = \left(\frac{\lambda-\kappa}{1+e}\right)\frac{dp_o}{p_o} \qquad 6.16$$

From equations 6.15 and 6.16

$$d\upsilon^p = \left(\frac{\lambda-\kappa}{1+e}\right)\left[1+\frac{1}{M}\left(\frac{dq}{dp}-\frac{q}{p}\right)\right]\frac{dp}{p} \qquad 6.17$$

Therefore

$$d\upsilon = \left(\frac{dp}{p}\right)\left(\frac{\lambda-\kappa}{1+e}\right)\left[1+\frac{1}{M}\left(\frac{dq}{dp}-\frac{q}{p}\right)\right]+\frac{\kappa\,dp}{p}$$

i.e. $$d\upsilon = \frac{1}{p}\left(\frac{\lambda}{1+e}\right)\left[\frac{\left(1-\frac{\kappa}{\lambda}\right)}{M}\left(dq-\eta\,dp\right)+dp\right] \qquad 6.18$$

Also

$$\frac{d\epsilon}{d\upsilon^p} = \left(\frac{1}{M-\eta}\right) \qquad 6.6(a)\text{ bis.}$$

ie $$d\epsilon = \left(\frac{\lambda-\kappa}{1+e}\right)\left(\frac{1}{M-\eta}\right)\left[1+\frac{1}{M}\left(\frac{dq}{dp}-\frac{q}{p}\right)\right]\frac{dp}{p} \qquad 6.19$$

The corresponding expressions for the modified theory are

$$\delta\upsilon^p = \left(\frac{\lambda-\kappa}{1+e}\right)\left[\frac{dp}{p}+\left(\frac{2\eta}{M^2+\eta^2}\right)d\eta\right] \qquad 6.20$$

Therefore $$d\upsilon = \left(\frac{\lambda-\kappa}{1+e}\right)\left[\frac{dp}{p}+\left(\frac{2\eta}{M^2+\eta^2}\right)d\eta\right]+\frac{\kappa\,dp}{p}$$

i.e. $$d\upsilon = \left(\frac{\lambda}{1+e}\right)\left[\frac{dp}{p}+\left(1-\frac{\kappa}{\lambda}\right)\left(\frac{2\eta}{M^2+\eta^2}\right)d\eta\right] \qquad 6.21$$

From equations 6.20 and 6.6(b)

$$d\epsilon = \left(\frac{\lambda-\kappa}{1+e}\right)\left(\frac{2\eta}{M^2-\eta^2}\right)\left[\frac{dp}{p}+\left(\frac{2\eta}{M^2+\eta^2}\right)d\eta\right] \qquad 6.22$$

The incremental stress-strain relationships given by equations 6.18, 6.19, 6.21 and 6.22 are only dependent on the three fundamental constants M, λ and k.

6.2.3 The prediction of the state boundary surface from the Cam-clay theory and the Modified theory

In the Cam-clay theory and the modified theory the equations for the state boundary surfaces are obtained by integrating equations 6.18 and 6.21 with dv = o. After simplification the corresponding equations are

$$\log\left(\frac{p_e}{p}\right) = \left(1 - \frac{\kappa}{\lambda}\right)\frac{\eta}{M} \qquad 6.23(a)$$ Cam-clay theory

and

$$\left(\frac{p_e}{p}\right) = \left(1 + \frac{\eta^2}{M^2}\right)^{\left(1-\frac{\kappa}{\lambda}\right)} \qquad 6.23(b)$$ Modified theory

where $p_e = \exp\left(\frac{e_a - e}{\lambda}\right)$

The pore pressure developed during constant volume tests is given by

$$u = (p_o + \tfrac{1}{3}q - p) \qquad 6.24$$

Combining equations 6.24 and 6.23(a) or (b), it is now possible to determine the pore pressure developed at any stage of an undrained test.

6.2.4 The comparison of experimentally observed strains with those predicted from the Cam-clay theory and its Modification

The theoretical strains are computed using the expressions derived in equations 6.18, 6.19, 6.21 and 6.22. The relevant constants λ, M and k are taken to be 0.26, 0.9 and 0.06 respectively (since these values were used by Roscoe and Burland (1968)). The value of M of 0.9 stated by these authors was obtained from strain controlled tests. It is considerably higher than the peak stress ratio (0.66 to 0.75) observed by the author in his stress controlled triaxial tests. No data from strain controlled tests is available for the batch of Kaolin used by the author.

The theoretically predicted strains are compared with those observed during experiments on samples initially isotropically consolidated to 30, 60 and 90 psi. Three different applied stress paths are considered at each of these stress levels. They include (i) a constant volume stress path where $dq > o$ and $dp < o$, (ii) a constant p stress path where $dq > o$ and $dp = o$,

(iii) a conventional fully drained test where $dq/dp = 3$ and $dq > o$, $dp > o$.

(a) The behaviour of the specimens initially isotropically consolidated to 30 psi

Figs.6.3 illustrate the volumetric and shear strains predicted from the Cam-clay theory and its modification during a constant volume test at an isotropic stress of 30 psi. The theoretical strains are calculated for the experimentally observed stress path. The Cam-clay theory predicts a volumetric strain of 1.3 p.c. at peak stress in this undrained test. The modified theory predicts a negative volumetric strain of the same order. The shear strain predicted by the Cam-clay theory is in close agreement with those observed during the undrained test. The modified theory predicts much smaller shear strains even at peak stress.

Fig.6.4 for constant p test and Fig.6.5 for fully drained tests indicate that (i) the Cam-clay theory overpredicts both the volumetric and shear strains in both constant p and fully drained tests, (ii) the modified theory also overpredicts the volumetric strain in both types of test, (iii) the shear strains predicted by the modified theory are in close agreement with the experimental observations for constant p and fully drained tests. These observations will be discussed further in section 6.3 in the light of the incremental stress-strain theory proposed by Roscoe and Poorooshasb (1963).

(b) The behaviour of specimens initially isotropically consolidated to 60 psi

Figs.6.6, 6.7 and 6.8 indicate that the overall comparison of the theoretical and experimental strain behaviour at 60 psi is very nearly the same as that at 30 psi, except that the modified theory tends to underpredict the shear strains in constant p tests. The volumetric strains predicted by the modified theory are in close agreement with the experimental observations in both constant p and fully drained tests.

(c) The behaviour of specimens initially isotropically consolidated to 90 psi

Figs.6.9, 6.10 and 6.11 illustrate that the overall comparison of theoretical and experimental strain behaviour at 90 psi is similar to that at 30 and 60 psi.

From the data presented in paragraphs (a), (b) and (c) it is seen that (i) the Cam-clay theory overpredicts the volumetric and shear strains in all types of drained tests, (ii) the modified theory underpredicts the shear strain in all types of tests, especially in the undrained and constant p tests, (iii) the volumetric strains predicted by the modified theory are in agreement with the experimental observations. These observations will be discussed in further detail in the subsequent sections.

6.3 The flow rule

As stated at the beginning of this chapter, the flow rule represents a relationship between the directions of the plastic strain rate vector and the stress vector. In the case of an "ideal plastic" material, at a smooth point on the yield surface the plastic strain rate vector is independent of the direction of the stress increment and is normal to the yield surface (Drucker 1959). Both the Cam-clay theory and the modified theory assume that the plastic strain rate vector is normal to the yield surface. The plastic strain rate vectors $d\upsilon^p/d\epsilon^p$ as derived from the energy balance equations of Roscoe, Schofield and Thurairajah (1963) and Roscoe and Burland (1968) are given in equations 6.6(a) and 6.6(b) respectively.

From equations 6.18, 6.19, 6.21 and 6.22 the <u>total</u> strain rate vectors are given by

$$\frac{d\upsilon}{d\epsilon} = \left(\frac{\lambda}{\lambda-\kappa}\right)(M-\eta)\left[\frac{\frac{dp}{p}+\frac{d\eta}{M}}{\frac{dp}{p}+\frac{1}{M}\left(1-\frac{\kappa}{\lambda}\right)d\eta}\right]^{-1} \qquad 6.25 \text{ Cam-clay theory}$$

and

$$\frac{d\upsilon}{d\epsilon} = \left(\frac{\lambda}{\lambda-\kappa}\right)\left(\frac{M^2-\eta^2}{2\eta}\right)\left[\frac{\frac{dp}{p}+\frac{2\eta}{M^2+\eta^2}d\eta}{\frac{dp}{p}+\left(1-\frac{\kappa}{\lambda}\right)\left(\frac{2\eta}{M^2+\eta^2}\right)d\eta}\right]^{-1} \qquad 6.26 \text{ Modified theory}$$

If k = o then equations 6.25 and 6.26 will reduce to

$$\left(\frac{d\upsilon}{d\epsilon}\right)_{\kappa=o} = M-\eta \qquad 6.27 \text{ Cam-clay theory}$$

and

$$\left(\frac{d\upsilon}{d\epsilon}\right)_{\kappa=o} = \frac{M^2-\eta^2}{2\eta} \qquad 6.28 \text{ Modified theory}$$

If k = o, then for constant stress ratios, equations 6.25 and 6.26 reduce to

$$\left(\frac{dv}{d\epsilon}\right)_\eta = \left(\frac{\lambda}{\lambda-\kappa}\right)(M-\eta) \qquad 6.29 \text{ Cam clay theory}$$

$$\left(\frac{dv}{d\epsilon}\right)_\eta = \left(\frac{\lambda}{\lambda-\kappa}\right)\left(\frac{M^2-\eta^2}{2\eta}\right) \qquad 6.30 \text{ Modified theory}$$

6.3.1 The flow rule based on the incremental stress-strain theory of Roscoe and Poorooshasb (1963)

The incremental stress-strain theory of Roscoe and Poorooshasb (1963) was presented in its original form in section 1.3.6. It will now be rewritten in slightly different form to facilitate comparison with other Cambridge theories. The basic equation is

$$(d\epsilon)_{\text{drained}} = (d\epsilon)_{\text{undrained}} + \left(\frac{d\epsilon}{dv}\right)_\eta dv \qquad 6.31$$

If it is assumed that (i) For stress paths starting from a given point on the state boundary surface, and provided the subsequent stress paths lie throughout on the state boundary surface, then ~~it is assumed that~~ v is a unique function of η and p. This assumption is equivalent to presuming there is a unique state boundary surface in (e,p,q) space. Expressed mathematically this assumption is

$$v = F(\eta, p) \qquad 6.32$$

and hence (ii) the shear strain in an undrained test is a continuous and differentiable function of the stress ratio (η),

$$\text{i.e.} \quad (\epsilon)_{\text{undrained}} = \int_o^\eta f_1(\eta)\, d\eta \qquad 6.33$$

and (iii) the slopes $\left(\frac{dv}{d\epsilon}\right)_\eta$ in the (v, ϵ) space of the anisotropic consolidation test paths are only a function of the stress ratio η

$$\text{i.e.} \quad \left(\frac{d\epsilon}{dv}\right)_\eta = f_2(\eta) \qquad 6.34$$

the equation 6.31 can therefore be expressed as

$$d\epsilon = f_1(\eta)\, d\eta + f_2(\eta)\, dF(\eta, p) \qquad 6.35$$

Also from 6.32 $$dv = \frac{\partial F}{\partial \eta} d\eta + \frac{\partial F}{\partial p} dp \qquad 6.36$$

In the case of a constant p stress path the second term in equation 6.36 becomes zero and therefore $dF/d\eta$ is given by the slope of the (v, η) relationship observed during a constant p test. Similarly in the case of an anisotropic consolidation stress path the first term in equation 6.36 becomes zero and dF/dp is given by the slope of the (v, p) relationship for the value of η corresponding to the particular anisotropic consolidation path under consideration. This slope is found to be independent of η and is $\frac{\lambda}{1+e}$

From equations 6.35 and 6.36 it can be seen that in general

$$\frac{dv}{d\epsilon} = \frac{\left(\frac{\partial F}{\partial \eta} d\eta + \frac{\partial F}{\partial p} dp \right)}{\left[f_1(\eta) d\eta + f_2(\eta) \left(\frac{\partial F}{\partial \eta} d\eta + \frac{\partial F}{\partial p} dp \right) \right]} \qquad 6.37$$

Equation 6.37 provides the relevant expression for the ratio of the total strain increments in terms of the functions $f_1(\eta)$, $f_2(\eta)$ and $F(\eta, p)$ and the differentials $d\eta$ and dp

It will be seen in section 6.3 that equations 6.34, 6.35 and 6.36 are valid for any stress path, for which the stress increment direction lies between the local undrained stress path and the local "anisotropic consolidation" path. The functions $f_1(\eta)$, $f_2(\eta)$ and $F(\eta, p)$ are determined directly from the experimental observations of a single undrained test and a series of anisotropic consolidation tests.

Since the above theory of Roscoe and Poorooshasb gives accurate strain predictions (and ~~are~~ is essentially based on experimental observations) it will be of interest to rearrange the terms in the equations (for the prediction of strains) of the Cambridge theory and the modified theory to obtain the equivalents of $f_1(\eta)$, $f_2(\eta)$ and $F(\eta, p)$. This will be carried out in the following section.

6.3.2 The conditions under which the Cam-clay theory and its modification will predict identical strains to those of the stress-strain theory of Roscoe and Poorooshasb

For the Cam-clay theory

$$dv = \left(\frac{\lambda}{1+e} \right) \frac{dp}{p} + \left(\frac{\lambda - \kappa}{1+e} \right) \frac{1}{M} d\eta \qquad 6.18 \text{ bis}$$

i.e. $$dv = \frac{\partial F^*}{\partial p} dp + \frac{\partial F^*}{\partial \eta} d\eta \qquad 6.38$$

where $$\frac{\partial F^*}{\partial p} = \left(\frac{\lambda}{1+e}\right)\frac{1}{p} \qquad 6.39(a)$$

and $$\frac{\partial F^*}{\partial \eta} = \frac{1}{M}\left(\frac{\lambda-k}{1+e}\right) \qquad 6.39(b)$$

from equation 6.19

$$d\epsilon = \left(\frac{\lambda-k}{1+e}\right)\frac{1}{M-\eta}\frac{dp}{p} + \frac{\lambda-k}{1+e}\frac{1}{M}\frac{d\eta}{(M-\eta)} \qquad 6.19 \text{ bis}$$

i.e. $$d\epsilon = f_1^*(\eta)\, d\eta + f_2^*(\eta)\, dF^*(\eta, p) \qquad 6.40$$

where $$f_1^*(\eta) = \left(\frac{\lambda-k}{1+e}\right)\frac{1}{M}\left(\frac{1}{M-\eta}\right)\cdot\frac{k}{\lambda} \qquad 6.41(a)$$

and $$f_2^*(\eta) = \left(\frac{\lambda-k}{\lambda}\right)\left(\frac{1}{M-\eta}\right) \qquad 6.41(b)$$

(Note: From equation 6.39(b) it is evident that the function depends only on the fundamental soil constants λ, k, M, and the voids ratio e; it is independent of the stress ratio η.)
From equations 6.39(b), 6.41(a) and (b) it can be shown that

$$f_1^*(\eta) = \left(\frac{k}{\lambda-k}\right) f_2^*(\eta)\cdot\frac{\partial F^*}{\partial \eta} \qquad 6.42$$

These relationships will be discussed further after deriving the corresponding relations for the Modified theory. Following the same procedure as that adopted for the Cam-clay theory and using the superfix ** for the expressions in the Modified theory it can be shown that

$$\frac{\partial F^{**}}{\partial \eta} = \left(\frac{\lambda-k}{1+e}\right)\left(\frac{2\eta}{M^2+\eta^2}\right) \qquad 6.43$$

$$\frac{\partial F^{**}}{\partial p} = \left(\frac{\lambda}{1+e}\right)\frac{1}{p} \qquad 6.44$$

$$f_2^{**}(\eta) = \left(\frac{\lambda-k}{\lambda}\right)\left(\frac{2\eta}{M^2-\eta^2}\right) \qquad 6.45$$

$$f_1^{**}(\eta) = \left(\frac{\lambda-\kappa}{1+e}\right)\left(\frac{2\eta}{M^2+\eta^2}\right)\left(\frac{2\eta}{M^2-\eta^2}\right)\frac{\kappa}{\lambda} \qquad 6.46$$

i.e. $$f_1^{**}(\eta) = f_2^{**}(\eta)\left(\frac{\kappa}{1+e}\right)\left(\frac{2\eta}{M^2+\eta^2}\right) \qquad 6.47$$

$$f_1^{**}(\eta) = \left(\frac{\kappa}{\lambda-\kappa}\right) f_2^{**}(\eta)\ \frac{\partial F^{**}}{\partial \eta} \qquad 6.48$$

Comparing equation 6.48 for the Modified theory with equation 6.42 for the Cam-clay theory, it is observed that the two equations are similar. Before proceeding with a detailed discussion of the relationships derived above, the author will study the equations 6.39(b) and 6.41(b) of the Cam-clay theory and the equations 6.43 and 6.45 of the Modified theory.

6.3.2(a) A relationship between $\frac{\partial F^{**}}{\partial \eta}$ and $f_2^{**}(\eta)$

In Appendix 3 it is shown that

$$\frac{\partial F^{**}}{\partial \eta} = \frac{\left(1-\frac{\kappa}{\lambda}\right)\left(\frac{\lambda}{1+e}\right)}{\left[1+\left(\frac{1-\frac{\kappa}{\lambda}}{M}\right)^2\left(\frac{1}{f_2^{**}(\eta)}\right)^2\right]^{\frac{1}{2}}} \qquad 6.49$$

which can be rearranged to give

$$f_2^{**}(\eta) = \frac{\frac{\partial F^{**}}{\partial \eta}}{\left[\left(\frac{\lambda}{1+e}\right)^2-\left(\frac{M}{1-\frac{\kappa}{\lambda}}\right)^2\left(\frac{\partial F^{**}}{\partial \eta}\right)^2\right]^{\frac{1}{2}}} \qquad 6.50$$

The function $\frac{\partial F^{**}}{\partial \eta}$ is the slope of the (v, η) characteristic of a constant p test. The function $f_2^{**}(\eta)$ is the slope of the anisotropic consolidation path in the (v, ϵ) space. Hence equation 6.50 indicates that there is a fundamental relation existing between the slope of the anisotropic consolidation line in the (v, ϵ) space and the slope of the constant p test path in the (v, η) space. Consequently in the calculation of the shear strains caused by any imposed stress increment using the incremental stress strain theory of Roscoe and Poorooshasb (1963), it is possible to obtain the magnitude of $(dv/d\epsilon)_\eta$ from a single constant p test. In other words it is not necessary to carry out an anisotropic consolidation test to find this relationship. In the stress-strain theory of Roscoe and Poorooshasb, the function F can be obtained from results of one undrained test,

provided the value of λ is obtained during the isotropic consolidation phase of the sample preparation. The function F, representing the state boundary surface, is therefore obtained from experimental observations. On the other hand the functions F* and F** for the state boundary surfaces of the Cam-clay theory and its modification come from the concept of normality and the respective energy equations. Hence for either the Cam-clay theory or the Modified theory to predict identical volumetric strains to those of the stress-strain theory of Roscoe and Poorooshasb (1963) it is clear that the conditions

$$F^* = F \qquad 6.51(a)\ \text{Cam-clay theory}$$

$$F^{**} = F \qquad 6.51(b)\ \text{Modified theory}$$

should be satisfied.

A further condition will be required if the shear strains as predicted from either of the two theories are to be identical to those obtained from the Roscoe and Poorooshasb theory and therefore to agree with those experimentally observed.

The general expression for the incremental shear strain in the Roscoe and Poorooshasb theory is

$$d\epsilon = f_1(\eta)\, d\eta + f_2(\eta)\, dF \qquad 6.35\ \text{bis}$$

Since the shear strains predicted from the Cam-clay, and the Modified theory are to be made to agree with those of Roscoe and Poorooshasb theory for all imposed stress paths they must be relevant for an undrained path, so that

$$f_1(\eta) = f_1^*(\eta) = f_1^{**}(\eta) \qquad 6.52$$

and also for a constant η path so that

$$f_2(\eta) = f_2^*(\eta) = f_2^{**}(\eta) \qquad 6.53$$

It has already been shown in equation 6.52, that identical volumetric strains in all three theories can only be obtained if $F = F^* = F^{**}$, hence the whole problem reduces to satisfying equations 6.51, 6.52 and 6.53. It should be recalled that $f_1(\eta)$ is the experimentally observed value of the shear strain in an undrained test, and it can be seen from equations 6.42 and 6.48, that if

$f_2^*(\eta) = f_2^{**}(\eta)$ and $F^* = F^{**}$ then $f_1^*(\eta) = f_1^{**}(\eta)$.

The energy equations used in the Cam-clay theory and the Modified theory determine the functions $f_2^*(\eta)$ and $f_2^{**}(\eta)$ respectively, and also F^* and F^{**} respectively. They therefore also fix $f_1^*(\eta)$ and $f_1^{**}(\eta)$ respectively. In the Roscoe and Poorooshasb theory the function $f_1(\eta)$, $f_2(\eta)$ and F are independent, whereas the corresponding functions for either of the two other theories are interrelated. Consequently if the energy equation of either of these two theories does not predict F correctly, then it will not predict $f_1(\eta)$ or $f_2(\eta)$ correctly.

6.3.2(b) The concept of an extra yield locus for shear distortion without plastic volume change for wet clays, proposed by Roscoe and Burland (1968) in their Modified Theory

Constant volume shear tests performed by Loudon (1967) on lightly and heavily overconsolidated Kaolin illustrated that considerable irrecoverable shear strain was experienced by the specimens during shear, even when the stress paths followed by these specimens lay inside the conventional undrained stress path of normally consolidated clay in a (p,q) space. For overconsolidation ratios in the range 1 to 2.2 Loudon found that the shear strain $\in$ was a unique function of q/p_e and for overconsolidation ratios greater than 2.2 the values of $\in$ at any specific (q/p_e) were dependent on the magnitude of q/p_e and Σ the overconsolidation ratio. Replotting the undrained test results of Loudon for lightly overconsolidated days in a (p,q) plot, Roscoe and Burland (1967) showed that for specimens of overconsoldation ratio 1 to 2.2 the contours of constant shear strain beneath the state boundary surface coincide with the contours of constant q. They further stated that for normally and lightly overconsolidated clays the contours of constant q can be considered as a series of yield loci. These "constant q yield loci" extend up to the conventional yield loci used in the modified theory. Also, since it is assumed that the specimen can only experience plastic volumetric strains when its stress path is directed outside the yield locus assumed in the modified theory, Roscoe and Burland named this yield locus the "volumetric yield locus". Thus for stress increments directed outside the volumetric yield locus, the stress point is assumed to move with the intersection of the constant q yield locus and its corresponding voluemtric yield locus.

However for stress increments directed inside the volumetric yield locus in a direction in which q is increasing the stress point is assumed to move through a series of constant q yield loci. Based on this new concept, Roscoe and Burland (1968) proposed revised flow rules. A brief summary of these revised flow rules which lead to what Roscoe and Burland (1968) called their "revised modified" theory, will be presented in 6.3.2(d). In the remainder of this thesis it will be called the "revised" theory.

6.3.2(c) The shear strain associated with the additional (constant q) yield locus used in the Revised-Modified theory

In Fig.6.12, for any particular value of the deviator stress q, let η be the magnitude of the stress ratio, at which the constant q line meets the volumetric yield locus.

Then the contribution to the shear strain from the constant q yield locus can be expressed as

$$\bar{\epsilon} = \phi(\eta) \qquad 6.54$$

Differentiating equation 6.54

$$\bar{d\epsilon} = \frac{\partial \phi}{\partial \eta} d\eta = \phi'(\eta)\, d\eta \qquad 6.55$$

where $\phi'(\eta) = \frac{\partial \phi}{\partial \eta}$

6.3.2(d) The revised flow rules of Roscoe and Burland (1968)

The following relationships were used by Roscoe and Burland (1967) for the determination of the incremental strains corresponding to the stress increments applied to a specimen, with its stress state lying on a volumetric yield locus.

For stress increments directed in the range

(i) $dq \leq 0$ and $dp \leq 0$ (Region ASB in Fig.6.12(a))

$$dv = \left(\frac{-\kappa}{1+e}\right) dp/p \qquad 6.56(a)$$

and $$d\epsilon = 0 \qquad 6.56(b)$$

provided the stresses are not decreased more than half of their previous maximum values.

(ii) $dp \geq 0$ and $-\infty \leq \frac{dq}{dp} \leq S_1$ (Region BSC in Fig.6.12(a))

where S_1 is the slope of the volumetric yield locus in the (p,q)

plane in a direction in which q is decreasing

$$d\upsilon = \left(\frac{-\kappa}{1+e}\right)\frac{dp}{p} \qquad 6.57(a)$$

and $$d\epsilon = 0 \qquad 6.57(b)$$

provided the stresses are not decreased more than half their previous maximum values.

(iii) $dp > 0$ and $\eta \geq \frac{dq}{dp} \geq S_1$ (Region CSD in Fig.6.12(a)) where S_1 is the slope of the volumetric yield locus in the (q,p) plane in a direction in which q is decreasing.

$$d\upsilon = \left(\frac{\lambda}{1+e}\right)\left[\frac{dp}{p} + \left(1-\frac{\kappa}{\lambda}\right)\left(\frac{2\eta}{M^2+\eta^2}\right)d\eta\right] \qquad 6.58(a)$$

and $$d\epsilon = \left(\frac{\lambda-\kappa}{1+e}\right)\left[\frac{2\eta}{M^2-\eta^2}\right]\left[\frac{dp}{p} + \left(\frac{2\eta}{M^2+\eta^2}\right)d\eta\right] \qquad 6.58(b)$$

(iv) $dp \geq 0$ and $\eta \leq \frac{dq}{dp} \leq \infty$ (Region DSE in Fig.6.12(a))

$$d\upsilon = \left(\frac{\lambda}{1+e}\right)\left[\frac{dp}{p} + \left(1-\frac{\kappa}{\lambda}\right)\left(\frac{2\eta}{M^2+\eta^2}\right)d\eta\right] \qquad 6.59(a)$$

and $$d\epsilon = \left(\frac{\lambda-\kappa}{1+e}\right)\left(\frac{2\eta}{M^2-\eta^2}\right)\left[\frac{dp}{p} + \left(\frac{2\eta}{M^2+\eta^2}\right)d\eta\right] + \phi'(\eta)\,d\eta \qquad 6.59(b)$$

(v) $dp \leq 0$ and $-\infty \leq \frac{dq}{dp} \leq S_1$ (Region ESF in Fig.6.12(a)) where S_1 is the slope of the volumetric yield locus in (p,q) space

$$d\upsilon = \left(\frac{\lambda}{1+e}\right)\left[\frac{dp}{p} + \left(1-\frac{\kappa}{\lambda}\right)\left(\frac{2\eta}{M^2+\eta^2}\right)d\eta\right] \qquad 6.60(a)$$

and $$d\epsilon = \left(\frac{\lambda-\kappa}{1+e}\right)\left(\frac{2\eta}{M^2-\eta^2}\right)\left[\frac{dp}{p} + \frac{2\eta}{M^2+\eta^2}d\eta\right] + \phi'(\eta)\,d\eta \qquad 6.60(b)$$

(vi) $dp < 0$ and $S_2 \leq dq/dp \leq 0$ (Region FSA in Fig.6.12(a)) where S_2 is the slope of the volumetric yield locus in the (p,q) space

$$d\upsilon = \left(\frac{-\kappa}{1+e}\right)\frac{dp}{p} \qquad 6.61(a)$$

and $$d\epsilon = \phi'(\eta)\,d\eta \qquad 6.61(b)$$

The flow rules specified by Roscoe and Burland and stated in sections (i-vi) fully describe the stress-strain behaviour for all increments of stress. Comparing the above set of equations with the incremental stress-strain theory of Roscoe and Poorooshasb (1963) it is evident that for stress increments applied in the ranges (iv) and (v) (where the applied stress path lies between the undrained stress path and the anisotropic consolidation line in the (p,q) space) the revised theory will predict identical strains if and only if

$$f_1(\eta) = f_1^{**}(\eta) + \Phi'(\eta) \qquad 6.62$$

If condition 6.62 is satisfied then the revised theory may be put in the form of the Roscoe and Poorooshasb theory

i.e. $$dv = \frac{\partial F^{**}}{\partial p} dp + \frac{\partial F^{**}}{\partial \eta} d\eta \qquad 6.63$$

and $$d\epsilon = \left[f_1^{**}(\eta) + \Phi'(\eta)\right] d\eta + f_2^{**}(\eta)\, dF^{**} \qquad 6.64$$

Or stated otherwise the presence of the function $\Phi'(\eta)$ in equation 6.6 leads to an expression for $dv^p/d\epsilon^p$ of the form

$$\frac{dv^p}{d\epsilon^p} = \frac{\left[\left(\frac{\lambda-\kappa}{\lambda}\right)\frac{\partial F^{**}}{\partial p} dp + \frac{\partial F^{**}}{\partial \eta} d\eta\right]}{\left[f_1^{**}(\eta) + \Phi(\eta)\right] d\eta + \left[f_2^{**}(\eta)\left(\frac{\partial F^{**}}{\partial p} dp + \frac{\partial F^{**}}{\partial \eta} d\eta\right)\right]} \qquad 6.65$$

where $$f_2^{**}(\eta) = \frac{\frac{\partial F^{**}}{\partial \eta}}{\left[\left(\frac{\lambda}{1+e}\right)^2 - \left(\frac{M}{1-\frac{\kappa}{\lambda}}\right)^2 \left(\frac{\partial F^{**}}{\partial \eta}\right)^2\right]^{\frac{1}{2}}} \qquad 6.50 \text{ bis}$$

and $$f_1^{**}(\eta) = \left(\frac{\kappa}{\lambda-\kappa}\right) f_2^{**}(\eta)\, \frac{\partial F^{**}}{\partial \eta} \qquad 6.48 \text{ bis}$$

From equation 6.65 it can be seen that when $d\eta > 0$, the plastic strain rate vector $dv^p/d\epsilon^p$ is now dependent, not only on the stress ratio η but also is dependent on the stress increment $d\eta$ and dp

When $d\eta = o$ the plastic strain rate vector is only dependent on the stress ratio η. The concept of normality and the energy balance used by Roscoe and Burland provides a possible method of obtaining the function F**, which satisfies equations 6.63, 6.50 and 6.48. Also the concept of the constant q yield loci provides a method of determining $\Phi(\eta)$.

Experimental observations will now be provided to illustrate that the function F** and $\Phi(\eta)$ can be used to predict strains for all stress paths lying in between the undrained and anisotropic consolidation paths (regions (iv) and (v) in Fig.6.12 (a)).

6.3.3 The experimentally observed form of $v = F(\eta, p)$ for stress increments from an initial state e_o, p_o.

In Fig.6.13 the volumetric strain contours are plotted from a variety of drained test paths each with different values of (dq/dp); the zero volumetric strain contour from an undrained test path AT_3 is also shown. The stress paths are indicated by the full lines. From the volumetric strain contours (shown dotted), it is evident that except for stresses close to the isotropic stress (from which the specimens are sheared) the contours are similar to that of the undrained stress path. All the specimens were sheared from 90 psi isotropic stress. Fig.6.13 illustrates that a state surface in (p,q,v) space exists for all specimens sheared from 90 psi isotropic stress with an increasing stress-ratio. It will be shown in a later section that except for stress paths with directions lying inside the tangent to the current volumetric strain contours (Fig.6.13), for all other increments of stresses, the volumetric strain contours plotted in Fig.6.13 are unique. This unique surface will now be used to calculate the shear strains experienced by specimens in drained tests similar to those shown in Fig.6.13 using the hypothesis of Roscoe and Poorooshasb (1963) (see section 6.3.1 and equation 6.32).

6.3.4 The $(dv/d\epsilon)_\eta$ of anisotropic consolidation paths for samples initially isotropically consolidated to 90 psi and subsequently sheared to the relevant value of

In this section the experimental observations on the compression tests with constant stress ratio (anisotropic consolidation) are presented. The author's results confirm the experimental finding of Roscoe and Poorooshasb (1963) that during the anisotropic consolidation (with constant stress ratio η), the

ratio of the incremental strains, namely $d\upsilon/d\epsilon$, is a constant and is dependent on the magnitude of the stress ratio η. The points in Fig.6.14 show the magnitude of $(d\upsilon/d\epsilon)_\eta$ corresponding to five different values of the stress ratio η as observed experimentally. The curves in Fig.6.14 give the predicted variation of $(d\upsilon/d\epsilon)_\eta$ with η as calculated from the expressions

$$f_2^*(\eta) = \left(\frac{d\upsilon}{d\epsilon}\right)_\eta = \left(\frac{\lambda}{\lambda-k}\right)(M-\eta) \qquad \text{6.29 bis Cam-clay theory}$$

and $$f_2^{**}(\eta) = \left(\frac{d\upsilon}{d\epsilon}\right)_\eta = \left(\frac{\lambda}{\lambda-k}\right)\left(\frac{M^2-\eta^2}{2\eta}\right) \qquad \text{6.30 bis Modified theory}$$

It can be seen that the variation of $f_2^{**}(\eta)$ as calculated from equation 6.30 (Modified theory) is in excellent agreement with the experimental observations which give $f_2(\eta)$. Therefore $f_2(\eta) = f_2^{**}(\eta)$. However for $\eta < 0.5$ it is evident that $f_2^*(\eta)$ for Cam-clay theory is much smaller than $f_2(\eta)$. Hence over most of the range of η from 0 to M, $f_2(\eta) \neq f_2^*(\eta)$.

6.3.5 The incremental volumetric strain during anisotropic consolidation

The changes in voids ratio with log p during anisotropic consolidation tests at three different values of η are presented in Figs.6.14(a-c)

The lines through the experimental points all have the same slope λ. Hence during anisotropic consolidation

$$d\upsilon = \left(\frac{-\lambda}{1+e}\right)\frac{dp}{p} \qquad 6.66$$

From equations 6.66, 6.36, 6.39(a) and 6.44

$$\frac{\partial F}{\partial p} = \frac{\partial F^*}{\partial p} = \frac{\partial F^{**}}{\partial p} = \left(\frac{-\lambda}{1+e}\right)\frac{1}{p} \qquad 6.67$$

In other words all three theories predict correctly the volumetric strains observed experimentally during anisotropic consolidation tests.

6.3.6 The volumetric strain observed in a constant p test and those predicted from the three stress-strain theories

The volumetric strain observed during a constant p test at 90 psi are represented by the points in Fig.6.15. The curves in this diagram refer to the predicted values from the various

stress strain theories. It is evident that the modified theory and the incremental stress-strain theory of Roscoe and Poorooshasb (1963) closely predicts the strains in a constant p test. The C-am-clay theory overpredicts the strains in constant p tests. Hence it is evident that

$$\frac{\partial F}{\partial \eta} = \frac{\partial F^{**}}{\partial \eta} \qquad 6.68 \text{ Modified theory}$$

and

$$\frac{\partial F}{\partial \eta} \neq \frac{\partial F^{*}}{\partial \eta} \qquad 6.69 \text{ Cam-clay theory}$$

6.3.7 The shear strains observed in a constant p test and those predicted from the three stress-strain theories

The shear strains observed in a constant p and in an undrained test are illustrated in Fig.6.16(a). In the same figure the predicted components of shear strain due to the anisotropic consolidation part of a constant p test is also indicated. The two components of shear strain are now added at each stress ratio, to give the Roscoe, Poorooshasb prediction. Excellent agreement is obtained between this prediction and the experimentally observed strains.

In Fig.6.16(b) the relationship between η and ε are shown for (i) the anisotropic component of the shear strains in a constant p test as calculated from the stress-strain theory of Roscoe and Poorooshasb. (ii) the shear strains predicted from the modified theory. (iii) the experimentally observed shear strains in a constant p test and (iv) the strains predicted from the Cam-clay theory. From this figure the following observations may be made. (a) the modified theory underpredicts the experimentally observed shear strain but agrees with the anisotropic component of the constant p test shear strains as calculated from the stress-strain theory of Roscoe and Poorooshasb (1963). (b) the Cam-clay theory overpredicts the shear strain in constant p tests. Therefore it can be concluded that

$$f_1^{**}(\eta)\, d\eta + f_2^{**}(\eta)\, dF^{**} = f_2(\eta)\, dF \qquad 6.70$$

and

$$f_1^{*}(\eta)\, d\eta + f_2^{*}(\eta)\, dF^{*} \geq f_1(\eta)\, d\eta + f_2(\eta)\, dF \qquad 6.71$$

Having seen that the modified theory predicts approximately the same amount of the shear strain as the anisotropic components, the undrained components of the shear strain ~~was~~ were added to give the strains as predicted by the revised theory. The result is presented in Fig.6.17 together with experimentally observed strains. Excellent agreement is observed between the experimentally observed strains and the theoretical strains.

It is therefore concluded that

$$f_1^{**}(\eta)\, d\eta + f_2^{**}(\eta)\, dF^{**} + \phi'(\eta)\, d\eta = f_1(\eta)\, d\eta + f_2(\eta)\, dF \qquad 6.72$$

In equation 6.72 $\phi'(\eta)\, d\eta = f_1(\eta)\, d\eta$

The above results indicate that the modified theory in its own form lacks the undrained component of shear strain used by Roscoe and Poorooshasb (1963) in the calculation of the shear strains in any tests with plastic volume change and for which $\eta \geq 0$ and $\delta\eta > 0$. Once this component is added to the shear strains predicted by the modified theory, the revised values are in close agreement with the strains predicted from the incremental stress strain theory of Roscoe and Poorooshasb (1963).

6.3.8 The strains predicted by the stress-strain theory of Roscoe and Poorooshasb (1963)

It has already been mentioned in Chapter 4 that the undrained stress path and the drained stress path (with slope 3) do not coincide in the $(q/p_e, p/p_e)$ plot, for tests carried out at 30 psi and 60 psi cell pressures, though they are coincident at 90 psi. The deviations at 30 psi being very much higher than those at 60 psi (see Fig.4.47). Therefore in calculating the shear strains in tests at 30 and 60 psi cell pressures (for all applied stress paths being between the undrained stress path and the anisotropic consolidation path ($\delta\eta \gg 0$)) the assumption of Roscoe and Poorooshasb (1963) that a unique state surface exists in (p,q,e) space is not strictly valid. Nevertheless this theory has been used to calculate the volumetric strains for three types of tests at 30 psi cell pressure (constant p test, constant cell pressure test and a drained test with applied stress path of slope < 3). The main assumptions made were (i) a unique state boundary surface does in fact exist in the (p,q,e) space and (ii) sections of this surface by constant voids ratio planes are geometrically similar to the undrained stress path at 30 psi cell pressure. The predicted and experimentally observed strains in the three types of

tests are presented in Figs.6.18 - 6.23. It is evident that the predicted values are very much larger than the experimentally observed volumetric and shear strains in all the three types of tests.

Similar, but smaller, differences between the predicted and the experimentally observed strains were found during tests on samples initially consolidated under an isotropic stress of 60 psi. These results are presented in Figs.6.24 to 6.29. The results for the three types of test when carried out from an initial isotropic stress of 90 psi are presented in Figs.6.30 to 6.33. In this case excellent agreement is obtained between the predicted strains and the experimentally observed strains for all three types of test. Before discussing the limitations of the stress-strain theory of Roscoe and Poorooshasb (1963) for other stress paths than those which have been considered above it will be appropriate to study the relationship between the strain increment vectors and the stress increment vectors at various levels of stress ratio.

6.3.9 The relationship between strain increment ratios, stress ratios, and stress increment ratios.

General In this section the magnitudes and the directions of strain increments for a variety of stress increments applied at five different values of stress ratio (i.e.($q/p=\eta$) of 0, 0.22, 0.33, 0.44 and 0.69) will be presented. All specimens were initially prepared under a 1-D stress of 22 psi and subsequently sheared from 90 psi isotropic stress. Figs.6.34 to 6.38 illustrate the directions of the stress increments in (q,p) space and the corresponding directions of the strain increments, in (v,ϵ) space. In Fig.6.34 the results of the extension tests (represented by dashed lines) have been derived from data obtained from extension tests carried out on samples initially isotropically consolidated at 60 psi. (This procedure was adopted because the standard Clockhouse triaxial cells employed were not suitable for carrying out extension tests with initial cell pressures higher than 60 psi.) All the data presented in Figs.6.35 to 6.38 inclusive refers to the results of compression tests. Dashed lines in these diagrams have not been obtained by direct experimental observation but by interpolation, from tests with neighbouring imposed stress paths. In Fig.6.35 the stress path labelled E_1 corresponds to an anisotropic consolidation line. The corresponding strain path was obtained directly from the

mean curve relating $(dv/d\epsilon)_\eta$ and η in Fig.6.14. The results presented in Figs.6.34 to 6.38 inclusive clearly show that the directions of the strain increment vectors in (v, ϵ) space are dependent on the directions of the stress increment vectors in (q,p) space.

From all the compression tests completed by the author initially consolidated isotropically to 90 psi, it was possible to prepare a number of curves, relating $dv/d\epsilon$ and dq/dp each for a given value of η. The unique relationship between $dv/d\epsilon$ and dq/dp for $\eta = o$ is shown by the curve in Fig.6.39. It will be noticed that $dv/d\epsilon$ axis is an assymptote when $dq/dp = o$, corresponding to isotropic consolidation. Furthermore, dq/dp tends towards ∞ in a constant p test, for which the initial stress path is represented by AO in Fig.6.34. It can be seen in the strain section of this diagram that $dv/d\epsilon$ is finite as represented by the strain path AO. The remaining curves in Fig.6.40 to 6.43 show corresponding relationships between $dv/d\epsilon$ and dq/dp for values of η ranging from 0.22 to 0.690. The range of the directions of the stress paths can be increased to include negative values of dq/dp (with p increasing) up to the magnitude which correspond to $dv/d\epsilon = \infty$ The unique curve relating $(dv/d\epsilon)$ with (dq/dp) at any particular stress ratio is seen to be dependent on the stress ratio. The $(dv/d\epsilon)$ (dq/dp) relationship in Figs.6.39 to 6.43 describe a surface in the three dimensional space $(dv/d\epsilon, dq/dp, q/p)$. This surface is shown in Fig.6.43(a). The chain dotted line drawn on the surface in this figure corresponds to $f_2(\eta)$ i.e. the variation of $(dv/d\epsilon)_\eta$ with η for the particular case of anisotropic consolidation (i.e. $\frac{dq}{dp} = \frac{q}{p} = \eta$).

6.3.10 Strain increment vectors for stress increment vectors of equal magnitudes but different directions

The magnitudes of the strain increment vectors corresponding to stress increments of 10 psi in a number of different directions at constant values of the stress ratio η of 0, 0.22, 0.33, 0.44 and 0.69 are presented in Figs.6.44 to 6.48 respectively. It can be seen that for any given initial stress state, the locus of the end points of the strain increment vectors is found to lie on an ellipse. The major axis of this ellipse is found to coincide with the v axis when $\eta = o$ (i.e. isotropic consolidation). However as η is increased the major axis of the ellipse rotates in a clockwise direction in (v, ϵ) space, until at the peak stress ratio the major axis of the ellipse lies along the ϵ axis.

Also the size of the ellipses corresponding to a finite stress increment is found to increase in size with increasing stress ratio η. These ellipses of strain increment vectors are again presented in Fig.6.49, superposed upon the (v, ϵ) characteristic of a fully drained ($dq/dp = 3$) test. The above observations again indicate that for a given magnitude of stress increment vectors the magnitude of the strain increment vectors are dependent upon the direction of the stress increment vector and upon the magnitude of the stress ratio η. However even if these ellipses were idealized to a single resultant vector coinciding with the major axis of the ellipse it is abundantly clear that the concept of one unique yield surface obeying "normality" cannot be true. If it were true the idealized resultant strain increment vectors should everywhere be tangential to the (v, ϵ) characteristic for the conventional drained test. It is implicit in the above argument that the effect of any recoverable elastic components of strains are negligible. The above investigation has been carried out with respect to total strains. It will be shown in Chapter 7 that the recoverable strains are an order of magnitude smaller than the total strains and therefore the strain increment ellipse shown in Figs.6.44 to 6.49 can be assumed to apply to the plastic strains. Hence the magnitude and direction of the plastic strain increment vector $\sqrt{(\delta v^p)^2 + (\delta \epsilon^p)^2}$ is dependent on the stress increment $\sqrt{\delta q^2 + \delta p^2}$. This observation indicates that a single yield surface of the form derived by Roscoe and Schofield (1963) is not sufficient to describe the rotation of the plastic strain rate vectors as the direction of the stress increment vector rotates. The concept of a second yield surface forming "singular" points with the first yield surface that was introduced by Roscoe and Burland (1968) is a method which can allow for such rotation of plastic strain rate vectors. However the hypothesis that the energy equation used by these authors is only applicable for the derivation of the volumetric yield locus and not the constant q yield locus needs further investigation.

In the conventional triaxial apparatus used by the Author, the principal axes of strain increments, stress increments and of stress are always coincident and two of the three principal stresses or strains are always equal. Under such conditions the Author found that the application of stress increments of the same magnitude in different directions caused the strain increments

to lie on an ellipse. It is therefore possible that in the general three dimensional stress system (σ_1 , σ_2 , σ_3) the application of a stress increment ($d\sigma_1$, $d\sigma_2$ and $d\sigma_3$) could cause the strain increments to lie on the surface of an ellipsoid in strain increment space ($\dot{\epsilon}_1$, $\dot{\epsilon}_2$ and $\dot{\epsilon}_3$). Further work is now in progress to verify this concept for the general three dimensional stress system.

The experimentally observed strain increment ellipses presented in Figs.6.44 to 6.45 are compared with those predicted from the stress-strain theory of Roscoe and Poorooshasb (1963) in Figs.6.50 to 6.54 inclusive. It can be seen that for stress increments lying between the conventional undrained stress path and the anisotropic consolidation path, the strain increment vectors obtained by employing the Roscoe and Poorooshasb theory lie on only part of the complete ellipse. This is because their method of predicting shear strains was restricted to stress paths lying between the undrained stress path and the anisotropic consolidation path. The Author has already shown that the revised theory of Roscoe and Burland (1968) predicts identical strains to those of Roscoe and Poorooshasb (1963). Hence this revised theory would also be capable of predicting the strain increment vectors corresponding to the stress increments lying between the undrained stress path and the anisotropic consolidation path.

The Author has not studied the variation of the strain increments with stress increments for initial state points within the state boundary surface. It is probable that similar strain increment ellipses may exist for stress increments applied on specimens at such initial state points. These ellipses if they exist will be smaller in magnitude than the ellipses described in Figs.6.44 to 6.48, which apply for states of stress lying on the state boundary surface. This will be so since the volumetric strains associated with stress increments lying inside the state boundary surface are of an order of magnitude smaller than the corresponding strain for state paths on this surface.

The volumetric and shear strains predicted from the Roscoe and Poorooshasb theory and the corresponding experimentally observed strains are compared for three state paths each with constant dq/dp lying between the conventional undrained path and the anisotropic consolidation path in Figs.6.55 to 6.60. Excellent agreement is noted between the experimentally observed strains and the theoretical strains.

6.4 Strains predicted by the stress-strain theory of Roscoe and Poorooshasb (1963) for stress paths with decreasing stress ratio

Roscoe and Poorooshasb (1963) in section 8(a) implied that their theory could be applied with confidence provided the value of the stress ratio η did not decrease at any stage when predicting strains caused by given imposed stress paths. They also suggested that it may be possible to relax this requirement. In this section the author makes attempts to compare predictions from their theory with his experimental results for imposed stress paths in which η was decreasing. For such stress paths it will be shown that this incremental stress-strain theory needs some modification. For example it is necessary, to obtain satisfactory agreement between predictions and observations, to neglect the undrained compohent of the shear strain on the right hand side of equation 6.31. This would lead to the following expression for shear strain

$$(\delta\epsilon)_{drained} = \left(\frac{d\epsilon}{dv}\right)_{\eta} \cdot \delta v \qquad 6.73$$

In equation 6.73 it is assumed that the value of $(d\epsilon/dv)_\eta$ which is given by $f_2(\eta)$ when η is increasing is also valid when is decreasing. This assumption may not be correct; it will in fact be shown later that $(d\epsilon/dv)_\eta$ for the phase in which the stress ratio η is decreasing is lower than that when η is increasing.

In an earlier section it has been shown that the volumetric strain increment dv associated with shear strain of equation 6.73 can be expressed in the form

$$dv = \frac{\partial F}{\partial \eta} d\eta + \frac{\partial F}{\partial p} dp \qquad 6.31 \text{ bis}$$

for stress paths in which η increases. The validity of equation 6.36 for stress paths in which the stress ratios decrease has not been ascertained. It will be shown that for stress paths with decreasing stress ratio and lying above the tangent to the conventional undrained stress path in the (q,p) plane, equation 6.36 is valid. Experimental observations on tests with decreasing values of stress ratio will now be presented.

Fig.6.61 (i) shows the imposed stress path ABC during a constant p shear test on sample BP AB followed by the stress path BC in which η decreases. The curves in Fig.6.61(ii) and (iii)

give the (η, ε) and (η, υ) curves predicted by the Roscoe and Poorooshasb theory and the points on these diagrams represent experimental observations during test BP. Similar results for other imposed stress paths in which η first increases and then decreases are given in Fig.6.62 for sample CO and in Figs.6.63 and 6.64 for samples BX. In these tests on samples BP, CO and BX the portion of the stress path BC with decreasing η is always outside the tangent to an undrained stress path through B in (q,p) space. For all these tests there is good agreement between predictions and observations for the volumetric strain relationships but the shear strains are somewhat overpredicted. This confirms the statement made in the paragraph immediately below equation 6.73 that $(d\epsilon/d\upsilon)_\eta$ is smaller when η is decreasing than when η is increasing. Figs.6.65 and 6.66 represent conditions for test CM in which the portion BC of the stress path with decreasing η is below the tangent to the undrained stress path through B. In this case both the strains are underpredicted. It must be remembered that Roscoe and Poorooshasb stated that their theory could not be used for predicting strains in this region.

The revised theory of Roscoe and Burland (1968) for the conditions of tests BP, CO and BX will not include the contribution of shear strain from the constant q yield loci for portions of the stress paths in which η is decreasing. Hence their Revised theory is identical to their Modified theory for such paths and both are the same as the Roscoe and Poorooshasb theory as used by the author above without the undrained component of shear strain.

From the above observations the following conclusions may be drawn:

(i) For stress increment vectors lying between the undrained stress path and the anisotropic consolidation path the original Roscoe and Poorooshasb theory and the Roscoe and Burland revised theory give accurate predictions of both volumetric and shear strains.

(ii) For stress increment vectors lying between the anisotropic consolidation path and the downward tangent to the undrained stress path in the (q,p) space, the Roscoe and Burland Revised theory and the Roscoe and Poorooshasb theory without the undrained component gives accurate predictions of volumetric strains but overpredicts the shear strains.

(iii) For stress increments directed inside the downward tangent to the undrained stress path in (q,p) space neither the volumetric nor the shear strains can be accurately predicted, by the Roscoe and Poorooshasb theory. The Revised Roscoe and Burland theory would predict that only elastic volumetric strains occur during the portion BC of the stress path on sample CM and that the shear strains are zero. It can be seen in Fig.6.66 that the observed shear strains are small for the path BC.

6.5 The behaviour of specimens when reloaded along stress paths with $d\eta > 0$ and $dp \geq 0$ subsequent to imposed paths in which $d\eta \leq 0$ and $dp \geq 0$

The stress-strain behaviour during subsequent unloading and reloading of initially sheared samples with p increasing all the time will now be considered. The type of stress paths imposed on the four samples CO, CL, BP and CP and their previous stress histories are shown in Figs.6.67, 6.70, 6.73 and 6.76 respectively. These specimens were initially sheared from the isotropic stress state A to stress states B with increasing stress ratios. Subsequently the specimens were sheared from B to C along stress paths with decreasing deviator stress (q) and increasing mean normal stress (p). This second phase of shear can be divided into two types depending on the slope of the applied stress path. In Fig.6.67(a) the stress path BC' lies above the tangent to the undrained stress path through B and stress path BC'' lies below this tangent. It has been shown in section 6.4 that the state C' of the specimen lies on the undrained state boundary surface and the state C'' lies inside the undrained state boundary surface. The third phase of reloading of the specimens from the stress states C' and C'' corresponding to the two paths C'D' and C'' D'' will now be studied separately.

(i) Reloading of specimens with initial states on the state boundary surface.

In the third phase of shear (CD) the specimens were subjected to stress paths with increasing stress ratio. For all specimens it can be seen in Figs.6.68, 6.71, 6.74 and 6.77 that the volumetric strains at the end of the second phase of shear corresponds approximately to those predicted from the undrained state surface. Also for all specimens during the reloading phase, the volumetric strains are very close to those predicted from the undrained state surface by the Roscoe and Poorooshasb theory

(which, of course, is the same as the Revised theory of Roscoe and Burland (1968)). The shear strains experienced by the specimens during the loading and reloading phases are illustrated in Figs.6.69, 6.72, 6.75 and 6.78. It has already been shown that there is little agreement between prediction and observation for the shear strains during the unloading process BC. Hence in these diagrams the predicted and observed values of the shear strains at points C (which is the start of the reloading process) have been made to agree at this point. The excellent agreement between the predicted and the experimental shear strains in these diagrams demonstrates that the theories can be used to calculate the volumetric and shear strains during reloading, provided the states of the specimen at the beginning of the reloading phase lies on the state boundary surface.

(ii) Reloading of specimens from states lying below the state boundary surface.

Fig.6.79 shows the stress path imposed on sample CM where the first shear loading AB is under approximately constant p (90 psi)conditions. During the unloading portion BC the deviator stress was reduced to about a third of its value at B, while the mean normal stress p increased by about 30 psi. In the portion CE, the sample was reloaded under a stress path $dq/dp = 3$ (corresponding to a conventional fully drained compression test). The portion BCD_2 is below the state boundary surface where D_2 is on the volumetric yield locus passing through B. The $(q/p, v)$ relationship during the first stage of shear is represented by the points between A and B in Fig.6.80, while the curve AB is the predicted relationship by both the Roscoe and Poorooshasb theory and the Revised theory of Roscoe and Burland. The same relationship as observed experimentally during the unloading process is given by the points between B and C in Fig.6.80. Over this range it is strictly not correct to use the Roscoe and Poorooshasb theory but as a matter of interest, the author has assumed that it can be applied when η is decreasing and $dp > 0$ and obtained the resultant curve BC_1 for the predicted behaviour during the unloading process. The Roscoe and Burland theory can be applied to predict the strains in this unloading process and of course the volumetric strain is in theory entirely elastic. Their predicted curve is represented by BC_2 in Fig.6.80. During the reapplication of the shear corresponding to the stress path CE in Fig.6.79 the Roscoe and Poorooshasb theory predicts the

curve C_1E in Fig.6.80, while the points between C and E were obtained from experiment. The Roscoe and Burland theory predicts elastic strains over the range CD_2 of the reloading path and thereafter, their predicted curve lies on that predicted by Roscoe and Poorooshasb. In calculating the elastic strains for the paths BC_2, C_2D_2 it was assumed that κ was 0.06. This value was taken to be consistent with its assumed value in the previous sections of this chapter. It is of interest to note that if κ had been equal to 0.03 then the point D_2 would have been on the curve C_1E. It is evident that the prediction begins to agree with observation during the reloading process as the volumetric strain increases (as has previously been indicated in Figs.6.71, 6.74, etc.). The initial divergence is probably due to plastic volume change during the unloading and reloading processes below the state boundary surface. The corresponding (q/p, ϵ) relationships for this sample CM are shown in Fig.6.81. in which the points are experimentally observed while the curves have been predicted for both theories except that no attempt has been made to predict shear strains from the Roscoe and Poorooshasb theory for the portions of the state paths BCD_2 below the state boundary surface. There is excellent agreement between the predicted and observed values.

Figs.6.82, 6.83 and 6.84 show corresponding information for the similar test on sample BO, in which (as can be seen in Fig. 6.82) the unloading path corresponded to reducing q to zero while p increased by about 10 psi and the state path lay very close to the state boundary surface as η was reduced. The agreement between prediction and observation is better than for the previous sample CM; in the case of the volumetric strains this may have been due to the much smaller range of change in p. The excellent agreement between predicted and observed values of q/p and v during the path D_2E is clearly evident.

6.6 Recoverable strains

It was shown in section 6.2 that the volumetric strain is only recoverable for stress paths applied within a narrow region below the state boundary surface (see D_1CD_4 in Fig.6.2e). What is implied by the statement that the volumetric strain is recoverable is that, in this region, the application of any closed cycle of stress (in which the unloading and reloading paths coincide) does not produce a net positive volumetric strain. In other words if the (q, ε) and (p, v) characteristics during such a reversal

of stress form hysteresis loops, the strains will be regarded as recoverable if the hysteresis loops are closed. If the loops enclose negligible area then the strains are not only recoverable but will also be called elastic.

The results of a number of cyclic loading tests on one sample (CG) from three initial states on the state boundary surface will now be presented. The first state point on the boundary surface is represented by point A_1 in Fig.6.85(a) (for which q = 50, p = 146). An imposed stress cycle is represented by $A_1B_1A_1$ in Fig.6.85(a) (in which B_1 has coordinates q = 1 and p = 115) and the corresponding (q, ε) and (p, v) relationships are shown in Fig.6.85(b) and (c) respectively. It can be seen that both strains were recoverable and elastic.

Two further cycles from the same point A_1 (q = 50, p = 146) were carried out to points B_2 (q = 1, p = 103) and B_3 (q = 1, p = 82) respectively. The results are shown in Fig.6.86 and Fig. 6.87 respectively. For the stress cycle $A_1B_2A_1$ the strains are recoverable and elastic. But for the cycle $A_1B_3A_1$, the strains are virtually recoverable but are not elastic in the sense defined above. It will be noticed that for all the three stress cycles the change of q is the same for each, but the change of p is considerably greater for the last cycle in which the closed hysteresis loops were observed. It has been shown in Chapter 3, that the strains were anisotropic under reduction of isotropic stress. Hence the above may be due to the development of preferred orientation of clay particles.

The second state point on the state boundary surface is represented by point A_2 in Fig.6.88(a) (for which q = 75, p = 145). The imposed stress cycle $A_2B_4A_2$ is such that B_4 has coordinates (q = 1, p = 100). Figs.6.88(b) and (c) show that despite reduction of p of 45 psi the strains are virtually recoverable and elastic. This however is not the case for the stress cycle A_2B_5 shown in Fig.6.89(a) where p was reduced by more than 100 psi, the volumetric strain is recoverable but not elastic (see Fig. 6.89(b)) while the shear strains are neither recoverable nor elastic (see Fig.6.89(c)). The later phenomenon indicates that the material has experienced reversed yielding (shear distortion) during the phase in which q was reduced, this may be attributed to the Bauchinger effect.

The third state point on the state boundary surface is represented by A_3 in Fig.6.90(a), which corresponded to a very high

stress ratio of η = 0.65 (A_2 corresponded to η = .52 and A_1 to η = 0.34). During the stress cycle p changed, by more than a 100 psi and the conclusions regarding the behaviour of the sample during the cycle A B A is the same as for the cycle $A_2B_5A_2$.
3 6 3

In Chapter 7 it is shown that during the unloading phase, the volumetric strains and the shear strains vary logarithmically with the mean normal stress p and the deviator stress q respectively. Hence if reversed yielding is prescribed by strains exceeding a given magnitude then it is possible to define a local stress region in the (q,p) plane within which the material can be assumed to be rigid.

The data already presented, and discussed above, has shown that during the reloading phase the (p,v) characteristic is linear for a wide range of stress paths. Consequently quantitative expressions relating the stress and strain during unloading and reloading may be defined and will be presented in Chapter 7.

6.7 Loading and Unloading of heavily Overconsolidated specimens

Consider specimen T_{19} which was normally consolidated to 90 psi and then isotropically swollen back to a pressure of 8 psi. This specimen was subsequently subjected to the stress path AB_1A indicated in Fig.6.91(a). The (q,ε) characteristic and the (q,v) characteristic corresponding to all three phases of shear are illustrated in Figs.6.91(b) and (c) respectively. During the first phase in which the specimen was loaded along AB_1, it experienced a compressive volumetric strain of 7 p.c. and a shear strain of 4 p.c. However during the stress path B_1A, a negative shear strain of 1.4 p.c. and a volumetric strain (swelling) of -4 p.c. is experienced. Hence in the stress cycle AB_1A, this specimen experienced an irrecoverable volumetric strain of 3 p.c. and an irrecoverable shear strain of about 2.9 p.c. The above behaviour of the overconsolidated specimens is therefore quite different from the behaviour exhibited by the normally consolidated specimens during the unloading and reloading phases (section 6.6). A detailed investigation of the stress-strain behaviour of overconsolidated specimens is presented in Chapter 7.

6.8 Stress-strain behaviour of specimens subjected to cyclic stress paths with $dq < 0$ and $dp > 0$ and lying inside the state boundary surface

Consider specimen BU initially isotropically consolidated to

A(0, 90) and subsequently sheared to point B (40, 57) in Fig. 6.92(a) along the stress path AB. The specimen was then subjected to the stress path BA. The (q, ε) characteristic and the (p, v) characteristic of this specimen are given in Figs. 6.92(b) and (c). During this phase of shear BA, the specimen experienced a positive volumetric strain of 2.8 p.c. and a negative shear strain of 1.8 p.c. as represented by BA in the strain diagrams. However, when this specimen was reloaded along the path AB the volumetric strain recovered was extremely small and the shear strain was about 0.6 p.c. (see $A'B'$ in Figs. 6.92(b) and (c)). A second application of the stress path BA, caused a volumetric strain of only 0.4 p.c. and a shear strain of -0.6 p.c. as represented by $B'A''$ in the strain diagrams. This observation indicates that the first application of the stress path BA causes large magnitudes of volumetric and shear strain, but subsequent stress applications only cause small s trains. The same phenomenon was observed during the second reloading along AB as represented by the curves $A''B''$. These results will be discussed further in Chapter 7.

6.9 Stress-strain behaviour of a specimen subjected to cyclic stress paths with increasing stress ratio ($\delta\eta > 0$) and decreasing deviator stress ($\delta q < 0$) and mean normal stress ($\delta p < 0$) during the unloading phases

Consider specimen T_{17} in Fig.693(a), which has been sheared to point A (q = 30, p = 90) on the state boundary surface along a constant p stress path from 90 psi isotropic stress. Subsequently the specimen was subjected to the cyclic stress paths AB_1A, AB_2A and AB_3A. For each of the stress paths the stress ratio (q/p) was increased while q and p were decreased and vice versa. The corresponding (q, ε) characteristics and the (p, v) characteristics are as indicated in Figs.6.93(b) and (c). It can be seen that the shear strain ε increased in all three stress paths for which the deviator stress q was decreasing. The deformation of Kaolin for stress paths of the form AB_1, AB_2 and AB_3 during which the stress ratio is increased therefore corresponds to unstable deformation, since the shear strain increased even though the deviator stress q was decreased. Insufficient experimental information was acquired by the author to study this region of unstable deformation in detail. However since the magnitudes of the shear strain and volumetric

strain were small for the initial phase of shear, it is possible to define regions in the stress plane for which, the deformation can be assumed to be small. In this way a region can be defined at each stress level within which the behaviour is rigid, and outside of which unstable deformation can take place. Now consider the stress paths B_1A, B_2A and B_3A during which the deviator stress was increasing while the stress ratio (η) was decreasing. It is again observed that the shear strain ϵ is positive for these stress paths even though the stress ratio (q/p) has been decreasing. It is therefore evident that for the stress region investigated, it is possible for the specimens to experience positive shear strain for any stress cycle of the type AB_1A both along AB_1 and along B_1A. This is the only region in the stress plane (q, p) within which a closed stress cycle can be applied on the specimen, such that the incremental deviator strain experienced by the specimen is always of the same sign for all values of stresses lying on the stress cycle. The author has classified this stress region as an unstable region since the application and the removal of deviator stresses along any stress path within this region cause an incremental shear strain of the same sign.

The major conclusions throughout this chapter have been presented at the end of each section. They will be reconsidered in Chapter 8 when they are discussed in the light of the whole of the work presented in this dissertation.

CHAPTER 7

CONSTITUTIVE EQUATIONS FOR THE STRESS-STRAIN BEHAVIOUR OF CLAYS IN BOUNDED STRESS REGIONS

7.1 General Introduction

Soils exhibit a wider variety of stress-strain behaviour than metals and it is difficult to establish a simple mathematical model that can adequately describe the mechanical behaviour for all possible forms of applied stress path. Even if such a model was developed it is likely to be so complicated as to be of limited use to the practising engineer. It is therefore necessary to make rational idealizations in order to derive simple constitutive equations. These equations are then only able to describe the stress-strain behaviour over a restricted range of applied stress paths. In this chapter the author studies the stress-strain behaviour of clays from experimental observations, and then attempts to develop equations that provide a framework within which the observed behaviour under a wider variety of stress paths can be correlated. These equations are found to describe characteristic surfaces in the stress-strain space and it may be appropriate to look for a possible correlation between these surfaces and the yield surfaces used in plasticity theories of the type developed at Cambridge.

The four variables that are considered in the present analysis are q, p, υ and ϵ. In general, the quantities υ and ϵ are heavily dependent on the stress path. Therefore before any attempt is made to set up simple mathematical expressions for strains based on scalar functions of q and p it is necessary to see whether it is possible to find specific stress paths for which the relationships among q, p, υ and ϵ are unique. If one can find the criterion which divides the stress paths into groups within which approximate equations can be derived for the stress-strain behaviour, then it is possible to set up mathematical models for the general behaviour, prescribing the particular stress region in which these models are valid. Depending on the magnitude of (dq/dp), the stress paths which originate from the isotropic consolidation pressure are divided into three groups as shown on section 7.2 and succeeding sections. In order to keep the effects of the initial one dimensional consolidation stress the same, all samples were initially prepared under the same 1-D stress and subsequently sheared from the same isotropic

stress state.

7.2 The first group of stress paths for which $d\upsilon \geq 0$ and $d\eta > 0$

Fig.7.1 illustrates the possible forms of stress paths in this first group. Except for the undrained stress path, all the other stress paths in this figure are linear. It will be shown in a later section that the stress-strain relationships derived for these linear stress paths are also applicable to non-linear stress paths, for which $dp \geq 0$, within this region. First the three applied stress paths OA, OB and OC with slopes (dq/dp) of ∞, 3 and 1.5 respectively, all starting from an isotropic stress of 90 psi, are considered.

7.2.1 The strain paths in (υ, ϵ) space for the first group of stress paths

Fig.7.2 shows the strain paths followed by the three specimens AO, AD and AY in (υ, ϵ) space. It is to be noted that the strain paths are convex to the ϵ-axis and have different slopes at the origin. The higher the initial value of $(d\upsilon/d\epsilon)$, the lower is the value of (dq/dp).

7.2.2 The contours of constant (q/p) in (υ, ϵ) space for the first group of stress paths

Fig.7.3 shows the contours of constant (q/p) on the strain paths in (υ, ϵ) space. These contours are found to be approximately linear and therefore it is possible to relate υ and ϵ by the relation

$$\epsilon = \psi(\eta) + \mathcal{Z}(\eta) \cdot \upsilon \qquad 7.1$$

where the function $\psi(\eta)$ gives the variation of shear strain in an undrained test (corresponding to the intercept on the -axis of the constant η lines) and $(1/\mathcal{Z}(\eta))$ corresponds to the slope of the constant $(\eta = \frac{q}{p})$ contours in (υ, ϵ) space. The $(q/p, \upsilon, \epsilon)$ surface corresponding to the relationship (7.1) is shown in isometric views from two directions in Figs.7.4(a) and (b). The projections of this surface on the $(q/p, \epsilon)$ and $(q/p, \upsilon)$ planes are given in Figs.7.5 and 7.6.

7.2.3 The constant volume (undrained) test in $(q/p, \upsilon, \epsilon)$ space for the first group of stress paths

In section 7.2 only stress paths with slopes ∞, 3 and 1.5 were considered, and the constant (q/p) contours were found to be linear in (υ, ϵ) space. The $(q/p, \epsilon)$ relationship corresponding

to zero volumetric strain is extrapolated from these contours and plotted as the crosses in Fig.7.7. The $(q/p, \varepsilon')$ relationship observed experimentally in an undrained test is also illustrated in this figure by the circles. The remarkable agreement between the two relationships illustrates that the undrained test too lies on the $(q/p, v, \varepsilon)$ surface corresponding to the three specimens with stress path slopes of ∞, 3 and 1.5. Wroth (1965) pointed out that at constant stress ratio the ratio of the shear strain observed in fully drained test (applied stress path of slope 3) to that in undrained test (constant volume) was a constant. While this observation is in agreement with the author's results, it should be borne in mind that the linear relationship observed by Wroth was derived from his mathematical model which includes an energy equation of the form

$$q = Mp + \left(\frac{p}{1+e}\right)\frac{\partial e}{\partial \epsilon} + \left(\frac{\kappa}{1+e}\right)\frac{\partial p}{\partial \epsilon} \qquad 7.2$$

This energy equation is identical to that originally proposed for the Cam-clay model by Roscoe, Schofield and Thurairajah (1963). Expressing the voids ratio term in equation 7.2 in terms of volumetric strain, it can be shown that

$$\frac{dv}{d\epsilon} = \frac{M-\eta}{\left(1-\frac{\kappa}{\lambda}\right)} \qquad 7.3$$

A comparison of $(dv/d\epsilon)_\eta$ derived from equation 7.3 and the function $1/Z(\eta)$ as observed experimentally is shown in Fig.7.8. It is evident that the two characteristics are different.

7.2.4 The $(q/p, v, \varepsilon)$ relationship at 60 psi isotropic stress for the first group of stress paths

Experiments performed with similar applied stress paths (to those shown in Fig.7.1) but on samples initially consolidated at 60 psi isotropic stress indicate a similar, but not identical, $(q/p, v, \varepsilon)$ relationship to that for the specimens sheared from 90 psi isotropic stress. The constant (q/p) contours in the (v, ε) space for tests starting from 60 psi isotropic stress are shown in Fig.7.9. This relationship is shown in an isometric view in Fig.7.10. The projections of this surface in the $(q/p, \varepsilon)$ plane and the $(q/p, v)$ plane are illustrated in Figs.7.11 to 7.12. It is appropriate at this point to comment on the use of total shear strain ε as a parameter in describing the stress-strain behaviour of soils. In addition to the parameters (p, q, e) used by Roscoe, Schofield and Wroth (1958) to describe the state

surface, Ladyani et.al.(1965) used total shear strain $\in$ as a state variable. From the experimental observations provided at the two isotropic stresses of 60 and 90 psi it is evident that the $(q/p, v, \in)$ surfaces corresponding to the two stress levels are displaced along the v axis as indicated in Fig.7.13. Hence there is no unique $(q/p, v, \varepsilon)$ surface, indicating that the use of ε as a state variable is not correct as pointed out by Roscoe and Poorooshasb (1963). Therefore the relationship 7.1 derived in section 7.2.2 is only applicable for specimens sheared from a given isotropic stress state.

7.2.5 The $(q/p, v, \varepsilon)$ surface of specimens sheared in extension from 60 psi isotropic stress for the first group of stress paths

So far the investigation has been confined to compression tests where the intermediate principal stress is always equal to the minor principal stress in a conventional triaxial system. Experimental observations will now be presented for extension tests where the intermediate principal stress is equal to the major principal stress, Since the maximum cell pressure that can be applied to the standard Clockhouse triaxial cell is limited to about 150 psi, it was necessary to carry out the extension tests from 60 psi isotropic stress. The (v, ε) characteristic for four types of tests are given in Fig.7.14. In these strain paths, the contours of constant (q/p) are also indicated. The results are presented in an isometric view in the three dimensional space $(q/p, v, \varepsilon)$ in Fig.7.15. The projections of these test paths are also given in Figs.7.16 and 7.17 in the $(q/p, \varepsilon)$ plane and $(q/p, v)$ plane respectively. From the experimental observations provided it is clear that the overall behaviour of the specimens on the extension side is very similar to that on the compression side.

7.2.6 The correlation of $(q/p, v, \varepsilon)$ surfaces for compression tests for the first group of stress paths.

It was shown in section 7.2.4 that the $(q/p, v, \varepsilon)$ surfaces originating from different isotropic stresses are displaced along the v-axis by the corresponding volumetric strain due to isotropic consolidation. Also ε_v^t was shown that v and $\in$ are related by an expression

$$\in = \psi(\eta) + \mathcal{I}(\eta)\, v \qquad 7.1 \text{ bis}$$

The function $\psi(\eta)$ corresponds to the shear strain ϵ experienced by a specimen in an undrained test. Experimental observations have been presented in Chapter 4 (see Figs.4.18 and 4.25) to illustrate that the function $\psi(\eta)$ is independent of the initial one dimensional stress history of the specimens and the subsequent level of isotropic consolidation. It therefore remains to investigate the last term of equation 7.1 containing v and the function $Z(\eta)$. Fig.7.18 shows the variation of $1/Z(\eta)$ with η for tests on samples prepared at 60 and 90 psi. It can be seen that the variation of $1/Z(\eta)$ with η is approximately unique for the two $(q/p, v, \varepsilon)$ surfaces at 60 and 90 psi isotropic stresses.

7.2.7 The comparison of the $(q/p, v, \varepsilon)$ surfaces of compression and extension tests at 60 psi isotropic stress for the first group of stress paths

It was shown earlier in section 7.2.5 that the extension tests also give a $(q/p, v, \varepsilon)$ surface, which was similar to that of the compression tests. It will be interesting to establish whether the two surfaces are identical. The (v, ε) projections of the two surfaces are shown in Fig.7.19 and are found to be similar, however significant differences are in evidence at the larger strains. The $(q/p, v)$ characteristics and the $(q/p, \varepsilon)$ characteristics are shown in Figs.7.20 and 7.21. These results also indicate that the compression and extension behaviour of the specimens are remarkably similar up to approximately 5 p.c. strain. During shear the major principal axes of the two types of tests (compression and extension) are perpendicular to each other, thus the results indicate that the specimens are nearly isotropic at the end of 60 psi isotropic consolidation.

7.2.8 Theoretical prediction of the $(q/p, v, \varepsilon)$ surface on samples prepared at 90 psi isotropic stress (First group of stress paths)

A detailed investigation of the stress-strain behaviour as predicted by the various stress-strain theories was presented in Chapter 6. It will be of interest to study how far these theories are capable of predicting the $(q/p, v, \varepsilon)$ surface generated by the types of tests specified in section 7.2.2. The Cam-clay theory predicts the (v, ε) characteristics for the three types of tests (AO constant p, AD fully drained with slope 3, and AY drained with slope 1.5) as shown in Fig.7.22. It can be seen that the differences between the (v, ε) characteristics predicted by the

Cam-clay theory for the three types of tests are small as compared with the experimental observations already presented in Fig.7.3. Also the predicted shear strain corresponding to zero volumetric strain as extrapolated from the constant (q/p) contours is small compared with the actually observed shear strain as shown in Fig.7.3. The (v, ε) characteristics predicted by the modified theory of Roscoe and Burland (1967) is illustrated in Fig.7.23. The constant (q/p) contours are also drawn on the strain paths. The shear strains at zero volumetric strain predicted by the theory (corresponding to the intercept of the constant (q/p) contours with the ϵ-axis) are again smaller than the experimentally observed shear strains presented in Fig.7.3. Fig.7.24 illustrates the (v, ε) characteristics and the constant (q/p) contours as predicted from the incremental stress-strain theory of Roscoe and Poorooshasb (1963). The remarkable agreement in this behaviour with the experimental observations presented in Fig.7.3 indicates that the ($q/p, v, \epsilon$) characteristic as observed experimentally can be successfully predicted by the theory of Roscoe and Poorooshasb (1963).

It has already been shown in Chapter 6 that the revised theory of Roscoe and Burland (1968) predicts the same strains as the theory of Roscoe and Poorooshasb for stress paths of the type discussed above. It also indicates that only under a restricted condition can the parameter ϵ be used as a state variable. Under this restriction, the ($q/p, v, \varepsilon$) surface employed by Ladyani et.al. (1963) is only a special case of the incremental stress-strain theory of Roscoe and Poorooshasb (1963). It will be logical to examine the relation between the incremental strain equation of Roscoe and Poorooshasb and the strain equation 7.1 which is

$$\epsilon = \psi(\eta) + Z(\eta) \cdot v \qquad 7.1 \text{ bis}$$

Differentiating $$d\epsilon = d\psi + v\,dZ + Z\,dv \qquad 7.4$$

The incremental stress-strain theory of Roscoe and Poorooshasb can be written in the form

$$d\epsilon = d\psi + \left(\frac{d\epsilon}{dv}\right)_\eta dv \qquad 7.5$$

From equations 7.4 and 7.5

$$\left(\frac{d\epsilon}{dv}\right)_\eta dv = v\,dZ + Z\,dv \qquad 7.6$$

This equation 7.6 becomes since $dZ = Z'(\eta)\,d\eta$

$$\frac{1}{\upsilon}\left(\frac{\partial \upsilon}{\partial \eta}\right) = \left[\frac{\mathcal{Z}'(\eta)}{f_2(\eta) - \mathcal{Z}(\eta)}\right] \qquad 7.7$$

where $f_2(\eta) = \left(\frac{d\epsilon}{d\upsilon}\right)_\eta$ and represents the slope of the anisotropic consolidation lines in the (ϵ, υ) space. It has been shown in Chapter 6 that υ is only a function of η and p, and this function can be obtained fron an undrained test and an isotropic consolidation test. $\mathcal{Z}(\eta)$ can be determined from a single undrained test and a conventional fully drained test with constant cell pressure. Therefore using the relation 7.7 the value of $f_2(\eta)$ i.e. the slope of anisotropic consolidation line in a (ϵ, υ) space can be obtained from an undrained test and a fully drained test.

7.2.9 The $(q/p, \upsilon, \gamma)$ surface for tests in the S.S.A. and the $(t/s, \upsilon^*, \epsilon^*)$ surface for tests in the biaxial apparatus for the first group of stress paths.

Only a limited amount of experimental data are available on the stress-strain behaviour of the Kaolin under plane strain conditions. Though an extensive series of tests were performed on the S.S.A. by Thurairajah (1961) and Walker (1967) the types of test carried out by these research workers were confined to undrained tests and fully drained tests in which σ' was kept constant. The volumetric strain (υ) and the shear strain (γ) relationships during the two types of test together with constant τ/σ contours are represented by data plotted along OA and OB in Fig.7.25. The other two dotted curves in this diagram have been extrapolated from this limited amount of data and are required to form an overall assessment of the $\frac{\tau}{\sigma}, \upsilon$ and $\frac{\tau}{\sigma}, \gamma$ relationships. The $(\frac{\tau}{\sigma}, \upsilon, \gamma)$ surface for the test paths followed by specimens in this apparatus is illustrated isometrically in Fig.7.26 and is similar to those obtained in the conventional triaxial apparatus. The author has had to limit further investigation into the correlation of the results from the S.S.A. with those from the triaxial apparatus until an assessment is made of the magnitude of the intermediate principal stress and its effect on the S.S.A. results. Preliminary experiments carried out by Hambly (1969) in his biaxial apparatus, under plane strain conditions indicate the existence of constant (t/s) contours in the (υ^*, ϵ^*) space (where $t = \sigma_1' - \sigma_3'$, $s = (\sigma_1' + \sigma_3')/2$, $\upsilon^* = \epsilon_1 + \epsilon_3$ and $\epsilon^* = \epsilon_1 - \epsilon_3$). Further experimental information from the biaxial machine is needed before a correlation between these results and the author's

triaxial test results can be fully explored.

7.2.10 A special type of test where the total strain ratio (υ/ϵ) is equal to the strain increment ratio ($d\upsilon/d\epsilon$) for the first group of stress paths from 90 psi isotropic stress

The experimental observations during drained triaxial tests provided in the previous sections were confined to linear imposed stress paths; the strain paths were observed to be convex in (υ, ε) space. The results of three tests in which linear strain paths, rather than linear stress paths, were followed will now be discussed. In contrast to the anisotropic consolidation paths (i.e. linear stress paths) in which $q/p = dq/dp = \eta$ (a constant) in these tests $\upsilon/\varepsilon = d\upsilon/d\epsilon = \zeta$ (a constant). These tests are now defined as constant ζ tests. The stress and strain paths followed by three specimens in constant ζ tests are shown in Figs.7.27 and 7.28. It can be seen that the stress paths of these specimens (BN, BT and BS) are convex to the p-axis in (q,p) space and are similar in form to the strain paths followed by constant (dq/dp) tests in (υ, ε) space. It is evident in Fig. 7.29 that the constant (q/p) contours obtained from the points plotted on this diagram for specimens BN, BT and BS all lie on the dotted line contours which have been transferred from Fig.7.3 and, of course, refer to specimens with linear stress paths. Hence these specimens have the same ($q/p, \upsilon, \varepsilon$) surface as that for the specimens sheared with linear stress paths from 90 psi (see Fig.7.3).

7.2.11 The (p,q, υ) surface for all tests from 90 psi with the first group of stress paths

The contours in q, p stress space corresponding to constant volumetric strain are similar to the undrained stress path from 90 psi isotropic stress as shown in Fig.7.30. Hence for specimens sheared from 90 psi isotropic stress, the state surface relating (p,q and υ) can be obtained as follows. In Fig.7.31 the undrained stress path AB can be expressed as

$$q = p_o' f(\eta) \qquad 7.8$$

i.e. $p_o = p_o' F(\eta)$ where $F(\eta) = \dfrac{f(\eta)}{\eta}$

Assuming the similarity of constant volumetric strain contours and defining υ as

$$\upsilon = \log\left(\frac{1+e_o}{1+e_o'}\right) \qquad 7.9$$

where $$e_o - e_o' = \lambda \log\left(\frac{p_o'}{p_o}\right) \qquad 7.10$$

From equations 7.9 and 7.10

$$p_o'/p_o = \exp\left[\left(\frac{1+e_o}{\lambda}\right)\left(1-\exp(-v)\right)\right] \qquad 7.11$$

eliminating p_o' from equations 7.8 and 7.11 therefore

$$p = p_o\left(\exp\left[\left(\frac{1+e_o}{\lambda}\right)\left(1-\exp(-v)\right)\right] F(\eta) \qquad 7.12$$

Equation 7.12 defines the state boundary surface relating q,p and v . This equation may be written in the form

$$v = -\log\left[1-\left(\frac{\lambda}{1+e_o}\right)\log\left\{\frac{p}{p_o F(\eta)}\right\}\right] \qquad 7.13$$

and when this equation is combined with equation 7.1 it follows that

$$\epsilon = \psi(\eta) - \mathcal{Z}(\eta)\log\left[1-\left(\frac{\lambda}{1+e_o}\right)\left\{\log\frac{p}{p_o F(\eta)}\right\}\right] \qquad 7.14$$

Equations 7.13 and 7.14 fully describe the stress-strain behaviour in terms of total strains. While equation 7.13 is identical with the state boundary surface used by Roscoe and Poorooshasb (1963), equation 7.14 is only a special case of their incremental stress-strain equation 7.1 , coupled with the equation 7.13

7.3 The second group of imposed stress paths which lie throughout below the state boundary surface.

Five different types of imposed stress paths which cause the states of the specimens to remain below the state boundary surface will be considered in the following subdivisions of this section.

7.3.1 Specimens sheared under swelling conditions ($dv<0$) and with increasing stress ratio .

The experimental observations on five specimens BU, T_{15}, BW, DA and DC will now be discussed in detail. The stress paths for these tests are represented by the dashed lines in Fig.7.32 together with contours of constant shear strain as shown by the continuous curves. Test T_3 is an undrained test and like the three specimens BU, T_{15} and BW were sheared from an isotropic stress

of 90 psi along the stress paths indicated. Samples DA and DC were isotropically swollen back to stresses of 56 and 30 psi respectively and then sheared along stress paths labelled DA and DC.

It will be shown later (in Fig.7.35) that the shear strains experienced by these specimens are of a much smaller order for a given stress ratio than those experienced by specimens which contract in volume when sheared from the normally consolidated state. In Fig.7.32 the shear strain contour corresponding to ϵ = 0.2 p.c. is approximately half way between the isotropic swelling line (i.e. the p-axis) and the current Hvorslev failure envelope. This would imply that the sample is virtually rigid in distortion for stress levels below this contour. Furthermore the shear strain contours appear to be spaced on a logarithmic space in the stress plane. If an empirical equation is derived to represent any one contour then from the geometrical similarity of the contours this equation could be generalised to give an expression for the shear strain ϵ in terms of the stresses q and p for all stress levels up to failure.

The corresponding contour of constant volumetric strain for these five tests are indicated in Fig.7.33. The datum for the volumetric strains recorded for all the tests is taken as zero at the maximum preconsolidation pressure (90 psi). It can be seen that the contours in Fig.7.33 are vertical throughout the observed range for all the paths thereby confirming the elastic wall concept of the Cambridge theories. However further experimental evidence is required to satisfactorily complete the upper ends of these constant volumetric strain contours in regions of high stress ratio near the undrained (υ = o) contour. Since no contours can cross, the upper ends of the contours for small values of υ have been sketched in convex to the p-axis as shown in Fig.7.33. Figs.7.34 and 7.35 show the volumetric and shear strain contour for stress paths lying outside, as well as inside, the undrained stress path. The volumetric strain contours in Fig.7.34 for the paths outside have been taken from Fig.7.30 and inside from Fig.7.33; it is evident that they are quite different in shape. Thus depending on the type of test, the deformation characteristics of the specimens can correspond either to those predicted from the state surface for the normally consolidated region (where the specimens contract) or to those predicted for the overconsolidated state (when the specimens expand). The

deformation characteristic will change from that corresponding to the normally consolidated region to that corresponding to the over-consolidated region at any pointon the state surface when the imposed stress path is directed inside the current volumetric yield locus. When $\kappa = o$ the current yield locus through a point on the state boundary surface coincides with the undrained state path through that point. The converse is only true when the stress path is directed outside the current volumetric yield locus that passed through the state point at which the state path of the specimen first began to go below the state boundary surface. A similar argument is relevant for the incremental shear strain contours in Fig.7.35.

7.3.2 Stress-strain behaviour of overconsolidated specimens sheared under contracting conditions ($d\upsilon \geq o$) and with increasing stress ratio ($\delta\eta > o$)(Second Group)

The results of nine tests (CZ, CX, T_{24}, DA_1, BH, BD, BJ, CY and T_3) on specimens of Kaolin "overconsolidated" from 90 psi are now presented and discussed. The stress paths followed by these specimens are shown in Fig.7.36. The stress path T_3 corresponds to an undrained test on a "normally consolidated" sample from an isotropic stress of 90 psi. The stress paths CY, BH, T_{24} and CZ refer to undrained tests on specimens overconsolidated from a maximum preconsolidation pressure of 90 psi, to isotropic stresses of 70, 56, 30 and 8 psi respectively. The stress paths BD and BJ correspond to a fully drained test (with constant Cell pressure) and a test with an applied stress path of slope 1.5 respectively. on specimens overconsolidated from an isotropic stress of 90 to an isotropic stress of 56 psi. The stress path CX corresponds to a test with applied stress path of slope $dq/dp = 1$ on a specimen previously overconsolidated from an isotropic stress of 90 psi to 30 psi. The stress path DA_1 corresponds to a test (with applied stress path of slope $dq/dp = 2.5$) on a sample previously overconsolidated from 90 to 30 psi. The shear strain contours of 0.2, 0.5, 1, 2 and 3 p.c., for all the nine tests described above are also shown. The shear strain contours are noted to be smooth and continuous for all the nine tests which included both lightly and heavily overconsolidated samples. It is also noted that the shear strain contour corresponding to 0.2 p.c. is approximately halfway between the p-axis and the Hvorslev failure envelope. This implies that the shear strains for deviator stresses of less than half peak value are quite small. For the heavily

overconsolidated specimens the shear strain contours may not be valid for stress paths in which dq/dp is small. For a detailed analysis of the shear strain contours in the heavily overconsolidated region additional experimental observations are required. These experiments should include (i) anisotropic consolidation tests for stress paths lying inside the state boundary surface and (ii) stress probes at various levels of stress ratio, to determine the directions of strain increments and their magnitudes for different directions of stress increments.) The volumetric strain contours for all the stress paths shown in Fig.7.36 are presented in Fig.7.37. The constant volumetric strain contours are found to change in shape from that of the undrained stress path (v = o) through the maximum preconsolidation pressure, as the overconsolidation ratio is increased. The constant volumetric strain contours can be used to obtain the unique surface relating (q,p and v) for stress paths lying inside the state boundary surface.

The contours of shear strain for "overconsolidated" samples which expanded during shear (shown in Fig.7.32) are superposed on those for samples which contracted during shear (shown in Fig.7.36) in Fig.7.38. In Fig.7.39 the volumetric strain contours of Figs.7.33 and 7.37 are superposed. The two types of contours, though appearing to be similar, are not identical. This difference in behaviour, may in part be due to the effect of anisotropy and in part due to nonuniform strains in the specimens which expanded. Experimental observations were provided in Chapter 3 to illustrate that the strains were anisotropic during swelling under isotropic stress conditions. (Further experimental and theoretical investigation is needed before the possible correlation that must exist within each family of contours with some fundamental soil constant or with the Hvorslev envelopes discussed in Chapter 5.)

7.3.3 The stress-strain behaviour of specimens sheared with stress paths where $d\eta > o$, with $dq < o$ and $dp < o$ (Second Group)

Experimental observations provided in the previous sections are such that the shear strain ϵ is always associated with stress paths where the deviator stress q was increasing. However it is possible to impose stress paths with decreasing deviator stress and cause positive shear strains. Typical stress paths of this

type were shown in Fig.6.9$^{3}_{\Lambda}$(a)(b) and (c) and were discussed in detail in section 6.9. In Test T_{17} the shear strain $\in$ was small when the deviator stress q was decreased from 30 to 20 psi, during which there was an increase in (q/p) from 0.33 to 0.4. However when the deviator stress was further decreased from 20 to 11 psi with an increase in stress ratio from 0.4 to 1, very large shear strains were experienced by the specimen. During this phase of shear, when the deviator stress q was decreasing and the stress ratio (q/p) was increasing energy was released from the specimen and was dissipated in plastic shear deformation. This phase of deformation is therefore unstable. The same specimen, T_{17}, was then sheared along the stress path B_1A_1 (see Fig,6.9$^{3}_{\Lambda}$(a)) retracing the original path AB_1, with the deviator stress q and the mean normal stress p now increasing and the stress ratio (q/p) being reduced. During this phase of shear the specimen was found to undergo positive volumetric and shear strains as indicated in Figs.6.9$^{3}_{\Lambda}$(b) and (c) respectively. In this cycle AB_1A_1 the specimen experienced shear distortion of the same sign both during the removal and the reapplication of deviator stress, which corresponded to an increase in (q/p) and a decrease in (q/p) respectively. Hence for stress paths of the form indicated in Fig.6.9$^{3}_{\Lambda}$(a), it is not possible to define a single yield surface, which is relevant to reversal of stress paths of the type described. At present the author has not sufficient information to define the general pattern of the stress-strain behaviour, and consequently to plot volumetric and shear strain contours within this region of the stress plane.

The specimen T_{17} was subsequently subjected to stress cycles $A_1B_2A_2$, $A_2B_3A_3$ and A_3B_4. The magnitudes of shear strains experienced by the sample during these subsequent stress cycles were small compared to those in the stress cycle AB_1A_1, even though the specimen was subjected to the same increase in stress ratio for all stress cycles. This indicates that most of the yielding takes place during the first cycle of stress, and the subsequent cycles produce only small strains.

7.3.4 The stress-strain behaviour of specimens sheared along stress paths with $d\eta<0$, $dq<0$ and $dp<0$ (second Group of stress paths)

The strains are only recoverable in a region in the stress domain in which $d\eta \leq 0$, $dq \leq 0$ and $dp \leq 0$. In this section, the stress-strain behaviour of specimens previously sheared to

stress ratios η of 0.34, 0.47, 0.58, 0.64 and 0.75 and subsequently unloaded along stress paths with $d\eta<o$, $dq<o$ and $dp<o$ are presented. The stress paths followed by the specimens are illustrated in Figs.7.40(a) to (e), in which the specimens are always unloaded from state points such as A which is always on the state boundary surface. A separate specimen was taken to each state point A and subsequently subjected to stress paths which are numbered in the order in which they were traversed. (The results of the reloading stress paths are presented in section 7.3.5.) Stress ratios lower than 0.34 are not considered for the reason that the magnitude of recoverable shear strains are small at low stress ratios. The $(q, \in)$ characteristics of the specimens are illustrated in Figs.7.41(a) to (e). In each of these figures the $(q, \in)$ characteristic is observed to be approximately unique and independent of (dq/dp), during the phase in which q and p are reduced. However it must be emphasisedthat there is a different unique curve for each initial state point A on the state boundary surface. It will be noted that as the stress ratio corresponding to this initial point A is increased the scatter of the (q, ε) data for all the stress paths from that point A increases in magnitude. For example the curves in Figs.7.41(b)(c) and (e) represent the upper and lower limits of this scatter.

Considering the scatter in the results of the recoverable shear strains, the author decided, on the evidence from scanning electron micrographs of the development of particle orientation, to use the lower limit of the (q, ε) characteristic for further analysis. These results are replotted on a semilogarithmic scale (ε, log q) in Figs.7.42(a) to (e). It was found that corresponding to each stress ratio, from which q and p were reduced, there is a unique straight line describing the recoverable shear strain in an ε, log q plot. The slopes of these lines, which are obviously a function of the stress ratio η_s of the starting point A on the state boundary surface, are plotted against η_s in Fig.7.43. It is interesting to note that a linear relationship exists between these slopes and η_s. Also this relationship indicates that this slope is zero when η_s = o corresponding to swelling under isotropic stress.

The (p, v) characteristics of the specimens will now be considered. These characteristics are presented in Figs.7.44(a) to (e). It is noted that corresponding to each initial stress ratio η_s (from which the stresses were reduced), a unique

relation exists between p and υ independent of the deviator stress and the direction (dq/dp) in which the stresses were reduced. These results are replotted on a semilogarithmic (υ, log p) scale in Figs.7.45(a) to (e), where the variation of υ is found to be linear with log p. The slopes of these straight lines are approximately constant and are therefore independent of the previous stress ratio to which each of these specimens was sheared.

(It would be interesting to know the consequences if the deviator stress were further reduced (i.e. below zero), so that the specimen was sheared in extension while swelling. Such experiments would indicate whether there is a discontinuity in the stress-strain curves as the deviator stress reverses in sign. If there is no discontinuity in the (q, ϵ) characteristic then it would be apparent, that the shear strains recovered during the phase in which the deviator stress was reduced are not truly elastic strains.) The recoverable volumetric and shear strains denoted by υ_{rs} and ϵ_{rs} are measured from the datum corresponding to the maximum stress ratio (i.e. the maximum deviator stress q and maximum mean normal stress p for the initial state point A on a state boundary surface.

Then $$\upsilon_{rs} = K_1 \log\left(p/p_s\right) \qquad 7.15$$

and $$\epsilon_{rs} = K_2(\eta_s) \log\left(\frac{q}{q_s}\right) \qquad 7.16$$

k_1 being a constant of magnitude 0.02 and k_2 is also a constant. Differentiating equations 7.15 and 7.16 it can be shown that the ratio recoverable strain rates is given by

$$\left(\frac{d\upsilon}{d\epsilon}\right)_r = \frac{K_1}{K_2}\,\frac{1}{\eta_s}\left(\eta \Big/ \frac{dq}{dp}\right) \qquad 7.17$$

i.e.

$$\left(\frac{d\upsilon}{d\epsilon}\right)_r = \frac{K}{\eta_s}\left(\eta \Big/ \frac{dq}{dp}\right) \qquad 7.18$$

where $K = \frac{K_1}{K_2}$

Equation 7.18 indicates that the ratio $\left(\frac{d\upsilon}{d\epsilon}\right)_r$ of the recoverable strains is also a function of the stress ratio and the stress increment ratio. This property was shown to be true for the deformation characteristic of normally consolidated clay (see section 6.3.9). Also the above equation indicates that for anisotropic swelling under constant stress ratio η the ratio

$(dv/d\epsilon)_r$ is a constant and is dependent only on the stress ratio η_s from which the stresses q and p are reduced. The deformation characteristics described by equations 7.15 and 7.16 are different from those of overconsolidated clays of the type dicussed in sections 7.3.1 and 7.3.2. The magnitude of the shear strains experienced by this type of overconsolidated clay is considerably higher than the magnitude specified by equation 7.16.

Also from equations 7.15 and 7.16

$$\eta = \eta_s \exp\left(\frac{\varepsilon_r}{v_r}\frac{1}{K\eta_s}\right) \qquad 7.19$$

Equation 7.19 describes the relationship between the stress ratio η and the strains ϵ_{vs} and v_{vs}. It is seen that this relationship describes a surface in the 3-D space (η , ε_{vs} and v_{vs}). The shape of this surface is dependent on the parameter η_s. The relation 7.19 may be compared with equation 7.1 for normally consolidated clays, which is

$$\epsilon = \psi(\eta) + \mathcal{F}(\eta).v. \qquad 7.1 \text{ bis}$$

7.3.5 The stress-strain behaviour of specimens during reloading when $d\eta > 0$, $dp > 0$ and $q \leq q_s$, $p \leq p_s$

(Second Group)

It has already been shown in section 6.6 that the (q, ϵ) characteristics and (p, v) characteristics of specimens for stress paths where q and p are reduced are different from the corresponding characteristics obtained by retracing the same stress path with increase in q and p. The stress-strain behaviour during the phase in which q and p are reduced is dealt in the section 7.3.4. In this section the (q, ε) characteristics and the (p, v) characteristics during the reloading phase in which q and p were increased are presented and discussed. The reloading stress path commences approximately at zero deviator stress, the corresponding mean normal stress being denoted by p_u. The specimens are reloaded to five different stress ratios, as shown in Figs.7.46 to 7.50 inclusive. In each figure the letters B,C,D.... indicate the initial stress level, from which the specimens are reloaded and A corresponds to the state point on the state boundary surface to which the specimens are reloaded and from which they were previously unloaded. The volumetric strain contains (measured from new datum points corresponding

to the initial stress state B,C,D....) are shown in Figs.7.51 to 7.55 inclusive. The contours are for volumetric strains of 0.1, 0.2, 0.5, 1 and 2 p.c. respectively, for each of the five specimens. These results indicate that for specimens reloaded from the stress states B,C,D... to A, a unique relation exists between the volumetric strains and the stresses q and p. The variation of υ with p for each path is shown in Fig.7.56 to 7.60 inclusive, and is linear with constant slope for any particular η_s. (Where η_s still refers to the point A.) Hence the volumetric strain contours during reloading can be approximated by the equation

$$\upsilon = k_3 (p - p_u) \qquad 7.20$$

where k_3 is a function of the maximum stress ratio η_s. The variation of k_3 with η_s is illustrated in Fig.7.61. Despite some scatter the results indicate that

$$k_3 = f(\eta_s) \qquad 7.21$$

The equations 7.20 and 7.21 are only approximate relations that describe the variation of volumetric strain with pressure during reloading of specimens which have been initially subjected to a maximum stress ratio η_s.

The corresponding shear strain contours of the specimens whose stress paths are illustrated in Figs.7.46 to 7.50 are presented in Figs.7.62 to 7.65. If these shear strain contours are assumed to lie approximately along lines of constant stress ratio, then the magnitude of shear strain during reloading can be expressed as

$$\epsilon = f_5 (\eta_s, \eta) \qquad 7.22$$

Fig.7.66 gives the $(\frac{q}{p}, \varepsilon)$ characteristics of the specimens when reloaded to different stress ratios η_s. In this figure the (η, ε) relation is found to be dependent on the values of η_s. No simple relationship is evident between η, ε and η_s.

7.3.6 The stress-strain behaviour of specimens sheared along stress paths with $dq<0$, $dp \geq 0$ and $|dq/dp| > |s|$ where s is the slope of the current volumetric yield locus. (Second Group)

The type of stress paths which satisfy the conditions specified above are paths which have been directed inside the

current volumetric yield locus (which coincides with the conventional undrained stress path if k = o) in the (q,p) plane in a direction in which q was decreasing and p was increasing. During the application of these stress paths the specimens experienced volumetric strains which were very much higher than the corresponding elastic component. In this section the volumetric and shear strains experienced by samples (CT, CR and BU) when sheared along three stress paths, as indicated in Fig.7.67, are presented. The datum for strains is taken as zero at the initial state point A on the state boundary surface. The volumetric strain contours are shown by dashed lines in Fig.7.68. It is noted that these volumetric strain contours are different in shape to those presented in section 7.3.1 which were deduced from specimens which had been sheared with an increase in stress ratio. The volumetric strain contours shown in Fig.7.68 would seem to intersect the current yield locus passing through A. The zero volumetric strain contour in Fig.7.68 can be expressed as

$$q = p_o' f^*(\eta) \qquad 7.23$$

where p_o' corresponds to the isotropic stress at which the zero volumetric strain contour meets the p axis. The variation of the volumetric strain with p_o is illustrated in Fig.7.69

where $$v = k_5 p_o' + k_6 \qquad 7.24$$

where k_5 and k_6 are constants.

The equations 7.23 and 7.24 approximately describe the volumetric strain contours plotted in Fig.7.68. The constants k_5 and k_6 may be functions of the stress ratio η_s from which the deviator stress was first unloaded.

The shear strain contours for the three specimens are shown in Fig.7.70. In this figure the shear strain contours approximate to the horizontal indicate that the shear strain is only dependent on the deviator stress and is independent of the mean normal stress p. The (q, ε) relationship as obtained from the constant shear strain contours are replotted in Figs.7.71 and 7.72, in the (q, ε) and $(\varepsilon, \log q)$ plots. The shear strain ε varies linearly with log q and therefore can be expressed as

$$\varepsilon = k_7 \log\left(\frac{q}{q_s}\right) \qquad 7.25$$

where k_7 is a constant.

7.4 The third group of stress paths for which $dp>0$ and $\eta > dq/dp > S$ where S is the slope of the current yield locus

The stress paths of the type specified above are shown in Fig.7.74. These paths all start from a point A on the state boundary surface which they reached by being sheared under constant p conditions from an isotropically consolidated state at 90 psi. These paths lie between the downward tangent to the yield locus through A and the constant η line through A. For these paths the ratio $(dv/d\epsilon)$ of the strain increments were found to be greater than those corresponding to the constant stress ratio line through A. The volumetric strain corresponding to these paths were predicted in section 6.4 using the state surface formed by the undrained stress paths. Excellent agreement was observed between the experimental volumetric strains and the predicted strains as shown in Figs. 6.71 and 6.73. However the predicted shear strains (from equation 6.73) using the values of $(dv/d\epsilon)_\eta$ obtained from anisotropic consolidation tests were greater than the experimentally observed shear strains. The magnitude of $(dv/d\epsilon)$ corresponding to any particular values of (dq/dp) was found to be a constant as shown for specimens CF and T_{12} in Fig.6.46. Hence for stress paths applied in this region it is reasonable to assume that $(dv/d\epsilon)$ will only be a function of (dq/dp) at any particular stress ratio but further data is required to confirm this. The shear strain, ϵ in relation to that for stress paths in which η was increasing, was found to be small.

7.5 Concluding Remarks

The main conclusions for each section have been presented at the end of each section but they will be presented in Chapter 8 in summary form and briefly discussed in the light of all the evidence presented in this thesis.

CHAPTER 8

CONCLUSIONS AND RECOMMENDATIONS FOR FUTURE RESEARCH

8.1 Conclusions on Chapter 3

8.1.1 One dimensional consolidation using the lead shot technique for measuring local strains

The friction measurements carried out during 1-D consolidation indicates that the percentage of load lost in friction can be reduced to as low as 10 p.c. by lining the inner surface of the consolidometer with a rubber membrane lubricated with a thin layer of silicone grease.

The local measurements of strains carried out with the lead shot technique show that the consolidation was uniform throughout the sample for the first increment of stress, when the clay (initially in the form of a slurry (160 p.c. m.c.)) was consolidated to about two thirds of its original height. For subsequent stress increments elements of clay nearest to the free draining surface were found to experience less consolidation than elements further from it.

The changes of overall average voids ratio as computed by summing the local values obtained from the local measurements of strains were in excellent agreement with those determined directly from the boundary measurements, at all stress levels.

The observed local voids ratio changes with time, when compared with the corresponding theoretical values as derived from the Modified theory of consolidation of Davis and Raymond (1965) (using the numerical procedure of Richart (1957)) illustrate:-

(i) The observed local voids ratio was in good agreement with the theoretical predictions for the top half of the specimen which was close to the free draining surface.

(ii) For elements far from the free draining surface the experimental observations deviated from the theoretical predictions.

The pore pressure isochrones determined from the local measurements of voids ratio were similar to those observed by actual local pore pressure measurements by Burland (1967).

8.1.2 Isotropic consolidation and swelling

For specimens contained between frictional ends, the axial and radial strains were found to be nonuniform during isotropic consolidation. With the use of lubricated ends this nonuniformity

in strains was reduced to a minimum. In both specimens the local volumetric strains were observed to be uniform throughout the sample.

The overall average voids ratio changes computed from the local measurements were in excellent agreement with those computed from the moisture content determination and the burette readings.

For isotropic stresses of similar magnitude to the initial one dimensional stress, the strains induced by increments of isotropic stress were found to be anisotropic. However for specimens which were isotropically consolidated to approximately three times the initial one dimensional stress, the effect of anisotropy was found to be small.

Experiments performed on 4 inch diameter samples showed that the axial and radial strains were uniform, but not equal, during swelling under isotropic stresses.

8.1.3 The displacement patterns and strain distributions during shear

The effects of end restraint on the axial and radial strain distributions were determined for 1.5 inch diameter specimens contained between (i) frictional ends and (ii) lubricated ends, in each case during a fully drained test ($dq/dp = 3$) and during an undrained test. The strain distributions plotted for all increments of stress up to failure showed that (i) marked non-uniformity in the strain developed in the specimens contained between frictional ends and (ii) substantially uniform strains (up to about 75 p.c. of the peak stresses) occurred throughout the specimens contained between lubricated ends.

A detailed investigation of the displacement patterns and the strains distributions on 1.5 inch diameter and 4.0 inch diameter samples both in compression and in extension indicated that (i) the axial and radial displacement patterns of the markers varied linearly with their vertical and horizontal positions respectively (ii) the axial and radial strains were moderately uniform up to about 75 p.c. of the peak stresses (iii) the principal axes of the local strains were coincident with the vertical and horizontal axes of the specimen (iv) the overall average axial and volumetric strains computed from the local strain measurements were in excellent agreement with the overall average measurements conventionally measured using a dial

gauge (for change in length) and a burette (for change in volume) (v) the local strains in the grids of the 4 inch diameter sample when plotted in the form of a histogram (i.e. the local strains number of grids) approximated to a normal distribution curve for each increment of stresses up to the peak value.

The local measurements of strains carried out on 1.5 inch diameter and 4 inch diameter on normally, and on lightly and heavily overconsolidated, samples revealed similar behaviour to that presented in the preceding paragraphs.

During progressive failure in compression, rigid zones were found to develop at the two ends of the specimens. These observed rigid zones, were symmetrical about the axis of the sample and were found to subtend an angle of approximately $\phi = 20^\circ$ with the end plattens. Theoretical analysis carried out by Haythornthwaite for triaxial compression tests predicted the formation of rigid zones, the boundaries of which subtend an angle with the end plattens of $(45 + \phi/2^\circ)$. No rigid zones were observed during progressive failure in extension tests, though Haythornthwaite's analysis would predict the formation of rigid zones subtending an angle of $(45 - \phi/2^\circ)$ with the base.

8.2 Conclusions on Chapter 4

8.2.1 The effect of initial moisture content of slurry on the stress-strain behaviour

The stress-strain behaviour and the $(q/p_e , p/p_e)$ characteristic of remoulded specimens were found to be dependent on the initial moisture content of the slurry from which the specimens were prepared. These effects became more marked as the initial moisture content of the slurry was made less than twice the liquid limit.

8.2.2 The effect of initial 1-D stress on the stress-strain behaviour

Fully drained compression tests (with constant cell pressure) on specimens prepared under different initial 1-D stresses and subsequently consolidated under the same isotropic stress showed that the $(q/p , v)$ characteristic, the $(q/p , \varepsilon)$ characteristic and the $(q/p_e , p/p_e)$ characteristic were dependent on the magnitude of the initial one dimensional stress. However the stress-strain behaviour of all these samples was found to be unique for shear stresses greater than had been imposed during the initial 1-D consolidation.

A set of undrained samples prepared in a similar manner showed that the (q/p, ε) characteristic was unique at all stress levels but the (q/p_e, p/p_e) characteristic depended on the initial 1-D stress. However this latter characteristic was found to be unique for shear stresses in excess of those imposed during the initial 1-D consolidation.

8.2.3 The effects of subsequent isotropic consolidation on the stress-strain behaviour

The stress-strain behaviour and the (q/p_e, p/p_e) characteristics for three types of tests (an undrained test, a constant p test and a fully drained test with $dq/dp = 3$) on specimens prepared with the same initial one dimensional stress condition and subsequently sheared from three different isotropic stress levels were studied in detail.

The observed (q/p, ε) characteristic for undrained tests was found to be independent of the previous isotropic consolidation stress level. However the (q/p_e, p/p_e) characteristics for these undrained tests were found to be dependent on the extent of the preliminary isotropic consolidation. A method based on the initial shear stress (as described in the preceding section) was suggested for the correlation of these results to give unique behaviour in the (q/p_e, p/p_e) space.

The (q/p, v), (q/p, ε) and the (q/p_e, p/p_e) relationships for the constant p tests and the fully drained tests were also found to be dependent on the magnitude of the isotropic consolidation subsequent to the initial 1-D stress prior to shear. These results were also correlated successfully to give unique behaviour.

8.2.4 The effects of time on the stress-strain behaviour

The deformation of Kaolin is considered in two phases; a time dependent phase in which the effect of time under constant applied stresses is predominant and a time stable phase in which the effect of time can be accounted for by using logarithmic relations (e.g. (ε, log t) and (v, log t)). The stress-strain behaviour of constant volume tests indicate that in the time dependent region, a unique relationship exists between (q, u, ε and t). For creep tests performed on specimens under undrained conditions with constant deviator stress, this relationship was studied by considering any one of the following four projections in the 3-D space relating (a) q, u and ε (b) q, ε and t (c) u, ε and t and (d) q, u and t.

For tests, in which the specimens contract, with stress increments applied at intervals of time which are longer than required for pore pressure dissipation, it was shown that the behaviour of the specimen was unique in the $(q/p, v)$, $(q/p, \varepsilon)$ and $(q/p_e, p/p_e)$ spaces. However in the time stable region the shear strains and the volumetric strains at any particular stress ratio were found to vary logarithmically with time. The rate of deformation $d\epsilon/d(\log t)$ was found to be a linear function of the stress ratio η and the rate of volumetric strain $dv/d(\log t)$ was found to be a constant for a given stress ratio. Thus the strain rate $(dv/d\epsilon)$ in the time stable region was only a function of the stress ratio η. The incremental stress-strain theory of Roscoe and Poorooshasb which was essentially derived to describe the stress-strain behaviour in a continuous test, was then modified to include the effects of time in the time dependent and the time stable regions.

8.2.5 The effects of local increment size and other miscellaneous factors on the stress-strain behaviour

The stress-strain behaviour of drained test $(dq/dp = 3)$ specimens was found to be dependent on the load increment size and this effect was shown to be entirely due to the difference in stress paths followed by specimens which had been subjected to different load increment sizes. The load increment size was then reduced to such an extent that its effect on the (q, ε) (q, v) and $(q/p_e, p/p_e)$ relationship during any application of load was within the limits of the experimental accuracy. This size of load increment was subsequently used in all tests in which the effects of stress paths were investigated.

Experiments performed on 4 inch x 4.5 inch samples indicated the same stress-strain behaviour as the 1.5 inch x 3 inch samples. This would imply that the stress-strain behaviour described in this dissertation is independent of the sample size.

8.3 Conclusions on Chapter 5

The investigation of the conditions at peak stresses showed that the peak stress envelopes in the (q,p), $(\Delta e_f, p_f)$ and $(\Delta e_f, q_f)$ spaces coincide with those of the conventional critical state line for tests covering a wide variety of stress paths where $p_f/p_o \geq 1$. However for values of $p_f/p_o < 1$ the peak stress points were found to lie on a Hvorslev type curve in the $(q_f/p_o, p_f/p_o)$ space. This curve has a unique projection in the

(Δe_f , p_f/p_o) and (Δe_f , q_f/p_o) spaces respectively. For specimens which experience only elastic volumetric changes from stress states with $\eta > 0$ it appears that a series of parallel curves (starting from the original unique envelope) exist in the (Δe_f , p_f/p_o) and (Δe_f , q_f/p_o) spaces. Further experimental work is needed before a proper interpretation can be made of these parallel curves.

8.4 Conclusions on Chapter 6

In Chapter 6 the stress-strain behaviour of Kaolin for all possible forms of loadings were presented. The observed strains were compared with the strains predicted from various stress-strain theories which were based on the concept of plasticity and other postulates.

8.4.1 The stress region in the (q,p) plane in which the volumetric strains are recoverable

Stress angles applied in all directions in the (q,p) plane from any initial state point on the state surface, indicated that the volumetric strains were only recoverable in a narrow region D_1CD_4 as shown in Fig.6.2(e). Outside this region the application of stress cycles on samples of Kaolin caused irrecoverable volumetric strains. According to the Cam-clay theory and its modification the regions in which plastic volumetric strains cannot take place are much wider than the limited zone indicated in Fig.6.2(e) showing that the yield surfaces predicted by the above theories are possibly oversimplifications.

8.4.2 The prediction of strains from the Cam-clay theory and the Modified theory

From the data presented in section 6.2 it was seen that (i) the Cam-clay theory overpredicts the volumetric and shear strains in all types of tests in which the samples contract and the modified theory underpredicts the shear strain in all types of tests especially in the undrained and constant p tests. The volumetric strains predicted by the modified theory are in agreement with the experimental observations.

8.4.3 The conditions under which the Cam-clay theory, the Modified theory and the Revised theory will predict identical strains to those of the Roscoe and Poorooshasb theory

The stress-strain theory of Roscoe and Poorooshasb was presented in a modified form to enable it to be compared with the

other theories developed at Cambridge based on an energy balance and the concepts of plasticity. Conditions were stated and verified experimentally to illustrate when the Cam-clay theory or the Modified theory or the Revised theory would predict identical strains to those of the Roscoe and Poorooshasb theory. This investigation showed that while all the four theories could be expressed mathematically in a similar form it is only the energy equation used in the Revised theory that can give an expression which is able to predict identical volumetric strains to those of the Roscoe and Poorooshasb (1963) theory. Also the additional (constant q) yield locus, used in the Revised theory is necessary for successful predictions of shear strains.

8.4.4 The flow rule

Experimental observations provided in section 6.3 illustrate that at any state point the magnitude of the strain increments vector $(d\upsilon/d\epsilon)$ is a function of the stress ratio η and the stress increment ratio (dq/dp). At constant stress ratio the relationship between $(d\upsilon/d\epsilon)$ and (dq/dp) is approximately hyperbolic and this relationship is dependent on the stress ratio η. The results when plotted in the 3-D space $(\frac{d\upsilon}{d\epsilon}, \frac{dq}{dp}, \frac{q}{p})$ were found to lie on a surface.

8.4.5 The strain increment ellipse for stress increment vectors of constant magnitude but different directions

For constant stress increment $(\sqrt{\Delta q^2+\Delta p^2})$ applied in different directions at any stress ratio η, the strain increment vector $\sqrt{\Delta\upsilon^2+\Delta\epsilon^2}$ was found to lie on the periphery of an ellipse. This strain increment ellipse at $\eta=\hat{o}$ has its major axis coincident with the v-axis in a (υ, ϵ) plot. However as η increases, this major axis rotates clockwise in (υ, ϵ) space until at failure it is approximately parallel to the ϵ axis. Assuming that the elastic strains are an order smaller than the plastic strains, the strain increment ellipse indicates that the direction of the plastic strain rate vector $d\upsilon^p/d\epsilon^p$ is dependent, not only on the stresses q and p, but also on the stress increments Δq and Δp. This observation indicates that a single yield surface satisfying the condition of normality as used by Roscoe, Schofield and Thurairajah (1963a) or Schofield and Wroth (1968)(i.e. the Cam-clay theory) is not sufficient to describe the rotation of the plastic strain rate vector at any state point. The stress strain theory of Roscoe and Poorooshasb or the Revised theory of Roscoe and Burland

provides a method which allows such a rotation of the plastic strain rate vector.

8.4.6 The regions in which the stress-strain theory of Roscoe and Poorooshasb and the Revised theory of Roscoe and Burland can predict the same strains as those observed experimentally

The Roscoe and Poorooshasb theory can predict (i) the volumetric and shear strains for all paths, with $\delta\eta > 0$, that lie in between the conventional undrained stress path and the anisotropic consolidation path. (ii) Only the volumetric strains for all paths that lie between the anisotropic consolidation path and the downward tangent to the conventional undrained stress path. The Revised theory is also valid for the above two types of stress paths and in addition is capable of predicting strains approximately for stress paths which lie inside the state boundary surface in a downward direction. Also during reloading on specimens which have been unloaded under increasing p conditions, both theories can predict the volumetric and shear strain for all stress paths that lie on the state boundary surface.

8.4.7 The stress-strain behaviour of specimens subjected to miscellaneous stress paths inside the state boundary surface

The region inside the state boundary surface was divided into four sections shown in Fig.8.1. The applications of stress cycles in regions b, c and d show that (1) the deformation is unstable in region (b) where a cycle of stress causes shear strain of the same magnitude and sign both during the phase in which q was decreasing as in the phase in which q was increasing.
(2) The volumetric strains are recoverable and elastic in region (c) for small reductions of p and the volumetric strains are recoverable but not elastic for large reductions of p. The shear strains are recoverable and elastic for unloading from low stress ratios but are neither recoverable nor elastic for unloading from high values of stress ratio for this region.
(3) In region (d), the application of stress cycles caused large irrecoverable volumetric strains and small irrecoverable shear strains.

8.5 Conclusions on Chapter 7

The stress paths are classified into three groups (see Fig.8.2)

depending on the magnitude of (dq/dp) and states of the specimens in relation to the state boundary surface. Group (1) of the stress paths are such that the states of the specimen always lie on the state boundary surface and η is always increasing. Group (2) of the stress paths are such that the states of the specimen always lie inside the state boundary surface, and group (3) of the paths is such that the states of the specimen lie on the state boundary surface but η decreases. Constitutive equations were proposed to describe the stress-strain behaviour in each region.

8.5.1 The stress-strain behaviour of specimens subjected to stress paths classified in Group 1

For all specimens sheared from an isotropic stress state under stress paths of the type classified in group 1, constitutive equations were developed for the prediction of shear strains and volumetric strains. These equations gave characteristic surfaces in $(q/p, v, \varepsilon)$ space, which are displaced along the v axis depending on the initial isotropic consolidation stress. Specimens sheared in extension also displayed similar behaviour to those sheared in compression. The surfaces predicted by the Cam-clay theory and the Modified theory were found to be similar to the experimentally observed surface but not identical. The stress-strain theory of Roscoe and Poorooshasb and the Revised theory of Roscoe and Burland successfully predicted the experimentally observed relationships.

8.5.2 The stress-strain behaviour of specimens sheared under stress paths classified in Group 2

The stress paths classified in group 2, where the states of the specimens always lie below the state boundary surface were again subdivided into 6 types as shown in Fig.8.3.

In Type (i) tests the specimens were sheared under the conditions $d\eta > 0$ and $dv \leq 0$. Volumetric and shear strain contours were then plotted in the (q,p) stress plane to describe the stress-strain behaviour. The shear strain contours were found to be similar to each other. Hence it was possible to derive equations to describe the shear strain. The volumetric strain contours were found to be vertical for all stress levels except for those states for which were close to the state boundary surface.

Similar volumetric and shear strain contours were observed

in the Type (ii) tests, where the specimens are sheared under the conditions $d\eta > 0$ and $dv \geq 0$. However these contours were found to differ from those obtained for the Type (i) tests. This difference is, in part attributed to the anisotropic deformation of Kaolin and in part to possible experimental errors for the specimens sheared under Type (i) stress paths.

The stress-strain behaviour in the Type (iii) tests (where $\Delta q \leq 0$, $\Delta p \leq 0$ and $\Delta \frac{q}{p} \geq 0$) is shown to be unstable since the specimens were capable of experiencing positive shear strain for all the stress states in a closed cycle of stress. The author did not obtain sufficient information to plot strain contours in this region of the (q,p) stress planes.

For the Type (iv) tests where the specimens were subjected to stress paths with $\Delta q \leq 0$ $\Delta p \leq 0$ and $\Delta q/p \leq 0$, the volumetric and shear strains (v and ϵ) were found to vary linearly with log p and log q respectively. Equations were derived to describe those variations and the expressions relating volumetric and shear strains were found to be similar to those for the Group 1 stress paths and the volumetric strains could be predicted by the Cam-clay and the Modified theories.

During shear under Type (v) stress paths where the specimens were reloaded under the condition $\Delta q > 0$, $\Delta p > 0$, $\Delta q/p > 0$ the volumetric and shear strain contours were plotted and equations are derived to describe the variation of strains with stresses.

For the Type (vi) tests, where the specimens were sheared under the condition $dv \geq 0$, $dq < 0$ and $dp > 0$ volumetric and shear strain contours were plotted and equations were derived to describe the strains in terms of the stresses.

8.5.3 Stress-strain behaviour of specimens sheared under stress paths classified in Group 3

Since the states of the specimens lie on the state boundary surface for all stress paths of this type (see Fig.8.2), the volumetric strains can be predicted from the stress-strain theory of Roscoe and Poorooshasb and the Revised theory of Roscoe and Burland. However the shear strains observed experimentally were smaller than those predicted from the above theories. The magnitudes of $(dv/d\epsilon)$ for this type of stress path were found to be a function of dq/dp and q/p. Further experimental investigation is needed to explore the exact relationship between $\frac{dv}{d\epsilon}$, $\frac{dq}{dp}$ and $\frac{q}{p}$ in this region.

Recommendations for further work

From the conclusions stated above it is evident that the stress-strain behaviour is broadly dependent on the stresses and is independent of the imposed stress path followed within the specific regions defined by the author. The author's experimental observations, though they cover all the possible forms of stress paths, are not complete. Many more tests must be carried out in which stress probes are applied to samples in initial states below the state boundary surface. The author has indicated the additional instrumentation and the experimental work required for future research under the various relevant sections in each chapter. The critical state parameters are found to be satisfactory for the description of the stress-strain behaviour in Group 1 tests. However the fundamental parameters that govern the behaviour of the specimens in Group 2 and Group 3 tests need further exploration.

Stress Increment psi	6.2 to 12.2	12.2 to 24.7	24.7 to 48.5	48.5 to 96.7	96.7 to 48.5	48.5 to 24.7	24.7 to 12.6	12.6 to 6.2
Duration of Time (days)	2	2	3	3	1	2	3	3
Voids ratio Change	2.16 to 1.95	1.95 to 1.75	1.75 to 1.50	1.50 to 1.304	1.304 to 1.31	1.31 to 1.35	1.35 to 1.39	1.39 to 1.428

(a) Perspex Consolidometer. Test Designation H

Stress Increment psi	5.6 to 11	11 to 22	22 to 44.2	44.2 to 88.6	88.6 to 44.2	44.2 to 22	22 to 11	11 to 5.6
Duration of Time (days)	3	2	2	1	1	1	1	3
Voids ratio Change	2.38 to 1.96	1.96 to 1.74	1.74 to 1.532	1.532 to 1.325	1.325 to 1.34	1.34 to 1.379	1.379 to 1.419	1.419 to 1.455

(b) Duralumin Consolidometer. Test Designation L

Stress Increment psi	5.8 to 11.6	11.6 to 22.8	22.8 to 45.8	45.8 to 91.7	91.7 to 45.8	45.8 to 22.8	22.8 to 11.6	11.6 to 5.8
Duration of Time (days)	2	1	1	3	1	2	2	1
Voids ratio Change	2.17 to 1.975	1.975 to 1.772	1.772 to 1.547	1.547 to 1.319	1.319 to 1.328	1.328 to 1.360	1.360 to 1.390	1.390 to 1.418

(c) Triaxial former Test Designation N

Table 2.1 (a) - (c) One dimensional Consolidation and Swelling tests

Stress increment in psi	24.9 to 46.5	46.5 to 65.9	65.9 to 88.5
Duration of Time (days)	1	3	1
Voids ratio Change	1.581 to 1.430	1.430 to 1.342	1.342 to 1.273

(a) Friction End. Test Designation J

Stress increment in psi	25 to 46	46 to 67	67 to 89
Duration of time (days)	4	3	4
Voids ratio Change	1.550 to 1.418	1.418 to 1.333	1.333 to 1.247

(b) Conventional lubricated end. Test Designation M

Stress increment in psi	25 to 46.2	46.2 to 66.6	66.6 to 89.2
Duration of Time (days)	1	1	1
Voids ratio change	1.591 to 1.437	1.437 to 1.338	1.338 to 1.265

(c) Enlarged end (Lubricated). Test Designation P

Table 2.2 (a) - (c) Isotropic Consolidation tests

Test Designation	Initial 1-D Stress psi	Isotropic Stress psi	Load increment during shear lb	Load increment duration days	Type of end condition	Type of test	Voids ratio at the end of isotropic consolidation
Q	22.6	60	10	2	Enlarged Lubricated	Fully Drained $\frac{dq}{dp}=3$	1.430
R	22.6	60	10	2	Conventional Lubricated	Fully Drained $\frac{dq}{dp}=3$	1.365
S	22.6	60	5	2	Conventional Rough	Undrained	1.368
T	22.6	60	10	2	Conventional Rough	Drained $\frac{dq}{dp}=3$	1.372
U	22.6	60	5	2	Enlarged Lubricated	Undrained	1.365

Table 2.3 Drained and Undrained Compression tests on $1\frac{1}{2}$ inch diameter sample with different end conditions.

Test Designation	Initial 1-D Stress (psi)	Isotropic stress (psi)	Load increment during shear (lbs)	Voids ratio at the end of Isotropic consolidation
AR	55	60	10	1.343
AB	22	60	10	1.366
AU	11	60	10	1.402

(a) Fully drained test

Test Designation	Initial 1-D Stress (psi)	Isotropic stress (psi)	Load increment during shear (lbs)	Voids ratio at the end of Isotropic consolidation
T_7	3	60	10	1.350
T_4	22	60	10	1.340

(b) Undrained test

Table 2.4 (a) and (b) Shear tests on specimens prepared with different initial one dimensional consolidation stress.

Test Designation	Initial 1-D Stress (psi)	Isotropic Stress (psi)	Load increment size (lbs)	Duration of Load increment hours	Voids ratio at the end of Isotropic consolidation
Z	22	60	1.0	5 increments a day at 3 hour interval	1.374
R	22	69	10	48	1.366
X	22	60	20	48	1.377
Y	22	60	40	48	1.389

Table 2.5 Shear tests with different load increment size.

Test Designation	Type of test	Initial 1-D stress (psi)	Isotropic stress (psi	Voids ratio at the end of Isotropic consolidation
OB	Drained Compression	22	30	1.538
OC	Drained Compression on Heavily over Consolidated	22	60	1.335
OE	Drained Extension on Normally Consolidated	22	30	1.50

Table 2.6 Tests on 4 inch diameter specimens

Test Designation	Initial 1-D Stress (psi)	Isotropic Stress (psi)	Load increment size (shear)	Load increment duration in days (shear)	Voids ratio at the end of Isotropic consolidation
T_5	22	30	5	2	1.565
T_4	22	60	10	2	1.340
T_3	22	90	15	2	1.231

Table 2. 7 Constant Volume Compression tests.

Test Designation	Initial 1-D Stress (psi)	Isotropic Stress (psi)	Load Increment size (lbs)	Number of load increments per day	Voids ratio at the end of Isotropic consolidation
AJ	22	30	0.5	5 at 3 hour interval	1.580
AQ	22	60	1.0	"	1.398
AO	22	90	1.5	"	1.252

Table 2.8 Constant p compression tests

Test Designation	Initial 1-D Stress (psi)	Isotropic Stress (psi)	Load increment size (lbs)	Number of load increments per day	Voids ratio at the end of Isotropic consolidation
Z	22	60	1.0	5 at 3 hour interval	1.374
AF	22	30	0.5	"	1.562
AD	22	90	1.5	"	1.283
AK	22	120	2.0	"	1.226

Table 2.9 Drained tests with applied stress path ($\frac{dq}{dp} = 3$)

Test Designation	Initial 1-D stress (psi)	Isotropic stress (psi)	Voids ratio at the end of 1-D consolidation	Applied stress path during shear
AP	22	30	1.569	2
AX	22	60	1.424	1.5
AY	22	90	1.277	1.5
CU	22	90	1.232	1
CV	22	90	1.242	0.65
CW	22	90	1.191	0.3

Table 2.10 Other drained tests with $dq > o$, $dp > o$ and $\infty \geq \frac{dq}{dp} > o$

Test Designation	Initial 1-D stress (psi)	Isotropic Stress (psi)	Voids ratio at the end of consolidation	Type of test
* PAL	22	60	1.373	Undrained
BB	22	60	1.366	Applied stress path 1.5
BE	22	60	1.375	Constant p
BG	22	60	1.344	Applied stress path 3

* PAL - Test from Loudon (1967)

Table 2.11 Extension tests

Test Designation	Initial 1-D stress (psi)	Isotropic Stress (psi)	Voids ratio at the end of Isotropic consolidation	Stress ratio η during Anisotropic consolidation	$\left(\frac{dv}{d\epsilon}\right)_\eta$
BF	22	90	1.286	0.205	2.80
BC	22	90	1.270	0.405	1.30
BT	22	90	1.237	0.51	1.00
BL	22	90	1.220	0.57	0.775
T_{10}	22	90	1.237	0.71	0.45

Table 2.12 Anisotropic Consolidation tests

Test Designation	Initial 1-D Stress (psi)	Isotropic Stress (psi)	Voids ratio at the end of Isotropic consolidation	Strain ratio $\left(\frac{v}{\epsilon}\right)$ (Shear)
BN	22	90	1.250	1.36
BT	22	90	1.237	0.66
BS	22	90	1.316	2.0

Table 2.13 Tests with linear strain paths i.e. v/ϵ = constant.

Test Designation	Type of test	Initial 1-D Stress (psi)	Maximum Isotropic Stress (psi)	Isotropic Stress st the end of swelling (psi)	Voids ratio at the end of swelling
CY	Undrained	22	90	70	1.233
BH	Undrained	22	90	56	1.263
T_{24}	Undrained	22	90	30	1.274
CZ	Undrained	22	90	8.2	1.397
BI	Constant p	22	91	56	1.262
BD	Applied stress path $\frac{dq}{dp} = 3$	22	90	56	1.278
BJ	Applied stress path $\frac{dq}{dp} = 1.5$	22	90	56	1.240
CX	Applied stress path $\frac{dq}{dp} = 1$	22	30	70	1.200
DA1	Applied stress path $\frac{dq}{dp} = 2.4$	22	90	30	1.290

Table 2.14 Tests on Over consolidated specimens

Test Designation	Initial 1-D Stress (psi)	Isotropic Stress (psi)	Applied Stress path during shear	Voids ratio at the end of Isotropic consolidation
BU	22	90	-1.5	1.227
BW	22	90	-0.5	1.243
DA	22	56	-0.55	1.234
DC	22	30	-0.50	1.307
T_{15}	22	90	-1.0	1.219

Table 2.15 Tests with stress paths where $dp < o$ $dq > o$ and below the undrained test path in a (p,q) space.

Test Designation	Initial 1-D Stress (psi)	Isotropic Stress (psi)	Stress level (q,p) at which the stresses are decreased	Voids ratio at the end of Isotropic consolidation
T_{17}	22	90	(30,90)	1.294

Table 2.16 Test with stress paths where $dp < o$, $dq < o$ and $d(\frac{q}{p}) > o$.

Test Designation	Initial 1-D Stress psi	Isotropic Stress psi	Stress levels (q,p) at which the stressed are decreased psi	Number of different stress paths followed during removal of stresses	Voids ratio at the end of isotropic consolidation
T_{20}	22	90	(30, 89)	5	1.243
T_{19}	22	90	(31, 68)	1	1.24
CB	22	90	(77, 127)	7	1.240
BP	22	90	(86, 134)	1	1.274
T_{16}	22	90	(42, 59)	6	1.230
CG1	22	90	(50, 146)	5	1.220
CG2	22	90	(77, 145)	5	1.220
CG3	22	90	(99, 145)	4	1.220

Table 2.17 Tests with stress paths where $dp < o$, $dq < o$ and $d(\frac{q}{p}) \leqslant o$.

Test Designation	Initial 1-D Stress (psi)	Isotropic Stress (psi)	Stress level (q,p) of which the constant q path is commenced	Voids ratio at the end of 1-D consolidation
BX	22	90	(40, 59)	1.238
BY	22	90	(31, 77)	1.254
T_{12}	22	90	(30, 90)	1.239
CB	22	90	(20, 83)	1.240

Table 2.18 Constant q tests.

Test Designation	Initial 1-D Stress psi	Isotropic Stress psi	Stress level (q,p) at which the stress paths are applied psi	Approximate Appl. Stress path	Voids ratio at the end of isotropic consolidation
CS	22	90	(38.5, 56)	-2.1	1.254
CT	22	90	(38.5, 56)	$-\infty$	1.232
BU	22	90	(39, 56.5)	-1.5	1.227
BO	22	90	(30, 90)	Tracing the locus of undrained stress path	1.242
CM	22	90	(56, 86)	-1.0	1.246
CN	22	90	(19, 89.5)	Tracing the locus of undrained stress path	1.231

Table 2.19 Tests with stress paths where $dp > o$, $dq < o$, $\frac{dq}{dp} < (\bar{s})$; $\bar{s}$ denoting the slope of undrained stress path in the (p,q) space in a direction in which q is decreasing.

Test Designation	Initial 1-D Stress psi	Isotropic Stress psi	Stress level (q,p) at which the stress paths are applied	Approximate Appl. Stress path	Voids ratio at the end of isotropic consolidation
CO	22	90	(20, 90)	-0.35	1.235
CL	22	90	(32, 90)	-0.30	1.235
BP	22	90	(30, 90)	-0.55	1.274
CP	22	90	(40, 90)	-0.65	1.226

Table 2.20 Tests with stress paths where $dp > o$, $dq < o$ and $d(\frac{q}{p}) > \bar{s}$; $\bar{s}$ denoting the slope of undrained stress path in the (p,q) space in a direction in which q is decreasing.

Test Designation	Initial 1-D Stress (psi)	Isotropic Stress (psi)	Previous stress history during shear	Applied stress path during shear	Voids ratio at the end of Isotropic consolidation
CO	22	90	Constant p path from (0,90) to (20,90) Linear stress path from (20,90) to (2,145)	3	1.235
CP	22	90	Constant p from (0,90) to (40,90) Linear stress path from (40,90) to (7,126)	3	1.226
CL	22	90	Constant p from (0,90) to (32,90) Linear stress path from (32,90) to (15,139)	3	1.235
BP	22	90	Constant p from (0,90) to (30,90) Linear stress path from (30,90) to (5,136)	Constant p	1.274
BO	22	90	Constant p from (0,90) to (30,90) Stress path tracing the locus of undrained stress path from (30,90) to(1,99)	3	1.242
CM	22	90	Constant p from (0,90) to (56,86) Stress path tracing the locus of undrained stress path from (56,86)to (21,105)	3	-

Table 2.21 Tests on specimens which have been initially sheared and subsequently subjected to stress paths where q and p increase.

Test Designation	Initial 1-D Stress (psi)	Isotropic Stress (psi)	The previous stress history	Applied Stress path slope	Voids ratio
CE	22	90	Constant p stress path from (0,90) to (37,90)	0.8	1.250
CF	22	90	Constant p stress path from (0,90) to (31.5,88.5)	0.15	1.240
CH	22	90	Constant p stress path from (0,90) to (29.5, 89)	0.6	1.237
CJ	22	90	Constant p stress path from (0,90) to (19,89)	1	1.247

Table 2.22 Tests with stress paths (where $\frac{dq}{dp}$ = constant) originating from stress ratios higher than zero.

Test Designation	Initial 1-D stress psi	Isotropic stress psi	Slope of Applied stress path	Type of end condition	q_f psi	p_f psi	$\frac{q_f}{p_f}$	$\phi = \tan^{-1}\frac{q_f}{p_f}$ degrees
Q	22.6	60	3	Enlarged end lubricated and with rubber membrane	58.6	79.5	0.738	19.2
R	22.6	60	3	Conventional lubricated end	63.2	81.1	0.768	20
T	22.6	60	3	Conventional rough end	60.6	80.2	0.755	19.5

Table 5.1 The effect of end restraint on the peak stresses

Test Designation	Initial 1-D stress psi	Isotropic stress psi	Slope of Applied stress path	Type of end condition	q_f psi	p_f psi	$\frac{q_f}{p_f}$
AU	11	60	3	Conventional lubricated	57	79	0.72
AB	22	60	3	-do-	60	80	0.75
AR	55	60	3	-do-	53.8	78	0.69

Table 5.2 The effect of initial 1-D stress on the peak stresses

Test Designation	Initial 1-D stress psi	Isotropic stress psi	Slope of Applied stress path	Type of end condition	q_f psi	p_f psi	q_f/p_f
AF	22	30 ~~60~~	3	Conventional lubricated	32.5	40.8	0.8
Z	22	60	3	-do-	63.5	81.2	0.785
AD	22	90 ~~60~~	3	-do-	88.5	119.5	0.740
AK	22	120 ~~60~~	3	-do-	116.9	159	0.735

Table 5.3 The effect on peak stresses of the isotropic consolidation prior to shear.

Test Designation	Initial 1-D stress psi	Isotropic Stress psi	Slope of Applied stress path	Type of end condition	q_f psi	p_f psi	q_f/p_f
AB	22	60	3	Conventional lubricated	59.9	80	0.75
N	22	60	3	-do-	61.1	80.3	0.762
R	22	60	3	-do-	63.2	81.1	0.768

Table 5.4 The effect of load increment duration on the peak stresses.

APPENDIX 1

Effects and Elimination of scattered radiation.

A1.1 General

A1.2 Practical Methods of eliminating scattered radiation

A1.2.1 Increasing the distance between film and object

A1.2.2 Use of filters

A1.2.3 Use of Parallel plate Collimators

A1.2.4 Use of Moving grids

(i) Mechanism to obtain uniform motion
(ii) Transmission of Primary radiation
(iii) Effect of Lateral decentering of grid
(iv) Effect of Error in focus grid distance
(v) Effect of Combined Lateral decentering and error in focus grid distance

A1.3 Tests Carried Out with Bucky grid

A1.4 Conclusion

A1.1 General

During the passage of radiation through a material medium, an initially homogeneous beam of rays becomes more and more heterogeneous due to the effect of scattered radiation. The scattered rays are of wave length longer than the primary beam and the effect at any point is due not only to the primary but also to the secondary radiation.

When a beam of parallel homogeneous radiation passes through any medium of thickness t, the intensity of radiation falls off according to the exponential law

$$I = I_o \exp(-\mu t) \qquad \text{A1-1}$$

where μ is the total absorption coefficient of the radiation in that medium. The decrease in intensity is due to three phenomena

(i) the conversion of quanta from the primary beam into photo-electrons

(ii) the compton effect in which part of the energy of a primary quantum is transferred to an electron and the remainder appears as a scattered quantum of lower energy than the primary

(iii) the nuclear disintegration which is negligible for all except the very short radiation

Hence μ can be expressed as

$$\mu = \tau + \sigma_a + \sigma_s \qquad \text{A1-2}$$

where σ_s referred to the scattered radiation and σ_a to the recoil radiation. If the material is of considerable thickness the scattered radiation can undergo multiple scattering and absorption.

Payne Scott (1936) calculated the quantity and the quality of the scattered radiation under varying conditions. In the quantitative analysis values of σ_a and σ_s are obtained by using the formulae derived by Klein and Nishina

By integrating their original formula, the expressions for ${}_e\sigma$ and ${}_e\sigma_s$ the absorption coefficients per electron corresponding to σ and σ_s is derived as

$${}_e\sigma = \frac{2\pi e^4}{m^2c^4}\left[\frac{1+\alpha}{\alpha^2}\left\{\frac{2(1+\alpha)}{(1+2\alpha)} - \frac{1}{\alpha}\log_e(1+2\alpha)\right\} + \frac{1}{2\alpha}\log_e(1+2\alpha) - \frac{(1+3\alpha)}{(1+2\alpha)^2}\right] \qquad \text{A1-3}$$

$$ {}_e\sigma_s = \frac{\pi e^4}{m^2c^4}\left[\frac{1}{\alpha^3}\log_e(1+2\alpha) + \frac{2(1+\alpha)}{\alpha^2}\frac{(2\alpha^2-2\alpha-1)}{(1+2\alpha)^2} + \frac{8\alpha^2}{3(1+2\alpha)^3}\right] \qquad \text{A1.4} $$

where $\alpha = h\nu/mc^2$

The values of ${}_e\sigma_a$ are obtained by subtraction.
Values of σ_a and σ_s are obtained by multiplying ${}_e\sigma_a$ and ${}_e\sigma_s$ by the number of electrons per unit volume.

Also τ had been derived using the empirical formula derived by Gray

$$ {}_e\tau = 2.24 \times 10^{-35} Z^3 \lambda^3 \qquad \text{A1.5} $$

for $\lambda > 100$ xU
and $\log_e \tau = 33.5102 + \log_{10} Z^3 + \log_{10} \lambda + 0.480(\log_{10}\lambda)^2$
for $0 < \lambda < 100$ xU *

Also at each scattering the incident quantum can be deflected through any angle between 0 and π
The corresponding wave length being given by

$$ \lambda = \lambda_0\left[1+\alpha(1-\cos.\theta)\right] \qquad \text{A1.6} $$

where λ_0 = the wave length of the incident radiation
λ = the wave length of the scattered radiation
$\alpha = h\nu/mc^2 = 24.2/\lambda_0$ when λ_0 is in X.U.

Thus at any point in the scattering medium the radiation comprises of the primary beam with wave length λ_0 and a band of scattered radiation with wave length varying from λ_0 to $\lambda_0 + 48.4$ xU

Also Klein-Nishina expressed the intensity per scattering electron of the medium of the radiation which has been scattered at an angle θ and which has travelled a distance γ in vacuo is given in terms of the intensity I_0 of the incident radiation by

$$ I = \frac{I_0 e^4}{2m^2c^4\gamma^2}\frac{1+\cos^2\theta}{\{1+\alpha(1-\cos\theta)\}^3}\left\{1+\frac{\alpha^2(1-\cos\theta)^2}{(1+\cos^2\theta)\{1+\alpha(1-\cos\theta)\}}\right\} $$

$$ = \left[\frac{I_0 e^4}{2m^2c^4\gamma^2} f(\theta)\right] \qquad \text{A1.7} $$

where $\alpha = h\nu/mc^2$

* X.U $\equiv$ 1 Angstrom unit $= 10^{-8}$ cm

If the total absorption coefficient in the scattering medium of the radiation scattered at an angle θ is μ' then the intensity at P (in Fig.A1.1) of the radiation which has travelled a distance is

$$\left[I_0 \exp\left(-\mu(d-r\cos\theta)\right)\right]\left[\exp\left(-\mu' r\right)\right]\frac{e^4}{2m^2c^4 r}\,f(\theta)$$

per scattering electron.

The number of scattering electrons in the elemental ring is given by

$$\left(\frac{\rho N Z}{A}\right)\left(2\pi r^2 \sin\theta\, dr\, d\theta\right)$$

∴ The intensity of the radiation received at P from this ring is $\left(\frac{\rho N Z}{A}\right)\left(2\pi r^2 \sin\theta\, dr\, d\theta\right)\left[I_0 \exp\left(-\mu(d-r\cos\theta)\right)\right]\left[\exp\left(-\mu' r\right)\right]\frac{e^4}{2m^2c^4 r^2}\,f(\theta)$

Hence the total intensity of the radiation scattered and reaching P can be calculated.

Expressing in terms of λ it is possible to calculate the intensity of the once-scattered radiation included in the wave length λ to $\lambda+d\lambda$

However the above analysis becomes too complicated in the case of granular media with varying geometry and hence such theoretical approach is of little use in the testing of soil specimens.

A1.2 Practical Methods of Eliminating scattered radiation.

A.1.2.1 Increasing the distance between film and object.

By increasing the distance between the film and object it is possible to reduce the influence of scattered radiation. The main objection to this method is the consequent reduction in definition due to the increased size of the penumbra caused by the finite size of the radiation source.

A1.2.2 Use of Filters

Though a certain portion of the scattered radiation can be attenuated by the use of some absorbent material like copper, tin or lead in between the film and object, yet the method is not 100 p.c. effective unless the absorbing material is very thick. However this would cause a large attenuation of the primary radiation reaching the film.

A1.2.3 Use of parallel plate collimators

The parallel plate collimator, Fig.A1.2 shows the variation in film density along the height of a film exposed at 90 KeV with a fine focal spot of 0.4 mm and a focal film distance of 48 inches.

The variation is about 12.4 p.c. The use of a parallel plate collimator as used by Sirwan (1965), reduced the above variation to about 7.7 p.c. (Fig.A1.3). From Fig.A1.3 it can be seen that the parallel plate collimator can be used efficiently only in small regions of the film, besides it leaves a permanent image of the lamellae on the film.

A1.2.4 Use of Moving grids

The most efficient method of counteracting the effect of scattered radiation is by the use of a Potter-Bucky diaphragm. This diaphragm consists essentially of thin strips of lead arranged in such a manner, when seen from the focus appear to be as narrow as possible. The scattered radiation in directions at not too small an angle to that of the primary rays are absorbed by the lead lamellae. The primary rays pass quite freely except when they strike the narrow edge of the lamellae and when attenuated by the material of the lamellae. The diaphragm is moved during the exposure to prevent the formation of any disturbing shadow strips on the film. It is necessary for the diaphragm to remain focussed during motion. There are two methods by which the lamellae can be arranged to be in focus while in motion.

In the first method the lamellae are arranged along the surface of a horizontal cylinder with axis passing through the focus as in Fig.A1.4. In the second method the lamellae are placed in the same plane, but radially with the axis of symmetry through the focus (Fig.A1.5). During the exposure the diaphragm rotates about the centre as shown in Fig.A1.5. The former method is not preferred because of the large distance between the film and the object which will result in a lack of definition of the image. While the latter method has the disadvantage that a white spot appears on the film at the point of rotation.

Hence let us consider the plane focussed grid shown in Fig. A1.6.

(i) Mechanism to obtain uniform motion:

The grid is mounted on a frame shown in Fig.2.8 carrying a roller at one end. The roller moves on the surface of a constant velocity cam. Fig.A1.7 shows the displacement of the grid with time. The cam is rotated at a constant velocity.

(ii) Transmission of primary radiation:

The transmission of primary radiation is given by

$$I_p = \left(1 - \frac{V}{h}\right) \exp(-\mu h)$$

where V is the specific lead volume $V = Ndh$, where N is defined

as the strip density i.e. the number of strips per unit length and h is the height of lead lamellae.

The part of the grid covered by lead = Nd = $'V/h$

By differentiating the above expression it can be shown that the intensity of the primary transmitted radiation I_p is a maximum when

$$h = \frac{1}{2} V \left(1 + \sqrt{1 + \frac{4}{\mu V}}\right)$$

where μ is the absorption coefficient of the organic inter spacing.

Since μ is generally ≤ 0.3

$$h_{opt} = \sqrt{\frac{V}{\mu}}$$

and hence $I_{p.max} \simeq e \times p(-2\sqrt{\mu V})$ Thus the optimum transmission is obtained when the absorption in the lead is approximately equal to that in the interspace .

Under optimum transmission there is a fixed relationship between the strip density N and ratio of the grid given by

$$\frac{N}{r} = -\mu + \sqrt{\mu/V}$$

(iii) Effect of lateral decentering of the grid:

From Fig.A1.8 it can be easily shown that a lateral decentering of the grid by a distance of b causes a reduction in the width of the exposed area by

$$e = \frac{r D b}{f_o} \qquad \text{A1.8}$$

This reduction is the same throughout the film at any distance from the centre line.

(iv) Effect of error in focus grid distance:

From Fig.A1.9 it can be easily shown that the error e in D due to any change in the focus grid distance from f_o to f_2 is

$$e = r d c \left[\frac{1}{f_o} - \frac{1}{f_2}\right] \qquad \text{A1.9}$$

Unlike the former case this error increases with increasing values of c.

Also an increase in the focal grid distance from f_o to f_2 is equivalent to a lateral decentering distance of $c\left[\frac{1}{f_o} - \frac{1}{f_2}\right] f_o$

(v) Effect of Combined Lateral decentering and error in focus grid distance:

The decrease in D by e is different at symmetrical positions

from the centre of the grid due to this error. The corresponding errors at equal distance c from the centre is given as

$$e_1 = \left[b + (c-b)\left(1 - \frac{f_o}{f_2}\right)\right] rd/f_o$$

and

$$e_2 = \left[b - (b+c)\left(1 - \frac{f_o}{f_2}\right)\right] rd/f_o \qquad \text{A1.10}$$

See Fig.A1.10

A1.3 Tests carried out with Bucky grid

The positive prints of radiographs taken with the parallel plate collimator and the static grid are shown in Figs.A1.11(a) and (b) respectively. Though the lines look uniform in Fig. A1.11(b) a closer look will reveal a considerable percentage of the nonuniformity in grid thicknesses. The thickness of these lamellae were measured using a Hensholdt Wetzlar Microscope. Accurate measurements of the grid lamellae are limited by the fading nature of the lamellae on the film at the edges. Also the suggested focus grid distance of 36 $\pm$ 3 inch give thicknesses of lamellae at the centre about 4 to 5 thou. greater than those at the edges. The approximate focus is found to be at 40.75 inch Figs.A1.12 and A1.13 show the variation in film density along the height of the film and across the film. While the percentage variation in the former is about 16 p.c., the one in the latter is only 1.325 p.c. Since the latter variation is not affected by the uniformity of grid thickness and the errors due to lateral decentering and focus grid distance, it is apparent that a finer grid with improved quality will give an even smaller variation in density across the film. Table A1.1 gives the percentage variation in film density with and without the parallel plate collimator and Bucky grid.

Table A1.1

	Type of Collimation	Along height of film 6 in.	Across the film about 6 in.
		Density Variation in p.c.	
1.	Without grid	12	5.6
2.	With Parallel plate Collimator	7.7	7.75
3.	With grid and Parallel plate Collimator	-	2.22
4.	With grid alone	16.0	1.33

Finally the efficiency of the grid in improving the contrast of the lead markers used in samples of sand about 7.5 inches thick is shown in Fig.A1.14(a-c).

A1.4 Conclusion

From the density measurement carried cut across the film it is apparent that with a good quality grid a constant film density can be achieved in one direction. It is possible to calibrate the variation in film density in the perpendicular direction. Since density measurements are generally carried out along the axis of a cylindrical sample it is always possible to oscillate the grid in a horizontal direction, thereby achieving constant density. The grid improves the contrast of the lead markers and reduces the fogging of radiographic film and therefore should lead to an increaase in the accuracy of the measurement of strains. The effect of a grid can be seen from Fig.A 1.14(a to c) which shows positions of radiographs of a sand sample without a grid, with a static grid and with an oscillating grid.

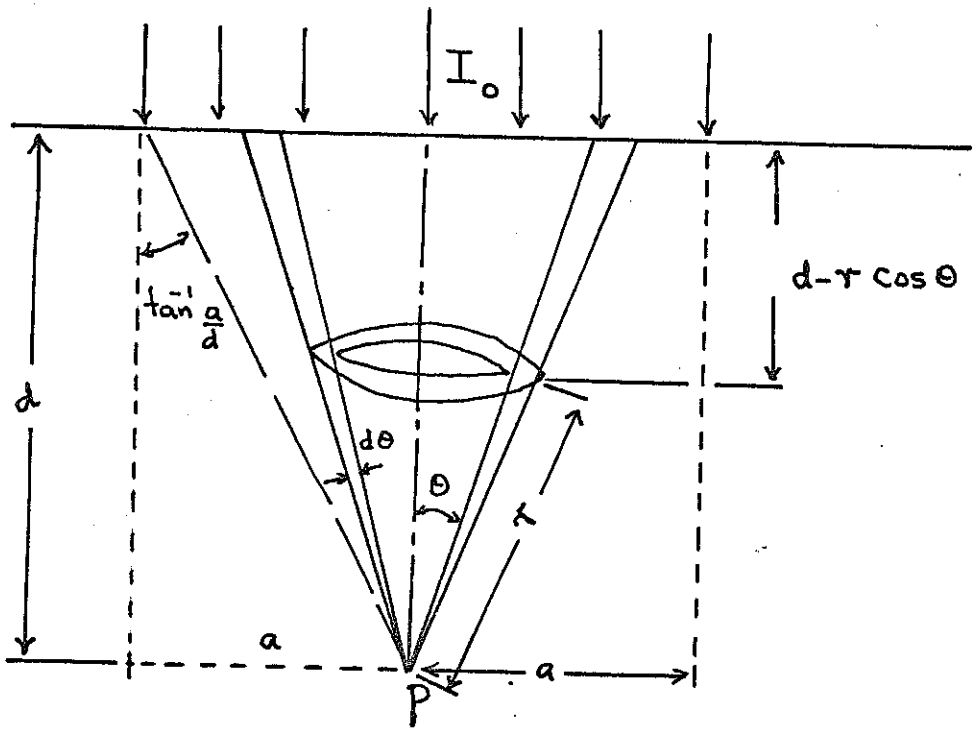

Fig. A1.1. The magnitude of scattered radiation reaching any point P.

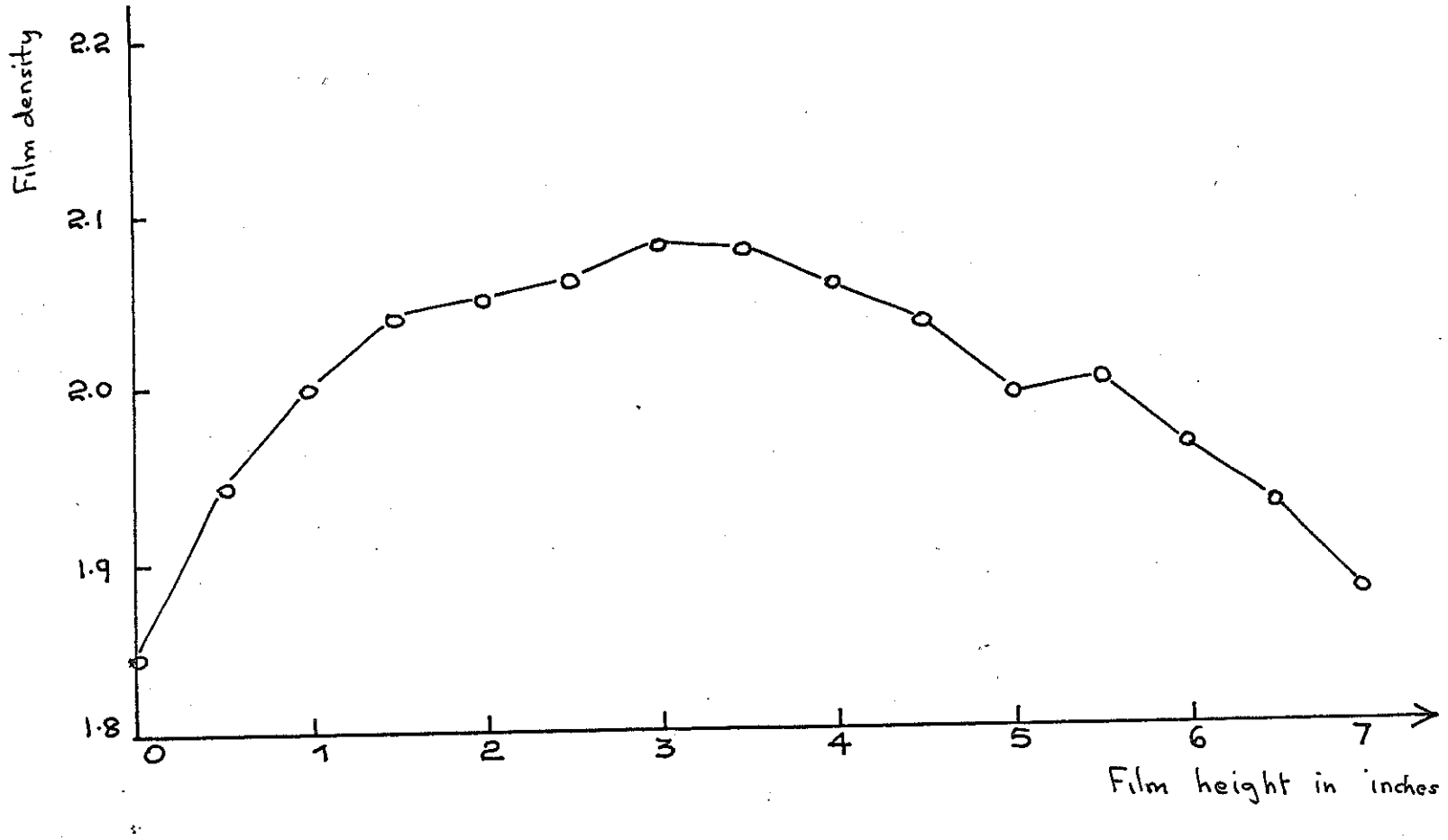

Fig. A1.2. Film density variation showing the effect of scattered radiations.

(90 keV)

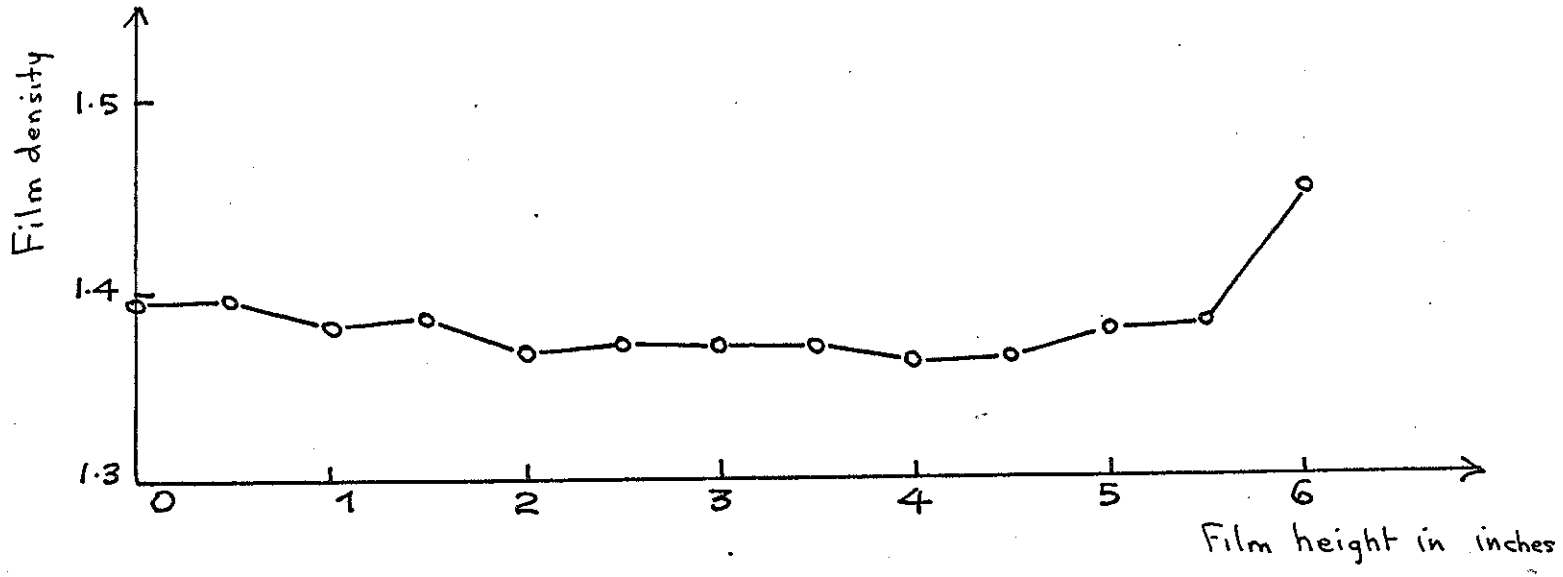

Fig. A1.3. Film density variation after reducing the effect of scattered radiation with the use of a parallel plate collimator.
(90 keV)

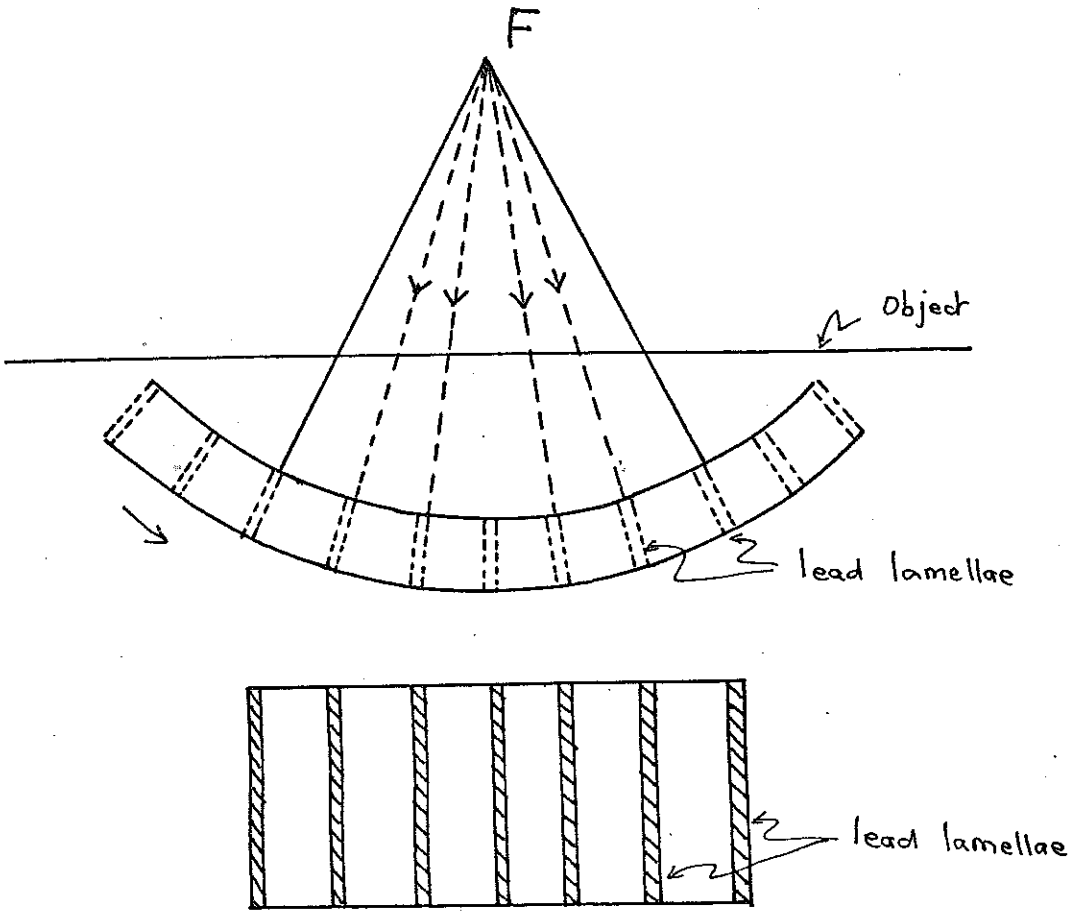

Fig. A1.4. Grid with lead lamellae arranged on a cylindrical surface.

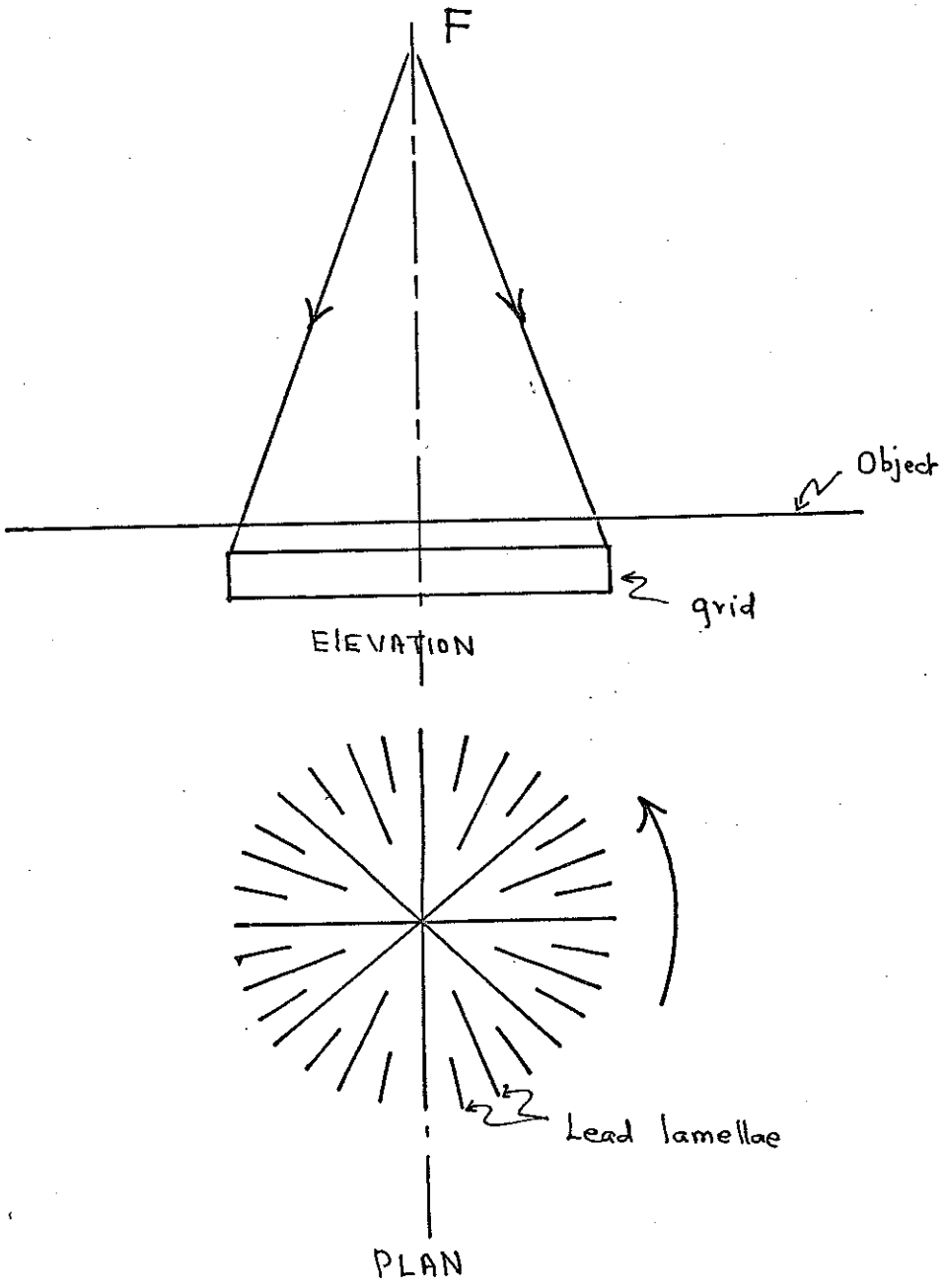

Fig. A1.5. Grid with radially placed lamellae.

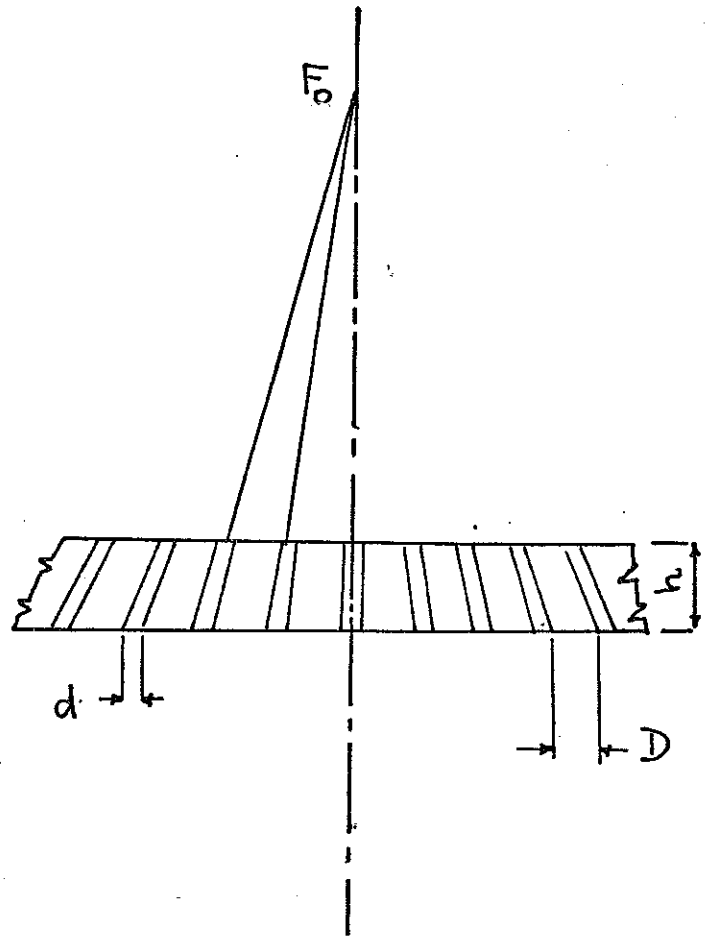

Fig. A1.6. Plane focussed Grid.

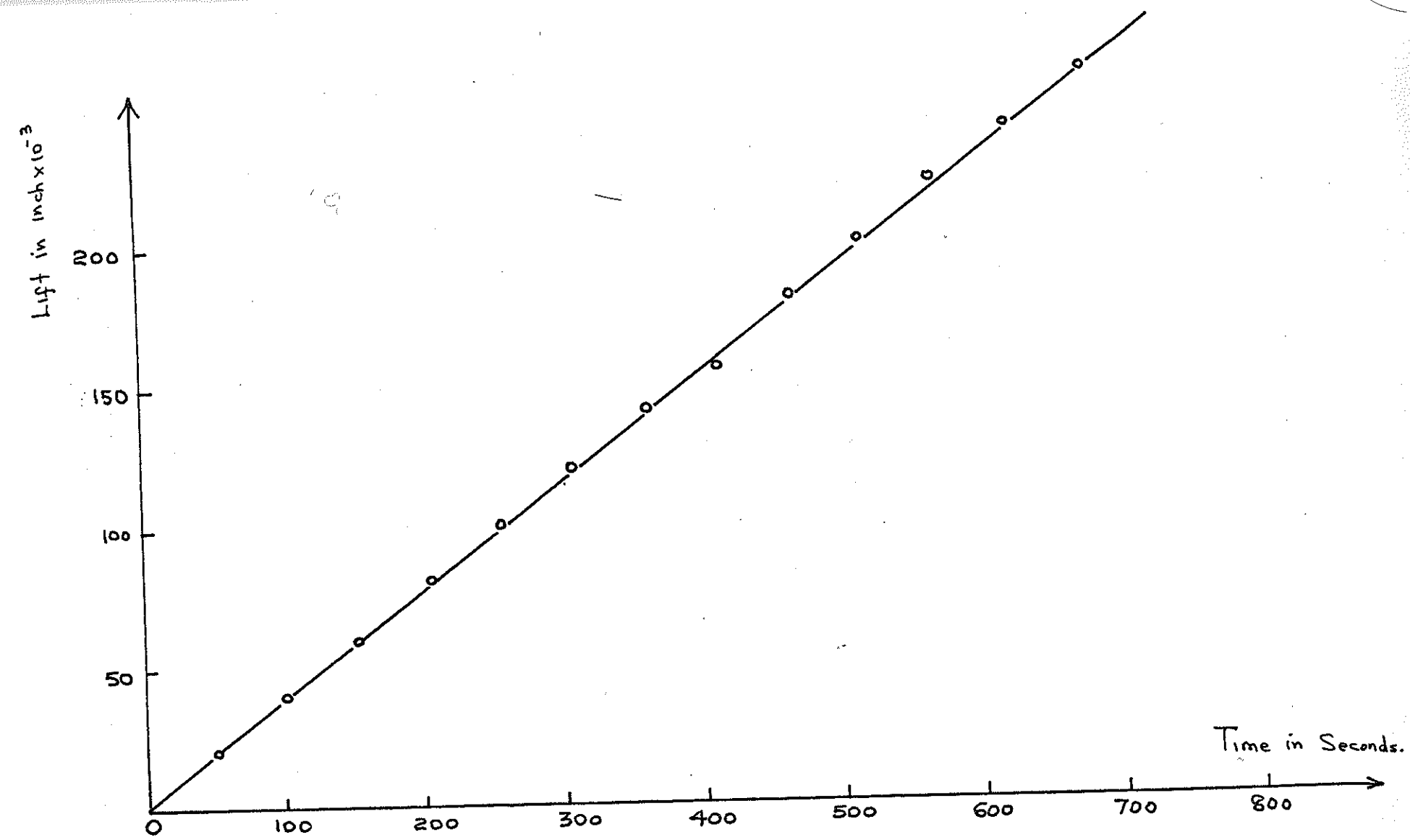

Fig. A1.7. The linear displacement of Grid with time.

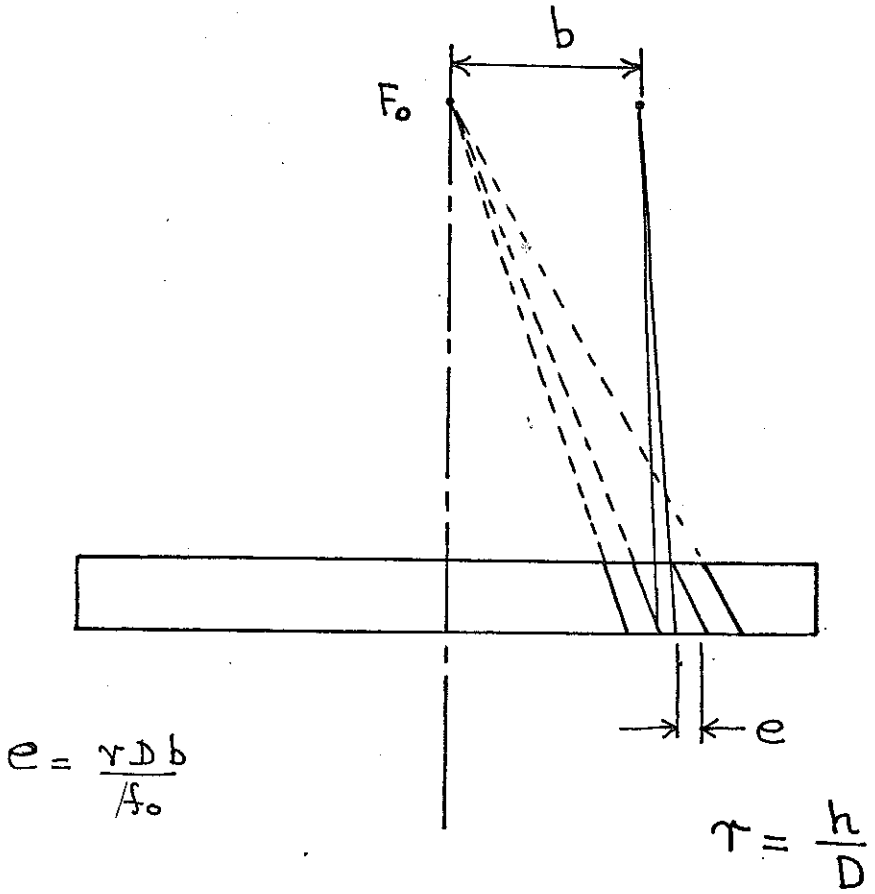

Fig. A1.8. Error in exposed area due to lateral decentering of Grid.

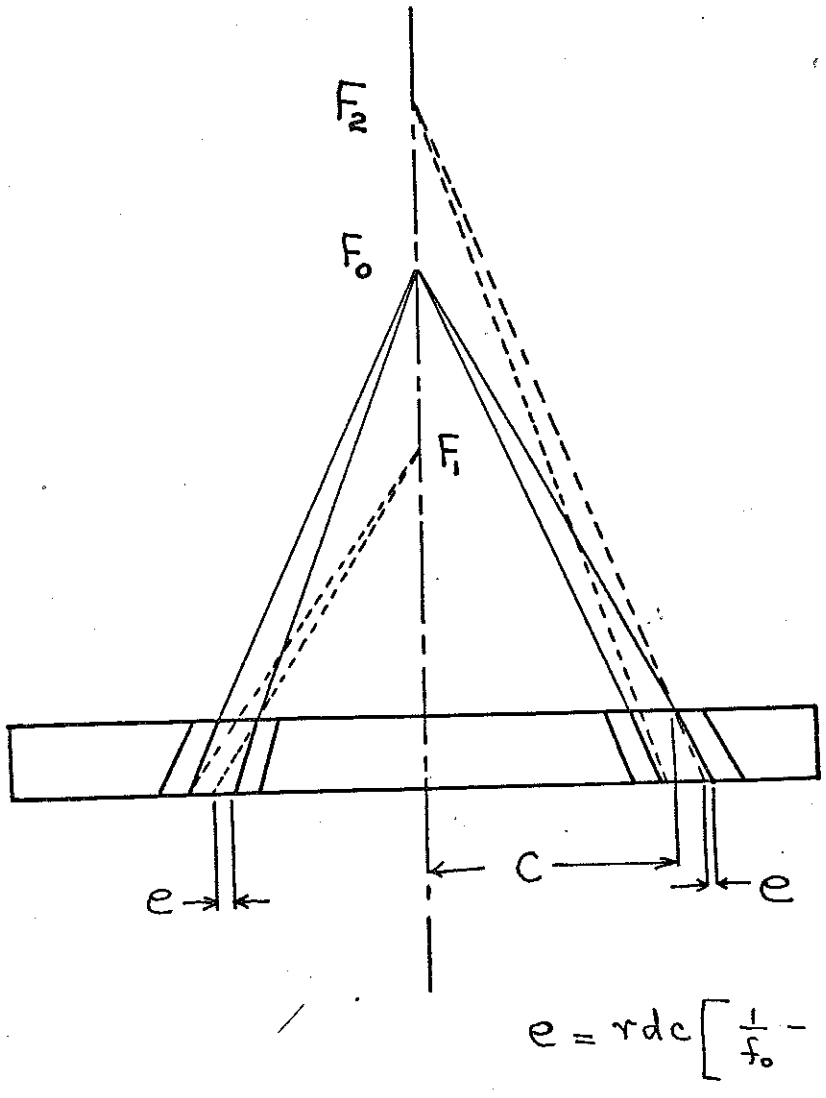

Fig. A1.9. Reduction in exposed area due to error in the focal ~~Groi~~ Grid distance.

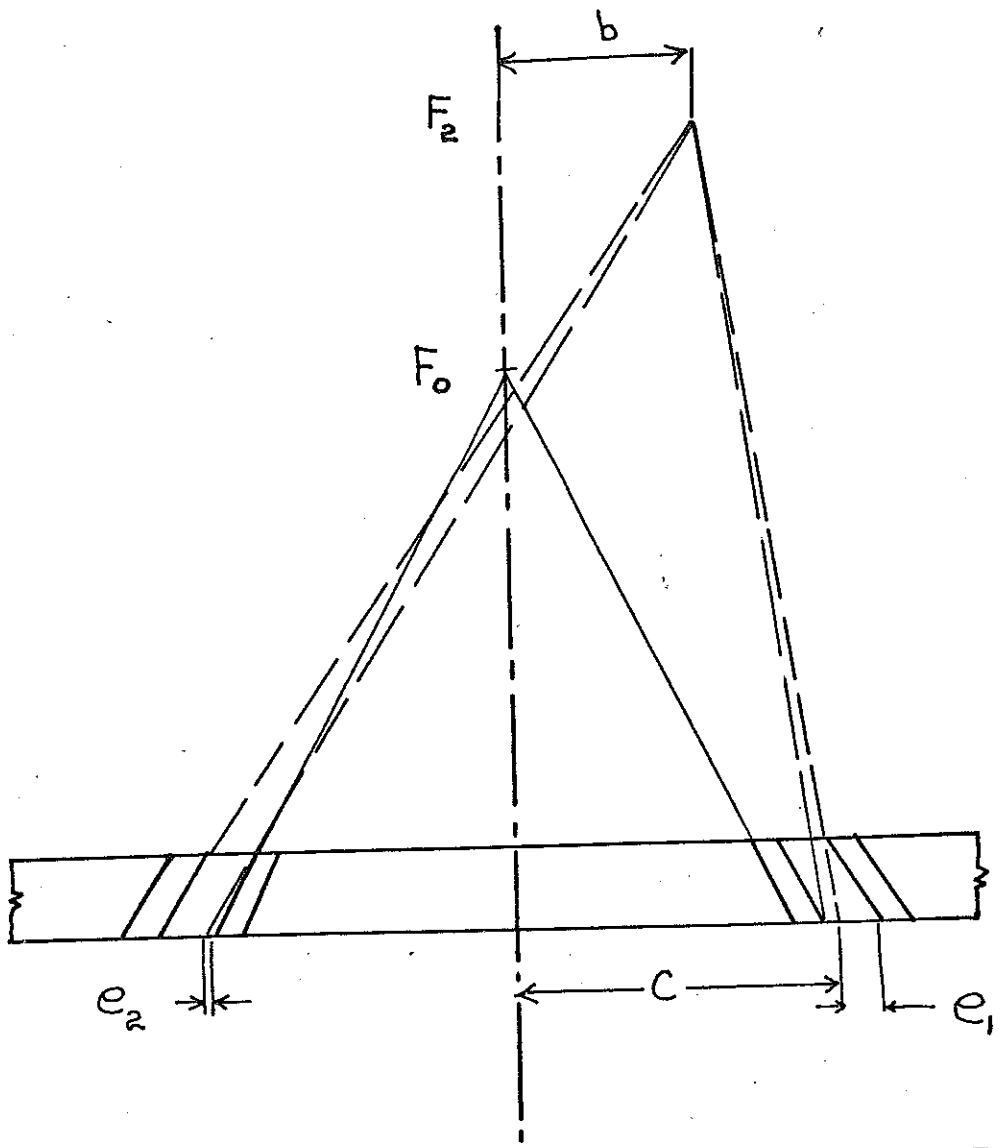

$$e_1 = \left[b + (c-b)\left(1 - \frac{f_o}{f_2}\right)\right] \frac{rd}{f_o}$$

$$e_2 = \left[b - (b+c)\left(1 - \frac{f_o}{f_2}\right)\right] \frac{rd}{f_o}$$

Fig. A1.10. Reduction in exposed area due to combined lateral decentering of the Grid and error in focal Grid distance.

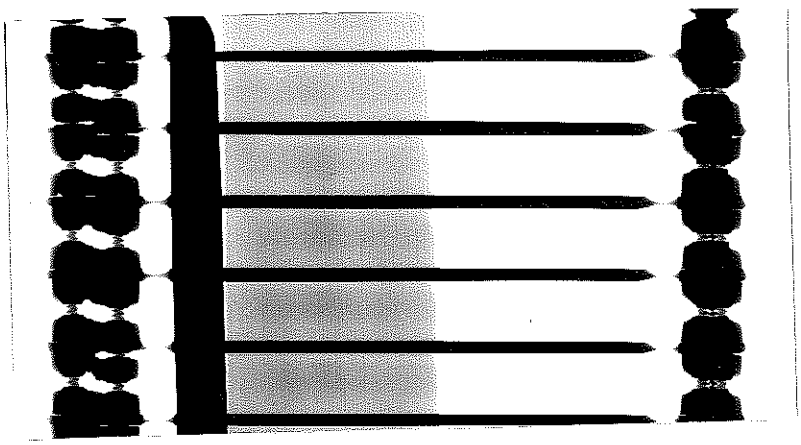

(a) With parallel plate Collimator.

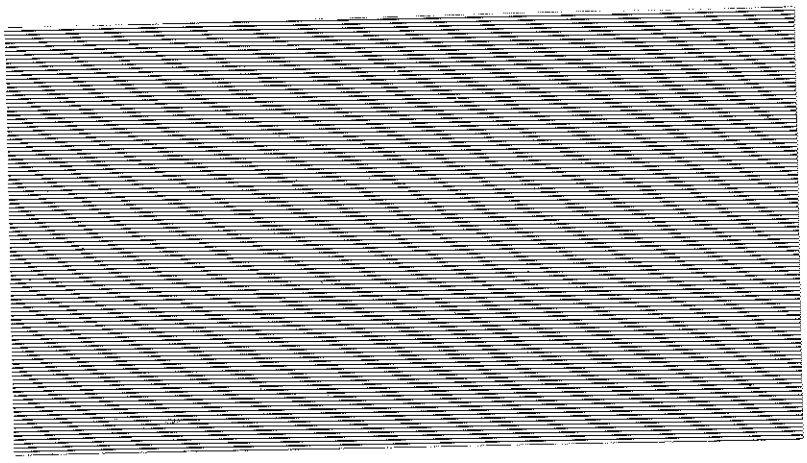

(b) With a Bucky Grid.

Figs. A1. 11 (a) and (b). Positive prints of radiographs taken with parallel plate Collimator and Bucky Grid.

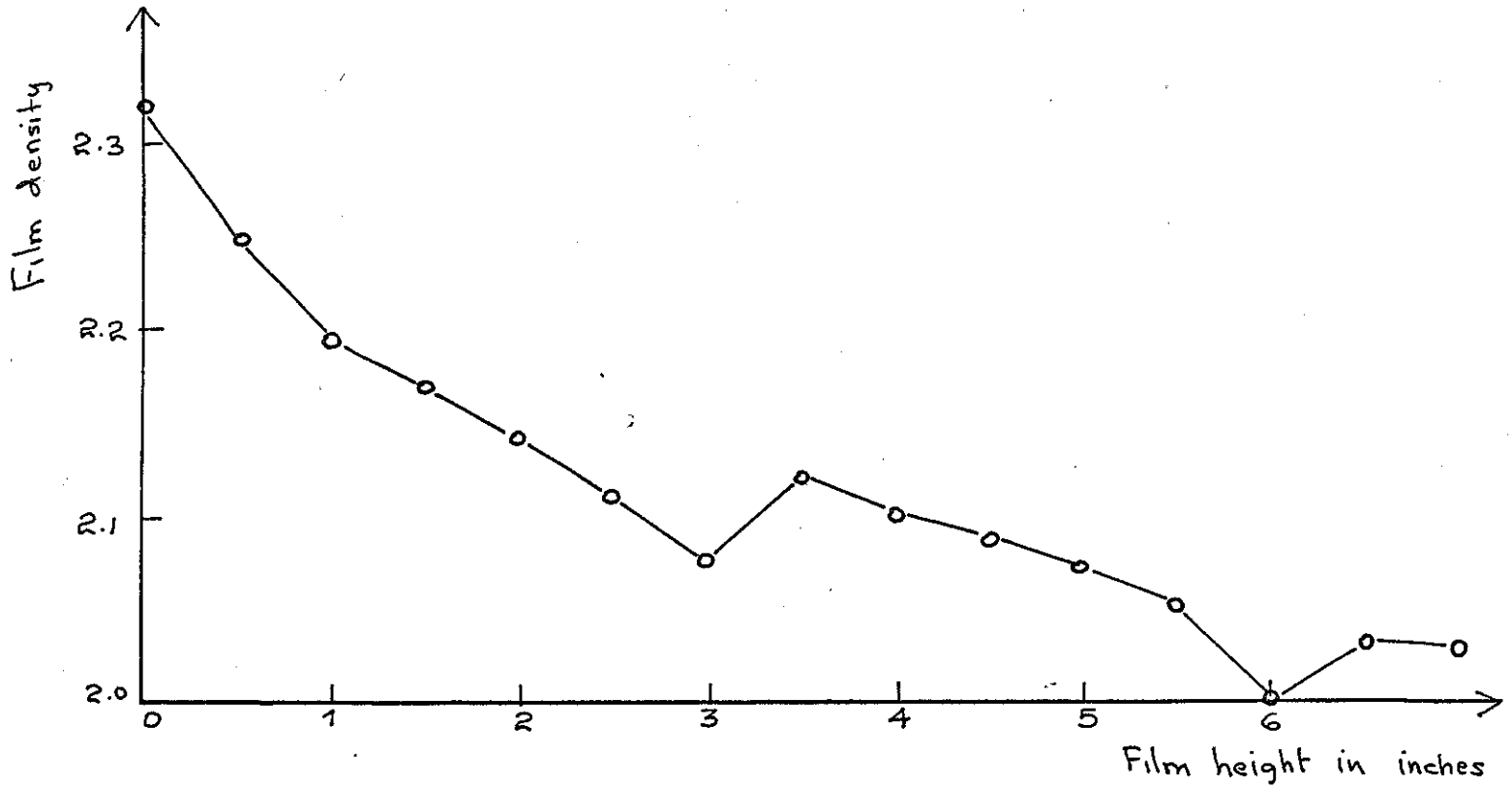

Fig. A1.12 Film density variation after reducing the effect of scattered radiation with the use of a Bucky Grid.
(I50 keV)

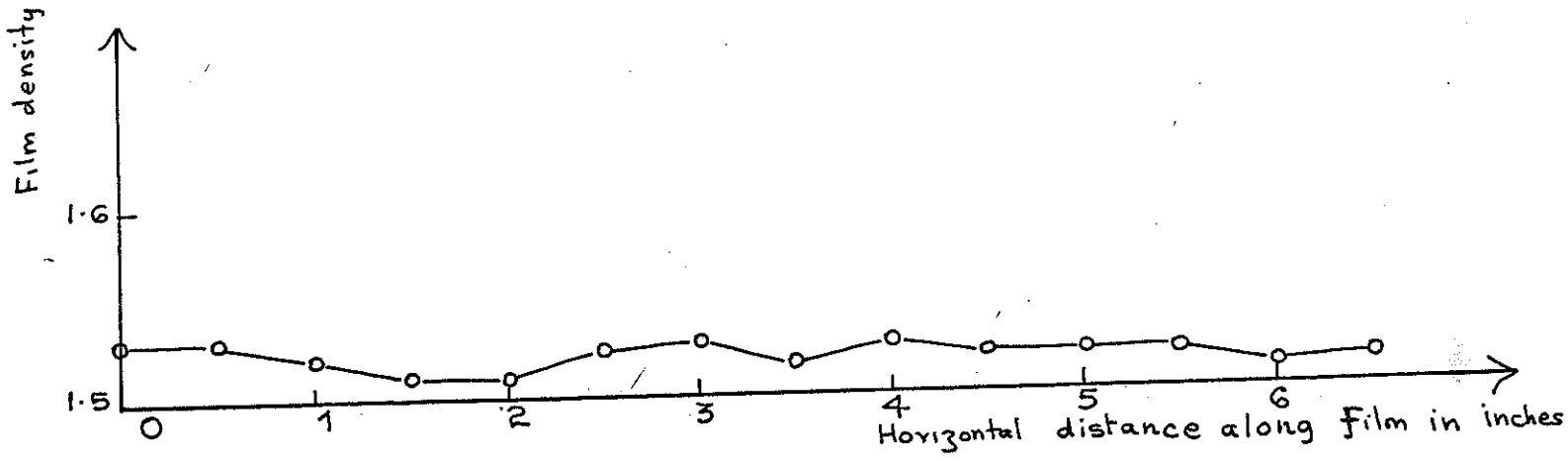

Fig. A1.13 Film density variation after reducing the effect of scattered radiation with the use of a Bucky Grid.
(90 keV.)

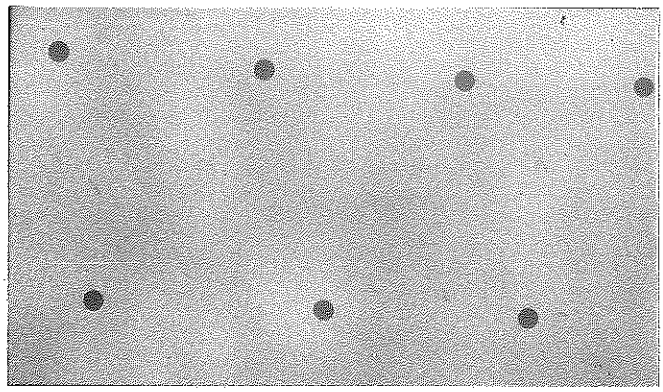

(a) Without using Bucky Grid

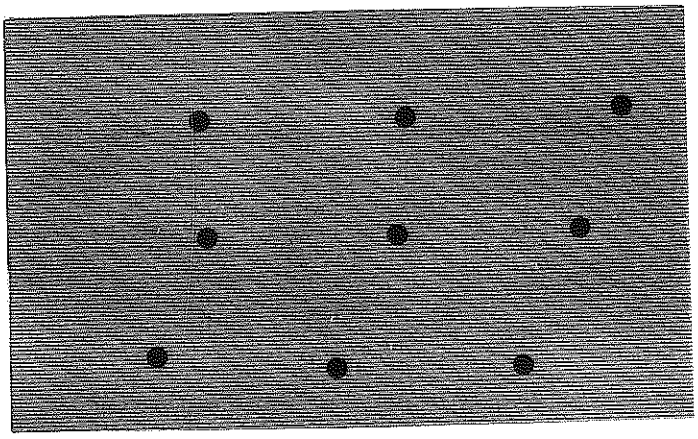

(b) With stationary Bucky Grid

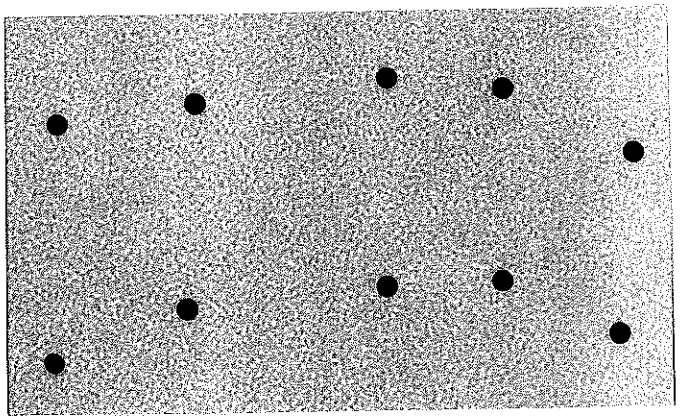

(c) With Oscillating Bucky Grid

Figs. A1.14 (a)-(c) Efficiency of a Bucky Grid in improving the contrast of lead markers

Appendix 2 The data of the peak stress points of all specimens sheared under Type 1, Type 2 and Type 3 tests are summarised in this Appendix in Tables A.2.1 to A.2.6.

Table A.2.1 The data of the test paths followed and the peak stress points of specimens sheared from 90 psi isotropic stress along Type 1 test path.

Test Designation	Test Ident. in graph	Coordinates of stress (q,p) and path followed	q_f psi	p_f psi	$\Sigma \delta e$	$\Sigma \delta \epsilon$
BD	1	(0,90) to (0,56) isotropic swelling. (0,56) to (57,75) applied stress path of slope 3	57	75	-0.082	16.8
BH	2	(0,90) to (0,56) isotropic swelling. (0,56) to (38.7, 43.3) undrained shear path	38.7	43.3	0.025	12.8
BI	3	(0,90) to (0,56) isotropic swelling. (0,56) to (44,55) constant p test path	44	55	-0.02	17.8
T_3	4	Undrained test from (0,90)	41.3	52.7	0	12.7
T_{11}	5	(0,90) to (35,85) applied stress path with constant (dq/dp) (35,85) to (49.5, 67.4) applied stress path with constant (dq/dp)	49.5	67.4	-0.051	11.9
T_{15}	6	(0,90) to (39.2, 44.0) applied stress path with constant (dq/dp)	39.2	44	0.005	17

Table A.2.1 continued.

Test Designation	Test Ident. in graph	Coordinates of stress (q,p) and path followed	q_f psi	p_f psi	$\Sigma \delta e$	$\Sigma \delta \epsilon$
BV	7	(0,90) to (7.1, 12.4) applied stress path with constant (dq/dp)	12.4	7.1	0.157	16.6
BZ	8	(0,90) to (0, 8.3) isotropic swelling (0, 8.3) to (16.5, 13.8) applied stress path with constant (dq/dp)	16.5	13.8	0.117	14.3
T_{24}	9	(0,90) to (0,30) isotropic swelling (0,30) to (31, 30) undrained test path	31	30	0.06	15

Table A.2.2. The data of the stress paths followed and the peak stress points of all specimens sheared from 90 psi isotropic stress along Type 2 test path

Test Designation	Test Ident. in graph	Coordinates of stresses (q,p) in psi and the stress path followed	q_f psi	p_f psi	$\Sigma\delta e$	$\Sigma\delta\epsilon$
AD	10	Applied stress path of slope 3 from (0, 90)	88.8	119.5	-0.183	16.5
AO	11	Constant p stress path from (0, 90)	64.9	88.6	-0.109	15.2
AY	12	Applied stress path of slope 1.5 from (0,90)	120	171.5	-0.291	21.2
CA	13	(0,90) to (31.5, 89.7) constant p stress path (31.5, 89.7) to (92, 138.7) applied stress path with constant slope	92	138.7	-0.213	16.4
CE	14	(0,90) to (39.3, 88.7) constant p stress path (39.3, 88.7) to (100.9, 141.3) applied stress path of constant (dq/dp)	100.9	141.3	-0.241	20.1
BK	15	(0,90) to (15, 137) applied stress path of constant (dq/dp) (15, 137) to (33, 143) applied stress path of constant (dq/dp) (33, 143) to (56, 143) constant p path (56, 143) to (80, 143) " (80, 143) to (100.5,143.4) "	100.5	143.4	-0.232	14.4

Table A.2.2 (continued)

Test Designation	Test Ident. in graph	Co-ordinates of stresses (q,p) in psi and the stress path followed	q_f psi	p_f psi	$\Sigma \delta e$	$\Sigma \delta \epsilon$
CJ	16	(0,90) to (18.5, 90) constant p path (18.5, 90) to (98.2, 141) applied stress path of constant (dq/dp)	98.2	141	-0.24	20.1
T_{13}	17	(0, 90) to (29, 89) constant p path (29, 89) to (29, 118) constant q path (29, 118) to (82.7,116) constant p path	82.7	116	-0.19	15.4
CQ	18	(0, 90) to (54.8, 87) approximately constant p path (54.8, 87) to (53, 126) approximately constant q path (53, 126) to (86.5,137) applied stress path of slope 3	86.5	137	-0.201	16.1

Table A.2.3. The data of the stress paths followed and the peak stress points of all specimens sheared from 90 psi isotropic stress along Type 3 stress paths.

Test Designation	Test Ident. in graph	Coordinate of stress (q,p) and the stress path followed	q_f psi	p_f psi	$\Sigma \delta e$	$\Sigma \delta \epsilon$
BC	19	(0, 90) to (31.8, 78) applied stress path with constant (dq/dp) (31.8, 78) to (62.4, 156) anisotropic consolidation (62.4, 156) to (110, 161) applied stress path with constant (dq/dp)	110	161	-0.273	23
BJ	20	(0, 90) to (0, 56) isotropic swelling (o, 56) to (68.2, 103.7) applied stress path of slope 1.5	68.2	103.7	-0.133	15.1
T_{10}	21	(0, 90) to (27.5, 38) applied stress path with constant (dq/dp) (27.5, 38) to (50, 109.5) anisotropic consolidation followed by constant q and constant p paths	72.8	117.1	-0.161	26.4

Table A.2.4. The stress paths followed and the peak stress points of all specimens sheared from 60 psi isotropic stress.

Test Designation	Test Ident. in graph	Type of Test	Coordinate of stress (q,p) psi and stress path followed	q_f psi	p_f psi	$\Sigma \delta e$	$\Sigma \delta \epsilon$
Z	26	Compression	Applied stress path with slope 3 from (0,60)	63.6	81.2	-0.20	19.1
AQ	27	Compression	Constant p stress path from (0,60)	44.5	58.5	-0.128	17
AX	28	Compression	Applied stress path of slope 1.5 from (0,60)	76	111	-0.279	17.3
T_4	29A	Compression	Undrained test from (o,60)	29	34.2	0	14.1
T_{21}	29B	Compression	Applied stress path of slope 1 from (0,60)	89.4	137.8	-0.324	14.8
PAL	35	Extension	Undrained test path from (0,60)	-26	35	0	
BB	36	Extension	Applied stress path of -1.5 from (0,60)	-69	100	-0.21	
BE	37	Extension	Constant p test path from (0,60)	-41	59	-0.097	
BG	38	Extension	Applied stress path of slope -3 from (0,60)	-44	73	-0.122	

Table A.2.5. The stress paths followed and the peak stress points of all specimens sheared from 30 psi isotropic stress.

Test Designation	Test Ident. in graph	Coordinate of stress (q,p) psi and stress path followed	q_f psi	p_f psi	$\Sigma \delta e$	$\Sigma \delta \epsilon$
AF	22	Applied stress path with slope 3 from (o,30)	32.5	40.8	-0.197	20.2
AJ	23	Constant p stress path from (0,30)	24.7	29.3	-0.134	19
AP	24	Applied stress path with slope 2 from (0,30)	39.5	50.5	-0.276	24.5
T_5	25	Undrained test path from (o,30)	14.4	16	0	17

Table A.2.6. The stress paths followed and the peak stress points of specimens sheared from miscellaneous isotropic stresses.

Test Designation	Test Ident. in graph	Coordinate of stress point (q,p) psi and the stress path followed	q_f psi	p_f psi	$\Sigma \delta e$	$\Sigma \delta \epsilon$
AK	30	Applied stress path of slope 3 from (0,120)	116.9	159	-0.194	19.4
BA	31	(0,145) to (0,90) isotropic swelling (0,90) to (90.6, 120.2) applied stress path of slope 3	90.6	120.2	-0.073	17
T_1	32	Applied stress path slope 3 from (0,25)	23.7	32.9	-0.125	16.9
T_2	33	Undrained test path from (0,25)	12.6	14.3	0	10.1
T_6	34	Undrained test path from (0,45)	21.6	23.6	0	14.4

APPENDIX 3

A relationship between the slope $\frac{\partial F^{**}}{\partial \eta}$ of the (v, η) characteristic of a constant p test and the slope $f_2^{**}(\eta)$ of the anisotropic consolidation paths in (v, ϵ) space

$$\frac{\partial F^{**}}{\partial \eta} = \left(\frac{\lambda - k}{1+e}\right) \frac{2\eta}{M^2+\eta^2} = x \qquad \text{A3-1}$$

$$f_2^{**}(\eta) = \frac{\lambda - k}{\lambda} \frac{2\eta}{M^2-\eta^2} = y \qquad \text{A3-2}$$

ie $$\frac{x}{y} = \left(\frac{\lambda}{1+e}\right) \frac{M^2-\eta^2}{M^2+\eta^2}$$

From which

$$\frac{\eta}{M} = \left[\frac{\left(\frac{\lambda}{1+e} - \frac{x}{y}\right)}{\left(\frac{\lambda}{1+e} + \frac{x}{y}\right)} \right]^{\frac{1}{2}} \qquad \text{A3-3}$$

From equations A3.3 and A3.2

$$x^2 = \left(\frac{1 - \frac{k}{\lambda}}{M}\right)^2 \left[\left(\frac{\lambda}{1+e}\right)^2 - \frac{x^2}{y^2} \right] \qquad \text{A3.4}$$

From equations A3.1, A3.2 and A3.4

$$\frac{\partial F^{**}}{\partial \eta} = \frac{\left(1 - \frac{k}{\lambda}\right)\left(\frac{\lambda}{1+e}\right)}{\left[1 + \left(\frac{1 - \frac{k}{\lambda}}{M}\right)^2 \left(\frac{1}{f_2^{**}(\eta)}\right)^2\right]^{\frac{1}{2}}} \qquad \text{A3.5}$$

or alternatively

$$f_2^{**}(\eta) = \frac{\frac{\partial F^{**}}{\partial \eta}}{\left[\left(\frac{\lambda}{1+e}\right)^2 - \left(\frac{M}{1-\frac{1}{\lambda}}\right)^2\left(\frac{\partial F^{**}}{\partial \eta}\right)^2\right]^{\frac{1}{2}}} \qquad \text{A3.6}$$

References

Andresen, A. and Simons, N.E., 1960. "Norwegian triaxial equipment and techniques." Res.Conf. on Shear Strength of Cohesive Soils, Boulder, Colorado. pp.695-709.

Arthur, J.R.F., R.G.James and K.H.Roscoe, 1964. "The determination of stress fields during plane strain of a sand mass." Geotechnique, Vol.14, pp.283-308.

Balla, A., 1960. "Stress conditions in Triaxial Compression." Proc. A.S.C.E., Vol.86, SM , pp.57-84.

Bernhard, R.K. and M.Chasek, 1955. "Soil density determination by direct transmission of Gamma rays." ASTM Proc. 1955, Vol.55, pp.1199-1223.

Bishop, A.W. and G.E.Green, 1965. "The influence of end restraint on the compression strength of a cohesionless soil." Geotechnique, Vol.15, No.3, pp.243-266.

Bishop, J.W., A.P.Green and R.Hill, 1956. "A note on the deformable region in a rigid plastic body." Journal Mech.Phys.Solids, Vol.4, 1956 p.256.

Bishop, A.W. and D.J.Henkel, 1962. "The measurement of soil properties in the triaxial apparatus." Arnold, London. 2nd edition.

Blight, G.E., 1963. "The effect of nonuniform pore pressures on laboratory measurements of the shear strength of soils." Symposium on "Lab.Shear Testing of Soils." Ottawa, 1963, pp.173-183.

Bucky, G., 1913. "Uber die Ausschaltung der im objekt entstehenden Sekundärstrahlen bei Röntgenaufnahmen." Verh. dtsch. Röntg-Ges. 9, (1913), 30.

Burland, J.B., 1965. "The yielding and dilation of clay." Correspondence, Geotechnique, Vol.15, pp.211-214.

Burland J.B., 1967. "Deformation of soft clay." Ph.D.Thesis, Cambridge University.

Cameron, J.F. and M.S.Bourne, 1958. "A Gamma scattering soil density gauge for subsurface measurements." Int.Journal of Applied Radiation Isotopes, 1958, Vol.3, pp.15-19.

Cole, E.R.L., 1967. "Behaviour of soils in the simple shear apparatus." Ph.D.Thesis, Cambridge University.

Coumoulos, D.G., 1967. "A radiographic study of soils." Ph.D.Thesis, Cambridge University.

D'Appolonia, E. and N.M.Newmark, 1951. "A method for the solution of the restrained cylinder under compression." Proc. 1st U.S.Nat.Cong.Appl.Mech., A.S.M.E., pp.217-226.

Davis, E.H. and G.P.Raymond, 1965. "A non-linear theory of consolidation." Geotechnique. 15:2:161.

Donnelly, W.P., 1967. "The use of Gamma radioscopy techniques on soil test apparatus." Internal report. Cambridge University.

Drucker, D.C., 1959. "A definition of stable inelastic material." Journal Appl.Mech.Trans., A.S.M.E., 26, pp.101-106, 1959.

Filon, L.N.G., 1902. "On the elastic equilibrium of circular cylinders under certain practical systems of load." Philosophical Transaction of the Royal Society, Vol.198(A), pp.147-223.

Geuze, E.C.W.A. and T.K.Tan, 1950. "The shearing properties of soils." Geotechnique, Vol.11, No.2, p.148.

Gray, L.H., 1931. Proc.Camb.Phil.Society 27 (1931) p.103.

Hambly, E.C., 1969. "Plane strain behaviour of soft clay." Forthcoming Ph.D.Thesis, Cambridge University.

Hambly, E.C. and K.H.Roscoe, 1969. "Observations and predictions of stresses and strains during plane-strain of wet clays." Paper accepted for publication in the 7th Int.Conf.Soil Mech., Mexico, 1969.

Hansen, J.B., 1961. "A model law for simultaneous primary and secondary consolidation." Proc. 5th Int.Conf. on Soil Mech., Vol.1, pp.133-136.

Haythornthwaite, R.M., 1960. "Mechanics of the triaxial test for soils." Journal of Soil Mech. and Found. Div., Proc., A.S.C.E., Vol.86, October.

Henkel, D.J., 1959. "The relationships between the strength, pore water pressure and volume change characteristics of saturated clays." Geotechnique, Vol.9, pp.119-135.

Henkel, D.J., 1960. "The relationship between the effective stresses and water content in saturated clays." Geotechnique, Vol.10, pp.41-54.

Henkel, D.J. and V.A.Sowa, 1963. "The influence of stress history on the stress path followed in undrained triaxial tests." ASTM-NRC Symposium on Lab. Shear Testing of Soils, Ottawa, Canada, pp.280-291.

Holubec, I., 1966. "The yielding of cohesionless soils." Ph.D.Thesis, University of Waterloo, Canada.

Hondius Boldingh, W., 1964. "Grids to reduce scattered X-rays in medical radiography." Phillips Res.Report. Suppl. No.1, pp.1-84.

Hvorslev, M.J., 1937. "Uber die Festigkeitseigenschaften gestörter bindiger Böden." Thesis, Ingeniörvidenskabelige, Skrifter, Series A, No.45.

Hvorslev, M.J., 1960. "Physical component of the shear strength of saturated clays." Research Conf. on Shear Strength of Cohesive Soils. A.S.C.E. June 1960, pp.169-273.

James, R.G., 1965, "Stress and strain fields in sand." Ph.D.Thesis, Cambridge University.

James, R.G., 1968. "Unpublished report on the new automatic film measuring device." Cambridge University.

Klein, O. and Y.Nishina, 1929. "Zeit für physik. 52 (1929) p.853.

Ladanyi, B., P.LaRochelle and L.Tanguay, 1965. "Some factors controlling the predictability of stress-strain behaviour of clay." Can.Geotech. Journal 2, pp.60-83, 1965.

Leonards, G.A. and P.Girault, 1961. "A study of the one dimensional consolidation test." Proc. 5th Int. Conf. Soil Mech., Vol.1, pp.213-218.

Lord, J.A., 1969. "Stresses and strains in an earth pressure problem." Forthcoming Ph.D.Thesis, Cambridge University.

Loudon, P.A., 1967. "Some deformation characteristics of Kaolin." Ph.D.Thesis, Cambridge University.

Mc.dermott, R.J.W., 1965. "The use of free ends in the triaxial testing of clay." M.Sc. Thesis, University of Manchester.

Mitchell, R.J., 1967. "Some applications of the critical state theories of yielding of soils." Ph.D. Thesis, Cambridge University.

Nadai, A., 1950. "Theory of flow and fracture of solids." McGraw-Hill, Vol.1.

O'Loughlin, M.W.B., 1964. "Radiological examination of granular materials." Ph.D. Thesis, Cambridge University.

Olson, R.E., 1962. "The shear strength properties of calcium illite." Geotechnique, Vol.12, pp.23-43.

Oosterlcamp, W.J., 1946. "Eliminating scattered radiation in medical X-ray photographs." Phillips Techn. Review, Vol.8, No.6, 1946, pp.183-192.

Palmer, A.C., 1965. "On stress-strain relations of soils." Division of Engineering, Brown University.

Pickett, G., 1944. "Application of the Fourier method to the solution of certain boundary problems in the theory of elasticity." Journal Appl.Mech., A.S.M.E., 11, A-176.

Poorooshasb, H.B., 1961. "The properties of soils and other granular media in simple shear." Ph.D. Thesis, Cambridge University.

Poulos, S.J., 1964. "Report on control of leakage in the triaxial test." Harvard Soilmechanics Series No.71, Cambridge, Massachusetts, 1964.

Rendulić, L., 1936. "Relation between voids ratio and effective principal stresses for a remoulded silty clay." Proc. 1st Int.Conf. on Soilmech and Foundation Vol.3, pp.48-51.

Richart, F.E., 1957. "A review of the theories for sand drains." Proc. A.S.C.E., 83:3:1957, pp.1301-1338.

Roscoe, K.H., 1953. "An apparatus for the application of simple shear to soil samples." Proc. 3rd Int.Conf. Soil Mech., Zurich, Vol.1, pp.186-191.

Roscoe, K.H., J.R.F.Arthur and R.G.James, 1963. "The determination of strains in soils by an X-ray method." Civ.Eng. and Pub.Wks.Rev., 58: pp.873-876 and 1009-1012.

Roscoe, K.H., R.H.Bassett and E.R.L.Cole, 1967. "Principal axes observed during simple shear of a sand." Proc. Conf. on "Shear Strength Properties of Natural Soils and Rocks." Oslo, 1967, pp.231-237.

Roscoe, K.H. and J.B.Burland, 1968. "On the generalised stress-strain behaviour of wet clay." Engineering Plasticity, Cambridge University Press, 1968, pp.535-609.

Roscoe, K.H. and H.B.Poorooshasb, 1963. "A theoretical and experimental study of strains in triaxial tests on normally consolidated clays." Geotechnique, Vol.13, pp.12-38.

Roscoe, K.H. and A.N.Schofield, 1963. "Mechanical behaviour of an idealised wet clay." Proc. 2nd Eur.Conf. Soil Mech., Wiesbaden, Vol.1, pp.47-54.

Roscoe, K.H., A.N.Schofield and A.Thurairajah, 1963a. "Yielding of clays in states wetter than critical." Geotechnique, Vol.13, pp.211-240.

Roscoe, K.H., A.N.Schofield and A.Thurairajah, 1963b. "A critical appreciation of test data for selecting a yield criterion for soils." Proc.Symposium on Laboratory Shear Testing of Soils, A.S.C.E. and N.R.C.C., pp.111-128.

Roscoe, K.H. and A.Thurairajah, 1964. "On the uniqueness of yield surfaces for 'wet' clays." Proc.Int. Symp.Rheology and Soil Mech., IUTAM, Grenoble, 1964, pp.364-381.

Roscoe, K.H., A.N.Schofield and C.P.Wroth, 1958. "On the yielding of soils." Geotechnique, Vol.8, pp.22-53.

Roscoe, K.H., A.N.Schofield and C.P.Wroth, 1959. "Correspondence on the yielding of soils." Geotechnique, Vol.9, pp.72-82.

Rowe, P.W. and L.Barden, 1964. "The importance of free ends in the triaxial test." Proc. A.S.C.E., Vol.90, SM 1.

Schofield, A.N. and C.P.Wroth, 1968. "Critical state soil mechanics." McGraw-Hill, London.

Scott, R.P., 1937. "The wavelength distribution of the scattered radiation in a medium transversed by a beam of X or Gamma rays. British Journal of Radiology, N.S.10 (1937), pp.850-870.

Shockley, W.G. and R.G.Ahlvin, 1960. "Nonuniform conditions in triaxial test specimens." Proc.Res.Conf. on Shear Strength of Cohesive Soils, A.S.C.E., pp.341-357.

Sirwan, K,Z., 1965. "Deformation of soil specimens." Ph.D. Thesis, Cambridge University.

Skopek, J., 1957. "Sand density determination using Gamma-radiation." Proc. 4th Int.Conf. Soil Mech. London, Vol.1, pp.107-110.

Thompson, W.J., 1962. "Some deformation characteristics of Cambridge Gault Clay." Ph.D. Thesis, Cambridge University.

Thurairajah, A., 1961. "Some shear properties of Kaolin and of Sand." Ph.D. Thesis, Cambridge University.

Ting, W.H., 1968. "Some effects of history on the stress-strain behaviour of Kaolin." Ph.D. Thesis, Cambridge University.

Tovey, N.K., 1969. "Electron Microscopy of clays." Forthcoming Ph.D. Thesis, Cambridge University.

Walker, A.F., 1965. "Stress-strain relationships for clays." Ph.D.Thesis, Cambridge University.

Walker, L.K., 1967. "The deformation of clay as a time dependent process." Ph.D. Thesis, Cambridge University.

Wroth, C.P., 1965. "The prediction of shear strains in triaxial tests on normally consolidated clays." Proc. 6th Int.Conf. Soil Mech., Montreal, Vol.1, pp.417-442.

Zelenin, A.N. and G.M.Lomize, 1961. "The compressive strength of soil samples in relation to limited plastic soil deformations." Proc. 5th Int.Conf. Soil Mech., Vol.1, pp.423-425.